PHOTOCATALYTIC HYDROGEN PRODUCTION

Dissertation

zur

Erlangung der naturwissenschaftlichen Doktorwürde

(Dr. sc. nat.)

vorgelegt der

Mathematisch-naturwissenschaftlichen Fakultät

der

Universität Zürich

von

Benjamin Probst

von Bäretswil ZH

Promotionskomitee

Prof. Dr. Roger Alberto (Vorsitz)

Prof. Dr. Peter Hamm

Zürich, 2010

to my family

This thesis presents the first successful application of rhenium(I) - tricarbonyl diimine – type complexes ($[ReX(CO)_3diimine]^+$) as photosensitiser (PS) and cobalt tetraene based water reduction catalyst's (WRC) for the photocatalysed up-conversion of triethanolamine (TEOA) and protons to oxidised TEOA and H_2. The reaction, although not economically interesting, presents an important step to the overall photocatalysed water splitting to give H_2 and O_2. Towards this end it could be shown for the first time that the reductive half reaction to H_2 is principally possible in H_2O as a solvent and substrate. Experiments in organic solvents have helped to identify the rate limiting steps and allowed to understand the kinetics of the full reaction cycle, thus allowing for improved catalysts both in terms of initial reaction yield and long-term performance. Furthermore a systematic screening on $[ReX(CO)_3diimine]^+$ helped to rationalise absorption and emission properties and thus allows the tailored syntheses of new complexes.

Diese Arbeit ist die erste erfolgreiche Anwendung von Rhenium(I) - tricarbonyl diimin Komplexen ($[ReX(CO)_3diimine]^+$) als Photosensitiser (PS) in Verbindung mit Kobalt tetraen basierenden Wasser Reduktions-Katalysatoren (WRC) für die photochemische Umsetzung von Triethanolamin (TEOA) und Protonen zu oxidiertem TEOA und Wasserstoff. Obwohl die Reaktion einem Netto Energiegewinn ergibt, ist sie wirtschaftlich nicht interessant. Sie stellt aber einen wichtigen Schritt in Richtung photochemischer Wasserspaltung zu H_2 und O_2 dar, indem sie erlaubt die reduktive Halbreaktion gesondert zu erforschen. In diesem Zusammenhang konnte zum ersten Mal überhaupt gezeigt werden dass der reduktive Teil der Wasserspaltung prinzipiell in reinem Wasser als Lösungsmittel und Protonen Quelle durchgeführt werden kann. Dies stellt einen Meilenstein in der Erforschung solcher Systeme dar. Des weiteren konnten wir durch kinetische Aufklärung den Reaktionszyklus die kritischen Schritte identifizieren und punkto Ausbeute und Langzeitstabilität optimieren. Eine systematische Reihe von Derivaten des Typs $[ReX(CO)_3diimine]^+$ erlaubte uns die Absorptions- und Emissionseigenschaften zu verstehen und somit massgeschneiderte, neue Verbindungen herzustellen.

The objective of this work was to contribute to the field of artificial photosynthesis, namely photocatalytic splitting of water into hydrogen and oxygen, by studying the reductive half reaction leading to H_2 using up to here unknown catalysts of the type $[ReX(CO)_3diimine]^+$ as photosensitisers (PS) and $[CoX_2(N_4)]$ as water reduction catalyst's (WRC). After establishing a working cycle in dimethylformamide (DMF) the subject was moved to understand catalysis and its rate limiting steps. Further research was then devoted to increase long-term stability of the process and later to understand solvent effects, with the ultimate goal to get catalysis from pure H_2O. This would not have been possible without profound knowledge of the photochemistry of rhenium type photosensitisers, which was studied by systematic ligand variation on the $\{Re(CO)_3\}$ core.

Further objectives will be to increase long-term performance in H_2O, increase overlap with visible spectra and to find a link to an oxidative counterpart.

[TBA](PF_6)	tetrabutylammonium hexafluorophosphate
3-H_2NCOpy	nicotinamide
4-H_2NCOpy	isonicotinamide
4-Me_2Npy	N,N-dimethylpyridin-4-amine
AcOH	acetic acid
bipy	2,2'-bipyridine
CNBz	benzyl isonitrile
CT	charge transfer
CV	cyclic voltametry
DMF	dimethylformamide
$dmgH_2$	dimethylglyoxime
DMSO	dimethylsulfoxide
DOH_2	2,3,9,10-tetramethyl-1,4,8,11-tetraazaundecane-1,3,8,10-tetraene-1,11-diol
Et_4N^+	tetraethylammonium cation
HPLC	high performance liquid chromatography
IR	infrared
LDA	lithium diisopropylamide
LED	light emitting device
MeCN	acetonitrile
MeOH	methanol
MeSH	methantiol
N_4	tetraene
$OTfls^-$	Trifluorosulfonate anion
pAmp	N-(pyridin-4-ylmethyl)-1,10-phenanthrolin-5-amine
pAp	N-(1,10-phenanthrolin-5-yl)-isonicotinamide
phen	1,10-phenanthroline
PhSH	thiophenol
ppy	2-phenylpyridine
PS	photosensitiser
PS I / II	photosystem I / II
py	pyridine
TEOA	triethanolamine

TIM	2,3,9,10-tetramethyl-1,4,8,11-tetraazacyclotetradeca-1,3,8,10-tetraene
TMSCl	trimethylsilylchloride
TOF	turn over frequency
TON	turn over number
WOC	water oxidation catalyst
WRC	water reduction catalyst

1 $[ReBr(CO)_5]$

2 $[Re(OTfls)(CO)_5]$

3 $[ReBr_3(CO)_3](Et_4N)_2$

10 $[ReBr(CO)_3bipy]$

11 $[Re(OH_2)(CO)_3bipy](TflsO)$

12 $[ReNCS(CO)_3bipy]$

13 $[Re(py)(CO)_3bipy](TflsO)$

14 $[Re(4\text{-}Me_2Npy)(CO)_3bipy](TflsO)$

15 $[Re(CNBz)(CO)_3bipy](TflsO)$

16 $[Re(NCMe)(CO)_3bipy](TflsO)$

17 $[Re(SPh)(CO)_3bipy]$

18 $[ReN_3(CO)_3bipy]$

19 $[Re(NO_2)(CO)_3bipy]$

20 $[Re(NO_3)(CO)_3bipy]$

21 $[ReCl(CO)_3bipy]$

22 $[Re(CN)(CO)_3bipy]$

30 $[ReBr(CO)_3phen]$

31 $[Re(OH_2)(CO)_3phen](TflsO)$

32 $[ReNCS(CO)_3phen]$

33 $[Re(py)(CO)_3phen](TflsO)$

34 $[Re(4\text{-}Me_2Npy)(CO)_3phen](TflsO)$

35 $[Re(CNBz)(CO)_3phen](TflsO)$

40 $[ReBr(CO)_3phenNH_2]$

41 $[ReBr(CO)_3pAp]$

42 $[ReBr(CO)_3pAmp]$

43 $[ReBr(CO)_3pImp]$

50 $[ReBr(CO)_3DHOCH_2bipy]$

51 $[Re(OH_2)(CO)_3DHOCH_2bipy](TflsO)$

52 $ReNCS(CO)_3DHOCH_2bipy]$

53 $[ReBr(CO)_3DH_3NCH_2bipy]Br_2$

54 $[Re(OH_2)(CO)_3DH_3NCH_2bipy](TflsO)_3$

55 $[ReNCS(CO)_3DH_3NCH_2bipy](TflsO)_2$

60 $[ReBr(CO)_3DMeCO_2bipy]$

61 [$Re(OH_2)(CO)_3DMeCO_2bipy$](TflsO)

62 [$Re(py)(CO)_3DMeCO_2bipy$](TflsO)

63 [$ReBr(CO)_3DMe_2NCObipy$]

64 [$Re(OH_2)(CO)_3DMe_2NCObipy$](TflsO)

65 [$Re(py)(CO)_3DMe_2NCObipy$](TflsO)

70 [$Co(OH_2)_2(dmgH)_2$]

71 [$Co(py)_2(dmgH)_2$](PF_6)

72 [$Co(py)_2(dmgH)(dmg)$]

73 [$CoBr(py)(dmgH)_2$]

74 [$CoCl(py)(dmgH)_2$]

75 [$CoCl(3\text{-}H_2NCOpy)(dmgH)_2$]

76 [$CoCl(4\text{-}H_2NCOpy)(dmgH)_2$]

77 [$CoCl(4\text{-}Me_2Npy)(dmgH)_2$]

80 2,2’-bipyridine (bipy)

81 4,4’-Dimethyl-2,2’-bipyridine (DCH_3bipy)

82 4,4'-Bis[(trimethylsilyl)methyl]-2,2'-bipyridine (4,4’-$DTMSCH_2bipy$)

83 4,4'-Bis(Chloromethyl)-2,2'-bipyridine (4,4’-$DClCH_2bipy$)

84 4,4'-Bis(acetoxymethyl)-2,2'-bipyridine (4,4’-$DAcOCH_2bipy$)

85 4,4'-Bis(hydroxymethyl)-2,2'-bipyridine (4,4’-$DHOCH_2bipy$)

86 4,4'-Bis(azidomethyl)-2,2'-bipyridine (4,4’-DN_3CH_2bipy)

87 4,4'-Bis(aminomethyl)-2,2'-bipyridine (4,4’-DH_2NCH_2bipy)

88 2,2’-bipyridine-4,4’-dimethylester ($DMeCO_2bipy$)

89 2,2’-bipyridine-4,4’-diamide ($DH_2NHCObipy$)

90 1,10-phenanthroline (phen)

91 5-nitro-1,10-phenanthroline ($phenNO_2$)

92 5-amino-1,10-phenanthroline ($phenNH_2$)

93 N-(1,10-phenanthrolin-5-yl)-isonicotinamide (pAp)

94 N-(pyridin-4-ylmethyl)-1,10-phenanthrolin-5-amine (pAmp)

1 Introduction

In evolution the invention of photosynthesis allowed a burst of life and biodiversity on planet earth. Before this invention free energy was obtained by fermentation of organic substrates present in the early atmosphere, which became scare with time. After the invention of photosynthesis the atomic fire of the sun became available as a source of free energy, with a massive impact on future evolution. On one hand oxygen was released into the early atmosphere, which eventually served as the ultimate electron acceptor in respiration for higher plants and animals, and on the other hand sunlight was converted into chemical bonds by photosynthesis.

Ludwig Boltzmann noted on the occasion of a lecture on a meeting of the Imperial Academy of Science in Vienna (1886) that "*The struggle for existence is the struggle for available energy*".[1] This statement must be related to the second law of thermodynamics, thus available energy does not mean absolute, but rather free energy, which can be used to accomplish work in a system. Clearly nature's breakthrough with the invention of photosynthesis and later on with respiration can be seen as major steps in this struggle for available energy.

Similar to evolution of life on earth, one could argue that the use of limited fossil and nuclear fuels presents an early evolutionary stage of mankind, which will eventually be overcome by the invention of techniques and their widespread use to capture sunlight to obtain free energy. The Italian photochemist Giacomo Ciamician noted in a lecture entitled 'The Photochemistry of the Future', which he held for the International Congress of Applied Chemistry 1912 in New York:

"*Where vegetation is rich, photochemistry may be left to the plants and by rational cultivation, as I have already explained, solar radiation may be used for industrial purposes. In the desert regions, unadapted to any kind of cultivation, photochemistry will artificially put their solar energy to practical uses.*

On the arid lands there will spring up industrial colonies without smoke and without smokestacks; forests of glass tubes will extend over the plains and glass buildings will rise everywhere; inside of these will take place the photochemical processes that hitherto have been the guarded secret of the plants, but that will have been mastered by human industry which will know how to make them bear even more abundant fruit than nature, for nature is not in a hurry and mankind is. And if in a distant future the supply of coal becomes completely exhausted, civilization will not be checked by that, for life and civilization will continue as long as the sun shines! If our black and nervous civilization, based on coal, shall be followed by a quieter civilization based on the utilization of solar energy, that will not be harmful to progress and to human happiness."[2]

With this picture he was more than a century ahead of his time, and he did not foresee that fossil oil and gas and nuclear energy would follow the use of coal. But he might be completely right in saying that ultimately humankind will have to master photosynthesis to overcome the problem of limited resources.

1.1 Analysis of Today's Energy Need

Today's primary energy supply largely comes from fossil fuels (81 %) and nuclear energy (6 %), thus giving a total of at least 87 % of our primary energy that stems from limited resources (see Figure 1, data for 2006). Even though we use close to twice the amount of primary energy as compared to 1973 (4.9×10^{20} vs. 2.6×10^{20} J/annum, respectively), the fraction of energy from limited resources remained constant. Only the relative shares between oil, coal, gas and nuclear energy changed.[3]

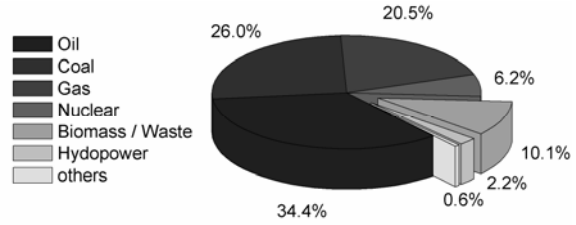

Figure 1. Primary energy supply, 2006.[3]

Nevertheless, some 12 % of our primary energy supply stem from renewable resources, namely biomass and waste (10 %), hydropower plants (2 %) and others (1 %, including geothermal, solar, wind, tide / wave / ocean energy, electricity and heat).[3]

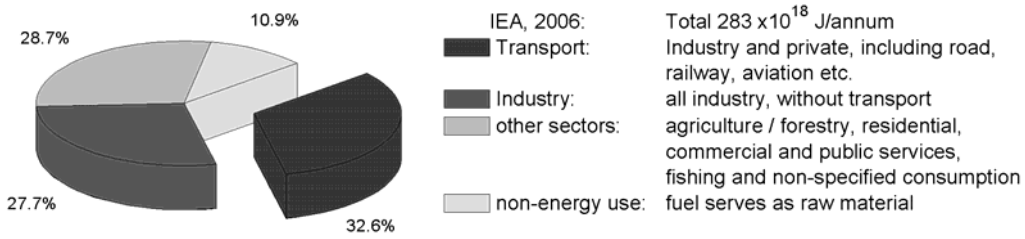

Figure 2. Use of fossil fuels by sectors.[3]

Given the high share of fossil fuels in world energy supply, it is interesting to note how fossil fuels are used (see Figure 2). Some 33 % are used as propellants in the transportation sector, thus accounting for 26 % of world energy use! Another 28 % go into the industry sector, 11 % are used as raw materials to be processed to higher value goods and 29 % go in various sectors including agriculture, forestry etc.

1.2 Energy in a post-fossil Society

To estimate how energy could be delivered in a post-fossil society, potentials of several non-fossil energy sources are estimated (see Figure 3).

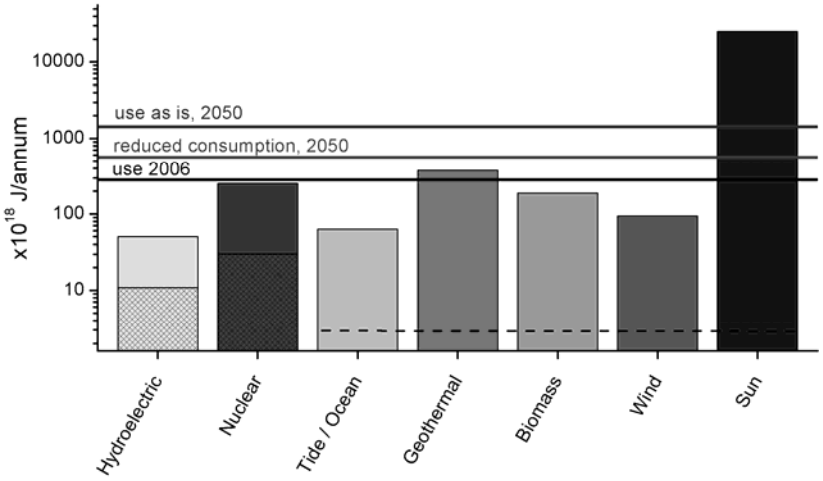

Figure 3. Potential of several renewable energy sources (Hydroelectric: technically feasible 1.6 TW; Nuclear: 8 TW, every 1.5 days a new power plant, forever; Tide / Ocean: 2 TW gross currents; Geothermal: 12 TW over land, small fraction recoverable; Biomass: 6 TW, all crop land use for energy production; Wind: 3 TW, up to 10 m; Sun: 1.2×10^5 TW on earth, 800 TW recoverable), projected consumption in 2050 (use as is and reduced consumption)[4-6] and today's use (black line).[3] Meshed black on hydroelectric and nuclear indicates their use in 2006, dotted black line on the other sources is their total use in 2006.[3] Note that a logarithmic scale is given for J/annum.

Clearly sun energy has a tremendous potential as compared to other energies. Only a very small fraction is used today.

It was noted before (section 1.1) that ~26 % of world energy supply goes into the transportation sector, mainly as diesel or gasoline. It is crucial to understand the characteristics of these two fuels when thinking about how to replace them in a post-fossil society. Figure 4 gives an idea of the energy density of several, randomly selected fuels, both in terms of weight and volume. Gasoline, diesel and kerosene are neither the energy densest fuels in terms of weight nor volume (these are hydrogen resp. aluminium). But Gasoline, diesel and kerosene have both a relatively high energy content in terms of weight and volume. They are relatively safe to handle due to

activation needed for ignition. The fact that they are liquids makes them furthermore very attractive for refuelling. No oxidant needs to be carried on board, since they can be burned with oxygen from air, and no oxidised fuel remains on board since CO_2 is released into the atmosphere.

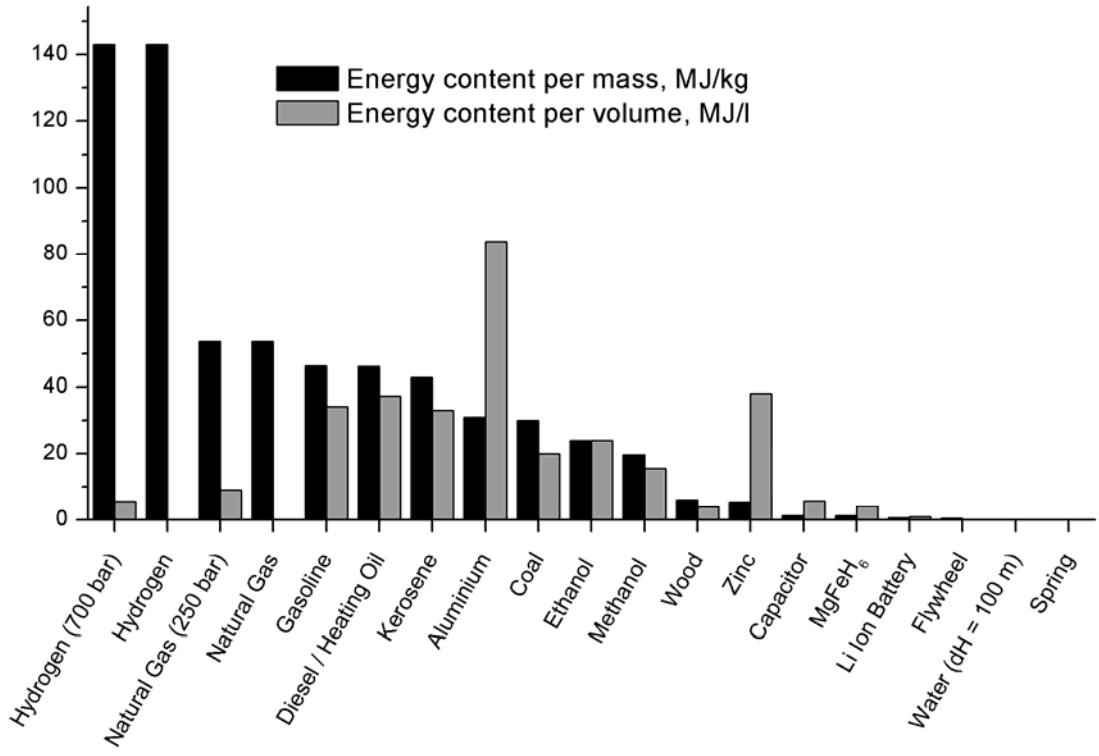

Figure 4. Energy density both in terms of mass (black) and volume (grey) for different storage devices.[7]

Clearly hydrogen and natural gas (no matter if used as gas or compressed) are too voluminous if used as propulsion fuel. Aluminium seems to be an interesting candidate as a propulsion fuel, although its combustion with O_2 is not trivial, and requires that the combustion product (AlO_3) be carried on board. Like for coal, wood and zinc refuelling would not be so easy. On the other hand both zinc and aluminium, like capacitors, hydrides (eg. $MgFeH_6$), Li-ion batteries, flywheels and springs could be recharged by electricity. In all the latter cases energy density both in terms of weight and volume forbids a use as propulsion fuel. More interesting is the situation for EtOH and MeOH: both are safe to handle liquids, have comparable energy densities to gasoline and diesel both in terms of weight and volume, and are easily combustible with O_2.

Interestingly enough, EtOH refined from crops is used today already as propulsion fuel in traditional Otto engines, without significant modifications. This scenario, even though very attractive at first glance, since using 'bio-ethanol', relies on agriculture to harvest sunlight and convert it into a fuel. Figure 3 clearly shows that this will never substitute fossil fuels, since even if all crops used for food supply today would go into ethanol production, only a fraction of world energy supply could be met, leaving alone the question of food supply.

A MeOH economy has been postulated before.[8] Key advantage of MeOH is, besides being combustible in traditional engines, that it could be used in a direct methanol fuel cell (DMFC) to produce electricity.[8,9] MeOH is the only substrate, besides H_2, that can be used in fuel cells at low temperature to produce electricity up to now. Clearly the question is how methanol would be produced.

It was stated before that the sun has an enormous potential for future energy conversion. If these two ideas were combined, eg. using the sun's tremendous energy supply and MeOH as an energy carrier, a very potent scenario for the post-fossil society results. Up to now, there is no direct way of producing alcohols from sunlight. Nowadays MeOH is produced mainly by steam reforming of fossil fuels (to give syn-gas), which is then processed to MeOH by a $Cu/ZnO/Al_2O_3$ catalyst dispersed in eg. a slurry-bubble column reactor (SBCR).[8-10] Other non-fossil sources of syn-gas are biomass or wood.[9,11] Alternatively fermentation of crops can give MeOH by distillation.[11]

An interesting scenario is the separated production of H_2 and O_2 from H_2O with sunlight (light reaction) and the capture of atmospheric CO_2 to combine them to MeOH (dark reaction).[8,10] In this case the most demanding step is the production of H_2 from H_2O, using sunlight. Several scenarios are given in section 1.3.

1.3 Solar Hydrogen

There are many ways to produce H_2 (or other fuels) with sunlight. It is fair to note that all fossil fuels used today arose from sunlight in ancient times. The question here is how to make efficient use of sunlight to meet today's society needs. Figure 5 gives an idea of how much land needs to be covered with photovoltaic (PV) power plants of 10 % efficiency to meet world energy demand. Even though 0.16 % is a respective fraction of worlds land surface, it is only a tenth of today's urban areas (1.5 %) and only about duple the amount of earths surface that is covered by roads today (~0.1%).[12]

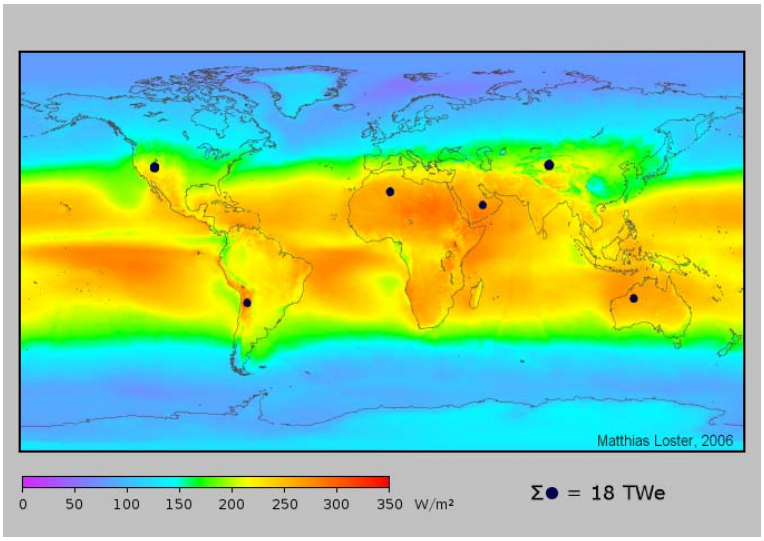

Figure 5. Schematic representation of world surface needed to cover 18 TW (optimistic projection for 2050) with 10 % efficient photovoltaic (PV) cells (0.16 % of continental surface).[6,13]

The coming discussion will briefly highlight several ways of obtaining H_2 or higher fuels from sunlight and H_2O / CO_2. Five possible pathways are outlined in Scheme 1.

Scheme 1. Randomly selected options discussed herein on how to convert H_2O with sunlight into H_2 / O_2 and finally to MeOH (PV = photovoltaic, SBCR = slurry-bubble column reactor).

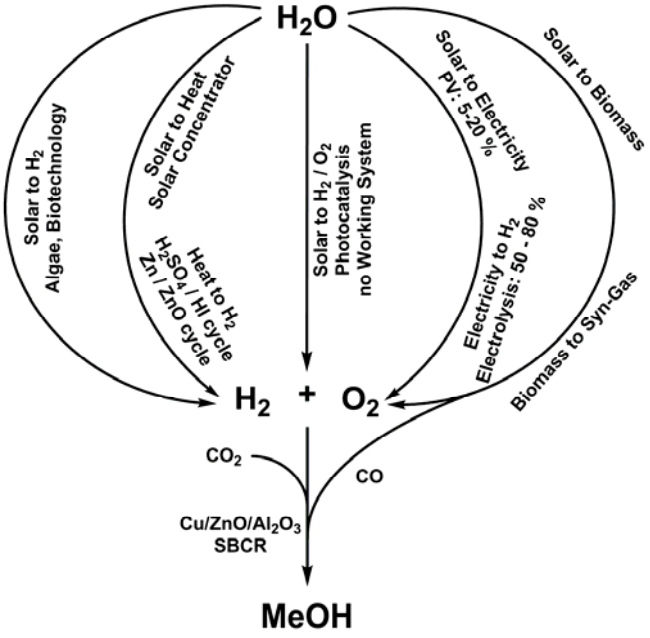

In *biological hydrogen production*, algae or bacteria are used for photocatalysis. No continuously working reactor has yet been demonstrated, and H_2 yields are very low.[6,14]

In a *solar thermal* assay, solar concentrators are used to concentrate light to give temperatures well above 1000°C. At these temperatures, besides producing electricity by well established steam engine technologies, endergonic reactions can be performed to achieve energy storage. Key advantage here is that the full solar spectrum, including the IR part, can be utilised. One example is the ZnO / Zn + O_2 cycle, where metallic zinc is obtained from the reactor, which can then by hydrolysed to give back ZnO and H_2.[15,16] Alternatively, the sulphur-iodine process, as outlined in Scheme 2, can be used to convert thermal energy in to H_2 and O_2.[17]

Scheme 2. Sulphur – Iodine process to split H_2O into H_2 and O_2 by heat.

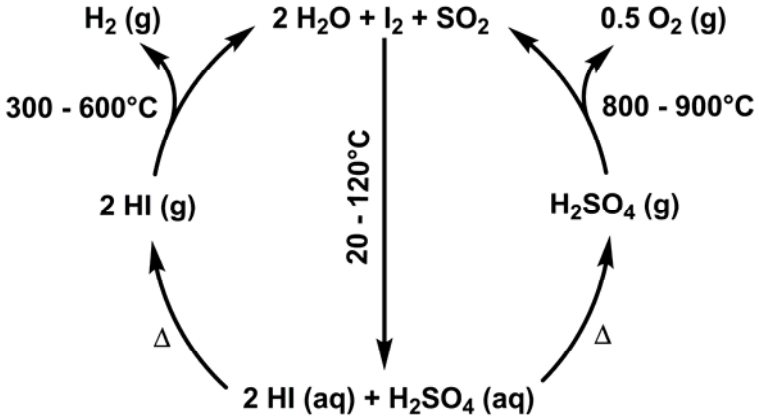

In *photocatalysis* bio-inspired, artificial chemical catalysts decompose water into H_2 and O_2 with light. Key to photocatalysis are photosensitisers (PS), to interact with light analogue to the pigments in natural photo system I & II, water oxidation catalysts (WOC) to oxidise water to O_2 and water reduction catalysts (WRC) to reduce water to H_2. A catalytic sequence is given in Scheme 3. Advantages are potentially cheap production, tuneability of absorption and efficiency. Disadvantages are potentially low turnovers, limited tuneability due to system complexity and low efficiency due to recombination. No working system has yet been presented, but research is increasing.[13,14,18-41]

Scheme 3. Photocatalysis to decompose H_2O into H_2 and O_2 by light using PS, WOC and WRC.

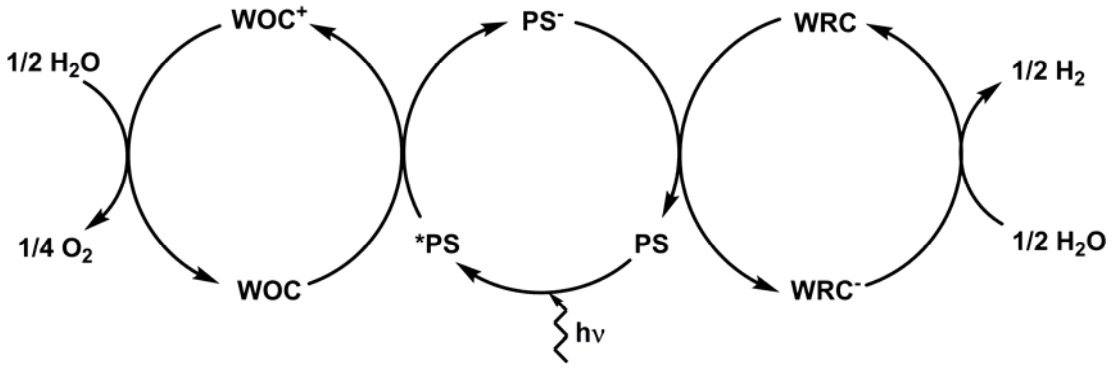

Alternatively, *sunlight* is converted *into electricity* by PV modules, solar concentrators or others, and the electricity is then used to *electrolyse* water. This approach is working with off-the-bench technology. PV modules convert

sunlight with a total efficiency of 5 – 20 % into electricity, and electrolysers convert electricity with 50 – 80 % yield into H_2 and O_2.[6,42] The advantage here is that electricity can be produced in remote, sunny areas, whereas water electrolysis can be done in areas with abundant rainwater. The disadvantage is that two processes need be coupled, thus the efficiencies for both processes need to be optimised. Up to now both PV cells and electrolysers relay on expansive materials, and PV cells are very energy intensive in production.[6,42]

An alternative approach is the use of waste *biomass* / *wood* to produce *syn-gas*, which can be reacted directly on to MeOH if the H_2 / CO ratio is correct.[9-11]

1.4 Photochemistry of Rhenium

Scheme 4. General representation of $[ReX(CO)_3diimine]^+$.

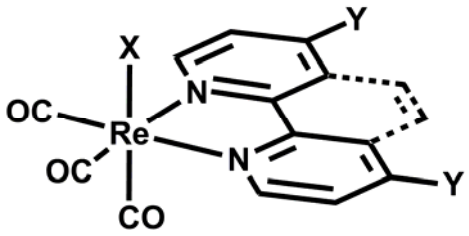

The first literature record for a rhenium tricarbonyl of the general formula $[ReX(CO)_3diimine]^+$ (see Scheme 4) appeared 1941 by H. Fuchs and W. Hieber. They synthesized $[ReX(CO)_3diimine]^+$ (X = Cl^-, Br^- and I^-; diimine = *o*-phenanthroline and $(pyridine)_2$) from $[ReX(CO)_5]$ by heating in the presence of pyridine or *o*-phenanthroline. Interesting is the observation that $[Re_2(CO)_{10}]$ reacts in a similar fashion, at even higher temperatures, to give compounds of the type $[Re(CO)_3diimine]$, which were described to be stable and most likely dimeric. It was noted that the former compounds are remarkably stable towards heat and solvents or acids. Only conc. H_2SO_4 or HNO_3 was found to decompose the compounds.[43] The first synthesis for $[ReI(CO)_3bipy]$ was reported in 1958 by G. Wilkinson and E. W. Abel.[44] First reports about $[ReX(CO)_3diimine]^+$'s excited state appeared in the 1980's by Mark Wrighton.[45-47] Remarkable at that time was that unlike for other metallo carbonyls, no CO loss occurred upon irradiation. It was anticipated correctly already in 1974 that the lowest absorption is of *d*-Re → π^*-diimine charge transfer (CT) character and that the emission occurs from a triplet state. Luminescence lifetimes, yields and triplet-triplet quenching rates were measured.[45] Later, a series of reductive and oxidative quenchers were shown to react with the excited state of $[ReX(CO)_3diimine]^+$. Quench rates were found to correlate with excited state oxidation- resp. reduction potentials.[47,48]
This allowed for real photochemistry with $[ReX(CO)_3diimine]^+$ type complexes. Examples for photochemistry in three component systems are given in section 1.6. The first such system for rhenium (two components) was established by J. Hawecker, J.-M. Lehn and R. Ziessel in 1983: visible light irradiation of a

dimethylformamide (DMF) solution containing triethanolamine (TEOA), $[ReX(CO)_3diimine]^+$ (X = Cl^- or Br^-, diimine = bipy or phen) under CO_2 atmosphere gave efficient formation of CO.[49] Whereas the initial steps of the reaction were elucidated readily,[49-52] only recently a complete picture of the system was obtained (see Scheme 5).[53-60] This has allowed the design of an optimised system for photochemical CO_2 reduction, as reported by O. Ishitani and col. in 2008, where $[Re(P(OEt)_3)(CO)_3(4,4'\text{-dimethoxy-bipy})]$ served as PS and $[Re(solv.)(CO)_3bipy]^+$ as a CO_2 reduction catalyst ($\Phi_{hv\rightarrow CO}$ = 0.59).[61]

Scheme 5. One possible pathway for catalytic CO_2 reduction by $[ReCl(CO)_3DMebipy]$, as proposed in literature.[57]

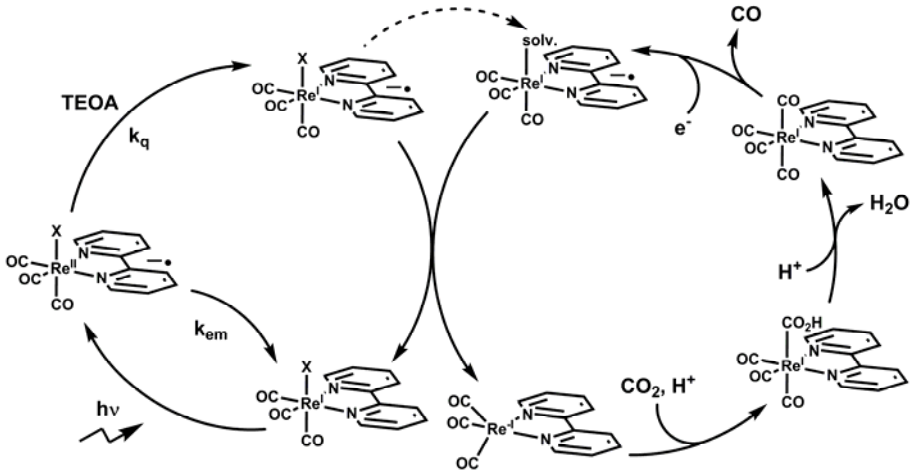

Further on the photochemistry of $[ReX(CO)_3bipy]^+$ was analysed in detail by time resolved methods,[62,63] DFT calculations[62,64] and structure activity relations.[65-67] Interesting systems were constructed which allowed the study of electron tunnelling,[68-70] electronics in hetero – dinuclear systems,[71] sigma bond homolysis[72] and so forth. All these efforts have lead to a profound understanding of the photochemistry of $[ReX(CO)_3diimine]^+$ – type complexes.

1.5 Electrochemistry of Cobaloximes

The first synthesis of a cobaloxime was presented by L. Tschugaeff in 1905, namely $[Co(NH_3)_2(dmgH)_2]^+$.[73] Already one year later, he reported on $[Co(NH_3)X(dmgH)_2]^+$ (X = NH_3, Cl^-, NO_2^-) and $[Co(NRH_2)_2(dmgH)_2]^+$ (R = H, Et), which he unambiguously identified with respect to the former compound both by the inertness of chloride towards silver(I) and by differing conductivity in water.[74] In 1907 he reported on $[Co(NH_3)X(dmgH)_2]^+$ (X = Cl^-, Br^-, I^-), $[Co(py)X(dmgH)_2]^+$ (X = Cl^- (**74**), Br^- (**73**), I^-, NCS^-, NO_2^-, NCO^-, N_3^-) and $[Co(py)Cl(R_1R_2gH)_2]^+$ (R_1 = Me, R_2 = Et).[75] In 1964 G. N. Schrauzer realised that cobaloximes were model compounds for vitamin B_{12}, namely in that they form cobalt – alkyl bonds if reacted with Grignard compounds, eg. MgXR, or if reduced to Co(I) and reacted with alkylhalogenides, alkenes or alkines.[76] He then gave a very convenient approach for the syntheses of various types of cobaloximes in 1968.[77] In the same year an interesting review on cobaloximes chemistry, including Co(I) and its reaction to Co(III)-H and finally H_2, appeared by the same author.[78] In 1971, G. N. Schrauzer gave an account on cobaloxime hydrides, and was even able to isolate one species, namely $[CoH(P(n\text{-}Bu)_3)(dmgH)_2]$, which he obtained by the reaction of $[CoCl(py)(dmgH)_2]$ with $NaBH_4$ at pH = 7 in an aqueous (50 % methanol), phosphate buffered solution. Attempts to isolate $[CoH(py)(dmgH)_2]$ failed due to its slow decomposition. Other axial bases than pyridine (imidazole, benzimidazole) gave even less stable hydrides.[79] J. H. Espenson carefully analysed the pathways for H_2 formation from hydride cobaloximes, and found both homolytic and heterolytic Co(III)-H cleavage, depending on cobaloxime hydride concentration and pH (see Scheme 6).[41] Much work focussed in the mean time on the hydrogenation of various substrates using $[Co(OH_2)_2(dmgH)_2]$ and H_2.[80-85] This research was hampered though by the tendency of the hydrides to intramolecular decomposition by hydride shift.[84] Others have used dimethylglyoxime ($dmgH_2$) for the electrochemical stripping analysis of nickel and cobalt.[86]

Scheme 6. General representation of three postulated pathways to H_2 release, eg. by homolytic (homo) or heterolytic Co^{III}-H cleavage (hetero) or by protonation and H_2 release from Co^{II}-H (Co^{II}-H).

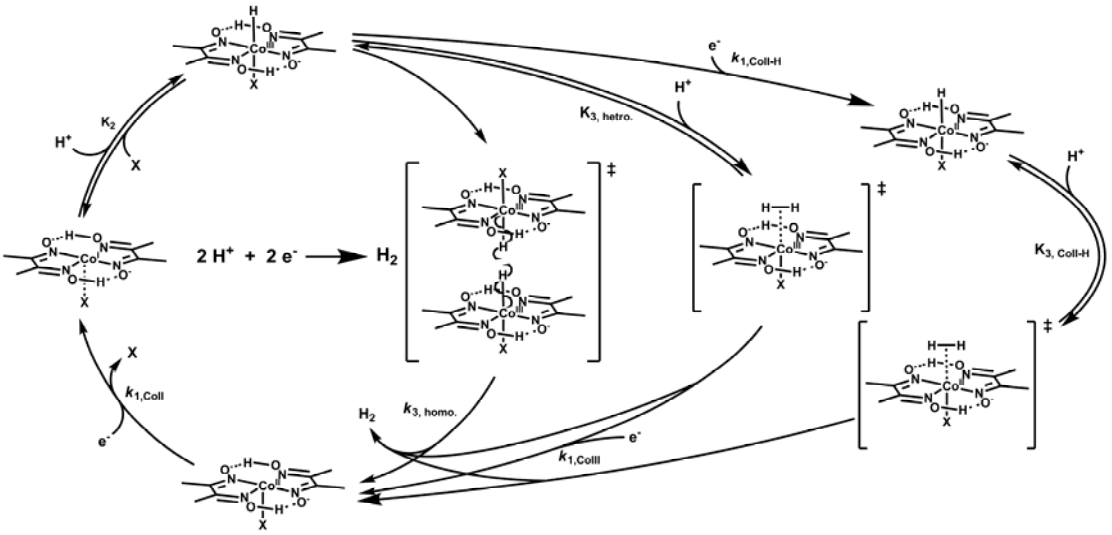

In 1983 J. Hawecker, J. M. Lehn and R. Ziessel showed consequently that [Co(dmgH)$_2$] type complexes could be employed as a WRC in a three component system (see section 1.6).[37] Starting in 2005, several interesting kinetic studies on cobaloximes appeared.[28,34,35] The key message was that, depending on the ligand framework, H_2 production proceeds by a modest to very low overpotential. However, it remained unclear if H_2 production occurred in a homolytic or heterolytic fashion, and both mechanisms seemed to be functional under certain conditions. Additionally, a mechanism referred to as Co^{II}-H pathway was postulated, involving reduction of Co^{III}-H to give a Co^{II}-H, which in turn is protonated to give Co^{II} and H_2 (see Scheme 6).[28,34] Further on, a systematic screening of the effect of the axial base on cobaloxime revealed a dramatic influence on the kinetics of H_2 release, eg. electron donating substituents increased the H_2 production rate and electron accepting substituents decreased the rate.[35]

1.6 Photocatalysis in three Component Systems

Overall water decomposition by visible light is a four electron process, and is typically thought to require three sophisticated catalysts, namely one for water oxidation (WOC), water reduction (WRC) and one for visible light absorption (PS), as in Scheme 3. Usually the system is then divided into a reductive and oxidative halfreaction, respectively, which can be studied independently. A three component system for photocatalysis thus consists of an irreversible electron donor / acceptor (D resp. A), a photosensitzer (PS) and a water reduction / oxidation catalyst (WRC resp. WOC), as outlined in Scheme 7 for one such case. Four general schemes are possible:

- reductive quenching of *PS by D to yield H_2
- oxidative quenching of *PS by WRC to yield H_2
- reductive quenching of *PS by WOC to yield O_2
- oxidative quenching of *PS by A to yield O_2

Scheme 7. One example for photocatalysis in a three component system, proceeding by reductive quenching of *PS by D to yield H_2.

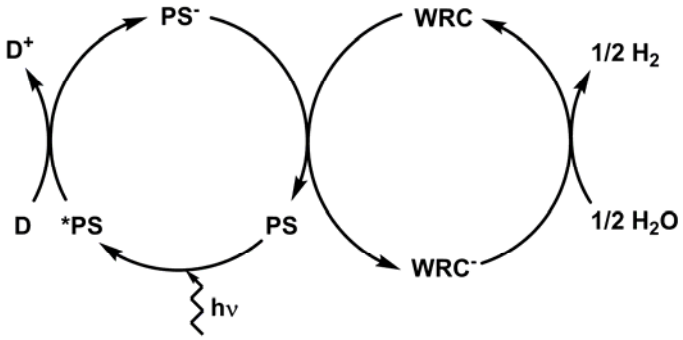

These four systems differ in that they produce H_2 or O_2 and proceed by reductive or oxidative interaction with *PS. Surely for proton reduction to H_2, the pathway via reductive quenching of *PS by D is simpler as compared to oxidative quenching of *PS by WRC. This is because the concentration of D is usually much higher than the concentration of WRC, thus allowing faster reaction at identical rates. The former pathway produces PS^{-}, which in turn reduces WRC, whilst the latter pathway produces PS^{+}, which then oxidizes D

in turn. In the former pathway, D needs to reductively quench *PS, whilst in the latter pathway only a simple reduction of PS^+ by D is required. So the former pathway requires PS^- to be stable and D to react efficiently with *PS, whilst the latter requires WRC to react efficiently with *PS and PS^+ to be stable. If considering a full water decomposition cycle (see Scheme 3), two scenarios can result: reductive quenching of *PS by WOC (as shown in Scheme 3) or oxidative quenching of *PS by WRC. The latter might be more realistic, especially when considering that the overall water decomposition is a four electron process, thus requiring the accumulation of four electron holes on WOC resp. two electrons on WRC. In the former case WOC has to interact with *PS four times before one molecule of O_2 could be produced, whilst WRC would 'only' have to strip off two electrons.

Up to date there is no example for a full water decomposition cycle in homogenous solution with visible light. Several examples using heterogeneous materials and UV light appeared,[87-89] although some of the results could not be reproduced by others.[89,90]

There are only two examples of homogenous systems for water oxidation; both of them appeared within the last year. Interestingly both of them make use of ruthenium complexes as WOC and use the well known $[Ru(bipy)_3]^{2+}$ as PS. The electron acceptor is $[Co(NH_3)Cl]^{2+}$ or $S_2O_8^{2-}$.[24,26] Besides ruthenium compounds[36,91-95] based on T. J. Meyers blue dimer,[96] also iridium complexes of the type $[Ir(ppy)_2(OH_2)_2]^+$,[97] cobalt[18] or ruthenium[98-100] polyoxometalates (POM's) and manganese compounds[101,102] are known as WOC's in homogenous solution. Apart from that, many heterogeneous WOC's are known, including titanium,[88,103] ruthenium,[104,105] iridium,[105] cobalt,[105,106] manganese[105,107] and iron[108] oxides. In one case, as in PS II, calcinated manganese oxides were shown to produce O_2 photochemically.[107]

On the reductive side, much more examples for three component systems in homogenous solution to reduce protons to H_2 exist. The first example appeared in 1979 by N. Sutin and colleagues. $[Ru(bipy)_3]^{2+}$ served as an PS, $[Co^{II}(Me_6[14]dieneN_4)(H_2O)_2]^{2+}$ as WRC, europium(II) or ascorbate served as electron donors and the system was run in buffered aqueous solution.[109] Later on, they report on the same system using $[Co(bipy)_n]^x$ as WRC.[38,39,110] In 1983, R. Ziessel and colleagues reported on a similar system using

$[Ru(bipy)_3]^{2+}$ as PS, in-situ prepared $[Co(dmgH)_2]$ as WRC and TEOA as electron donor in DMF.[37] Besides these work in homogenous solutions, many systems using $[Ru(bipy)_3]^{2+}$ as PS, $[M(bipy)_3]^x$ (M = Rh or Co) or MV^{2+} as electron relay and TEOA, Eu^{2+}, $EDTA^{2+}$, ascorbate etc. as electron donor and colloidal Pt or Pd as WRC were presented.[40,111-118] In 1997, N. Sutin, C. Creutz and E. Fujita give a comprehensive review of literature up to that date.[58]

Starting in 2005, a series of new system for proton reduction by visible light appeared, following in essence the same principles as in the 1980thies, namely using three component systems. Remarkable high turnovers in PS (up to 5000) were obtained by S. Bernhard's group using $[Ir(ppy)_2bipy]^+$ – type PS's.[33,119] One year later several investigations using supramolecular architectures of a $[Ru(bipy)_3]^{2+}$ type PS covalently linked to a Pt, Pd or Rh WRC centre appeared,[120-122] but the homogenous character of these systems was put in question.[123] In 2008 a bio-inspired system using $[Ru(bipy)_3]^{2+}$ as PS, Fe – only hydrogenase mimics as WRC and ascorbic acid as electron donor in MeCN / H_2O mixtures appeared, although turnover numbers in WRC did not exceed 5 and in PS did not exceed 100.[124] A similar system published in 2010 using also a Fe – only hydrogenase mimic achieved a TON of 200.[19] On the other hand a system published in 2009 using conventional $[Fe_3(CO)_{12}]$ along with an iridium based PS achieved up to 300 TON's in WRC.[25] Also in 2008 appeared a work by M. Fontecave and colleagues, using ruthenium and iridium supramolecular assemblies, which were linked to a cobaloxime WRC. TON's were below 300, and the three component system with $[ReBr(CO)_3phen]$ PS and the cobaloxime based WRC was superior to the supramolecular assemblies.[29,30] The group of R. Eisenberg presented several systems using a new PS of the [Pt(ttpy)(acetylide)] – type along with cobaloxime based WRC's and TEOA as electron donor in MeCN / H_2O mixtures. Respective turnovers of 2150 were obtained with high [TEOA] and little H_2O in MeCN.[27,31] In 2009 the same group presented a system using xanthine type PS under otherwise identical conditions.[23] Our own work uses $[ReX(CO)_3diimine]^+$ – type PS, cobaloxime or related WRC's and TEOA as an electron donor in DMF (more than 7000 TON's in PS, more than 1000 in WRC)[20,21] or H_2O (up to 200 TON's in PS, 16 in WRC).[125]

2 Results and Discussion

This section will first give a brief overview of the general aspects in syntheses of rhenium tricarbonyl diimine type complexes ($[ReX(CO)_3diimine]^+$), cobaloximes ($[CoY_2(dmgH)_2]$) and respective diimine ligands (2.1). Then a characterisation of the chemistry and spectroscopic properties of the rhenium (2.2) and the cobalt (2.3) complexes follows. In sections 2.4, 2.5, 2.6 and 2.7 examples for photocatalysis in a three component system for H_2 production are given. Section 2.4 describes a system in DMF using $[ReBr(CO)_3bipy]$ as photosensitiser (PS) along with $[Co^{II}(dmgH)_2]$ as water reduction catalyst (WRC) and gives an insight in the kinetics of the cycle. Section 2.5 describes a system in DMF using $[ReNCS(CO)_3bipy]$ as PS, $[Co^{II}(dmgH)_2]$ as WRC and gives insights into long-term stability of the cycle. Section 2.6 describes the first such system in H_2O using $[Re(py)(CO)_3bipy]^+$ and derivatives as PS and $[Co^{III}(py)_2(dmgH)_2]^+$ and derivatives as WRC. Section 2.7 gives an insight about the solvent effects in H_2 production using $[ReX(CO)_3diimine]^+$ and cobalt-tetraene type complexes.

2.1 Syntheses

2.1.1 General approach to $[ReX(CO)_3diimine]^+$ – type complexes

Scheme 8. Syntheses of $[ReX(CO)_3diimine]^+$ complexes from $[Re_2(CO)_{10}]$.

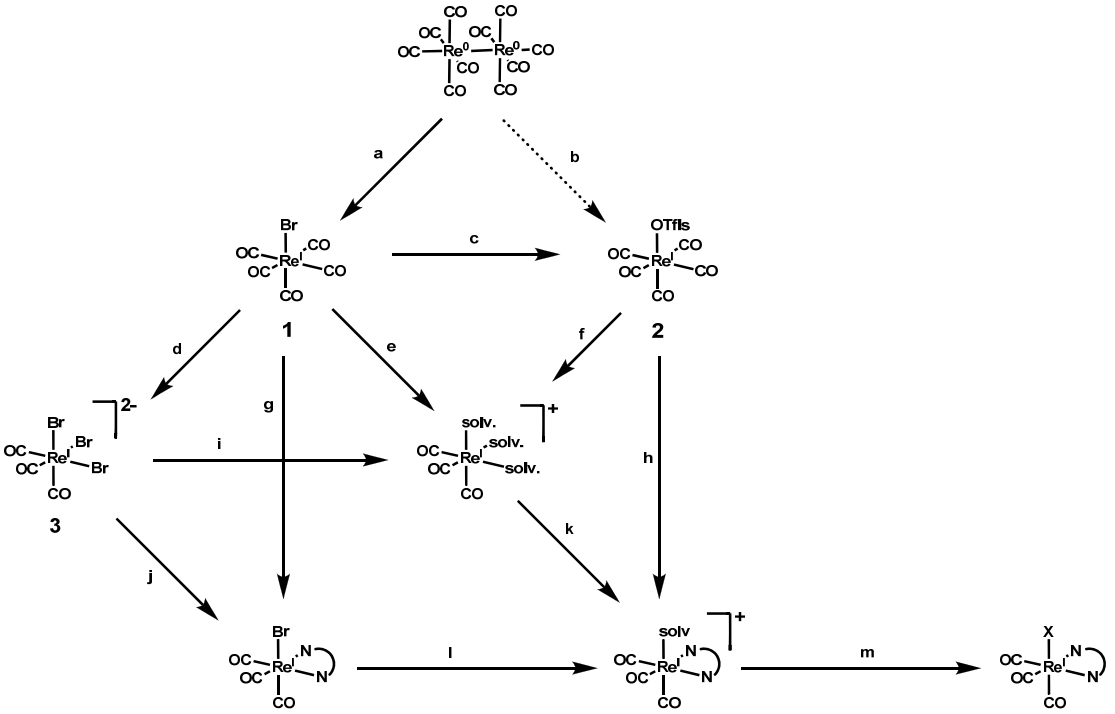

$[ReX(CO)_3diimine]^+$ – type complexes in this work were obtained by different routes, depending on the axial ligands (neutral or anionic / strong or weak binders) and the diimines used (neutral or ionic), as illustrated in Scheme 8. The most versatile intermediate is $[ReBr(CO)_5]$ (**1**), which is easily obtained from $[Re_2(CO)_{10}]$ (route a)[126] and is quantitatively converted to $[ReBr(CO)_3diimine]$ by route g (see Scheme 11). Replacement of axial bromide is achieved by reaction with silver salts (route l, Scheme 13), followed by substitution (route m, Scheme 14). Alternatively, axial bromide is removed on the $\{Re(CO)_5\}$ – core already (route c, Scheme 9) to obtain $[Re(OTfls)(CO)_5]$ (**2**), which is then readily converted in one pot via $[Re(CO)_3(solv.)_3]^+$ to $[Re(solv.)(CO)_3diimine]OTfls$ (route f and k resp. h, Scheme 10).

The 'classical' approach via $[ReBr_3(CO)_3](Et_4N)_2$ (**3**, route d, i and j), although a nice precursor, was found to be inconvenient for most syntheses in this work either because of additional reaction steps needed to obtain $[ReBr(CO)_3$diimine] (neutral diimines) or because $[Et_4N]^+$ salts were hard to remove after reaction with ionic diimines. As for the direct reaction of **1** to $[Re(solv.)_3(CO)_3]Br$ (route e),[127] apart from the long reaction time (1 day), bromide was still present as an anion and disturbed in the following steps (routes k, m), where explicitly weakly coordinating, innocent anions were wanted.

Since the use of silver salts might be problematic later on (photochemistry, small impurities might disturb) alternative routes circumventing the use of silver were searched. Several trials to prepare **2** directly from $[Re_2(CO)_{10}]$ (route b) by use of acid or the respective anhydrides failed. Possibly the known reduction of $[Re_2(CO)_{10}]$ to $Na[Re(CO)_5]$ by sodium amalgam[128] and subsequent reaction with acids (eg. TflsOH) might be more successful.

Scheme 9. Synthesis of $[Re(OTfls)(CO)_5]$ from $[ReBr(CO)_5]$.

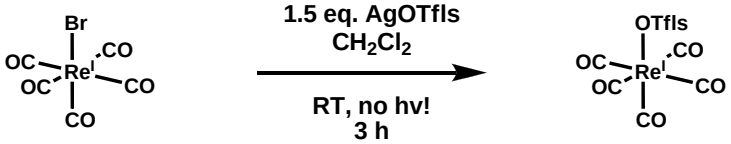

1 **2**

Route c. The reaction of **1** with AgOTfls was first described by Trogler and colleagues[129] and yields the corresponding pentacarbonyl-rhenium(I)-trifluoromethansulfonato complex **2** in good yields by recrystallisation (Scheme 9). The compound is described as light stable, but was found to be slightly hygroscopic, thus prohibiting storage of excessive amounts. Additional column chromatography might be useful to assure complete removal of silver.

Scheme 10. Reaction of $[Re(OTfls)(CO)_5]$ with diimine to give $[Re(solv)(CO)_3$diimine]OTfls.

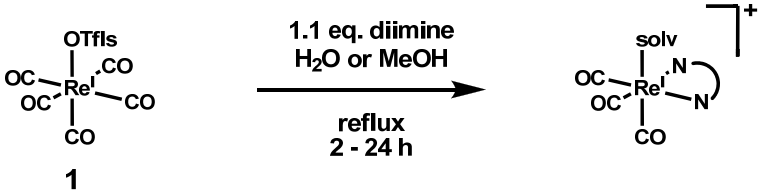

1

Route h. **2** readily dissolves in polar solvents such as MeOH or H_2O, possibly by formation of $[Re(solv.)_3(CO)_3]^+$ (route f) and reacts with diimines to give the corresponding $[Re(solv.)(CO)_3diimine]^+$ complexes as a trifluoromethansulfonato salt in quantitative yields upon removal of solvent and washings to remove excess diimine (route k resp. h, Scheme 10). The advantage of this route versus route e / k is that no bromide is present from the beginning and that removal of solvent / lyophilisation directly yields the pure product with no need to remove tetraethylammonium salts, a problem often encountered in route i / k. This route was though preferred if the diimine ligand was ionic or did not react in route g (compound **53**). If necessary, $[Re(solv.)(CO)_3diimine]OTfls$ was then applied to column chromatography (AlO_3, CH_2Cl_2) to completely remove silver salts. The compounds readily exchanged coordinated solvent (MeOH or H_2O) to $OTfls^-$, which can be replaced by solvent again by refluxing in the appropriate solvent.

Scheme 11. Conversion of $[ReBr(CO)_5]$ to $[ReBr(CO)_3diimine]$.

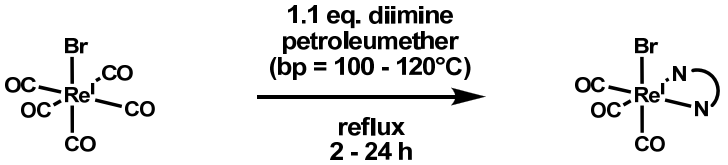

1

Route g. This reaction was found to be applicable to most of the diimines studied here, eg. for bipy, phen and $DMeCO_2bipy$, giving complexes **10** (see Figure 6), **30** and **60**.

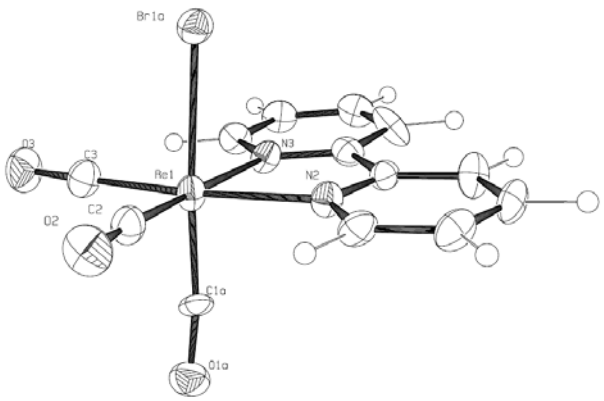

Figure 6. ORTEP drawing of **10** (bp070607) at 50 % probability level.

Refluxing a suspension of **1** with the appropriate diimine in high boiling solvents leads to [$ReBr(CO)_3$diimine] in quantitative yields after washing with hexane / MTBE (see Scheme 11). The reaction is best monitored by IR spectroscopy, as a characteristic shift from {$Re(CO)_5$} to {$Re(CO)_3$} occurs (see Figure 7). Reaction times vary depending on the diimine used. For this work petroleum benzine (boiling range = 100 – 120 °C) gave best results, as it can be removed easily by washing with hexane / MTBE. The reaction works as well in toluene, but removal was found to be more cumbersome, possibly due to staking interaction with the product. Most likely aromatic components in the solvent used play a crucial rule for activating the {$Re(CO)_5$} core, possibly by a [η^6-arene-$Re(CO)_3$]$^+$ intermediate.

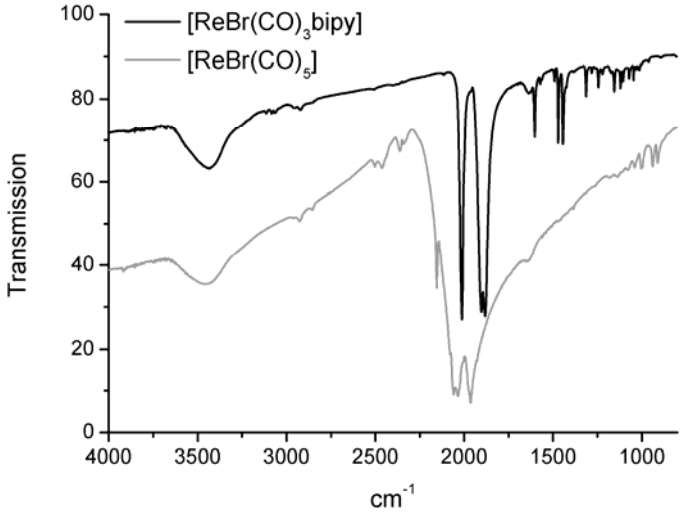

Figure 7. FT-IR spectra of [$ReBr(CO)_3$bipy] and [$ReBr(CO)_5$] (KBr pellet).

Scheme 12. Complexation of **3** by diimine to give [$ReBr(CO)_3$diimine].

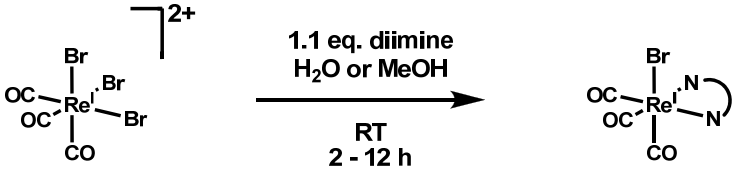

3

Route j. Usually reaction of diimines with [$ReBr_3(CO)_3$](Et_4N)$_2$ in MeOH or other polar solvents was rapid (Scheme 12). If the educts were dissolved before the reaction and provided that diimine was a neutral molecule, it often led to a precipitate of the product, which could then be removed by filtration and subsequent washings. If the diimine was ionic or led to otherwise well soluble products, separation was more difficult, especially because of the

tetraethylammonium salts present in the solution. This route was chosen for complexes **40**, **41**, **42**, **50** and **53**.

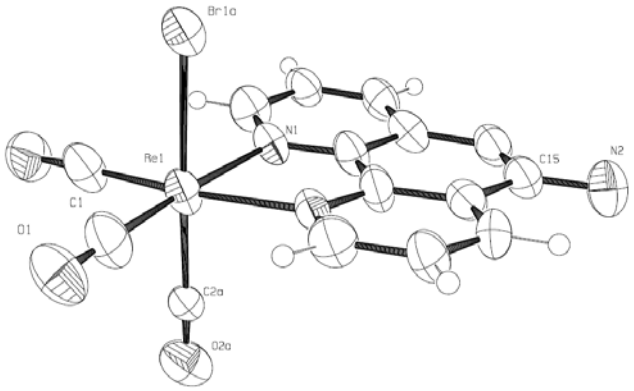

Figure 8. ORTEP drawing of **40** (bp100706) at 50 % probability level.

[ReBr(CO)$_3$phenNH$_2$] (**40**, see Figure 8) could be obtained in pure form after filtration of the methanolic reaction solution. Compounds [ReBr(CO)$_3$pAp] (**41**) and [ReBr(CO)$_3$pAmp] (**42**) were applied to column chromatography after reaction, as impurities accumulated in the product, possibly by the partial coordination of the pendant isonicotinyl – moiety.

Scheme 13. Removal of axial bromide by silver precipitation.

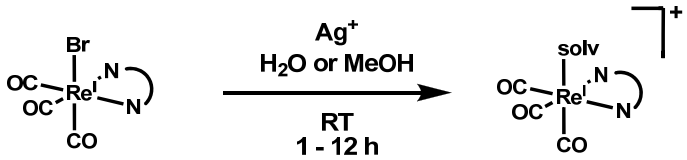

Route I. Removal of bromide from [ReBr(CO)$_3$diimine] by reaction with AgOTfls gave best results for this study. Other silver salts were tested, but OTfls$^-$ was found to be a nice compromise between a non-coordinating anion, water solubility of the products and ease in handling of the respective silver salt (hygroscopicity). If eg. $AgNO_3$ was used instead, and diimine was 2,2'-bipyridine, [Re(ONO$_2$)(CO)$_3$bipy] (**20**) was formed (see Figure 9) instead of the respective solvato complex, and replacement of NO_3^- was rather difficult

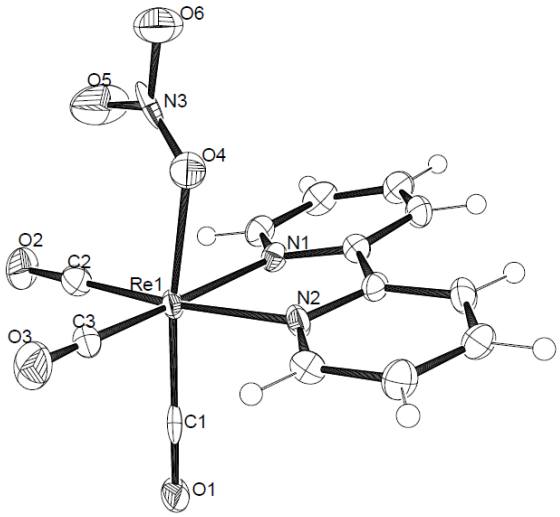

Figure 9. ORTEP drawing of **20** (bp030609) at 50 % probability level.

Even if the reaction according to route I was run stoichiometrically, and AgBr was removed quantitatively, minor impurities of silver were found to remain, which in some cases influenced the outcome of photochemical studies. [Re(solv.)$(CO)_3$diimine]OTfls was thus applied to column chromatography (AlO_3, CH_2Cl_2, MeOH) to remove traces of Ag^+. After column the axial solvent was replaced by $OTfls^-$, which could be reversed by refluxing the product in water or MeOH, where complete conversion to the solvate complex was observed. Coordinated OH_2 resp. MeOH can be observed in the ^{1}H-NMR in DMSO. Actually a 1 to 1 equilibrium between the aquo- and solvato-complex was observed, as shown in Figure 10 for the 2,2'-bipyridine analogue, but as observed for all diimines in this study.

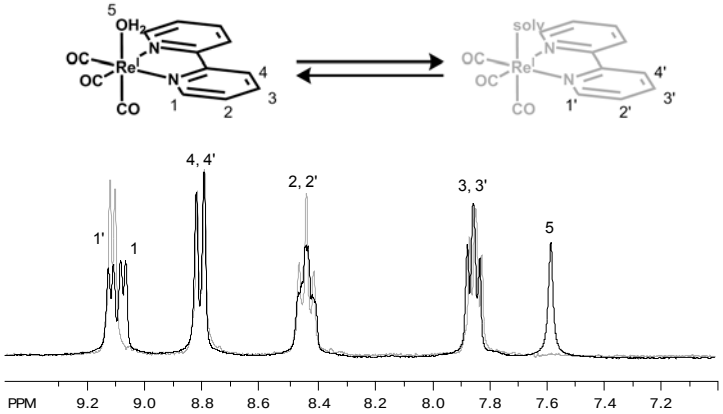

Figure 10. Aromatic region in ^{1}H-NMR spectra of [Re(OH$_2$)(CO)$_3$bipy]OTfls (**11**, black) as opposed to [Re(OTfls)(CO)$_3$bipy] (grey) in d^6-DMSO, 300 MHz.

A demonstration of the weak binding of OH_2 to [Re(OH$_2$)(CO)$_3$diimine]$^+$ was obtained by growing x-ray quality crystals by vapour diffusion of a saturated solution of **31** in CH_2Cl_2 versus pentane. As shown in Figure 11, axial OH_2 was replaced by OTfls$^-$.

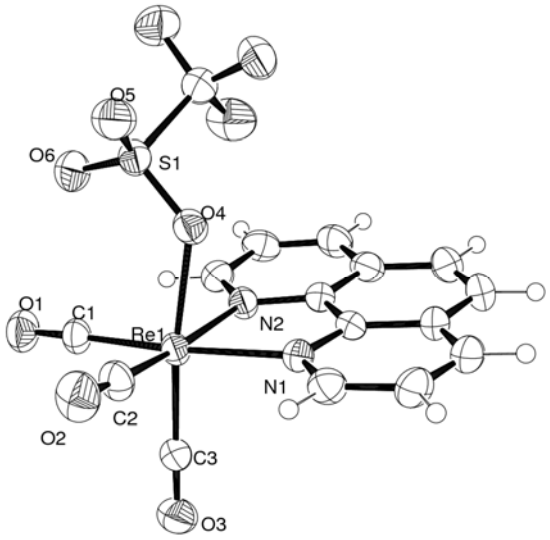

Figure 11. ORTEP drawing of **31** (bp221209) at 50 % probability level.

If, par contra, crystals were grown from a saturated aqueous solution (in this case for **11**), axial water remains in place, as shown in Figure 12.

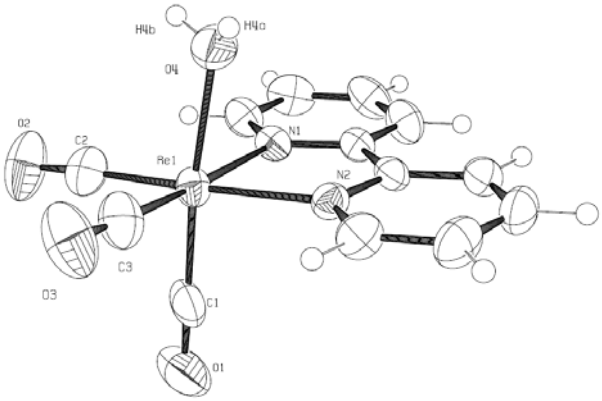

Figure 12. ORTEP drawing of **11** (bp061109) at 50 % probability level, $OTfls^-$ is omitted for clarity.

Scheme 14. General scheme for the synthesis of $[ReX(CO)_3diimine]^+$.

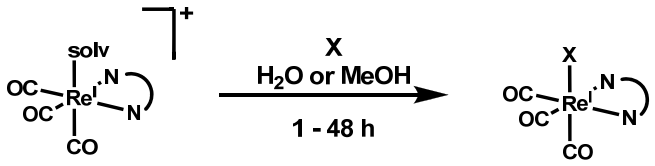

Route m. $[Re(solv.)(CO)_3diimine]OTfls$ was the most versatile precursor for the syntheses of $[ReX(CO)_3diimine]^+$ – type complexes, where X could be a neutral or anionic, monodentate ligand. HPLC analysis of the reaction progress was found to be very helpful in determining the reaction time or if excess of the axial ligand and / or heating was required. For anionic axial ligands the product could be obtained by filtration in a classical in phase – out of phase reaction, followed by washing (compounds **12**, **17**-**22**, **32** and **52**). If X was a neutral ligand, isolation was usually achieved by evaporation of the polar solvent and washing in an apolar solvent such as MTBE (compounds **13**-**16**, **33**-**35**, **62** and **65**).

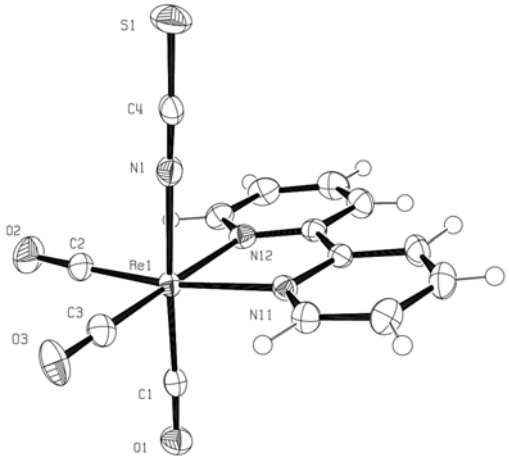

Figure 13. ORTEP drawing of **12** (bp160909) at 50 % probability level.

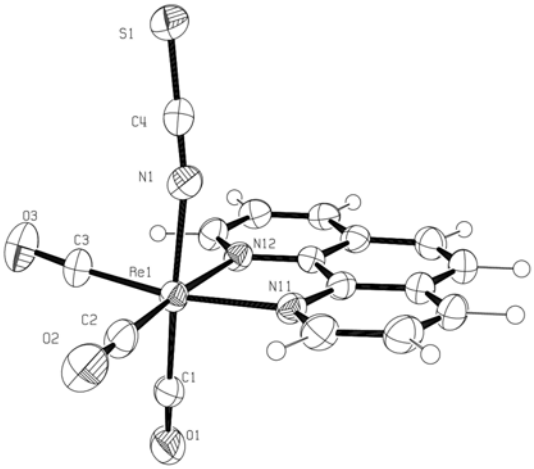

Figure 14. ORTEP drawing of **32** (bp120110) at 50 % probability level.

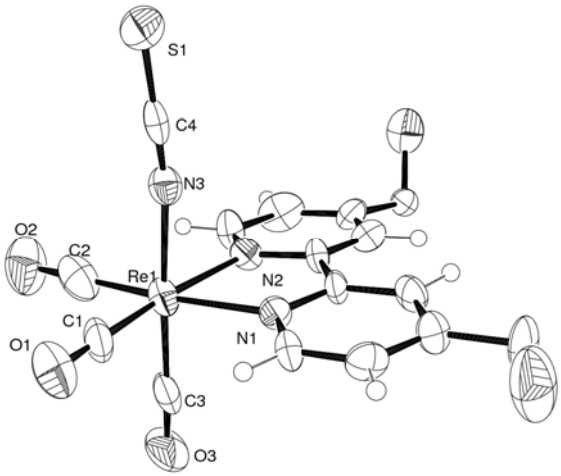

Figure 15. ORTEP drawing of **52** (bp171108) at 50 % probability level.

Of special interest are the syntheses of complexes **12**, **32**, **52** and **55** incorporating the thiocyanate motive (see Figure 13 to Figure 15). It usually only required a small excess (max. 10 equivalents) of NaNCS and, even at room temperature, led to a fast precipitation of a corresponding product (except for the di-cationic compound **55**). It was found though that first a kinetic product, most likely of the form [Re(SCN)(CO)$_3$diimine], was formed in equilibrium with a corresponding thermodynamic product [Re(NCS)(CO)$_3$diimine]. The two products could be differentiated by HPLC and ^{1}H-NMR (see Figure 16 and Figure 17). If the reaction mixture was refluxed for ~3 h complete conversion to the Re-NCS compound was usually observed. As reaction times might vary, checking by eg. HPLC was required.

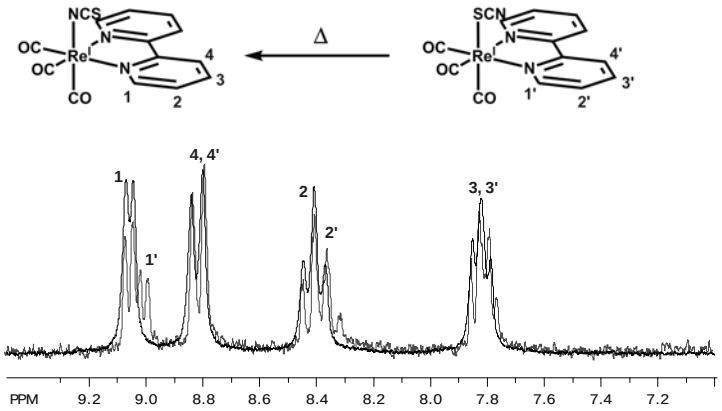

Figure 16. ^{1}H-NMR of **12** before (grey) and after (black) heating (d^6-DMSO, aromatic region shown only).

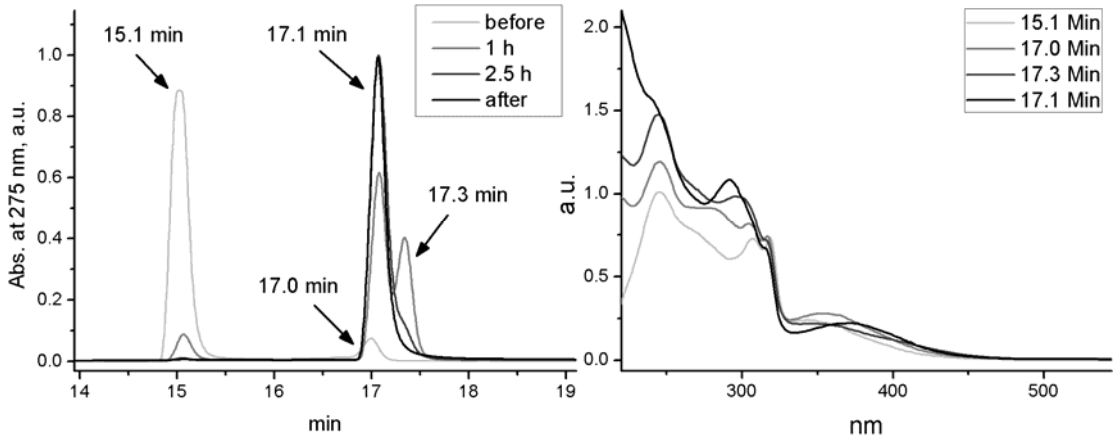

Figure 17. Left: HPLC traces for the reaction to [ReNCS(CO)$_3$bipy] (**12**) according to route m (before heating, 1 resp. 2.5 h of heating and after complete formation; peaks at 15.1 and 17.0 min are typical for [Re(solv)(CO)$_3$bipy]$^+$, at 17.1 min for the product **12** and at 17.3 min for the

hypothetical [ReSCN(CO)$_3$bipy]). Right: Spectra of the species at respective retention times, absorbance is set to arbitrary units for comparison).

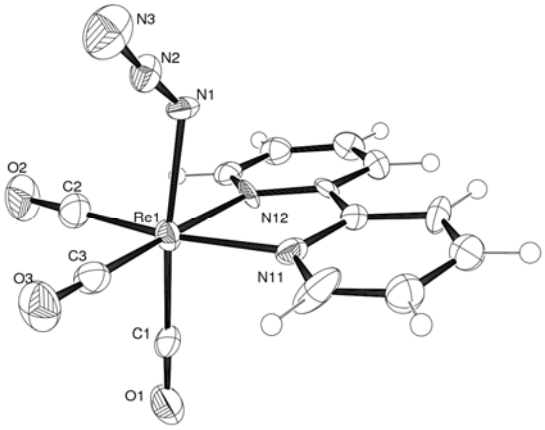

Figure 18. ORTEP drawing of **18** (bp070110) at 50 % probability level.

The reaction of **11** with NaN_3 in H_2O was straightforward and gave **18** after filtration. Crystals of x-ray quality could be obtained by vapour diffusion of **18** in CH_2Cl_2 versus pentane (see Figure 18). It is, however, interesting to note the tilted binding mode of N_3^- (Figure 18, Re1-N1-N2 = 127°) versus NCS^- (eg. **12**, Figure 13, Re1-N1-C4 = 175°), although N_3^- and NCS^- are iso-electronic. Surely this difference arises from the fact that in N_3^- double bonds are preferred as compared to NCS^-, where a triple bond between nitrogen and carbon and a single bond between carbon an sulphur are preferred, due to bad overlap of the respective π – orbitals.

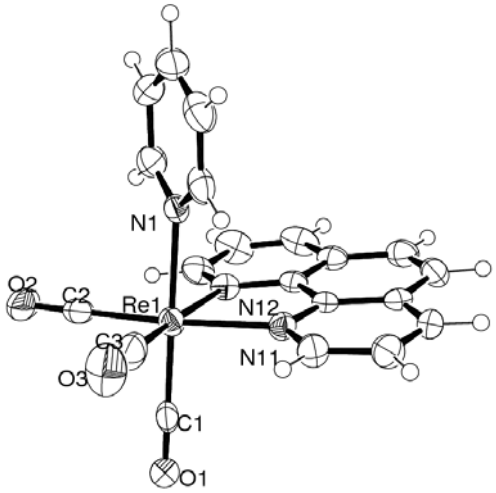

Figure 19. ORTEP drawing of **33** (bp230909) at 50 % probability level, $TflsO^-$ and solvent molecules are omitted for clarity.

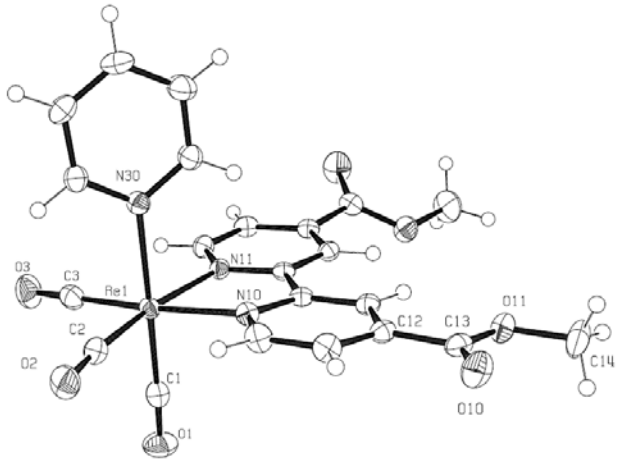

Figure 20. ORTEP drawing of **62** (bp090610) at 50 % probability level, $TflsO^-$ molecules are omitted for clarity.

The syntheses of complexes containing the pyridine motive, $[Re(py)(CO)_3diimine]^+$ (see eg. Figure 19 and Figure 20), was straight forward, but heating or an excess of pyridine was required. Water solubility of complexes **13** and **33** was, after gentle heating, maximal 2 mM. Complexes **62** and **65** dissolved by simple stirring 2 mM in H_2O and might dissolve in even higher concentration. The former two complexes do not show any sign of instability under thermal treatment or light exposure, whilst the latter two tend to hydrolyse on the methylester resp. dimethylamide moiety if heated in H_2O.

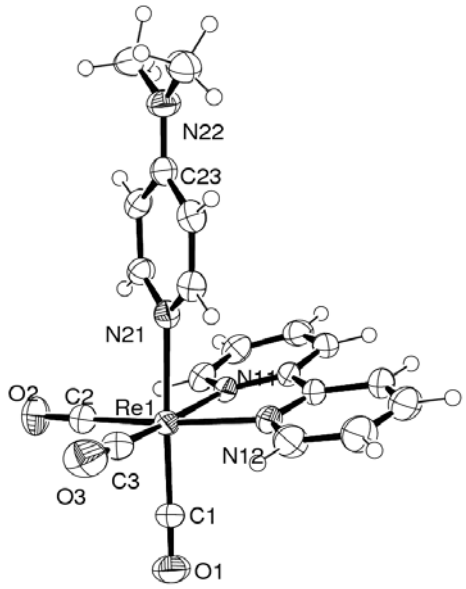

Figure 21. ORTEP drawing of **14** (bp151209) at 50 % probability level, $TflsO^-$ and solvent molecules are omitted for clarity.

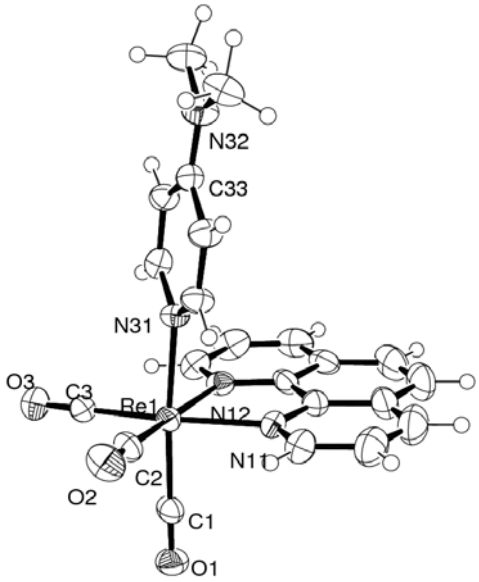

Figure 22. ORTEP drawing of **34** (bp210410) at 50 % probability level, $TflsO^-$ is omitted for clarity.

The 4-dimethylaminopyridine analogues **14** and **34** form readily, although reaction times were usually longer for these compounds as compared to the respective pyridine analogues. Also, if 4-dimethylaminopyridine was added to the aquo-precursor, an immediate colour change to orange – red occurred, although HPLC clearly indicated that the reaction did not yet take place. This colour change was thus ascribed to a kinetic product, presumably to an amine bound species, which would be stabilized by $\pi - \pi$ stacking, thus giving rise to

the red shift in absorption. This hypothesis was not further pursued, since heating allowed the formation of the thermodynamic product in most cases (see Figure 21 and Figure 22). The reaction with 4-dimethylaminopyridine was also tried in the case of [Re(OH_2)($CO)_3$DMeCO_2bipy](TflsO) (**61**) and [Re(OH_2)($CO)_3$DMe_2NCObipy](TflsO) (**64**), since the products were expected to absorb to higher wavelengths, a property sought for in photocatalysis. This hypothesis could be confirmed by HPLC / PDA of the reaction mixtures, but isolation of the products was not successful. In these cases the prolonged heating required for complete reaction caused hydrolysis of the ester resp. amide bonds. Solubility of **14** and **34** was low, and after heating a maximum of 500 µM was obtained. The complexes did not show any sign of instability neither by thermal treatment nor by exposure to light in H_2O.

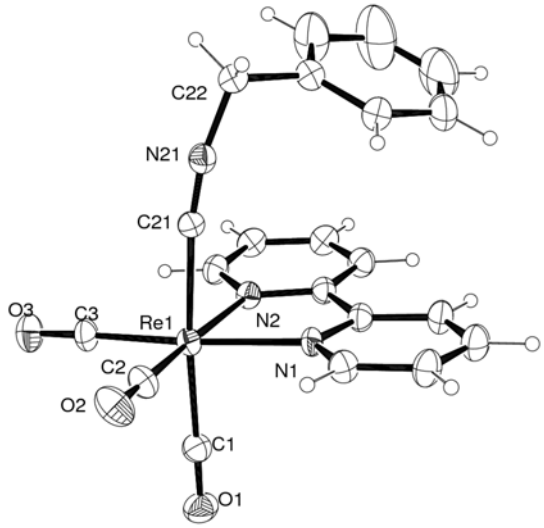

Figure 23. ORTEP drawing of **15** (bp280510) at 50 % probability level, $TflsO^-$ is omitted for clarity.

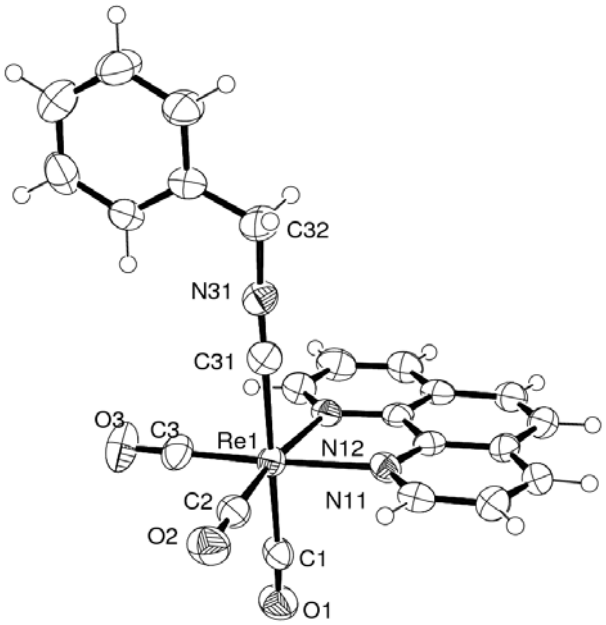

Figure 24. ORTEP drawing of **35** (bp031209) at 50 % probability level, $OTfls^-$ is omitted for clarity.

For the benzonitrile complexes (**15** and **35**, see Figure 23 and Figure 24) reaction occurred much faster and no heating was required. These complexes showed low water solubility, and only after heating solutions of maximum 500 µM could be obtained. The complexes were stable towards thermal treatment and light in H_2O. Solutions of **35** showed some decomposition when exposed to light in DMF.

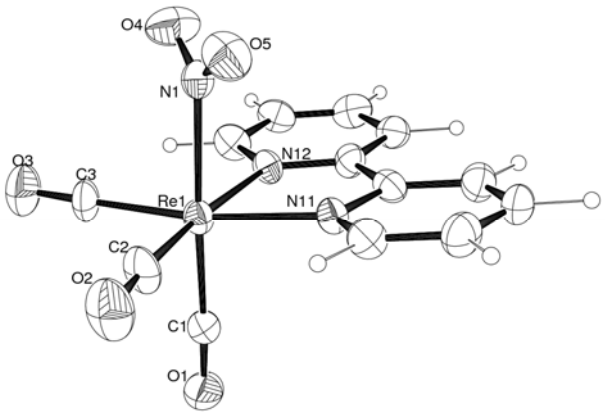

Figure 25. ORTEP drawing of **19** (bp271109) at 30 % probability level.

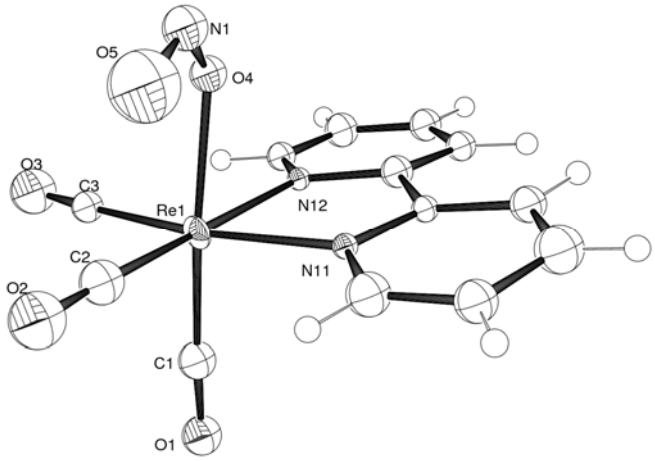

Figure 26. ORTEP drawing of **19** (bp081209_twin) at 50 % probability level.

The reaction of **11** and 5 eq. $NaNO_2$ was carried out in H_2O. It was found to proceed quite fast by HPLC in the first 2 h at room temperature, and an immediate formation of precipitate occurred. If the mixture was stirred for an additional 24 h, the product peak did not increase significantly (about 90 % conversion). Refluxing for 5 h did not bring about a major increase, and even if the precipitate was filtered and washed with H_2O, HPLC still showed 90 % product and 10 % educt. According to ^{1}H-NMR in DMSO there was a 3:4 ratio between two species, and none of them was an aquo- or solvato- complex, nor could any $TflsO^{-}$ from the educt be detected by ^{19}F-NMR. Elemental analysis was perfect. This all indicated that two products in equilibrium were present, eg. a Re-NO_2 and a Re-ONO species. This hypothesis could be confirmed by X-ray crystallography (Figure 25 and Figure 26). Interestingly enough, the equilibrium observed in DMSO was not the same as in HPLC (H_2O, 10 % MeOH, 0.1 % TFA). Possibly a proton catalysed isomerisation is taking place under these conditions, deserving to be explored in more detail.

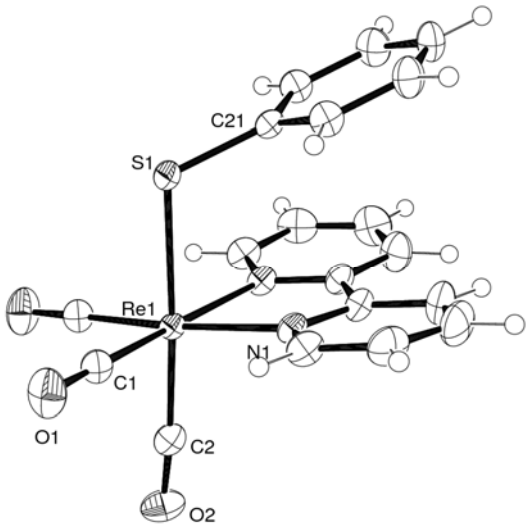

Figure 27. ORTEP drawing of **17** (bp180509) at 50 % probability level.

The reaction of **11** with thiols was examined by using either MeSH or PhSH with K_2CO_3 as a base in H_2O, MeOH or CH_2Cl_2. Where as repeated attempts with MeSH failed to produce a species stable enough to be detected by ^{1}H-NMR or HPLC, the latter reaction run to completion without major problems in H_2O and gave rise to a stable, reddish product. Under HPLC conditions 5 % solvate complex could still be detected, indicating an equilibrium between **17** and **11** under acidic conditions. In DMSO only one species was observed. X-ray analysis showed significant $\pi - \pi$ stacking between 2,2'-bipyridine and the thiophenol moiety (r = 3.6 ± 0.2 Å), thus explaining the reddish colour and the increased stability of **17** as compared to the MeSH analogue.

Only few derivatization reactions on diimines coordinated to rhenium were successful. For **41** the reaction with isonicotinylchloride was tried in several assays, but without satisfactory results. Compound **43** was prepared by reaction of **40** and isonicotinylaldehyde in dry THF, and crystals of x-ray quality were obtained directly from the reaction (see Figure 28). All attempts for further analysis were hampered by the high tendency of **43** to hydrolyse on the imine moiety, thus yielding **40** and isonicotinylaldehyde.

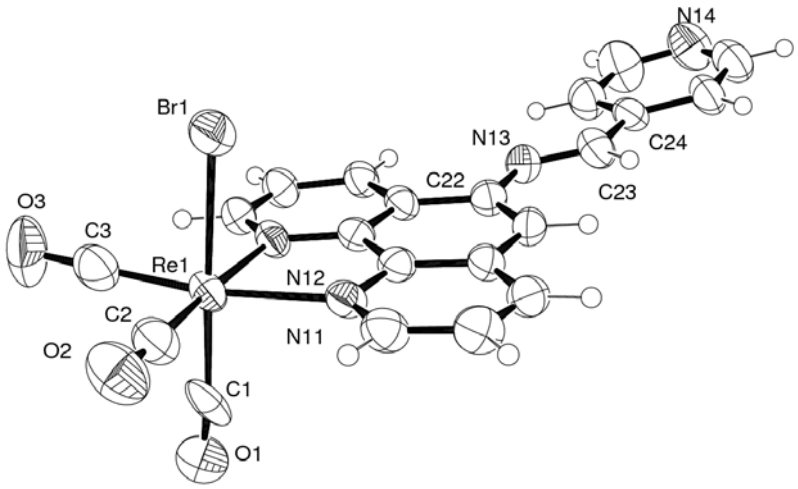

Figure 28. ORTEP drawing of **43** (bp050906) at 50 % probability level.

An interesting observation was made for compound **60**: it formed from a solution of unreacted DH_2NCObipy and **3** in conc. H_2SO_4 and MeOH. **63**, on the other hand, was obtained by the reaction of **60** with Me_2NH in MeOH.

2.1.2 General approach to cobaloximes

A very general approach to various types of cobaloximes is given in the account of G. N. Schrauzer in Inorganic Syntheses.[77] Generally, cobalt(II) salts are mixed in a 1:2 ratio with dimethylglyoxime ($dmgH_2$) under an inert atmosphere in the presence of the desired axial ligands and one equivalent of base per cobalt. The so formed Co^{II} complex usually precipitates from solution, and only after oxidation it dissolves again. Care should be taken to account for the protons lost in complexation – usually a base is added to do so. If the required amount of base is calculated it should be taken into account that O_2 will serve as a base after oxidation. Thus only one equivalent of base per cobalt is required (see Scheme 16).

Scheme 15. Synthesis of $[Co^{II}(OH_2)(dmgH)_2]$ (**70**).[77]

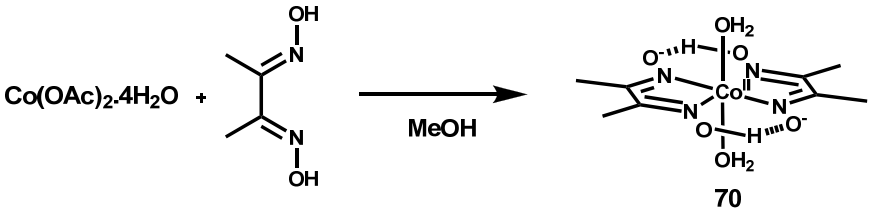

The synthesis of **70** is straight forward, but requires strictly anaerobic conditions (Scheme 15). The compound can be stored under inert atmosphere, but oxidises readily upon exposure to air. If dissolved in H_2O or DMF, after some time, aggregation occurs. The same was already noted by Schrauzer and col., and was explained by a dimerization of the compound to give a Co^{II}-Co^{II} – type species.

Scheme 16. Synthesis of $[Co^{III}X(py)(dmgH)_2]$ – type complexes.[77]

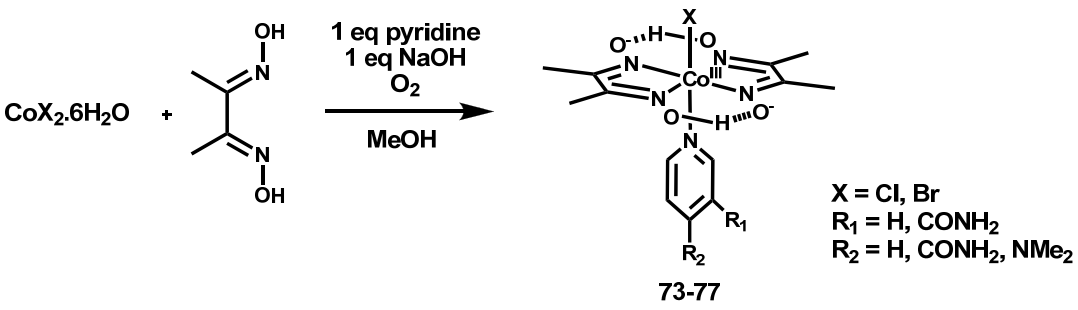

Compound **73** – **77** were synthesised as depicted in Scheme 16, following Schrauzer's procedure. It needs to be noted that this synthesis might also produce $[Co^{III}(py)_2(dmgH)_2]([Co^{III}X_2(dmgH)_2])$, which would be indistinguishable in some respects. Thus some groups propose to choose a cleaner synthesis instead, eg. producing the di-halogenido-cobaloxime first and substituting one halogenide afterwards.[27,130] In our hands, Schrauzer's one pot approach worked fine, as could be seen by ^{1}H-NMR in DMSO and by ESI-MS.

Scheme 17. Synthesis of $[Co^{III}(py)_2(dmgH)_2]PF_6$ (**71**).

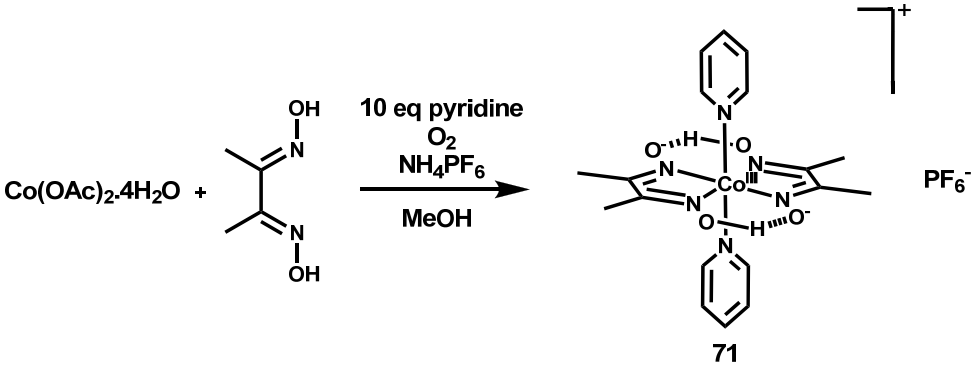

The synthesis of the di-pyridine analogue **71** was run in MeOH using an excess of pyridine both as axial ligand and as base. Before oxidation the corresponding neutral $[Co^{II}(py)_2(dmgH)_2]$ complex precipitates, but upon exposure to air it redisolves. Filtration was then used to remove insoluble material, and precipitation was achieved by adding NH_4PF_6 (Scheme 17).

Scheme 18. Synthesis of $[Co^{III}(py)_2(dmgH)(dmg)]$ (**72**).

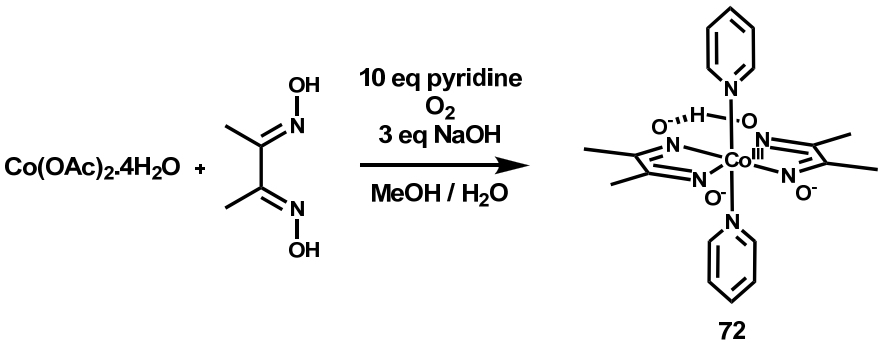

Alternatively to using NH_4PF_6, MeOH was removed and the residue taken up in H_2O, filtered and precipitated by the slow addition of NaOH (~3-5 equivalents, Scheme 18) to give the deprotonated complex **72** in crystalline

form (see Figure 29). The pK_a of **72** in H_2O was determined to be 7.36. This complex is soluble in pure H_2O up to 2 mM, likely in an equilibrium to the protonated form.

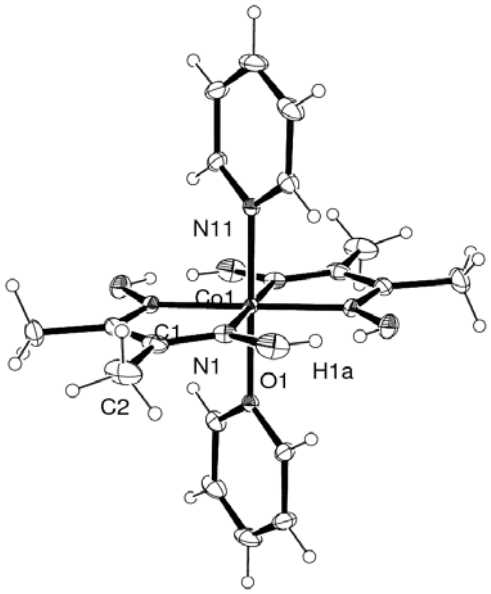

Figure 29. ORTEP drawing of **72** (bp300310) at 50 % probability level (H1a is occupied to 25 % only).

2.1.3 Ligand modifications on 4,4'-dimethyl-2,2'-bipyridine

Scheme 19. Scheme for the synthesis of 4,4'-dimethyl-2,2'-bipyridine derivatives. Dotted lines indicate products that were not isolated.

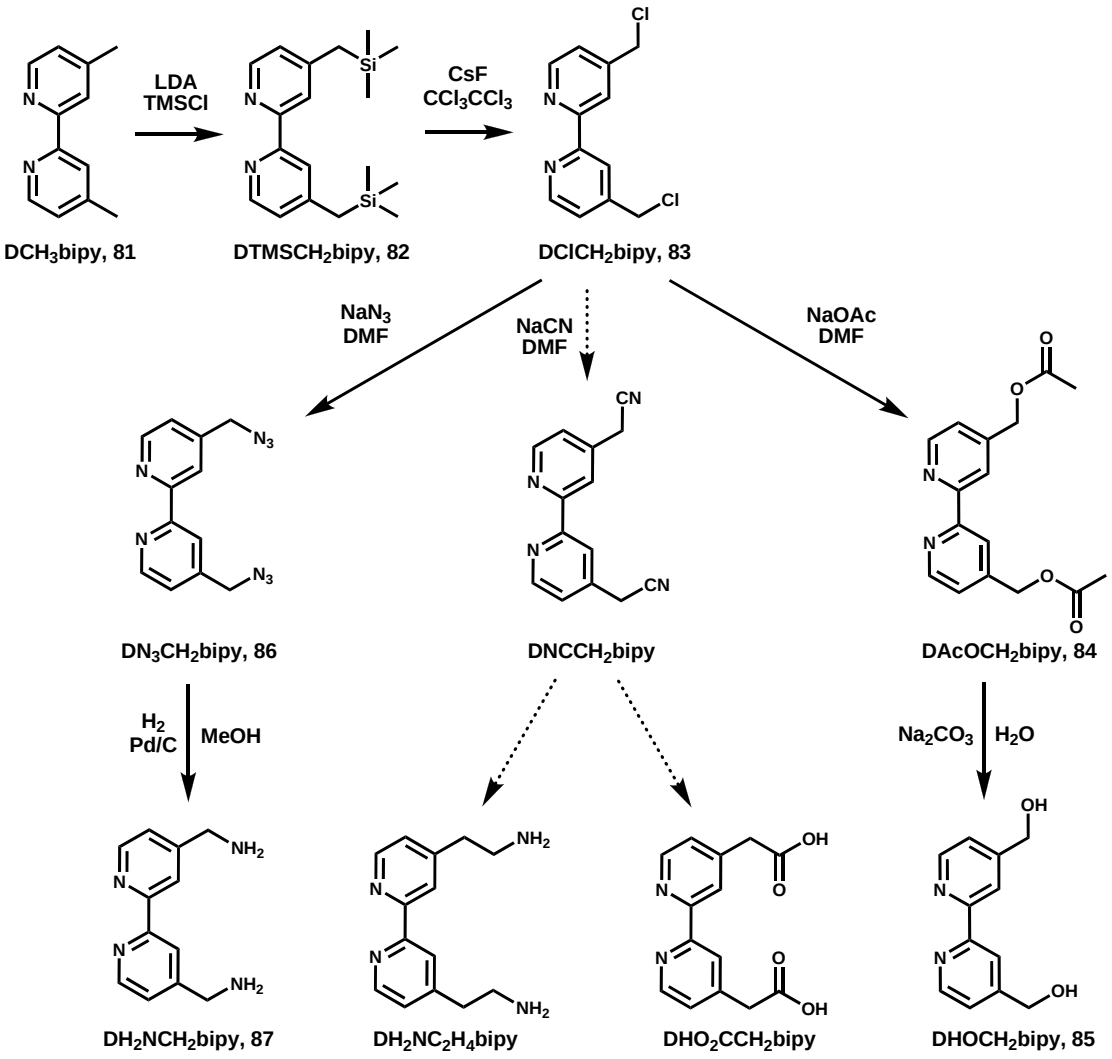

A very convenient approach to 4,4'-dimethyl-2,2'-bipyridine derivatives is given by C. L. Fraser and col.[131,132] The synthesis starts with **81**, which is commercially available. **82**, **83**, **84** and **85** were synthesized according to this literature procedure (see Scheme 19).

Reaction of **81** with LDA at low temperature yields kinetically controlled the highly reactive 4,4'-dimethyl-2,2'-bipyridine dianion, where the methyl groups are selectively deprotonated. This species reacts within seconds with TMSCl to the corresponding trimethylsilyl – derivative. The latter can then by reacted (without workup) with CCl_3CCl_3 upon activation with [TBA]F. Both reactions

run perfectly both in terms of yield and selectivity, provided that care is taken to avoid water.

The high reactivity of **83** in DMF with nucleophiles such as AcO^-, which might be surprising at the first glance, results from their high pK_a's in DMF (eg. pK_a(AcOH, H_2O) = 4.75; pK_a(AcOH, DMF) ≈ 13).[133] Direct conversion of **83** into the diol **85** using aqueous NaOH resulted in a mixture of species, whereas hydrolysis of the acetate yielded the diol **85** very nicely.

Several nucleophiles where thus tested for reaction with **83** in DMF, namely NaN_3, NaCN, sodium oxalate, sodium malonate and sodium gluconate. Whereas a reaction was observed in all cases, only in the case of the first two nucleophiles the desired product could be detected. The reaction with NaN_3 was finished within one hour at room temperature. The diazide was then reduced using Pd/C and H_2 in MeOH at room temperature (higher temperatures caused complete reduction to the dimethyl derivative **81**). The dicyanide could not be obtained in pure form, but was without doubts detected by HPLC (12.05 min) and HPLC-MS (*m/z* = 235.2 $[M+H]^+$,100 %). Prolonged reaction times led to an increase of side products in that case, as observed by HPLC. DMF, DMF/H_2O and EtOH where used, but the DMF gave best results (~30 % dicyanide). If the dicyanide could be obtained in pure form, it would be an interesting building block for further derivatization. First tests towards acid hydrolysis to DHO_2CCH_2bipy (see Scheme 19) gave promising results (HPLC: 9.0 min, broad; HPLC-MS: *m/z* = 273.1 $[M+H]^+$, 100 %). But impurities arising from the synthesis of the dicyanide could not be eliminated by extractions only. The reduction of the dicyanide using 1 M BH_3 in THF, followed by workup and extraction gave promising results as well, and $DH_2NC_2H_4$bipy (see Scheme 19), along with a dimeric species could be identified by HPLC-MS (HPLC: 2.4 min, HPLC-MS: *m/z* = 243.3 $[M+H]^+$ (30 %), 507.3 $[2M+Na]^+$ (100 %); HPLC: ~4 min, HPLC-MS: *m/z* = 423.2, 100 %). The latter species likely forms by dimerization of the diamine with unreacted diazide, and is often encountered in reduction of azides.[134] Thus the reaction could be done in the presence of CO_2, to convert the amine into the carbamic acid to prevent dimerization. Release of CO_2 would cause the carbamic acid to equilibrate with the amine and CO_2.[134]

2.1.4 Ligand modification on 4,4'-dicarboxylicacid-2,2'-bipyridine

Scheme 20. Scheme for the synthesis of 4,4'-dicarboxylicacid-2,2'-bipyridine – derivatives.

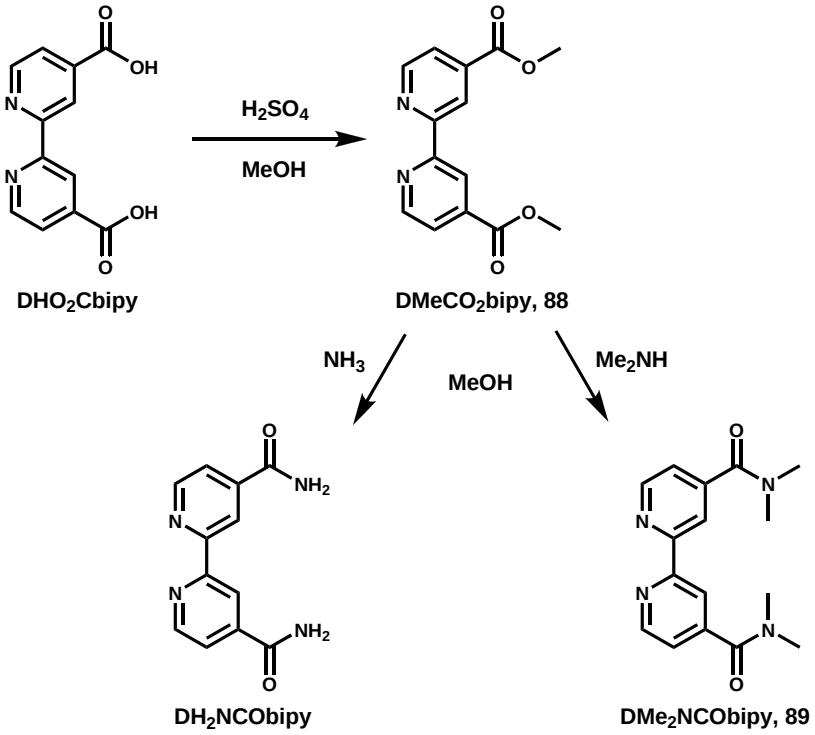

The syntheses of the 4,4'-dicarboxylicacid-2,2'-bipyridine – derivatives started with commercially available DHO_2Cbipy, which was converted to the ester $DMeCO_2bipy$ (**88**, see Scheme 20). This reaction runs smoothly from H_2SO_4 and MeOH,[135] and in one instance even at the rhenium complex! $DMeCO_2bipy$ is prone to hydrolysis, but can easily be stored as a solid. The reaction to the amide is performed in MeOH saturated with the amine of choice. In this work ammoniac was tested, which resulted in the clean formation of $DH_2NCObipy$ (characterised by EA, IR). The latter compound does not dissolve in any solvent tested, which prohibited reaction to the corresponding complexes. $DMe_2NCObipy$ forms as quickly as the former from methanolic Me_2NH solutions, but its solubility is enhanced by the two methylamine groups, thus facilitating complexation reactions. The latter compound was not found to hydrolyse as quickly as compared to **88**.

2.1.5 Ligand modifications on 1,10-phenanthroline

Scheme 21. General scheme for the synthesis of 1,10-phenanthroline (phen, **90**) derivatives.

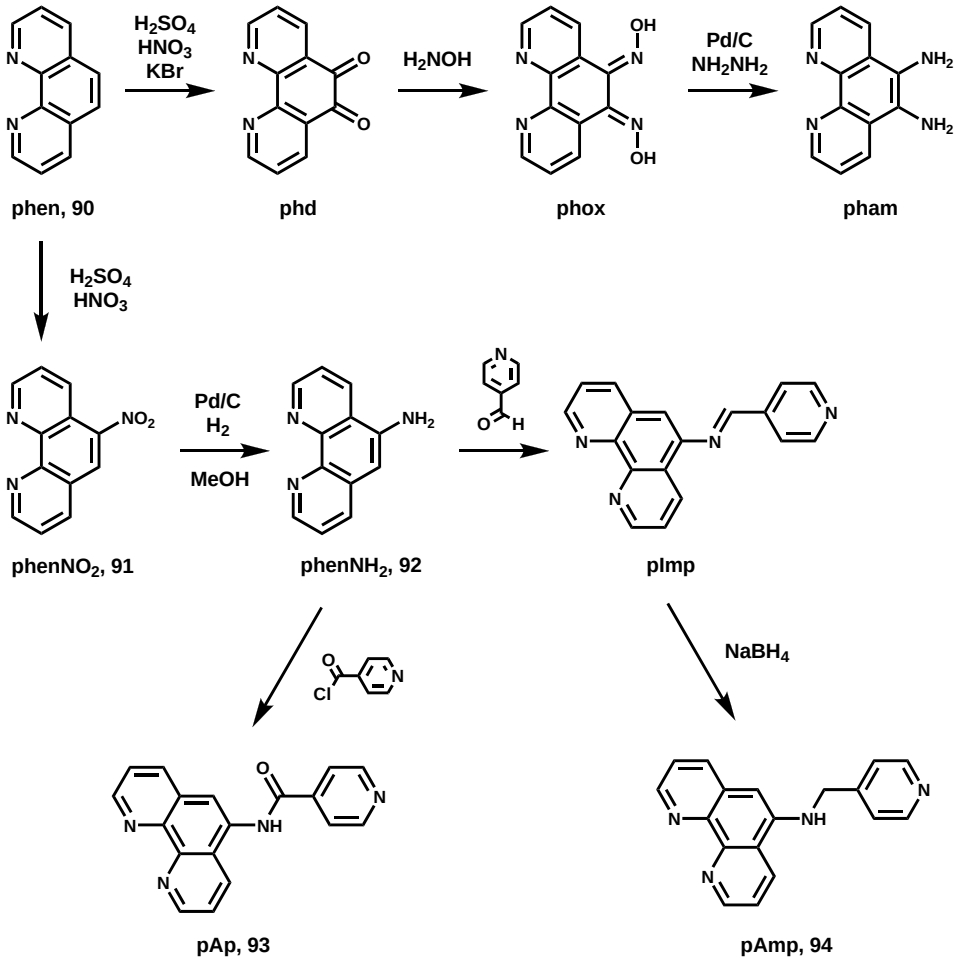

Syntheses of 1,10-phenanthroline derivatives on the 5,6-positions was achieved by activating phen (**90**) oxidatively in H_2SO_4 / HNO_3 mixtures. Whereas the classical method results in clean formation of phenNO_2 (**91**), along with minor impurities of phd,[136] addition of KBr to the mixture results in clean formation of phd only.[137] The latter is a building block for condensation with diamines of various forms, but reacts readily with hydroxylamines aswell to eventually lead to the diamine.[56,138] PhenNO_2 (**91**) on the other hand is reduced to the monoamine phenNH_2 (**92**), which in turn can be readily functionalised by amide couplings or condensation to aldehydes and subsequent reduction (see Scheme 21).

The synthesis of phenH_2 crucially depended on the supply of H_2 (for large batches a H_2 balloon was insufficient!), the quality of the Pd/C (need be fresh, active), elevated temperature (as an intermediate 5-hydroxylamine-1,10-phenanthroline was observed, which cold even be isolated in one case) and that all the educt is dissolved in MeOH. Retituration from H_2O was found very useful for product purification and separation from greenish impurities that formed during reduction. The compound is very stable, and shows very little sign of decomposition even in methanolic solution after 4 years.

The reaction with isonicotinyl chloride was very sensitive to H_2O. Rigorous exclusion of water was a prerequisite, but even then the products could only be obtained by using reflux conditions along with DMF and TEA as co-catalysts in acid chloride formation resp. amide formation. This might be due to the fact that phenNH_2 and isonicotinyl chloride are of rather unreactive nature, especially when compard to aliphatic amines / acid chlorides. Since the product was of low purity as obtained after reaction, column chromatography was applied to yield **93** in pure form. Isonicotinyl chloride can also be obtained from commercial sources.

Alternatively phenNH_2 was reacted with isonicotinyl aldehyde, and formation of the imine product pImp was observed by TLC and ^{1}H-NMR, but the compound was prone to hydrolysis. If the crude reaction mixture was reacted with a reducing agent such as $NaBH_4$, the corresponding secondary amine **94** was obtained in good yield after washing with H_2O. Column chromatography was applied to obtain pure **94**. The compound was found to be quiet hydroscopic.

2.2 (Photo-)Chemistry of Rhenium

$[ReX(CO)_3diimine]^+$ complexes were assayed as photosensitisers (PS's) in photocatalytic hydrogen production (see section 2.4 – 2.7). Four key prerequisites can be defined for a complex to do so: absorption in (the visible part of) the solar spectrum, an excited state lifetime of at least several nanoseconds (to undergo photochemical reactions), a LUMO of appropriate energy for (reduction of a co-catalyst for) proton reduction and (photo-)stability of all intermediates (on the respective timescales). Modification of the ligand structure around the $\{Re(CO)_3\}$ – core thus served to understand this various aspects.

2.2.1 Spectrochemical Properties

Most $[ReX(CO)_3diimine]^+$ – type complexes absorb on the blue edge of the solar spectrum, showing characteristic yellow to orange colours (see Figure 30 and Figure 31). One motivation for studying the various ligands was to understand how this absorption comes about and how to influence it, to potentially design complexes with increased overlap with the solar spectrum. A systematic screening of axial ligands (X) and bidentate ligands (diimine) with a spectrochemical analysis of all complexes should thus reveal the factors governing absorption properties. A further focus of this study was on the excited state lifetimes of the complexes, since photochemistry in a bimolecular scheme requires diffusion controlled reactions with the excited state (eq. 1 and 2).

$$PS + hv \rightarrow {}^*PS,\ k_{abs} \quad (1)$$

$$^*PS + Q \rightarrow PS^- + Q^+,\ k_q \quad (2)$$

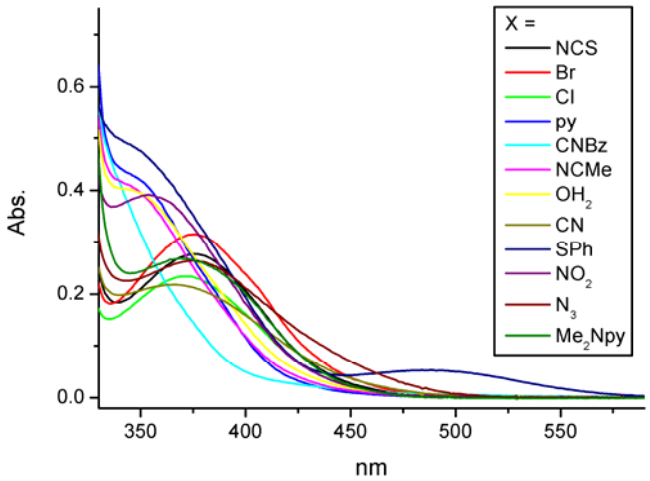

Figure 30. Absorption spectra of 0.1 mM solutions of [ReX(CO)$_3$bipy] in DMF.

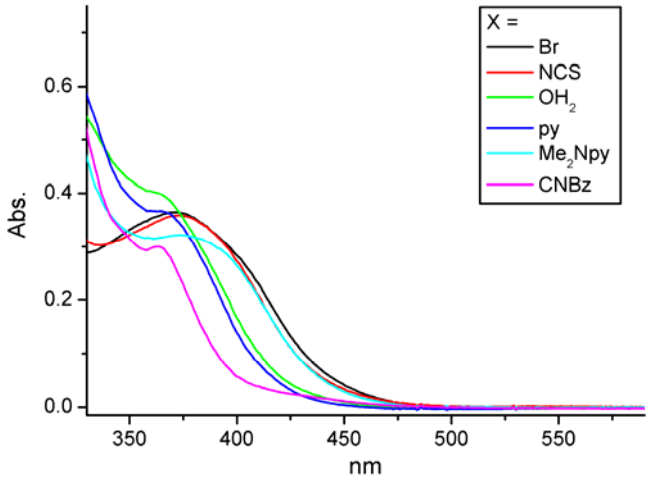

Figure 31. Absorption spectra of 0.1 mM solutions of [ReX(CO)$_3$phen] in DMF.

If a quencher (Q) was available at c = 1 M and k_q was diffusion controlled (~10^9 $M^{-1}s^{-1}$), reaction with the excited state still takes 1 ns. Since k_q is usually below diffusion control (10^7 – 10^8 $M^{-1}s^{-1}$), excited state lifetimes in the µs range are needed if [Q] should also be lowered to practically relevant concentrations (eg. 1 mM).

Table 1 and Table 2 give a summary of some physicochemical parameters for the complexes under study in DMF and water, respectively. The absorption maximum, usually assigned to a metal-to-ligand charge transfer (MLCT) band,[45] only shifts within a small window (342 to 378 nm). Nevertheless this results in a pronounced shift of the colour of the respective complexes, ranging from off-yellow to orange. The spectrochemical series (reported based on data for $[Co(NH_3)_5X]^{2/3+}$) for all ligands under question is shown

below (sorted by increasing ligandfield splitting induced, bold atoms coordinate):[139]

$Br^- < \mathbf{S}CN^- < Cl^- < \mathbf{O}NO_2^- < N_3^- < OH^- < \mathbf{O}NO^- < \mathbf{O}H_2 < \mathbf{N}CS^- < CH_3C\mathbf{N} <$ py < bipy < phen < $\mathbf{N}O_2^- < \mathbf{C}N^-$

The series as found in this study for $[ReX(CO)_3diimine]^+$:

X = pyridine: $DMeCO_2$bipy < phen < DMe_2NCObipy < bipy

diimine = bipy: Br^-, N_3^-, $\mathbf{N}CS^-$ < $Me_2N\mathbf{py}$, Cl^- < $\mathbf{C}N^-$ << NO_2^- < $^-\mathbf{S}$Ph, py < $CH_3C\mathbf{N}$, $\mathbf{O}H_2$ < $\mathbf{C}$NBz

diimine = phen: $\mathbf{N}CS^-$, $Me_2N\mathbf{py}$ < Br^- < $\mathbf{C}$NBz, $\mathbf{O}H_2$, py

Obviously there is little correlation with the spectrochemical series recorded for cobalt pentamine complexes, likely due to the difference in the metalfragment ({$Re(CO)_3$} vs. {$Co(NH_3)_5$}). It is known that ligand field splitting is usually much larger for 2. and 3. row transition metals than compared to 1. row transition metals (~1:1.5:2).[139] Nevertheless there is a trend starting with π-donor ligands and ending with π-acceptor ligands. This is somewhat unexpected for N_3^- and NCS^-, but calculations clearly show the presence of low lying π-donor orbitals. Also pyridine (py) and the modified 4-dimethlyaminopyridine (DMe_2Npy), containing the dimethlyamino donor group, follow the expected trend. It is unclear, however, why OH_2 causes such a high ligandfield splitting.

An example of a MO scheme (valence orbitals, calculated) is given for [$ReNCS(CO)_3$bipy] (**12**) in Figure 32. As can be seen, the lowest transitions (S1 and S2) are clearly of MLCT (*d*-Re – π^*-bipy) and LLCT (π-NCS – π^*-bipy) character, whereas the (destructive) *d* – *d* transition (S2) is of higher energy (as opposed to $[Ru(bipy)_3]^{2+}$ – type complexes).[140] At even higher energies the ILCT (S3, π-bipy – π^*-bipy) transitions occur. Thus it is not surprising, given the nature of the lowest transition, that variation of axial ligands / diimines influences the lowest transition (MLCT/LLCT).

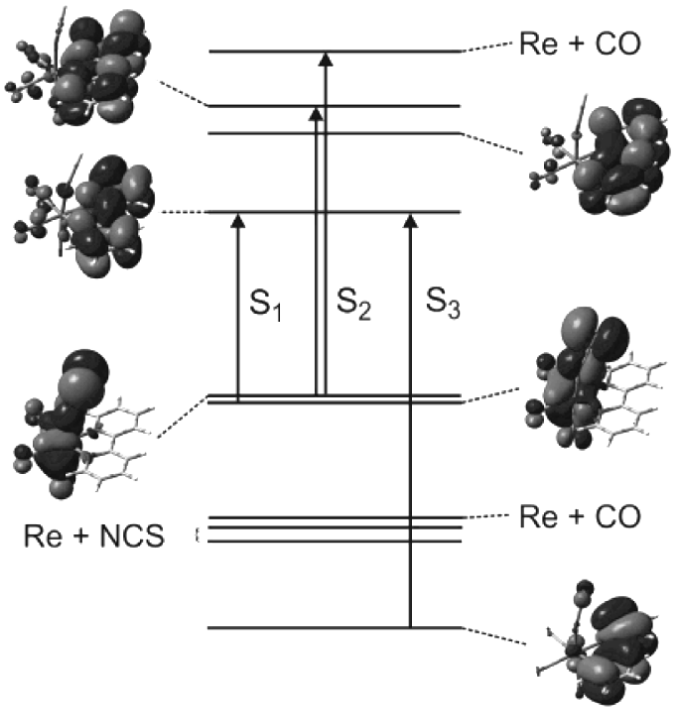

Figure 32. MO scheme for **12** showing valence bands only.[62]

Based on the nature of the MLCT band, it can be anticipated that variations of the axial ligand will have a most pronounced effect on the HOMO (*d*-Re orbitals) and variations of the diimine on the LUMO (π^*-bipy orbitals). This can be seen when comparing the symmetric CO stretching frequencies ($\nu_{CO,sym}$) in Table 1, since they are a sensitive probe for the electron density on the rhenium core. Increased electron density leads to increased backbonding, thus increasing the CO bond length and decreasing $\nu_{CO,sym}$. If diimine is altered (phen, bipy, $DMe_2NCObipy$ and $DMeCO_2bipy$), while the axial ligand remains pyridine, emission is shifted significantly to lower energies (561, 575, 600 and 640 nm, respectively, see Figure 33 for absorption spectra), while at the same time $\nu_{CO,sym}$ only shifts by about 10 wavenumbers to higher energies (2030, 2026, 2035 and 2034 cm^{-1}, respectively).

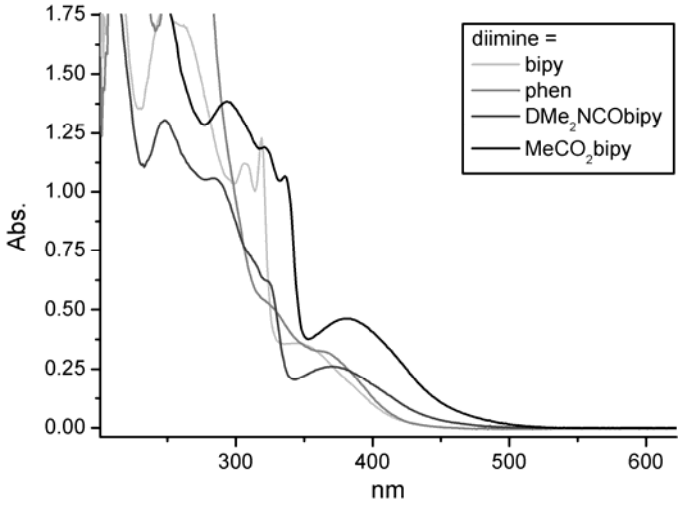

Figure 33. Absorption spectra of 0.1 mM solutions of [Re(py)(CO)$_3$diimine] in H_2O.

Whereas this trend in $\nu_{CO,sym}$ is readily explained by the acceptor properties of the diimines, it only has an insignificant effect as compared to the shift in emission. The latter is explained by the fact that a variation of the diimine mainly influences the LUMO, thus narrowing the MLCT.

If, on the other hand, the axial ligand X is varied (CNBz, py, OH_2, Me_2Npy, Br^- and NCS^-) while diimine is phen, a shift of the emission to lower energies (524, 561, 585, 593, 595 and 597 nm, respectively) is observed along with a shift of $\nu_{CO,sym}$ to lower energies (2044, 2030, 2035, 2024, 2018 and 2024 cm^{-1}, respectively. This trend is exactly opposite to the previous one (see Figure 34), and is readily explained by a stabilisation of the HOMO with increasing acceptor ability of X, thus decreasing backbonding on CO and increasing the CO bondlength.

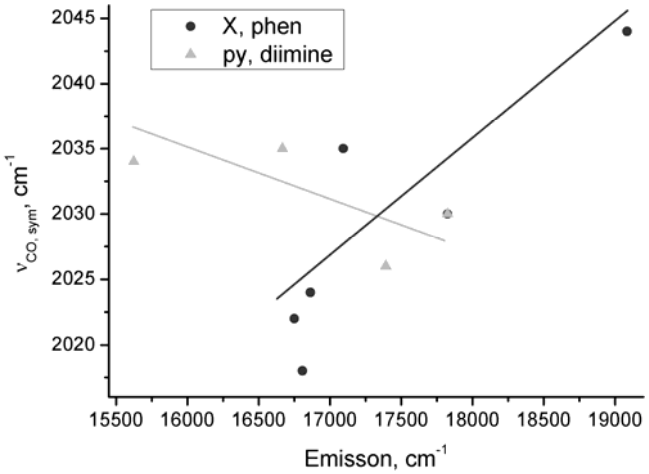

Figure 34. Correlation of $\nu_{CO,\ sym}$ with emission energies (in DMF) for [ReX(CO)$_3$diimine]$^+$ (▲: X = py; ●: diimine = phen). Straight lines were placed manually.

As to be expected for a MLCT band, solvatochromism occurs. Thus all the diimine = bipy or phen complexes display absorption / emission at slightly higher energy in H_2O as compared to DMF, consistent with the decrease in solvent polarity.[65] This is not true for the two complexes holding the 4,4'-X_2bipy ligand (**62**, **65**). This might arise from other interaction with the solvent in the latter complexes, where the π^*-bipy orbital is expected to have significant contribution from the X – substituent.

Other authors found linear correlations between the logarithm of luminescence lifetime and emission resp. absorption energies (energy gap law, EGL).[65,66] The same correlation is found for the $[ReX(CO)_3diimine]^+$ – type complexes (see Figure 35). All complexes seem to fall within the linear trend, and only minor derivations for bipy, phen and 4,4'-X_2bipy – derivatives are seen. The effect of solvent is very small.

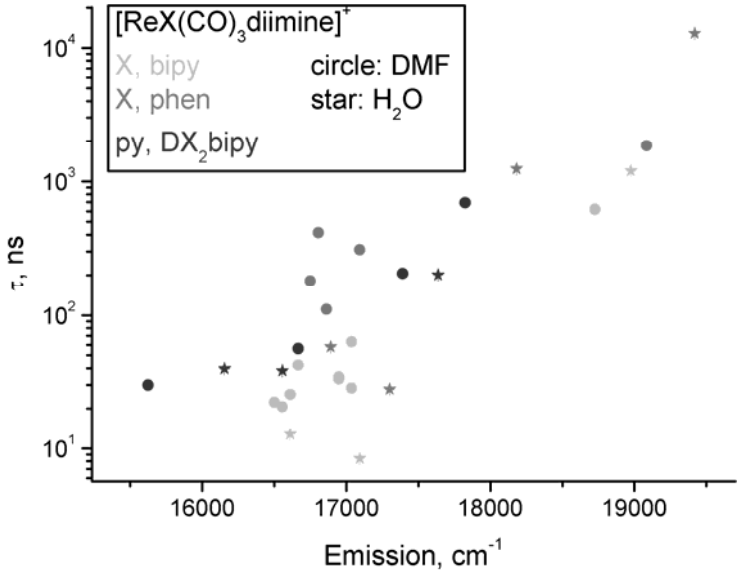

Figure 35. Plot of emission energies versus luminescence lifetimes (logarithmic scale; DMF resp. H_2O, RT).

Luminescence lifetimes (τ) depend on radiative (phosphorescent) decay rates (k_{phos}) and non-radiative decay rates (k_{nr}), according to eq. 3 and 4. It is known that k_{nr} contributes most to the relaxation of the excited state for room temperature phosphorescence. k_{nr} can be approximated by an Arrhenius-like temperature dependent part and k_0, representing the so-called 'weak coupling' of the excited to the ground state, according to equation 5:[65]

$1/\tau = k_{phos} + k_{nr}$ (3)

$1/\tau \times \Phi_{phos} = k_{phos}$ (4)

$$k_{nr} = k_0 + A\exp\left(\frac{-E_a}{k_B T}\right) \quad (5)$$

The exponential term stands for deactivation via a higher lying excited state (hence E_a is the energy difference to the relaxed excited state). The k_0 term stands for 'weak coupling', briefly by promoting vibrations and/or by spin – orbit interaction (for a detailed account see ref. [65]). -ln(k_0) is proportional to E_{em}, and the slope of the correlation depends on the inverse of the mean acceptor frequency of the ground state. This correlation holds true for all complexes investigated here bearing the $[ReX(CO)_3diimine]^+$ core (Figure 36).

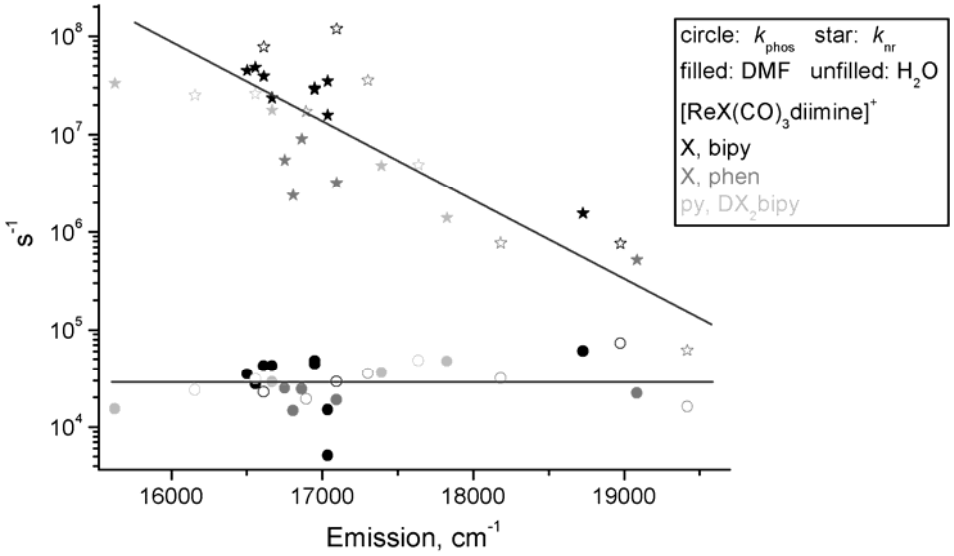

Figure 36. Plot of emission energies versus k_{phos} (●) resp. k_{nr} (✱).

Despite the general trend indicated for k_{nr} in Figure 36, it appears as if the slopes for the data from H_2O are slightly steeper than compared to those measured in DMF, indicating differences in solvation. Also the slopes for the bipy series seem to be slightly steeper than the slopes for the phen series, indicating less efficient coupling to the acceptor modes of the ground state for the latter. Even though only three examples of $[Re(py)(CO)_3(4,4'\text{-}X_2bipy]^+$ – type complexes are shown, it appears as if the correlation is less pronounced. This trend deserves to be explored in more detail, eventually with other axial ligands than pyridine or with variations of substituents on phen, potentially yielding long lived complexes with increased overlap to the visible spectrum.

Table 1. Spectroscopic properties of $[ReX(CO)_3(diimine)]^+$ in DMF.

X / diimine	$\lambda_{max,\,abs}$, (nm)	$\varepsilon_{\lambda max}$, ($M^{-1}\,cm^{-1}$)	$\lambda_{max,\,em}$, (nm)	Φ_{em} (x 10^{-3})	τ, (ns)	k_{phos} (x $10^3\,s^{-1}$)	k_{nr} (x $10^6\,s^{-1}$)	$k_{q,TEOA}$, (x $10^6\,s^{-1}$)	E_{red}, (V)[c]	$\nu_{CO,sym}$, (cm^{-1})[d]
NCS^- / bipy	376	2760 (± 27)	602	1.08 (± 0.046)	25.5 (± 0.22)	43 (± 1.8)	39.2 (± 0.34)	92 (± 1.2)	-1.185	2020
Br^- / bipy	375	3110 (± 50)	600	1.8 (± 0.106)	42.2 (± 0.19)	43 (± 2.5)	23.7 (± 0.11)	64.8 (± 0.4)	-1.235	2011
Cl^- / bipy	371	2325 (± 17)	606	0.78 (± 0.033)	22.23 (± 0.04)	35 (± 1.5)	44.9 (± 0.07)	[h]	[h]	2018
pyridine / bipy [a]	350 (*sh*)	4145 (± 32)	575	9 (± 1.00)	206.0 (± 0.91)	47 (±)	4.81 (±)	[h]	[h]	2026
Me_2Npy / bipy	370	2695 (± 57)	604	0.57 (± 0.015)	20.6 (± 0.12)	27.7 (± 0.7)	48.5 (± 0.28)	[h]	[h]	2029
CNBz / bipy	342 (*sh*)[e]	3910 (±23)	534	37 (± 3.4)	618 (± 2.4)	60 (± 5.5)	1.56 (± 0.01)	[h]	[h]	2041
MeCN / bipy [a]	347 (*sh*)	4000 (± 31)	590	1.67 (± 0.041)	34.6 (± 0.14)	48 (± 1.2)	28.8 (± 0.12)	[h]	[h]	2043
OH_2 / bipy	347 (*sh*)	3950 (± 20)	590	1.49 (± 0.073)	33.3 (± 0.16)	45 (± 2.2)	29.9 (± 0.14)	236 (± 3.2)	-1.085	2035
CN^- / bipy [a]	365	2140 (± 30)	587	0.95 (± 0.069)	63.2 (± 0.62)	15 (± 1.1)	15.8 (± 0.15)	55 (± 10)	[h]	2020
SPh^- / bipy	349 (sh)[f]	4785 (± 25)	–[g]	–[g]	–[g]	–[g]	–[g]	–[g]	[h]	2009
N_3^- / bipy	375	2605 (± 40)	–[g]	–[g]	–[g]	–[g]	–[g]	–[g]	[h]	2018
NO_2^- / bipy [a]	354	3770 (± 39)	587	0.146 (± 0.006)	28.5 (± 0.44)	5.1 (± 0.23)	35.0 (± 0.54)	[h]	[h]	2024
Br^- / phen	371	3525 (± 9)	595	6.1 (± 0.11)	414.9 (± 0.85)	14.7 (± 0.27)	2.40 (± 0.01)	32.3 (± 0.7)	-1.250	2018
OH_2 / phen [a]	363 (sh)	3845 (± 35)	585	5.9 (± 0.44)	310.1 (± 0.82)	19 (± 1.4)	3.21 (± 0.01)	[h]	[h]	2035
NCS^- / phen	373	3485 (± 12)	597	4.5 (± 0.12)	181.4 (± 0.42)	24.9 (± 0.68)	5.49 (± 0.01)	[h]	[h]	2022
pyridine / phen [a]	364 (sh)	3540 (± 8)	561	33 (± 1.6)	692 (± 3.2)	48 (± 2.4)	1.40 (± 0.01)	[h]	[h]	2030
Me_2Npy / phen	373	3235 (± 23)	593	2.70 (± 0.085)	110.8 (± 0.5)	24.4 (± 0.78)	9.01 (± 0.04)	[h]	[h]	2024
CNBz / phen [b]	363 (sh)	2890 (± 19)	524	41.1 (± 0.59)	1'845 (± 4.5)	22.3 (± 0.32)	0.520 (± 0.001)	[h]	[h]	2044
py / $DMe_2NCObipy$	359	3010 (± 36)	600	1.6 (± 0.16)	56.1 (± 0.29)	29 (± 2.8)	17.8 (± 0.1)	[h]	[h]	2035
py / $DMeCO_2bipy$	378	4835 (± 41)	640	0.46 (± 0.035)	30.0 (± 0.21)	15 (± 1.2)	33.3 (± 0.2)	[h]	[h]	2034

Data measured in DMF, [a]: partial conversion to solvato complex (3 - 30 %, see stability of PS); [b]: photolabile; [c]: 0.1 M $[TBA]PF_6$, DMF, vs Ag/AgCl, $Fc^{0/+1}$ at 500 mV; [d]: in KBr pellet; [e]: small shoulder at 410 nm (320 $M^{-1}\,cm^{-1}$); [f]: maximum at 488 nm (528 $M^{-1}\,cm^{-1}$); [g]: no room temperature emission; [h]: not measured.

Table 2. Spectroscopic properties of $[ReX(CO)_3(diimine)]^+$ in H_2O.

X / diimine	$\lambda_{max,\ abs}$, (nm)	$\varepsilon_{\lambda max}$, ($M^{-1}\ cm^{-1}$)	$\lambda_{max,\ em}$, (nm)	Φ_{em} (x 10^{-3})	τ, (ns)	k_{phos} (x $10^3\ s^{-1}$)	k_{nr} (x $10^6\ s^{-1}$)	$k_{q,TEOA}$, (x $10^6\ s^{-1}$)[b]	E_{red}, (V)[c]	$\nu_{CO,sym}$, (cm^{-1})[d]
OH_2 / bipy	339 (sh)	4025 (± 93)	585	0.25 (± 0.01)	8.40 (± 0.02)	29 (± 1.4)	119.0 (± 0.3)	–[e]	-1.085	2035
pyridine / bipy	343	3625 (± 26)	567	9.8 (± 0.3)	201.5 (± 0.4)	48 (± 1.5)	4.91 (± 0.01)	51 ± 1	[g]	2026
Me_2Npy / bipy	368	2470 (± 52)	602	0.29 (± 0.01)	12.80 (± 0.06)	22.9 (± 0.6)	78.1 (± 0.4)	[f]	[g]	2029
CNBz / bipy	337 (sh)	3800 (± 24)	527	87 (± 3.1)	1'195 (± 1.4)	73 (± 2.6)	0.764 (± 0.003)	[f]	[g]	2041
MeCN / bipy [a]	340 (sh)	3675 (± 45)	543	5.8 (± 1.3)	8.46 (± 0.03)	684 (± 157)	117.5 (± 0.4)	[g]	[g]	2043
OH_2 / phen	360 (sh)	3380 (± 27)	578	0.99 (± 0.02)	28.0 (± 0.2)	35.4 (± 0.6)	35.7 (± 0.2)	–[e]	[g]	2035
pyridine / phen	362 (sh)	3360 (± 25)	550	39.1 (± 0.5)	1'241 (± 1.7)	31.5 (± 0.4)	0.775 (± 0.001)	78 ± 3	[g]	2030
Me_2Npy / phen	368	3005 (± 22)	592	1.12 (± 0.07)	58.0 (± 0.4)	19 (± 1.2)	17.2 (± 0.1)	[f]	[g]	2024
CNBz / phen	360 (sh)	2615 (± 21)	515	208 (± 3.7)	12'830 (± 58)	16.2 (± 0.3)	0.0617 (± 0.0004)	[f]	[g]	2044
py / $DMe_2NCObipy$	371	2590 (± 21)	604	1.20 (± 0.03)	38.4 (± 0.2)	31.2 (± 0.8)	26.0 (± 0.1)	[g]	[g]	2035
py / $DMeCO_2bipy$	381	4630 (± 30)	619	0.96 (± 0.03)	39.8 (± 0.3)	24.0 (± 0.6)	25.1 (± 0.2)	[g]	[g]	2034

Data measured in H_2O, [a]: slow conversion to solvato complex (see stability of PS); [b]: from time resolved FT-IR experiment in 1 M TEOA, 0.1 M HBF_4, ~95 % D_2O; [c]: 0.1 M $[TBA]PF_6$, DMF, vs Ag/AgCl, $Fc^{0/+1}$ at 500 mV; [d]: in KBr pellet; [e]: no reductive quenching observed, deprotonation of exited state occurs instead; [f]: solubility issues; [g]: not measured.

2.2.2 Stability of the Conjugates

Not all combination's of {$Re(CO)_3$diimine} and monodentate axial ligands X gave stable complexes of the form $[ReX(CO)_3diimine]^+$. As pointed out in section 2.1.1, $[ReBr(CO)_3bipy]$ (**10**), along with other complexes with $X = Br^-$ (**30**, **50**, **53**, **60**, **63**), all reacted readily with Ag^+ salts in MeOH, H_2O or CH_2Cl_2 to give AgBr and the respective solvato complex (in MeOH or H_2O) or silver anion complex (in CH_2Cl_2). These reactions usually run at room temperature within less than 1 hour to completeness, if not hindered by the solubility of the reactants. This already gave evidence that axial bromide is quite labile, since reaction with Ag^+ would be accelerated by a pre-equilibrium of bromide dissociation from $[ReBr(CO)_3diimine]$.

Further evidence came from HPLC, as depicted in Figure 37. For all bromo complexes two peaks were observed. In the case of **10** this was at 15.04 and 16.57 min. These two peaks were readily assigned according to their absorption spectra and by HPLC-MS to the solvato complex **11** and the bromo complex **10**, respectively. Depending in what solvent **10** was dissolved before injection, 50 – 80 % were detected as solvato complex. Clearly this showed that **10**, already in the solvent, but also on the HPLC, equilibrated with its solvato form. In DMSO and DMF, **10** remained completely stable, as evidenced by ^{1}H-NMR and CV. In H_2O (upon heating) and MeOH partial conversion to the solvato complex occurred.

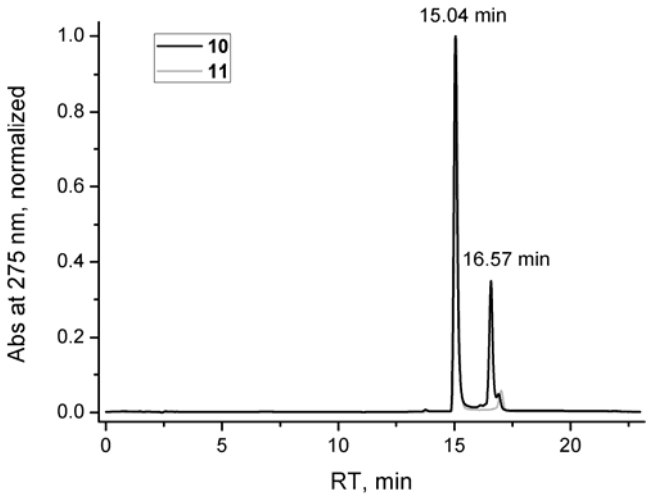

Figure 37. HPLC traces of methanolic solutions of **10** (black) and **11** (grey), showing the solvato complex **11** at 15.04 min and the bromo complex **10** at 16.57 min (the peak at 17.01 min is probably a trifluoroacetato adduct).

Judging the stability of the MeCN complex **16** was more difficult: although the synthesis clearly yielded the MeCN adduct, as obvious from elemental analysis, IR and MS data (see section 4.1.1), HPLC and spectrochemical analysis was not unambitious. HPLC analysis gave a peak very close to the solvato complex **11** (15.04 vs 15.18 min), thus making distinction difficult. Only upon careful analysis of the spectral signature at least partial assignment to **16** became possible. ^{1}H-NMR analysis from D_2O and d^6-DMSO, on the other hand, always showed free MeCN along with coordinated MeCN. The ratio free MeCN / coordinated MeCN could be observed to increase during the measurement in d^6-DMSO. Accordingly the resonances for the bipy – ligand of **16** were split in to two subsets, relating to **16** and a solvato adduct. If emission properties of **11** and **16** were compared, very similar data were obtained in DMF (regarding lifetime, emission maxima and Φ_{phos}), thus suggesting MeCN replacement by DMF again. In water, on the other hand, emission maxima were 585 nm and 543 nm, and Φ_{phos} was 0.25 ‰ and 5.8 ‰ for **11** and **16**, respectively. The lifetime of both compounds was 8.4 ns. This clearly indicated that, at least partially, two different species were present in H_2O. Thus the series of the nitrile complexes deserves further investigation, with emphasis on their water chemistry.

Unlike other complexes, $[ReN_3(CO)_3bipy]$ (**18**) did not form readily. The reaction was run in H_2O using **11** and NaN_3 (2 eq.). Refluxing for 5 h in was necessary to obtain a satisfactory yield. Also after this procedure HPLC still indicated 5 – 10 % solvato complex (15.05 min) along with the product (16.53 min). ^{1}H-NMR from d^6-DMSO, on the other hand, showed a pure compound. Thus an acid assisted dissociation is likely to occur in H_2O. Unfortunately, the compound was silent in terms of phosphorescence.

Axial water was probably the most labile axial ligand, and most substitution reactions were thus carried out with **11** or its analogues as educts. Nevertheless, axial bound water as well as MeOH was visible from ^{1}H-NMR in d^6-DMSO (see section 2.1.1). If the trifluoromethansulfonate anion occupied the axial position, substitution was more difficult, which is somewhat contra-intuitive.

Some attempts to the synthesis of compounds bearing thiolates in the axial position were made, but only thiophenolate gave a stable complex (**17**). This compound was most likely stabilized by $\pi - \pi$ interaction between the bipy and thiophenolate moiety (see section 2.1.1 and Figure 27). The analogue methanthiolate complex did not form.

Complexes bearing an axial NCS^- ligand (**12**, **32**, **52**, **55**) were quite stable, and only after prolonged heating in dilute H_2O could an evidence for decomplexation to the solvato complex be observed for **52**. If allowed to stand, the NCS – complex reformed upon cooling. Also the pyridine (**13**, **33**, **62** and **65**) and benzoisonitrile (**15** and **35**) complexes were very stable in all solvents tested and showed no sign of decomplexation even after refluxing in H_2O. Compound **35** did show signs of decomposition under irradiation in DMF.

2.2.3 Electrochemistry of the Rhenium Complexes

Electrochemistry of $[ReX(CO)_3diimine]^+$ complexes is well explored and mostly well understood.[56,141-145] Two characteristic experiments are given in Figure 38 for **10** and in Figure 39 for **12**.

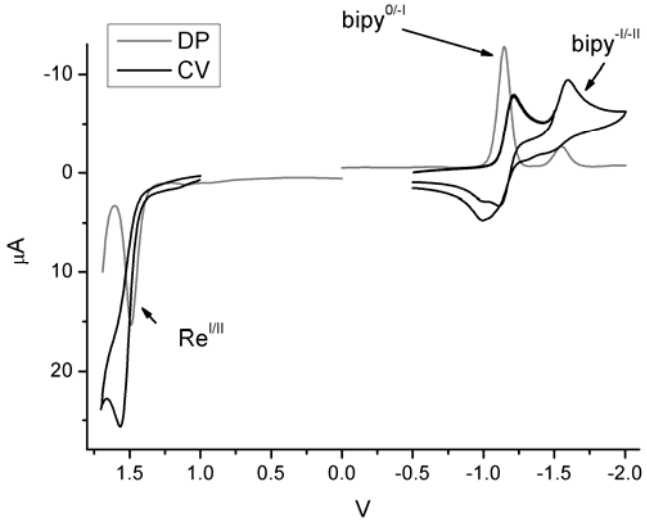

Figure 38. Electrochemistry on a 1 mM solution of **10** in 0.1 M $[TBA]PF_6$, DMF, N_2 ($Fc^{0/I}$ at 500 mV, WE is glassy carbon, ID = 2 mm). Grey lines are differential pulse scans, black lines are cyclic voltametry scans. The oxidation ($Re^{I/II}$ couple; E_{pa} = 1.490 V) resp. the second reduction ($bipy^{-I/-II}$ couple; E_{pc} = -1.670 V) of **10** are irreversible, the first reduction ($bipy^{0/-I}$ couple; $E_{1/2}$ = -1.235 V) is quasi-reversible (see **Figure 40**)

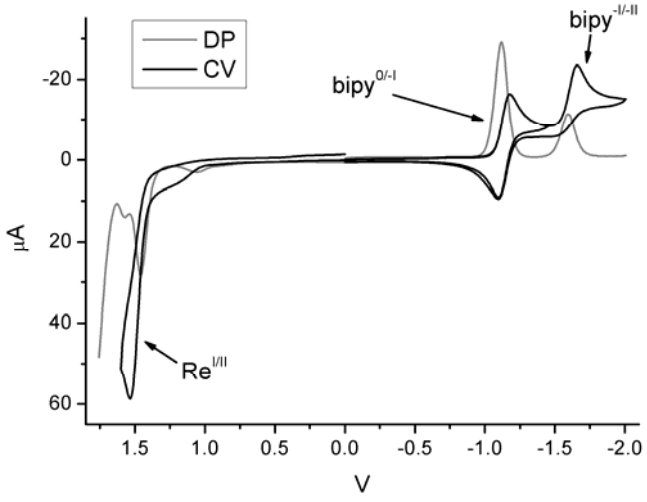

Figure 39. Electrochemistry on a 1 mM solution of **12** in 0.1 M $[TBA]PF_6$, DMF, N_2 ($Fc^{0/I}$ at 500 mV, WE is glassy carbon, ID = 3 mm). Grey lines are differential pulse scans, black lines are cyclic voltametry scans. The oxidation ($Re^{I/II}$ couple; E_{pa} = 1.485 V) resp. the second reduction ($bipy^{-I/-II}$ couple; E_{pc} = -1.705 V) of **10** are irreversible, the first reduction ($bipy^{0/-I}$ couple; $E_{1/2}$ = -1.185 V) is reversible.

Both sets of data show an irreversible oxidation at relative high potential (~1.5 V). The oxidation would deplete the HOMO, thus a Re – X based orbital. The irreversibility of this process is either due to CO loss (decreased backbonding from Re^{II})[144] or oxidative elimination of an axial ligand (since the HOMO is Re – X in character),[146] but deserves further investigation, with emphasis on the time scale and the nature of follow up reactions. Evidence is that decomposition occurs between the µs and the ms timescale (from time resolved FT-IR and CV, respectively). This is of particular interest when designing three component systems for photocatalysis in which excited PS is oxidatively quenched by eg. a cobalt based WRC.

The first reduction is, depending on the axial ligand X, quasi-reversible for X = Br^- (see Figure 38 and Figure 40) resp. fully reversible for X = NCS^- (see Figure 39). This reduction is ligand based, thus assigned as $diimine^{0/-I}$, in accordance with a mainly diimine based LUMO.

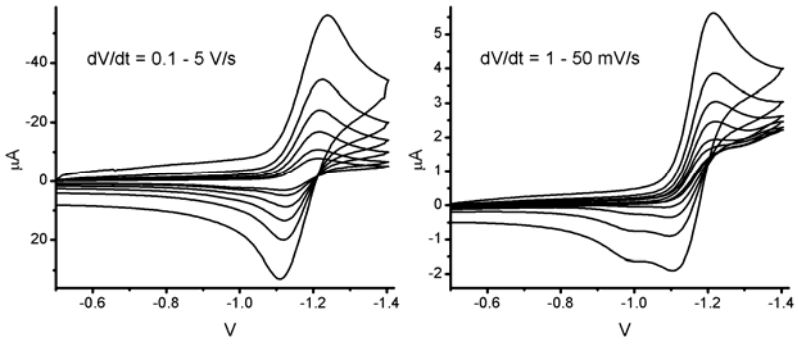

Figure 40. Cyclic voltametry study on the reduction of **10** (1 mM **10**, 0.1 M $[TBA]PF_6$, N_2, DMF, WE is glassy carbon, ID = 2 mm, $Fc^{0/I}$ at 500 mV).

Bromide dissociation from $[ReBr(CO)_3bipy]^-$ (**10**$^-$) was observed before (in THF and MeCN), and results in $[Re(solv)(CO)_3bipy]$. The latter eventually dimerizes through a pentacoordinate $[Re^0(CO)_3bipy]$ species (17 e^-) to form a Re-Re bond (18 e^-), as depicted in Scheme 22.[141,143-145] To assay the stability of **10**$^-$ in DMF cyclic voltametry (CV) at various scan rates was performed on the **10**/**10**$^-$ couple (see Figure 40). Whereas the couple is perfectly reversible with scan rates of 1 – 5 V/s, a new anodic peak at -1.05 V is observed if scan rates were lowered (see Figure 40). If several sweeps were performed in a row, a corresponding cathodic peak could be detected at -1.12 V (see Figure

41). This species is readily assigned to $[Re(solv)(CO)_3bipy]^+$. Time dependent analysis of the CV data allowed an estimate for bromide dissociation above 1 s. After 1 minute at -1.2 V or -1.4 V an equilibrium is achieved, with roughly equal concentrations of $[ReBr(CO)_3bipy]^-$ and $[Re(solv)(CO)_3bipy]$. This did not change if the applied potential was kept for longer times.

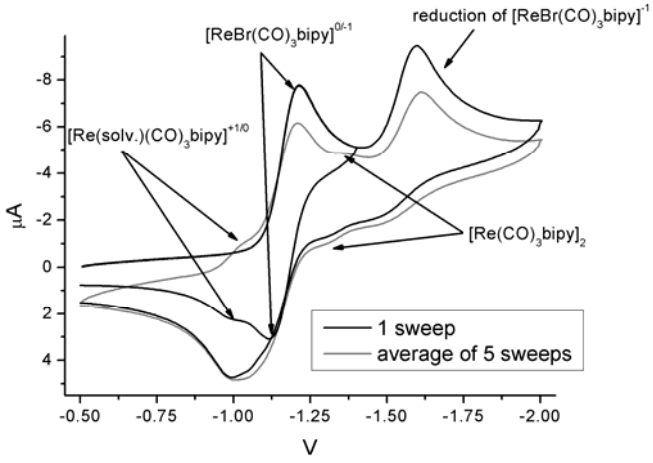

Figure 41. Cyclic voltametry study on the reduction of **10** (1 mM **10**, 0.1 M $[TBA]PF_6$, N_2, DMF, WE is glassy carbon, ID = 2 mm).

The first reduction of **12**, on the other hand, was completely reversible on a scan rate between 1 mV/s and 5 V/s, thus underscoring the strong binding of the NCS^- ligand, even in the reduced state. This feature is of particular importance in photocatalysis.

The second reduction is irreversible for both compounds. The reduction is still bipy based, thus giving formally rise to a dianion $bipy^{2-}$, in accordance with the diimine based LUMO-1. This dianionic ligand, however, is an excellent electron donor to the rhenium core, and labilizes the axial ligand even more, thus causing prompt formation of the 18 e^- species $[Re(CO)_3bipy]^-$ (see Scheme 22).[141,143-145] This species is obtained as well by reduction of $[Re(solv)(CO)_3bipy]$ or $[Re(CO)_3bipy]_2$. Evidence for the dimeric species was obtained in a CV experiment using 5 repeated sweeps across the two reduction waves (Figure 41). A small anodic peak for $[Re(CO)_3bipy]_2$ at -1.36 V was already seen in the first scan. In the consecutive scans a corresponding cathodic signal appears at -1.43 V. In the given experiment neither $[Re(solv)(CO)_3bipy]^+$ nor $[Re(CO)_3bipy]_2$ accumulate to more than

10 %. Upon re-oxidation prompt re-coordination of X occurs, thus underscoring the reversibility of ligand dissociation from the one electron reduction product $[ReX(CO)_3bipy]^{-}$.

Scheme 22. Reduction sequence for $[ReX(CO)_3bipy]$.

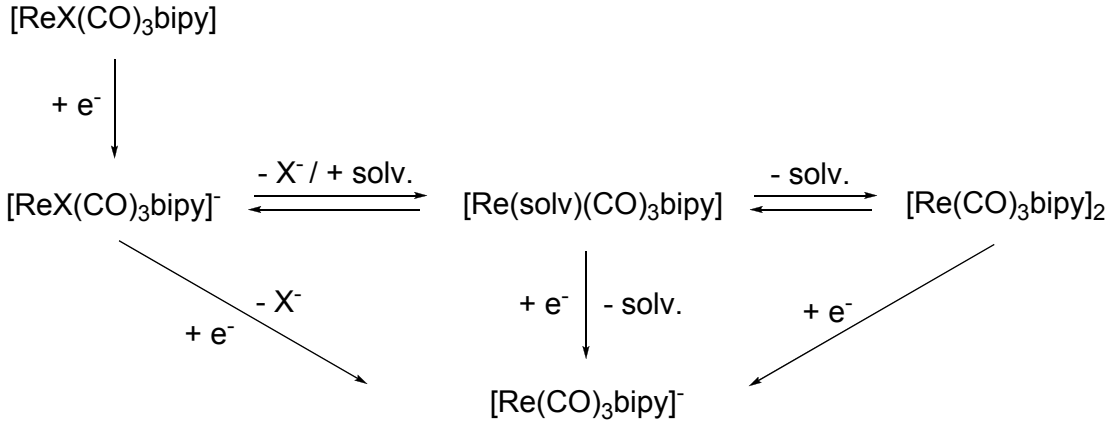

2.2.4 Quenching of the exited state of [ReX(CO)$_3$diimine]$^+$

Excited states of many [ReX(CO)$_3$diimine]$^+$ complexes are long lived enough for bimolecular quench reactions to occur in room temperature solutions (see eq. 1 and 2). Several different quenchers were thus assayed for their abilities to interact with ***10** according to the Stern – Vollmer relation (see eq. 6 and 7). If a steady state concentration for *PS is assumed, equation 1 and 2 can be transformed to the following rate law:

$$[*\mathrm{PS}]_{\mathrm{SS}} = \frac{k_{abs}[\mathrm{PS}]}{k_{nr} + k_{phos} + k_q[\mathrm{Q}]} \tag{6}$$

With the excited state lifetime $\tau^{-1} = k_{nr} + k_{phos}$ and the luminescence intensity $\mathrm{I} \propto [*\mathrm{PS}]_{\mathrm{SS}}$, this transforms into

$$\frac{\mathrm{I}_0}{\mathrm{I}} = 1 + k_q\tau[\mathrm{Q}], \tag{7}$$

for two experiments with (I) and without (I_0) added quencher. Thus plotting of (I_0/I)-1 gives a linear correlation with intercept 0 and slope $k_q\tau$ if equation 1 and 2 are fulfilled and no other factors (such as absorption of the quencher) disturb the measurement. A series of such experiments are plotted in Figure 42 for **10**.

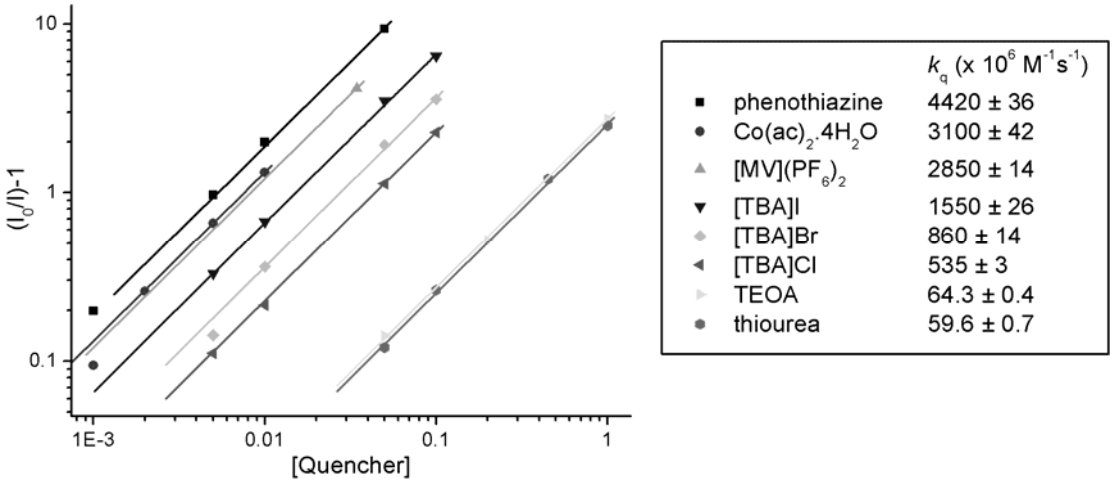

Figure 42. Stern – Vollmer Plot of luminescence intensity decrease for **10** using different quencher molecules in DMF (logarithmic scale for better comparison). Inset: k_q as calculated from the slope of the fit and $\tau_{\mathbf{10}}$ = 42.5 ± 0.2 ns.

As is seen immediately, the quench rate k_q for different quenchers differs by 2 orders of magnitude. It was of special interest to determine the character of the quench event, eg. if it was reductive, oxidative or energy transfer quenching. Time resolved vibrational spectroscopy was applied to elucidate the different mechanism of action of the quenchers studied (see Table 3).

Besides establishing the nature of the quench event, analysis of the time resolved FT-IR data allowed to determine k_q and Φ_{cage}. Exponential fitting of the data gives τ_1 resp. τ_2, according to eq. 8. τ_1 then transforms into k_q according to eq. 9 if the lifetime of the excited PS, τ_{PS}, is known. For back electron transfer only τ_2 is calculated, since a correct analysis according to a second order rate law (eq. 10) was not possible due to unknown [PS^-].

$$y = y_0 + A_1 e^{-\frac{t}{\tau_1}} + A_2 e^{-\frac{t}{\tau_2}}, \text{ with } \tau_1 < \tau_2 \quad (8)$$

$$\tau_1 = \frac{1}{k_{nr} + k_r + k_q[Q]} = \frac{1}{\tau_{PS}^{-1} + k_q[Q]} \quad (9)$$

$$[PS^-]_t = \frac{1}{k_{back} t + [PS^-]_0} \quad (10)$$

The cage escape yield of the reductive / oxidative quench event is given by the fraction of successful separations of the encounter complex into products as compared to the total amount of encounter complex formed. Or, in other words, the cage escape yield shows how much of the initial excited PS that formed an encounter complex is converted into products. The maximal cage escape yield ($\Phi_{q,max}$) is given by eq. 11. Φ_{red} is the fraction of reduced / oxidized PS as compared to the excited PS, and is directly accessible from the pre-exponential terms of eq. 8, namely by eq. 12. Φ_{cage} is then the ratio of Φ_{red} and $\Phi_{q,max}$ (eq. 13).

$$\Phi_{q,max} = \frac{k_q[Q]}{k_q[Q] + k_{nr} + k_r} \quad (11)$$

$$\Phi_{red} = \frac{A_2}{A_1 + A_2} \quad (12)$$

$$\Phi_{cage} = \frac{\Phi_{red}}{\Phi_{q,max}} \quad (13)$$

Table 3. Observed lifetimes of **10** in the presence of different quencher molecules (pump-probe FT-IR setup, 1 mM **10**, DMF, Ar unless otherwise noted, 415 nm pump pulse).

quencher	τ_1 (ns)[a]	τ_2 (µs)[a]	k_q (x 10^6 $M^{-1}s^{-1}$)[b]	$\Phi_{q,max}$[c]	Φ_{red}[d]	Φ_{cage}[e]
–	50 ± 1.5	–	–	–	–	–
1 M TEOA	15.1 ± 0.2	–	46 ± 1.1	0.70 ± 0.02	0.32 ± 0.03	0.47 ± 0.05
1 M TEOA[f]	14.2 ± 0.2	0.17 ± 0.01	50 ± 1.0	0.71 ± 0.02	0.36 ± 0.02	0.51 ± 0.03
1 M TEA[g]	11.0 ± 0.3	8 ± 3.2	71 ± 3.0	0.78 ± 0.04	0.39 ± 0.06	0.50 ± 0.07
1 M TEA[f]	10.5 ± 0.1	0.18 ± 0.01	75 ± 1.0	0.79 ± 0.01	0.41 ± 0.02	0.51 ± 0.02
0.1 M TBACl	13.6 ± 0.1	7 ± 1.1	536 ± 3	0.73 ± 0.01	0.02 ± 0.01	0.02 ± 0.01
0.1 M TBABr	10.1 ± 0.1	9 ± 3.1	787 ± 5	0.80 ± 0.01	0.01 ± 0.01	0.01 ± 0.01
0.1 M TBAI	5.6 ± 0.2	4.7 ± 0.9	1600 ± 71	0.89 ± 0.01	0.06 ± 0.02	0.07 ± 0.02
0.1 M Pth[h,i]	1.9 ± 0.03	0.56 ± 0.05	4960 ± 84	0.96 ± 0.02	0.79 ± 0.03	0.82 ± 0.04
1 M Thiourea	13.1 ± 0.1	14 ± 1	56.2 ± 0.3	0.74 ± 0.01	0.05 ± 0.01	0.07 ± 0.02
34.4 mM MV[j]	7.7 ± 0.1	14 ± 1	3180 ± 24	0.85 ± 0.01	0.06 ± 0.01[k]	0.07 ± 0.01

[a]: exponential fitting according to eq. 8, times above 1 µs are possibly error affected by trace levels of O_2 present due to incomplete purging; [b]: according to eq. 9; [c]: according to eq. 11; [d]: according to eq. 12; [e]: according to eq. 13; [f]: normal atmosphere, 21 % O_2; [g]: a second rise time was observed at 240 ± 25 ns; [h]: phenothiazine; [i]: a second rise time was observed at 121 ± 4.3 ns, and a second bleach at 2.2 ± 0.1 µs; [j]: methylviologen as an hexafluorophosphate salt; [k]: oxidative quenching.

A rather good agreement for quench rates as observed by Stern – Vollmer analysis of luminescence intensities and as observed by time resolved FT-IR was found. For all quenchers studied in Table 3 reductive quenching of the excited state was observed, except for $[MV](PF_6)_2$, which showed oxidative quenching. Interestingly enough, in all cases except for TEOA, the quench event was reversible in rhenium. If back electron transfer occurred, it was about 3 orders of magnitude slower than the quench event. This is related to the large excess of quencher added as compared to the concentration of quenched PS. Thus back electron transfer (k_{back}), even if it occurred at rates close to diffusion control, would be substantially slower than the quench event. Interesting was the observation that in the presence of oxygen (normal atmosphere) quenching by TEOA was virtually unaffected. Obviously the quench process by TEOA (1 M) was faster than quenching by O_2. On a timescale of 200 ns PS^- was converted back into PS, supposedly by oxidation through O_2.

Due to the small number of compounds it was found inappropriate to do an analysis of k_q in this study. Others have compared reductive resp. oxidative quench rates to the excited state oxidation resp. reduction potentials (see

Figure 43).[47] As expected quench rates decrease as ΔG for the reaction decreases, reaching a maximum close to diffusion control.

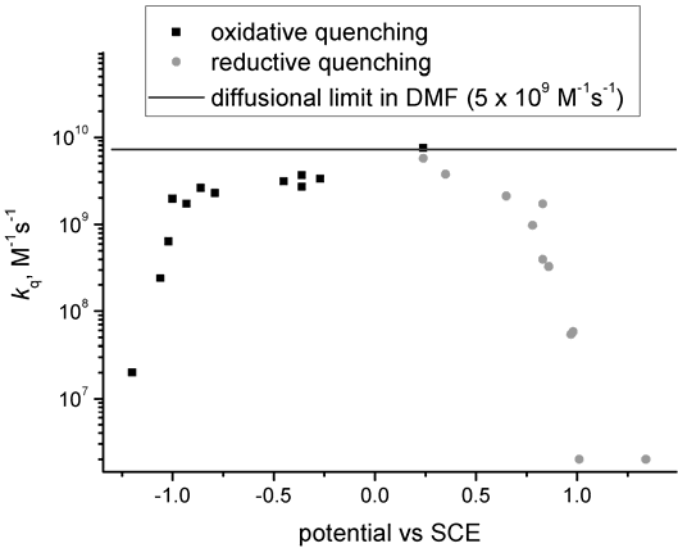

Figure 43. Plot of k_q versus the oxidation resp. the reduction potential of various electron donor's resp. acceptor's (grey resp. black) for [ReCl(CO)$_3$phen] in MeCN (note the excited state redox potentials are +1 resp -1 V vs SCE).[47]

Cage escape yields varied between 1 and 80 % for the quenchers tested in this study. Almost no effect could be observed for [TBA]Cl and [TBA]Br, in accordance to the relatively high oxidation potential associated with the $Cl^-/Cl^\bullet$ resp. $Br^-/Br^\bullet$ couple. In the case of [TBA]I, thiourea and methylviologen a Φ_{cage} of close to 10 % was obtained. The next class were the tertiary amines, for which a Φ_{cage} of about 50 % was observed. Quite remarkable is the case of phenothiazine, where a consecutive transfer of two electrons was observed, yielding a total 200 % of $\mathbf{10}^-$ as compared to ***10** (see Figure 44). A value of 80 % was obtained for the first electron. As to now, the factors governing the cage escape yields remain to be unravelled.

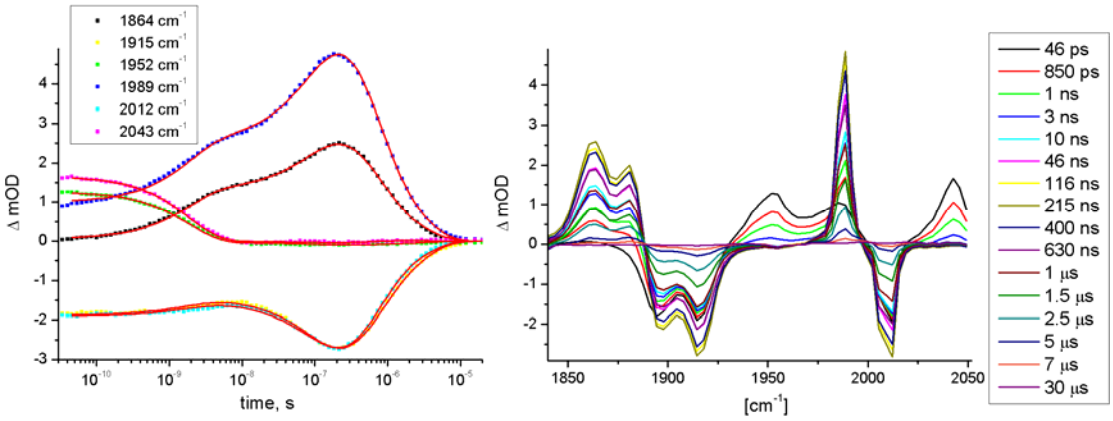

Figure 44. Spectral changes in the IR region showing characteristic ν_{CO} of **10** upon a 415 nm laser pulse (1 mM **10**, 0.1 M phenothiazine, DMF, Ar). Negative bands (1915 and 2012 cm^{-1}) are due to depletion of the ground state, positive bands are new transients formed after by excitation and subsequent reactions (***10** at 1952, 1989 and 2043 cm^{-1} and $\mathbf{10}^-$ at 1864 and 1989 cm^{-1}, respectively).

Possibly this behaviour is related to the structure of phenothiazine: upon one electron oxidation (localised at central N)[147] the pK_a drops significantly (~1 in MeCN)[148] and deprotonation will occur. A second electron could then be released through aromatization of the central thiazine moiety (see Scheme 23). Others have found similar fast quench rates for 10-methyl-phenothiazine.[47,149] This is related to a good match of ΔG for the reaction according to the Marcus theory of electron transfer.[47] No note is given regarding the second electron in the case of 10-methyl-phenothiazine, in contrast to our observations with phenothiazine, underscoring the difference in reactivity, as observed elsewhere.[147] As observed here, very fast back electron transfer occurs, at rates close to diffusion control.[149]

Scheme 23. Hypothetical redox sequence for phenothiazine.

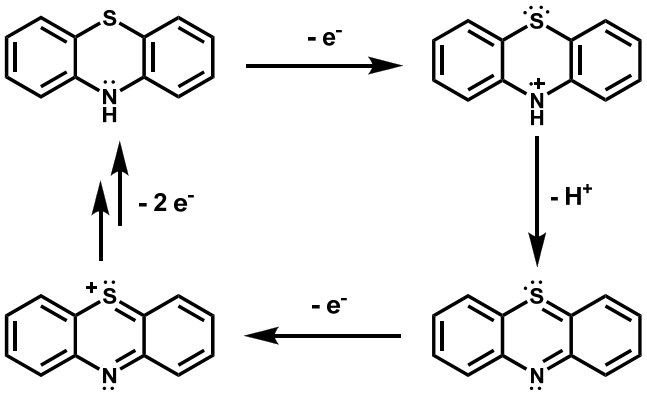

Also in the case of TEOA the transfer of a second electron was observed, although at much slower timescales.[20] This was observed before[48,52] and is related to the decomposition of once oxidised TEOA according to Scheme 24. Note that the quench process in this case is irreversible. Surprisingly, no transfer of a second electron was observed (up to 40 µs) if the same experiment was run with **13** or **33** in D_2O.

Scheme 24. Schematic representation for the oxidative degradation of TEOA.

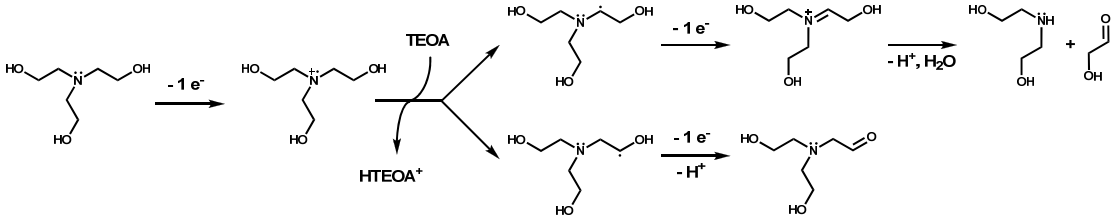

Quench rates with TEOA are almost unaffected by the type of $[ReX(CO)_3diimine]^+$ complex employed and whether DMF or water was used as a solvent (see Table 4). From the limited number of data available it seems as if though Φ_{cage} is higher in water then in DMF.

Table 4. Lifetimes and quench rates for reductive quenching with TEOA for $[ReX(CO)_3diimine]^+$ in the respective solvent.

X / diimine / solvent	τ (ns)[a]	k_q (x 10^6 $M^{-1}s^{-1}$)[b]	Φ_{cage}[c]
Br^- / bipy / DMF	42.5 (± 0.21)	64.3 (± 0.4)	0.47 ± 0.05
OH_2 / bipy / DMF	33.0 (± 0.2)	238.2 (± 3)[f]	–[h]
NCS^- / bipy / DMF	25.3 (± 0.2)	93 (± 1.3)	–[h]
CN^- / bipy / DMF[d]	63 (± 3.9)	55 (± 10)	–[h]
Br^- / phen / DMF	405 (± 1.3)	33.1 (± 0.7)	–[h]
Br^- / phenNH_2 / DMF	4.2 (± 0.10)	114 (± 12)	–[h]
Br^- / pAp / DMF	356 (± 7)	56 (± 1.4)	–[h]
Br^- / DHOCH_2bipy / DMF	50.5 (± 0.2)	40 (± 1.1)	–[h]
OH_2 / bipy / H_2O[e]	9.0 (± 0.2)	–[g,c]	–[g]
py / bipy / H_2O	202.0 (± 0.4)	50 (± 4)[c]	0.76 ± 0.03
OH_2 / phen / H_2O[e]	28.0 (± 0.2)	–[g,c]	–[g]
py / phen / H_2O	1257 (± 2)	90 (± 5)[c]	0.74 ± 0.06

[a]: measured luminescence lifetimes; [b]: according to eq. 7; [c]: as measured by time resolved FT-IR spectroscopy ; [d]: 25 % of solvato complex; [e]: measured in 1 mM TflsOH, pH = 3; [f]: possibly deprotonation and reductive quenching compete; [g]: deprotonation of exited state occurs; [h]: not measured.

The case of the two aquo complexes **11** and **31** in H_2O deserves further discussion. First of all it was noted that luminescence intensity critically depended on the pH of the solution and could be fitted to a pK_a of 8.3 ± 0.1 (see Figure 45). The two species in equilibrium are assigned to $[Re(OH_2)(CO)_3bipy]^+$ and $[Re(OH)(CO)_3bipy]$, respectively. Dimerization to $[\mu\text{-}O(Re(CO)_3bipy)_2]$ can not be precluded in the latter case. Obviously the deprotonated form does not display room temperature solution luminescence, or in other words, Φ_{phos} is considerably smaller than for the protonated form (0.25 ± 0.01).

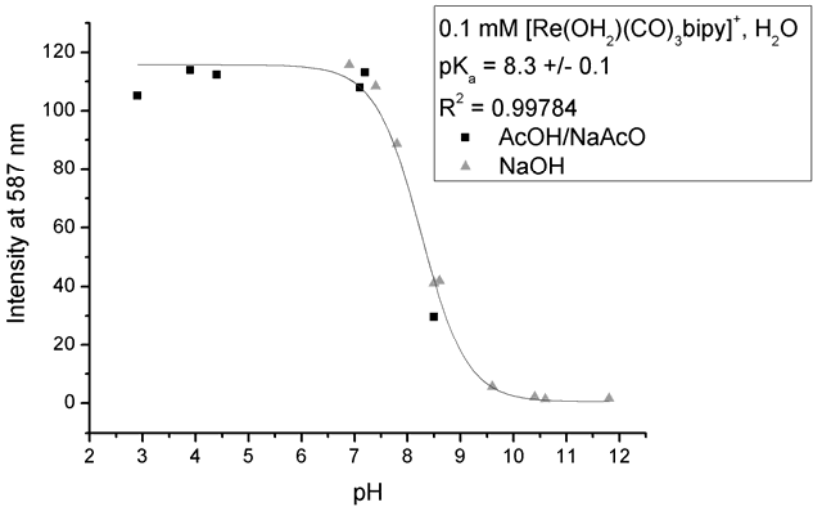

Figure 45. Dependence of luminescence on pH (0.1 mM **11**, H_2O, different buffers).

UV-Vis titration gave about the same pK_a value (8.4 ± 0.1) and confirmed the presence of two species only (see Figure 46). Interestingly, the deprotonated species exhibits similar absorbance as the complexes with π - donating axial ligands (see Figure 30). This confirmed the above assignment to a deprotonation of the axial water ligand, as OH^- is a better π - donor then OH_2. About the same pK_a value (8.6 ± 0.1) was also obtained independently by a volumetric titration with NaOH.

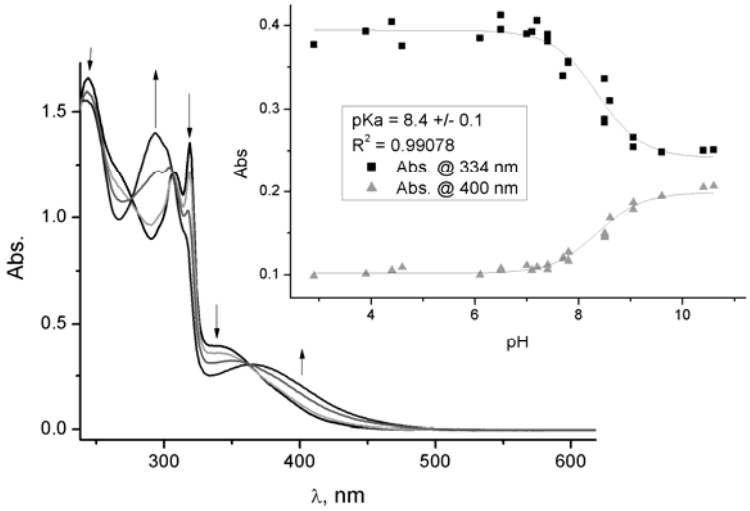

Figure 46. Spectral changes for a 0.1 mM aqueous solution of **11** upon increasing the pH.

Analysing reductive quenching by TEOA by means of traditional Stern – Vollmer plots of luminescence intensities versus quencher concentration (according to eq. 7) was thus not possible due to deprotonation of the ground state by TEOA. Time resolved FT-IR spectroscopy was thus used for **11** and **31** to establish if reductive quenching with TEOA occurred and if, to determine how fast it was. Plots of spectral changes and the characteristic ν_{CO} versus time are given in Figure 47 and Figure 48. As to be expected from the pK_a, under the experimental conditions (1 M TEOA / 0.1 M HBF_4 buffer, pH = 8.7) an equilibrium between the two protonation states occurs (~1:2). After the laser pulse prompt formation of two new species was observed, characterised by their $\nu_{CO,\,sym}$ at 2019 and 2036 cm^{-1} for **11** and 2019 and 2032 cm^{-1} for **31**, respectively. Based on the aforementioned arguments the species at lower energy is assigned to the Re-OH complex, whereas the species at higher energy is assigned to the Re-OH_2 complex. This assignment was positively tested by FT-IR of the ground state of complex **11** at varying pH. The transient of Re-OH decays with 470 ± 12 ps for **11** and 1.33 ± 0.06 ns for **31**, respectively. The transient for Re-OH_2, on the other hand, undergoes a chemical change at 6.6 ± 0.8 ns resp. 4.8 ± 0.6 ns for **11** and **31** to lower energies. This would be expected for reductive quenching by TEOA, but on the other hand we see as well disappearance of the latter species on 61 ± 34 resp. 72 ± 24 ns for **11** and **31**. This would be unexpected for electron transfer to cobalt, as it is above diffusion control ($\tau_{min,diff.controlled.}$ = 200 ns). Back

electron transfer to $TEOA^+$ was not observed so far. Furthermore, from the diffusional limit of $k_{2.order}$ in H_2O (~10^{10} $M^{-1}s^{-1}$) and since $[*PS]_{max}$ = 50 µM, τ_{min} is 10 µs. This is much longer then the observed times.

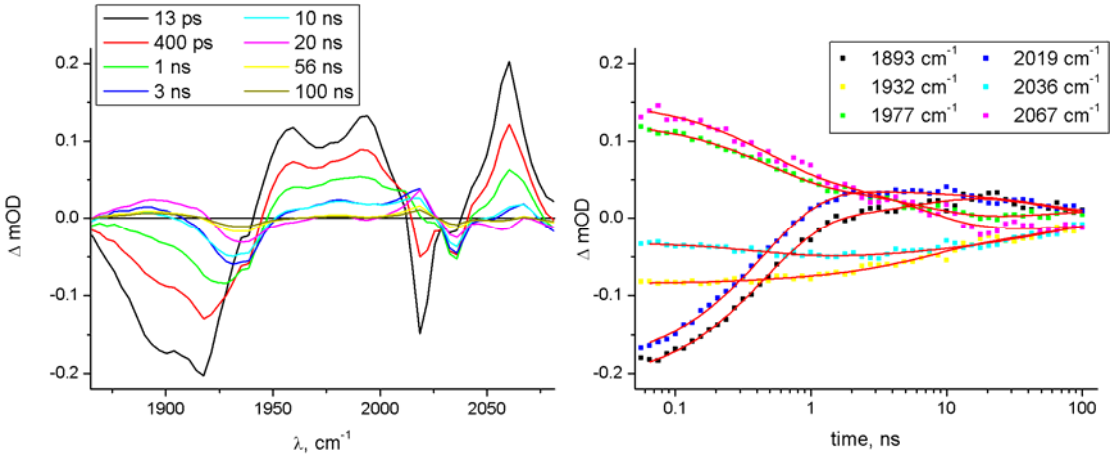

Figure 47. Spectral changes in the IR region following a 400 nm laser pulse (0.5 mM **11**, 0.5 mM **72**, 1 M TEOA, 0.1 M HBF_4, 95 % D_2O).

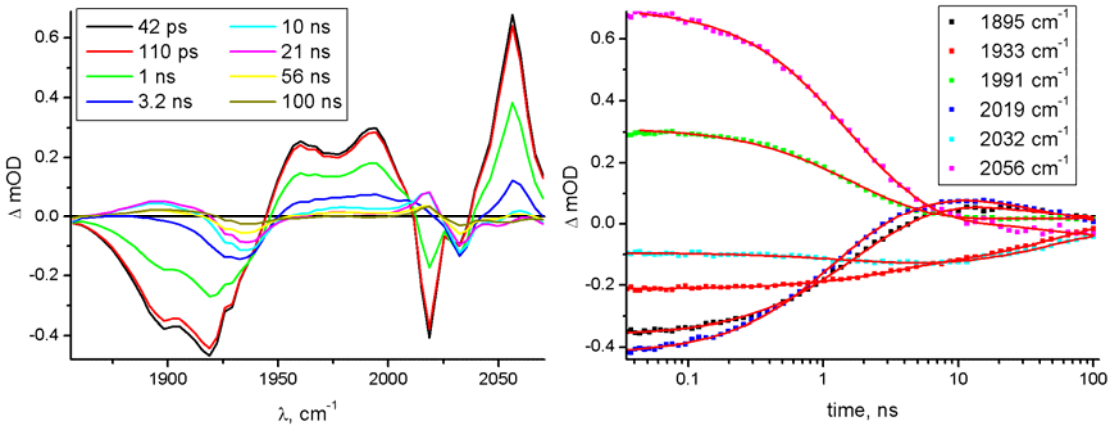

Figure 48. Spectral changes in the IR region following a 400 nm laser pulse (0.5 mM **31**, 0.5 mM **72**, 1 M TEOA, 0.1 M HBF_4, 95 % D_2O).

Alternatively deprotonation of the excited state can be considered. This would certainly explain the shift to lower energies, but also the rapid relaxation to the ground state, as reprotonation can occur by solvent. As the formal oxidation state of rhenium in the excited state is two, a significantly lower pK_a would be predicted for the excited state as compared to the ground state. Measurements of excited state lifetime as a function of pH would thus allow determining the pK_a of the excited state. Further studies on the system might help to develop a photo acid that is activated by visible light. Generally

speaking quenching by TEOA in the case of the aquo complexes occurs, but is not of reductive nature and thus not of interest for photocatalysis.

Quenching of **10** by $Co(AcO)_2.4H_2O$, as described in Figure 42, was investigated since it was of relevance in photocatalysis (see section 2.4 and 2.5). It is assumed to be ascribable to triplet-triplet annihilation.[150]

Quenching of **10** by MV^{2+}, as described in Figure 42, was investigated as an example for oxidative quenching. It is expected to be of oxidative nature due to the redox potentials of MV^{2+}. Time resolved FT-IR confirmed this hypothesis (Figure 43), as formation of a new species with absorbance at higher energies than the ground- and excited state was observed (namely at $\nu_{CO,\ sym}$ = 2086 cm^{-1}). Oxidative quenching by MV^{2+} (and other reductive resp. oxidative quenchers) was described before for $[ReCl(CO)_3phen]$ in MeCN.[47]

Table 5. Quench rates as obtained from Stern – Vollmer analysis of lifetimes of ***12** in DMF vs [Co]**.**

Quencher	k_q, ($\times 10^9$ M^{-1} s^{-1})[a]	E (V vs Ag/AgCl)[b]
$[Co^{III}(py)_2(dmgH)_2](PF_6)$ (**71**)	2.86 ± 0.16	-0.24 (E_{pc}, $Co^{III/II}$)
$[Co^{III}Cl(py)(dmgH)_2]$ (**74**)	2.05 ± 0.04	-0.61 (E_{pc}, $Co^{III/II}$)
$[Co^{II}(solv)_2(dmgH)_2]$	1.23 ± 0.02	-1.04 ($Co^{II/I}$)

[a]: DMF, 1 mM **12**, 60 mM $dmgH_2$; [b]: 0.1 M $[TBA](PF_6)$, DMF.

Quenching of **12** by $[CoX_2(dmgH)_2]$ – type complexes was of interest for photocatalysis. It was investigated by means of time resolved luminescence spectroscopy, since a direct measurement according to eq. 7 was not possible due to absorption of the cobalt complexes at the concentrations of quencher required (1 – 10 mM). The results are summarized in Table 5. It is assumed that, at least for **71** and **74**, oxidative quenching is operative, as found before.[27] For the complex $[Co^{II}(solv)_2(dmgH)_2]$ both oxidative and reductive quenching along with energy transfer could be operative. Further analysis is needed to elucidate the nature this quench processes. Nevertheless all complexes display very fast quench rates, following the trends as observed in reduction potentials.

2.2.5 Conclusion

$[ReX(CO)_3diimine]^+$ represents a very versatile building block for an light absorbing and conversion unit. A detailed understanding of its photochemistry, electrochemistry, synthesis and stability allows the design of tailored antennas for solar energy conversion schemes. Key features include the ease of assembly, the tuneability of its derivatives by variations of the diimine and axial ligands and the match of reduction- and oxidation potential to water splitting.

Variation of diimine allows to fine tune the LUMO of the complexes. Acceptor- or donor substituent's at the bipyridine moiety decrease resp. increase the bipy based LUMO, thus shifting the MLCT into the red resp. blue. The lifetimes of the conjugates follow the energy gap law. Extending the diimine from bipy to phen only slightly affects absorption, because the MLCT is related with a bipy based MO, which is no longer the LUMO for diimine = phen etc. The actual LUMO (from where emission occurs) is located further away from the rhenium core on the extended diimine, thus spatially separating the hole and the electron, thus giving rise to longer lived charge separated states. This significantly affects lifetime, but goes with a relative small change in reduction potential end emission wavelength.

The axial ligand X influences the rhenium based HOMO of the complex. An electron donor resp. acceptor ligand increases resp. decreases the HOMO energy, thus shifting absorption into the red resp. blue. This can have a tremendous effect on lifetime, but also on absorption. It is shown that here as well the energy gap law is valid. The complex with the highest lifetime was $[Re(CNBz)(CO)_3phen](OTfls)$ (**35**) with close to 13 µs in H_2O, the shortest was $[Re(OH_2)(CO)_3bipy](OTfls)$ (**11**) with about 9 ns in H_2O. The complex with the highest energy transition was $[Re(CNBz)(CO)_3bipy](OTfls)$ (**15**) with 340 nm and the one with the smallest transition $[Re(py)(CO)_3(DMeCO_2bipy)](OTfls)$ (**62**) with 380 nm.

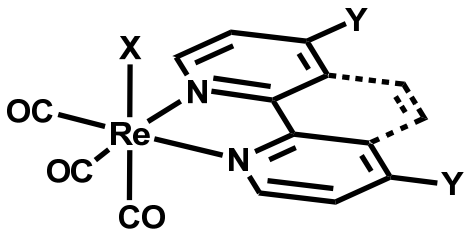

Figure 49. General representation of [ReX(CO)$_3$(4,4'-Y$_2$-diimine)].

The only photolabile complex was [Re(CNBz)(CO)$_3$phen](OTfls) (**35**) in DMF, possibly due to it's high lifetime. More serious is the situation with catalytic intermediates in photochemistry such as PS^+ or PS^-. Whereas for both species no decomposition was observed up to 40 µs by time resolved methods, no PS^+ was stable on the CV timescale (ms and above). Some of the PS^- showed decomposition below 1 ms as well (eg. **10** in DMF and **13** in H_2O), others were at least stable for seconds (eg. **30** and **12** in DMF). Thus fast reaction with a substrate will be crucial for photocatalysis.

2.3 Introduction to Cobaloximes

Cobaloximes of the general formula $[CoXY(dmgH)_2]$ ($dmgH_2$ = dimethylglyoxime), but also $[CoX_2DOH]$ (DOH_2 = 2,3,9,10-tetramethyl-1,4,8,11-tetraazaundecane-1,3,8,10-tetraene-1,11-diol) and $[CoX_2TIM]$ (TIM = 2,3,9,10-tetramethyl-1,4,8,11-tetraazacyclotetradeca-1,3,8,10-tetraene) were used as water reduction catalyst's (WRC's) in photocatalytic hydrogen production (see section 2.4 – 2.7). Several key prerequisites for a WRC to do so can be defined: matching redox potentials for proton reduction (overpotential), mechanistic pathway for oxidative addition of H^+ resp. reductive elimination of H_2, thermodynamic stability of the catalyst and kinetic inertness during catalysis. The following section will highlight this various aspects mainly for the family of cobaloximes.

2.3.1 Electrochemistry

Figure 50 displays a typical cyclic voltametry (CV) experiment for a cobaloxime, in this case $[Co(py)_2(dmgH)_2]PF_6$ (**71**), in DMF. Two reduction stages occur, from Co^{III} to Co^{II} and from Co^{II} to Co^{I}.

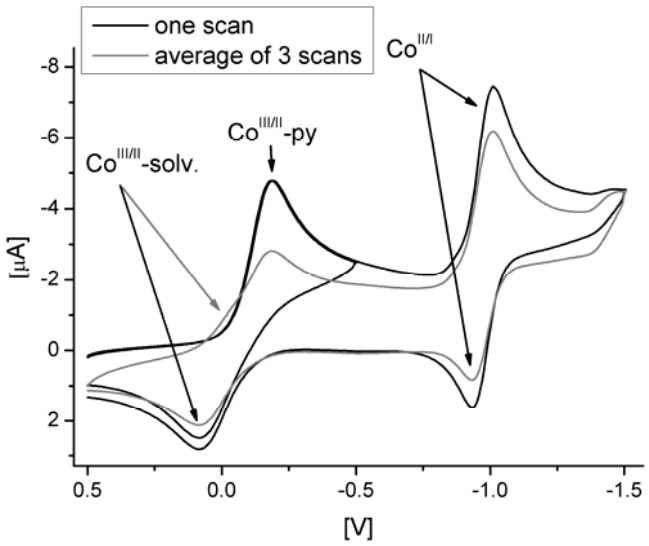

Figure 50. Cyclic voltametry on a 1 mM solution of **71** in DMF, 0.1 M $[TBA]PF_6$, N_2, 0.1 V/s (E_{pc} ($Co^{III/II}$-py) = -0.24 V, $E_{1/2}$ ($Co^{II/III}$-solv.) = -0.03 V, $E_{1/2}$ ($Co^{II/I}$) = -1.03 V; $Fc^{0/+}$ at 500 mV).

The first reduction from Co^{III} to Co^{II} is irreversible, as judged from the peak separation to the reoxidation wave (ΔE = 260 mV), whereas the second reduction is reversible (ΔE = 84 mV). It is assumed[35] that the first reduction results in loss of one axial pyridine and formation of $[Co^{II}(solv)py(dmgH)_2]$. Consequently, if several scans on the system are averaged (Figure 50, grey line) a new shoulder at -0.07 V appears, attributable to the reduction of $[Co^{III}(solv.)py(dmgH)_2]^+$. Thus the loss of pyridine from **71** is reversible, and an equilibrium is achieved if the experiment is cycled, resulting approximately in a ratio of 1:4 $[Co^{III}(solv)py(dmgH)_2]^+$: $[Co^{III}(py)_2(dmgH)_2]^+$. Further investigations on the association of pyridine are given in section 2.3.3.

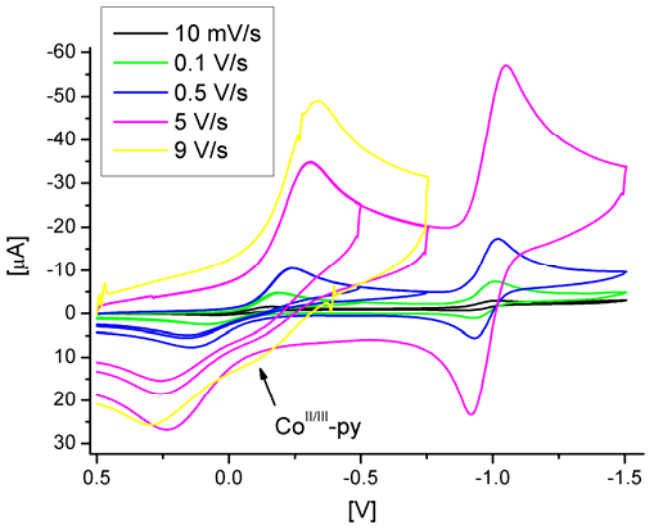

Figure 51. CV on a 1 mM solution of **71** in DMF, 0.1 M $[TBA]PF_6$, N_2, varying scan speed.

If, on the other hand, scan speed is varied (Figure 51), a new anodic peak at -0.17 V, attributable to the oxidation of $[Co^{II}(py)_2(dmgH)_2]$, is observed from 5 V/s upwards. In other words, the dissociation of pyridine occurs on a timescale faster than 200 ms.

Scheme 25. Summary of observations regarding the electrochemistry of **71** in DMF.

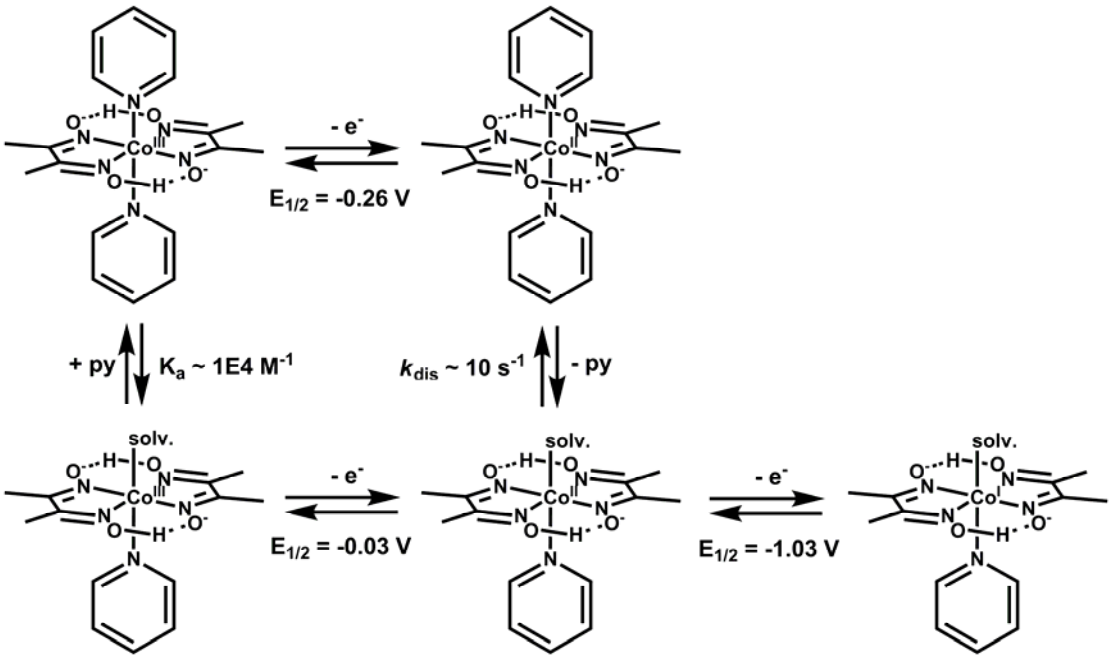

The example of **71** is characteristic for the electrochemistry of cobaloximes. Scheme 25 gives a summary of these results. If one axial pyridine is replaced by Cl^- or Br^-, as in **74** and **73**, respectively, only the position of the first cathodic peak changes (Table 6), in accord with the mechanism as pointed out before, only that now Cl^- or Br^- dissociates from reduced **74** and **73**, respectively, instead of pyridine as in reduced **71**. Consequently the position of the anodic peak resp. the half potential for the $Co^{II/I}$ couple do not change.

Table 6. Summary of electrochemical parameters for **71**, **73** and **74**, respectively, in DMF containing 0.1 M [TBA]PF_6 (referenced to $Fc^{0/+}$ at 0.50 V).

$[Co^{III}Xpy(dmgH)_2]^+$	E_{pc} ($Co^{III/II}$-X), V[a]	E_{pa} ($Co^{II/III}$), V[a]	$E_{1/2}$ ($Co^{II/I}$), V[b]
X = py (**71**)	-0.24	0.02	-1.03
X = Br (**73**)	-0.47	0.07	-1.02
X = Cl (**74**)	-0.61	0.01	-1.04

[a]: E_{pc} and E_{pa} are the peak potentials of the cathodic and anodic peaks, resp.; [b]: half wave potential.

2.3.2 Proton Reduction Electrocatalysis

In photocatalytic water reduction the WRC will be reduced photochemically to an oxidation state low enough for proton reduction. WRC's alone can be investigated for this ability electrochemically. Thus, if a certain amount of acid of a specific pK_a is added to a CV experiment as described in section 2.3.1, catalysis is expected to take place. This is manifested in the CV spectra by a catalytic peak at a potential where it would not appear if no WRC was added to the solution. The exact position of the catalytic wave with respect to the reduction waves of the parent WRC complex, its shape and its dependence on [acid] and scan speed thus all bear further information regarding the kinetics of H_2 evolution.[34,151]

Scheme 26. Schematic representation of proton reduction catalysed by $[Co(dmgH)_2]$ – type complexes. The smaller cycle represents the pathway via homolytic, the bigger via heterolytic H_2 release.

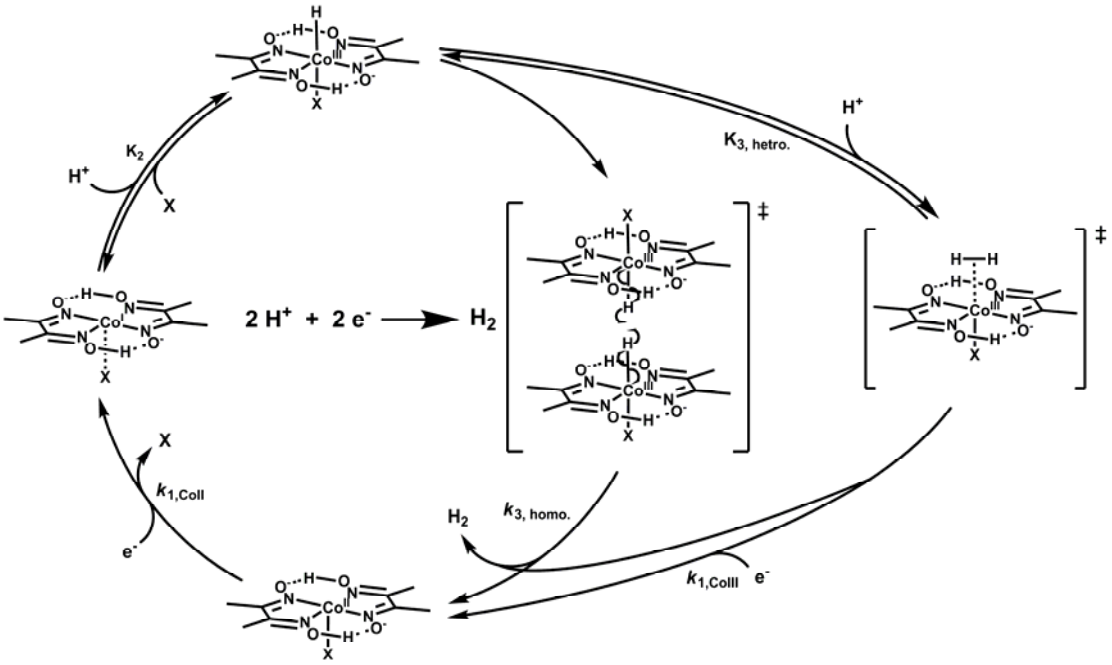

As many of the WRC's studied herein have already been assayed electrochemically,[34,35] no detailed kinetic analysis of the voltagrams will be given, but rather a yes / no answer whether or not proton reduction by these

WRC's works. A general pathway to protonreduction, either by a homolytic or by a heterolytic H_2 formation step, is given in Scheme 26.

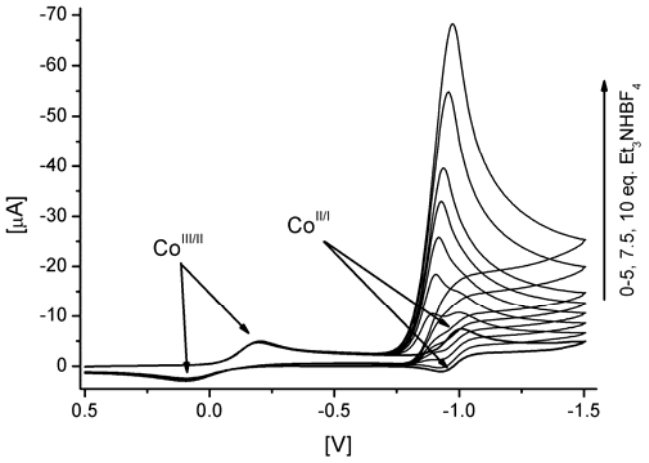

Figure 52. 1 mM $[Co(py)_2(dmgH)_2]PF_6$ (**71**) in 0.1 M $[TBA]PF_6$, DMF, varying amounts of $[Et_3NH]BF_4$.

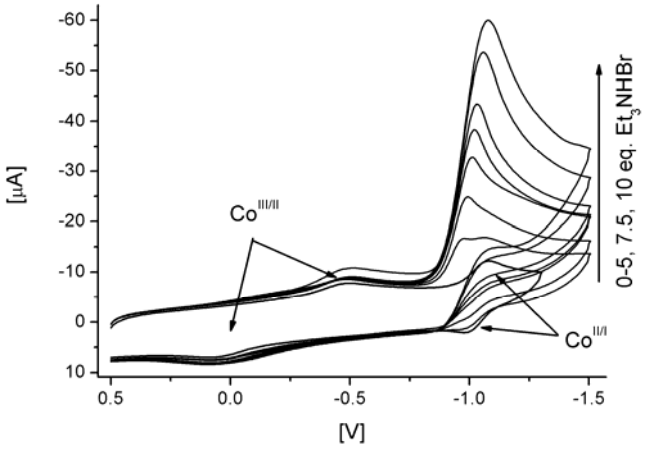

Figure 53. 1 mM $[CoBr(py)(dmgH)_2]$ (**73**) in 0.1 M $[TBA]PF_6$, DMF, varying amounts of $[Et_3NH]Br$.

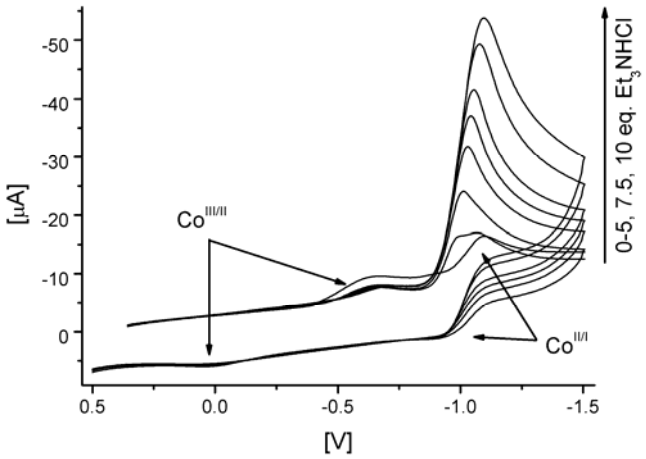

Figure 54. 1 mM $[CoCl(py)(dmgH)_2]$ (**74**) in 0.1 M $[TBA]PF_6$, DMF, varying amounts of $[Et_3NH]Cl$.

Figure 52 – Figure 54 show electro catalysis of proton reduction by **71**, **73** and **74**, respectively. As $[Et_3NH]^+$ is added, a catalytic wave is observed on the onset of the $Co^{II/I}$ couple, indicating proton electro reduction to take place. As $c([Et_3NH]^+)$ is increased, the catalytic wave increases, indicating that diffusion of $[Et_3NH]^+$ to the electrode is limiting the process. The catalytic peak then levels off for $c([Et_3NH]^+) > 10$ mM, indicating that now the catalyst becomes rate limiting. It has been shown before that the mechanism for H_2 release for these complexes can be both heterolytic and homolytic, depending on the solvent and concentration of acid and catalyst.[34,35,41]

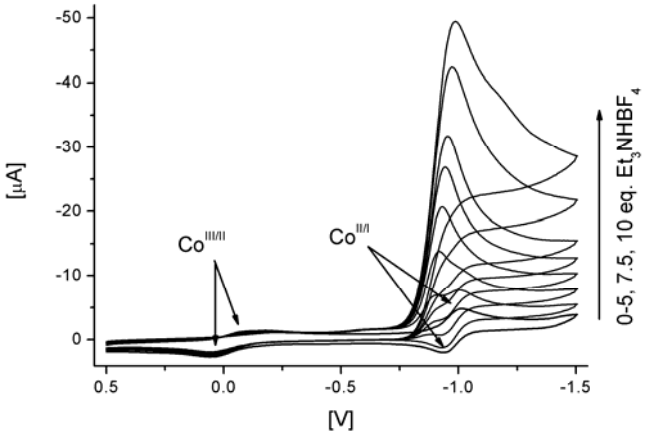

Figure 55. DMF, 0.1 M $[TBA]PF_6$, 1 mM **70**, 2 mM pyridine and varying amounts of $[Et_3NH]BF_4$.

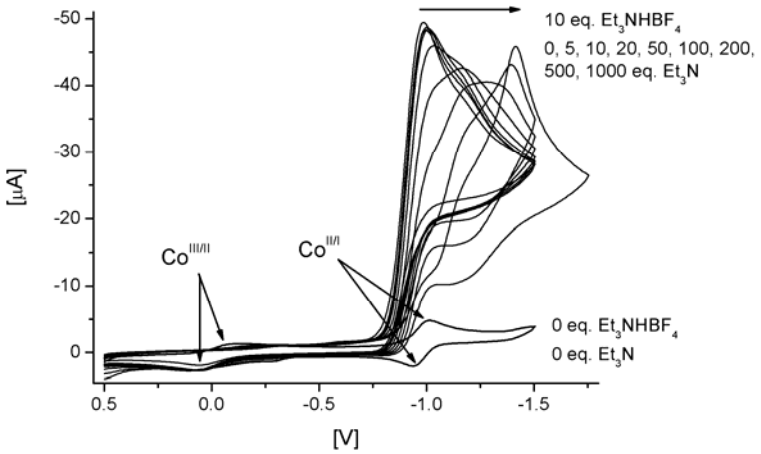

Figure 56. DMF, 0.1 M $[TBA]PF_6$, 1 mM **70**, 2 mM pyridine, 10 mM $[Et_3NH]BF_4$ and varying amounts Et_3N.

Figure 55 and Figure 56 show proton electro reduction by a 1 mM solution of $[Co(OH_2)_2(dmgH)_2]$ (**70**) in the presence of pyridine. The experiment resembles that with **72**, thus indicating pyridine coordination to **70**. Again c($[Et_3NH]^+$) was increased to 10 mM, giving rise to an increase in peak current (Figure 55). Addition of Et_3N to the latter experiment will increase the pH of the solution. Simultaneously a shift in the position of the catalytic wave occurred (Figure 56). This indicates that a modified route to H_2 is operative at these conditions. None of the two mechanisms as proposed in Scheme 26 accounts for the fact that the catalytic wave is now shifted cathodically with respect to the $Co^{II/I}$ couple. An explanation could be the mechanism as proposed in Scheme 27 and as postulated for similar systems before.[28,34] Thus the new wave could be attributed to the reduction of Co^{III}-H to Co^{II}-H. These results are of particular relevance when comparing to photocatalysis in section 2.4 and following, where similar buffers were used.

Scheme 27. Schematic representation of the alternative heterolytic cycle via Co^{II}-H.

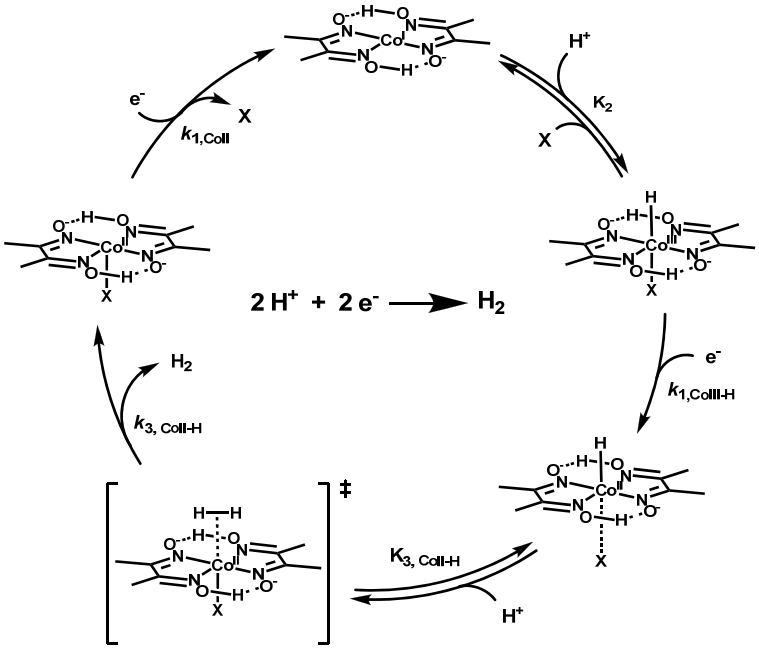

The situation in H_2O solvent is more complex, although the pH is much better defined. If a CV on $[Co(py)_2(dmgH)(dmg)]$ (**72**) is run in 0.1 M KNO_3 electrolyte only, the same result as in a buffered experiment in Figure 57 for pH 9.92 was obtained, even though the pH in the former experiment was only 8.65. This clearly indicated the need for a buffer in H_2O, as electro catalysis otherwise changes the pH locally at the electrode too rapidly.

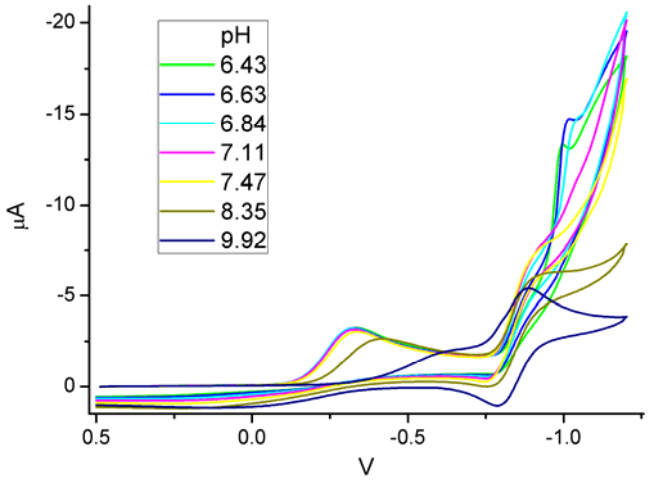

Figure 57. CV of **72** in H_2O, 1 M PO_i, pH as indicated.

Thus an experiment in phosphate buffer was performed (Figure 57). At pH 9.92 no catalysis took place, as can be seen by the absence of a catalytic

wave and from the reversible $Co^{II/I}$ couple. Since the pK_a for the $[Co(py)_2(dmgH)(dmg)]$ / $[Co(py)_2(dmgH)_2]^+$ couple is 7.4, the deprotonated form will be the dominant species at pH 9.92. If the pH was slowly lowered, the shape of the CV respondent promptly: there is an anodic shift in the $Co^{III/II}$ couple, as to be expected from its pK_a (the protonated form should have a higher E_{pc} ($Co^{III/II}$) than the deprotonated one, judging simply from it's charge). On the other hand, the $Co^{II/I}$ couple was no longer fully reversible. Judging the shape of the catalytic wave is difficult due to the appearance of a peak (tail) caused by proton reduction at the glassy carbon electrode at only modestly lower potentials than the $Co^{II/I}$ couple. Nevertheless it seemed as if catalysis did take place in H_2O solvent for the protonated form of **72**, but only in buffered solution where pH can be assumed to be constant. It would be interesting to repeat those experiments with varying concentration of buffer and with buffer's at varying pH's. Preliminary results showed, to our surprise, that **72** remains stable down to a pH of 3.

2.3.3 Stability of the WRC

The stability of $[Co(dmgH)_2]$ was of particular interest for photocatalysis. Thus the complexation of Co^{II} by $dmgH_2$ was studied by differential pulse amperometry according to eq. 14 and 15.

$$Co^{II}(AcO)_2.4H_2O + 2\ dmgH_2 \rightarrow [Co(dmgH)_2] \quad (14)$$

$$K_{cond} = \frac{[Co(dmgH)_2]}{[Co(AcO)_2][dmgH_2]^2} \quad (15)$$

If the titration curve in Figure 58 was fitted according to eq. 15, a conditional equilibrium constant of 10^6 M^{-2} was obtained. In other words, at 1 mM $Co(AcO)_2.4H_2O$ and 6 mM $dmgH_2$, $[Co(dmgH)_2]$ accounts for 95 % of all cobalt. Interesting was the fact that the same K_{cond} was obtained no matter if neat DMF or 1 M TEA in DMF were used. The reason for this might be the relatively high pK_a of AcO^- in DMF (13),[133] which facilitates proton uptake from the complex formed.

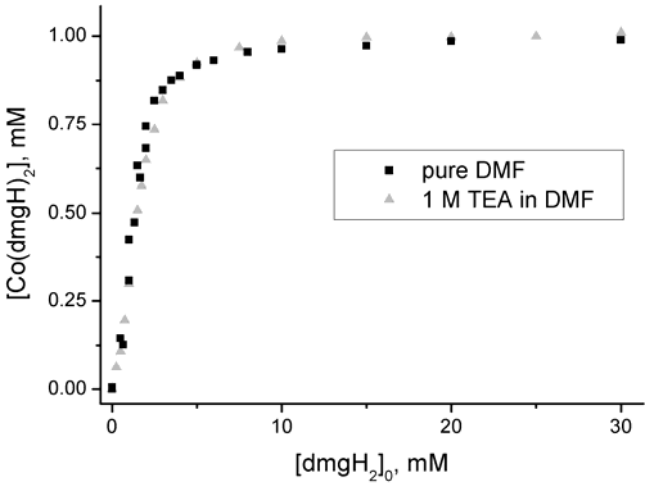

Figure 58. Titration of 1 mM $Co(AcO)_2.4H_2O$ with $dmgH_2$ in 0.1 M $[TBA]PF_6$, DMF (I_{pc} of the $Co^{II/I}$ couple in the DP mode served as a reference to concentration of $[Co(dmgH)_2]$).

2.4 The first Example of a three component System using a Rhenium type Photosensitiser as Photocatalyst to produce Hydrogen

This section refers to Appendix I. The publication showed for the first time that [ReBr(CO)$_3$bipy] (**10**) acts as PS for in a three component system using [Co(dmgH)$_2$] and TEOA in DMF.[21] Hydrogen production in this scheme using [Ru(bipy)$_3$]$^{2+}$ was observed before.[37] It was shown however, that the rhenium based PS is superior to the ruthenium based PS in terms of turn over numbers (TON), possibly resulting from improved stability of the PS. Further highlights were the detailed kinetic analysis of the PS cycle by time resolved FT-IR analysis, the mechanistic insights into the WRC cycle obtained by studying the dependence of H_2 production on c([Co(dmgH)$_2$]), the determination of the quantum yield and proof of the homogenous character of the reaction.

The paper thus presents an important contribution to the field of homogenous, photocatalysed decomposition of water into O_2 and H_2. Although only published in 2009, its track of citations shows that is has been well taken up by the community. Notably is also the fact that the new kinetic methods have become standard to the study of such systems.[27,30]

2.4.1 Summary of Probst, B. *et al.*, *Inorg. Chem.* 2009, *48*, 1836.

It could be shown that, under otherwise identical conditions, the [ReBr(CO)$_3$bipy] (**10**) PS is superior to [Ru(bipy)$_3$]$^{2+}$ PS in terms of H_2 yield (TON_{Re} = 300 vs TON_{Ru} = 140) after 9 h of irradiation with visible light ($\lambda \geq$ 400 nm), as shown in Figure 1 of Appendix I. Further analysis showed that H_2 production in the new system proceeded by reductive quenching of the PS ($k_q = 6 \times 10^7$ M^{-1}s^{-1}), electron transfer to Co^{II} ($k_1 = 2.5 \times 10^8$ M^{-1}s^{-1}), protonation of Co^{I} (K_2) and subsequent H_2 release second order in cobalt ($k_{2.order}$), as depicted in Scheme 28.

Scheme 28. From Appendix I, Scheme 2.

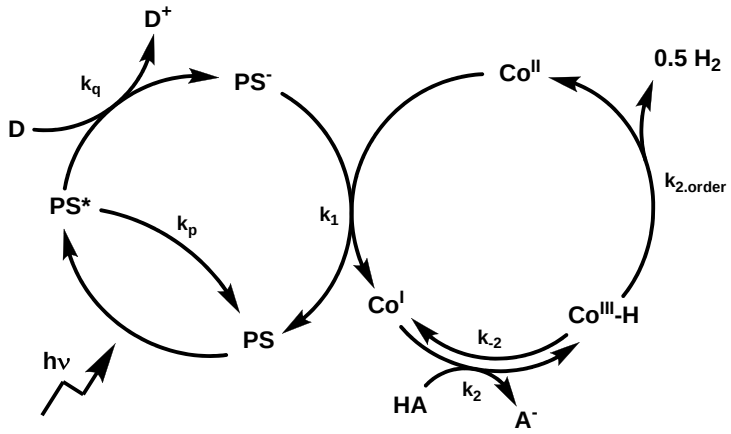

Apart from the traditional methods (luminescence lifetime measurements by photon counting, Stern Vollmer analysis of luminescence intensities as a function of [TEOA]) to determine k_p and k_q, time resolved FT-IR was applied to study the rhenium cycle. This allowed, apart from a confirmation of k_p and k_q, the determination of k_1, the forward electron transfer to Co^{II} (see Figure's 2 and 3 in Appendix I). The cage escape yield for reductive quenching was determined by an exact analysis of the time resolved FT-IR data (Φ_{cage} = 0.4). Further on the cycle, a second order dependency of H_2 production on $[Co]_{tot}$ was found (see Figure 4, Appendix I), indicating that the final H_2 release step is a concerted homolytic cleavage of two Co^{III}-H bond's. Interesting was also the observation that a plateau in H_2 production rate is reached if [Co] was increased above 1 mM. It could be shown that this was related to photon flux control of the reaction (see SI 1, SI 5 in Appendix I). A further observation concerns the fact that a strong dependence was found on [$dmgH_2$]. As mentioned before (2.3.3), the formation of [$Co^{II}(dmgH)_2$] from $Co(AcO)_2.4H_2O$ and $dmgH_2$ in DMF has a K_{cond} of 10^6 M^{-2}. This alone could not explain the dependency of H_2 production on [$dmgH_2$] (see Figure 5, Appendix I). It was found though that $Co(AcO)_2.4H_2O$ is an efficient quencher of *PS ($k_q = 2.6 \times 10^9$ $M^{-1}s^{-1}$), and thus did not only the incomplete formation of [$Co^{II}(dmgH)_2$] at low [$dmgH_2$] decrease H_2 production rate, but also quenching of *PS by $Co(AcO)_2.4H_2O$. The acid used in this system was AcOH, and a strong dependency on its concentration was found (see Figure 6, Appendix I). Interesting was the observation that, apart from the dependency on the H_2

production rate, catalysis performed much more constant over the tested time range of 9 h when low [AcOH] were used. Within a linear correlation between H_2/s and hv/s a quantum yield of 0.25 was obtained by two independent methods (see section 3, Appendix I). The homogenous character of the system was shown by light scattering experiments (see SI 6, Appendix I).

2.4.2 Further Observations

As for the [$ReBr(CO)_3$bipy] / $Co(AcO)_2.4H_2O$ / $dmgH_2$ / TEOA / AcOH / DMF system, further, unpublished observations are given below.

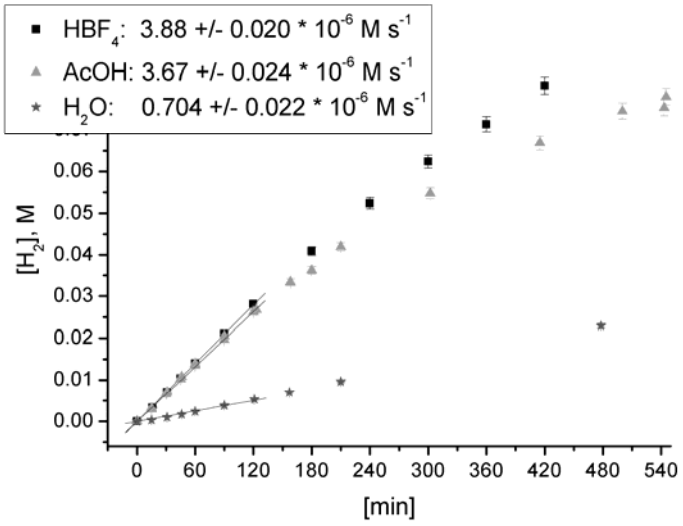

Figure 59. Dependency of H_2 production on the type of acid added (0.5 mM **10**, 1 mM $Co(AcO)_2.4H_2O$, 6 mM $dmgH_2$, 1 M TEOA, 0.1 M H^+, DMF, 10 ml, hv > 400 nm).

One observation was on the type of acid used for catalysis. Acetic acid (pK_a in DMF 13 ± 1)[133] was compared to HBF_4 (which will protonate TEOA to give [HTEOA](BF_4), pK_a TEOA in DMF = 7.5)[133] and H_2O (0.05 M). AcOH and HBF_4 perform about at the same initial rate, whereas H_2O is considerably slower. It is, however, difficult to judge if this was related to the respective pK_a's in DMF. Especially in the case of AcOH it remained unclear if AcOH itself acted as a acid for protonation of Co^I or if small concentrations of $[HTEOA]^+$, stemming from the dissociation of $[TEOA]^+$ (vide infra) are responsible for this effect. As in the case of H_2O, no pK_a value could be found

in the literature for DMF. The other observation concerned long term stability, which seems to be inferior in the case of HBF_4 as compared to AcOH.

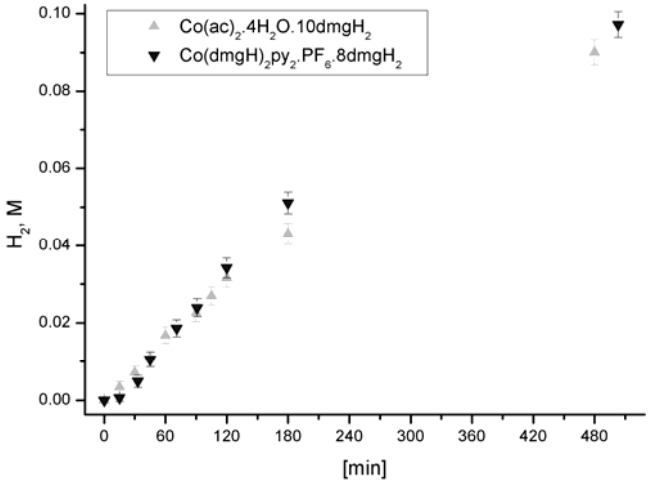

Figure 60. Comparison of H_2 production for two different WRC's (0.5 mM **10**, 1 mM Co, total 10 mM $dmgH_2$, 1 M TEOA, 0.2 M AcOH, DMF, 10 ml, hv > 400 nm).

An other interesting observation was came from using different WRC's: little difference was observed for in-situ prepared $[Co(dmgH)_2]$ and preassembled $[Co(py)_2(dmgH)_2]PF_6$ (**71**, see Figure 60), apart, maybe, from a longer induction period for the latter due to reduction of Co^{III} to Co^{II} before H_2 evolution can take off. Also if $[Co^{II}(OH_2)_2(dmgH)_2]$ (**70**), $[Co(py)_2(dmgH)_2]PF_6$ (**71**), $[Co(py)Br(dmgH)_2]$ (**73**), $[Co(py)Cl(dmgH)_2]$ (**74**) and in-situ prepared $[Co(dmgH)_2]$ were compared no significant differences could be observed.

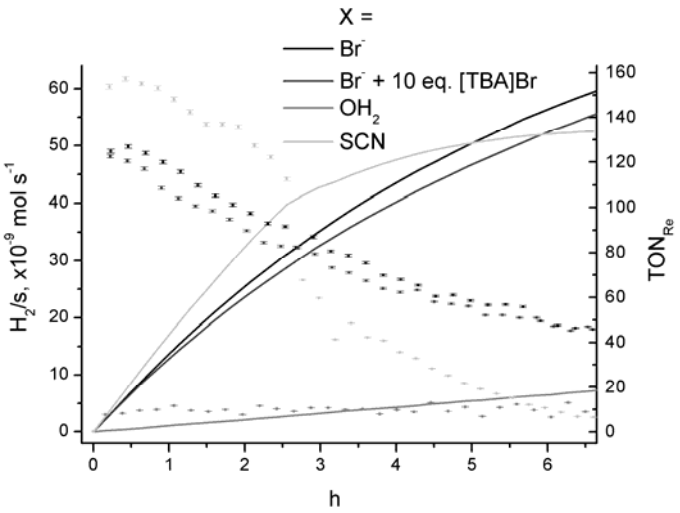

Figure 61. H_2 production with PS = **10**, **10** plus 10 eq. Br^-, **11** and **12** (0.5 mM PS, 1 mM $Co(AcO)_2.4H_2O$, 6 mM $dmgH_2$, 1 M TEOA, 0.1 M AcOH, DMF, 10 ml, hv > 400 nm). Left scale: H_2 production rates (dots), right scale: TON_{Re} (lines).

If, on the other hand, PS was varied (see Figure 61), a marked dependence was found. Whereas the addition of [TBA]Br to an experiment with **10** did not alter catalysis significantly, the use of **12** had a marked influence, resulting in higher initial rates and a reproducible, sudden stop of catalysis. The use of **11** gave very stable H_2 production over time, although at much lower rates.

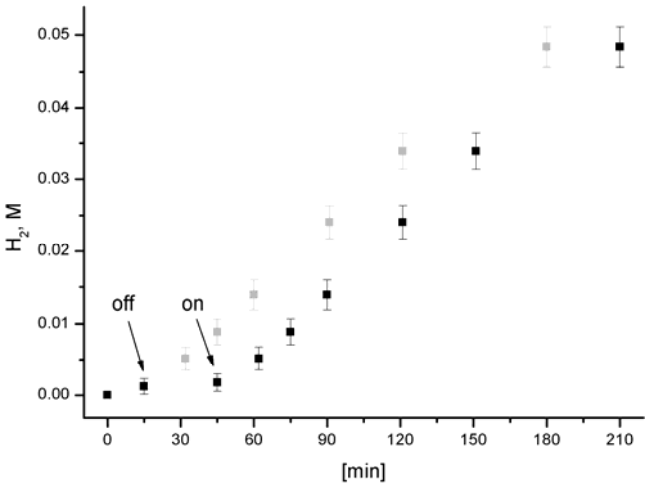

Figure 62. H_2 production curves illustrating the effect of light (0.5 mM **10**, 1 mM **71**, 4 mM $dmgH_2$, 1 M TEOA, 0.2 M AcOH, DMF, 10 ml, hv > 400 nm).

The effect of light is illustrated in Figure 62, showing that catalysis critically depends on light.

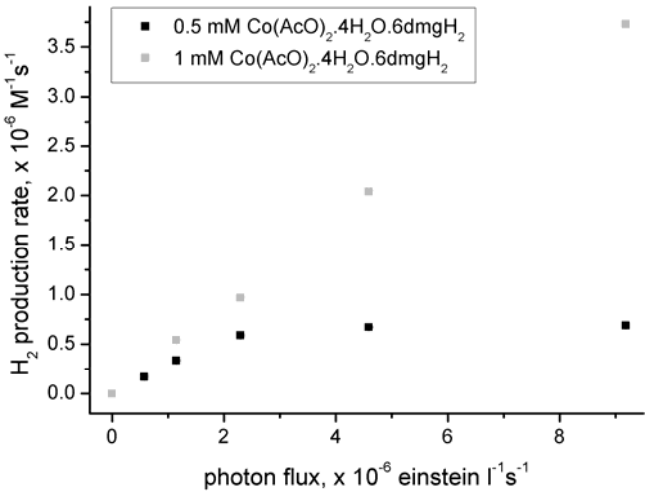

Figure 63. H_2 production as a function of photon flux (0.5 mM **10**, vary [$Co(dmgH)_2$], 1 M TEOA, 0.1 M AcOH, DMF, 10 ml).

Clearly two domains for reaction control could be identified: the one is photon flux (Figure 63, 1 mM [$Co(dmgH)_2$] and up to 2×10^{-6} einstein $l^{-1}s^{-1}$ for 0.5 mM [$Co(dmgH)_2$]) and the other a cobalt dependence assigned to the homolytic Co^{III}-H cleavage, as mentioned before (Figure 63, 0.5 mM [$Co(dmgH)_2$], from 2×10^{-6} einstein $l^{-1}s^{-1}$ upwards). This observation is of relevance for future applications, because only if catalysis is run under photon flux control a stable system can be achieved. This because otherwise one of the catalytic intermediates will eventually accumulate, and for all involved states the ground state is the most stable configuration. Also, of course, quantum yield is affected if catalysis is not performed under photon flux control.

2.5 Improved long-term Stability in Photocatalysis by a three Component System to produce Hydrogen

This section refers to Appendix II. In the mean time since the publication of our last work[21] several studies on the reductive photocatalytic half-reaction to H_2 in three component systems appeared.[19,22,23,25,27,29-33] As already pointed out before, we observed changes in long-term stability related to the type of acid and to the type of PS used. Furthermore, we were now set to do long-term studies over several days thanks to an automated setup for H_2 measurements. This work was though devoted to the analysis of long-term stability. We could show that in the previous system catalysis was limited by the decomposition of **10** due to the presence of AcO^-. Thus significantly higher turnovers in rhenium were achieved by using the more stable analogue **12** ([ReNCS(CO)$_3$bipy]) along with the [HTEOA]BF_4 buffer system, which besides the avoidance of AcO^- gave the benefit of having a much more defined proton source. All together turnovers in rhenium above 6000 (H/Re) could be obtained. We could show that catalysis is now limited by the cobalt WRC (no more than TON_{Co} = 1000 could be obtained, H_2/Co). Furthermore we showed again that catalysis proceeded by reductive quenching of ***12** by TEOA ($k_q = 9 \times 10^7$ $M^{-1}s^{-1}$) and subsequent electron transfer to [$Co^{II}(dmgH)_2$] ($k_1 = 1.3 \times 10^8$ $M^{-1}s^{-1}$). Thanks to an improved setup for time resolved FT-IR we could further show that decomposition of oxidised TEOA results in the transfer of a second electron to **12**. Again a quadratic dependence on $[Co]_{tot}$ was found and indicated that H_2 release occurred by a homolytic splitting of the Co^{III}-H bond. The same dependence of H_2 production rate as before on [$dmgH_2$] was found, but furthermore also an interesting dependence of TON_{Co} on $dmgH_2$ was observed. This along with a detailed study of the decomposition of PS, WRC and $dmgH_2$ during catalysis clearly indicated that the instability of WRC is caused by $dmgH_2$ consumption, supposedly by a intramolecular hydride shift in Co^{III}-H. A quantum yield of 0.9 was measured. We confirmed again the homogenous character of the experiments by mercury poisoning studies.

2.5.1 Summary of Probst, B. *et al.*, *Inorg. Chem.* 2010, *49*, 6453.

A comparison of catalysis using **10** and **12** is given in Figure 1 of Appendix II. Clearly the use of HBF_4 and **12** are superior to the combination **10** and AcOH. It was shown that in the latter case efficient decomposition of **10** into a solvato / acetato adduct occurred. Up to 2000 turnovers were now possible in PS, as compared with 300 for **10** and AcOH. It was of interest to compare electron transfer from $\mathbf{12}^-$ to Co^{II} with electron transfer from $\mathbf{10}^-$ to Co^{II}. As expected the rate was only slightly smaller ($k_{1,NCS}$ = 1.3 × 10^8 $M^{-1}s^{-1}$ vs $k_{1,Br}$ = 2.5 × 10^8 $M^{-1}s^{-1}$). This difference was readily explained by the Marcus Theory of electron transfer (Appendix II, section 'electron transfer steps'). Interesting was the observation that a second electron was transferred to **12** on a timescale of 3 µs in the absence of cobalt. This was attributed the decomposition of oxidised TEOA, and $k_{2.electron}$ = 3.3 × 10^8 $M^{-1}s^{-1}$ and a yield of 0.7 was estimated (see Appendix II, Scheme 2 and Figure 2). Decomposition of oxidised TEOA was observed before and was know to result in the release of a second electron. As the buffer system was changed it was of interest to study the dependence of H_2 production on $[Co]_{tot}$ again. A quadratic relation was found along with a higher k_{obs} than in the AcOH system (25 $M^{-1}s^{-1}$ vs. 4 $M^{-1}s^{-1}$, see Appendix II, Figure 4).

Scheme 29. General representation of photocatalysis (from Appendix II, Scheme 3).

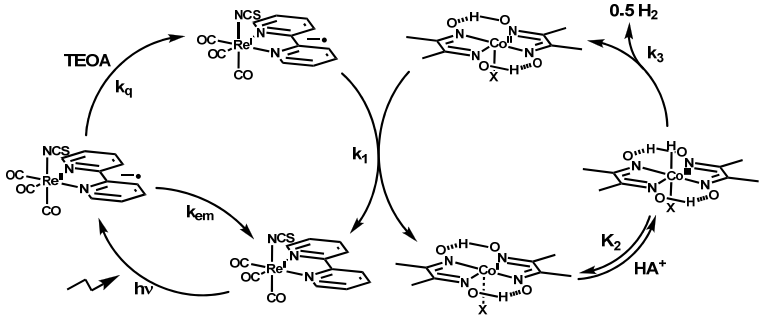

The value of k_{obs} in the new system could now be compared with equation 4 in Appendix II, thus allowing an estimate for $c \times K_2 \times k_3$ of 2025 $M^{-1}s^{-1}$ (c is the fraction of $[Co^I]$ with respect to $[Co]_{tot}$, K_2 and k_3 as indicated in Scheme 29). A pronounced dependence of H_2/s and TON_{Re} on [acid] was found. At high

[acid] TON_{Re} decreased sharply, while H_2/s remained constant. At low [acid] both TON_{Re} and H_2/s decreased. Reaction analysis during catalysis indicated that first excess $dmgH_2$ and only then PS was consumed (see Appendix II, Table 2). The dependence of initial H_2 production on [$dmgH_2$] indicated again that formation of [$Co^{II}(dmgH)_2$] in DMF is crucial for catalysis. Furthermore we could observe that, at high values of $dmgH_2$, even though at the same initial rate, higher TON_{Co} were obtained (Appendix II, SI 3). This was a further indication that consumption of $dmgH_2$ limits catalysis. If [PS] was lowered, an increase in TON_{Re} (up to 6000) could thus be observed (see Appendix II, Figure 6), indicating once more that WRC limits long-term stability. A quantum yield of 0.9 was obtained by actinometry. Mercury poisoning studies indicated that the character of the system was truly homogenous.

2.5.2 Further Observations

These observations are unpublished. Some of them are still unclear to the author. The first concerns the acid dependence (Figure 64), which is summarized in Appendix II, Figure 5.

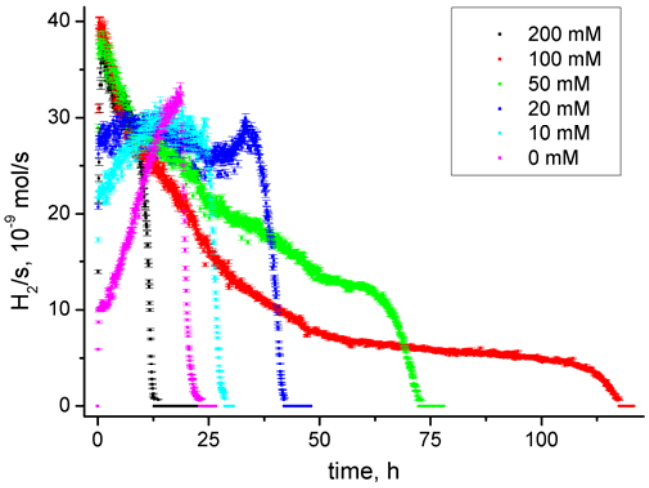

Figure 64. H_2 production rates as a function of time, as in Appendix II, Figure 5 (0.5 mM **12**, 0.5 mM $Co(BF_4)_2.6H_2O$.6$dmgH_2$, 1 M TEOA, varying amounts HBF_4 as indicated, DMF, Ar, 10 ml, 480 nm).

Appendix II, section Acid Dependence, states that at [HBF_4] ≤ 0.1 M presumably protonation of Co^I becomes rate limiting, thus resulting in low H_2 production rates. It is noteworthy however, when looking at the H_2/s profile in Figure 64, that H_2/s increases for low [HBF_4] before H_2 production suddenly stops. This abrupt stop was explained in Appendix II, Table 2 for the experiment in Figure 64, 0.1 M HBF_4, by a successive consumption of free $dmgH_2$ before [$Co(dmgH)_2$] becomes too small so that PS^- accumulates in solution and eventually decomposes. On the other hand, one might expect this to happen much earlier when comparing to Appendix II, Figure 4 and SI 3. The reason for it to take so long in certain cases (120 h in Figure 64, 0.1 M HBF_4) might be a fragile balance of production of PS^- (which becomes smaller with higher concentration of free Co^{II} due to triple-triplet quenching of *PS, see Appendix I, SI 3) and its reaction with remaining [$Co^{II}(dmgH)_2$]. It remains unclear however, why such a situation is not achieved when [$dmgH_2$] is altered (see Figure 66). It remains also unclear as to why H_2/s increases initially for low [HBF_4] in Figure 64. It seems though as if pH changes during catalysis, the reason for which remains to be explained.

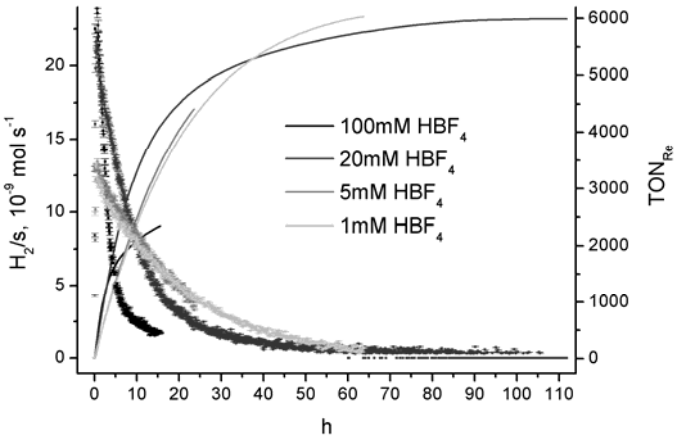

Figure 65. H_2 production profiles for different [HBF_4] at low [PS] (30 µM **12**, 500 µM $Co(BF_4)_2.6H_2O.6dmgH_2$, 1 M TEOA, varying HBF_4, DMF, 10 ml, Ar, 380 nm).

An interesting observation was made when the above experiments were run at 380 nm and 30 µM **12**. This setup was chosen because the absorption of **12** peaks at 375 nm (see Table 1) and thus allowed much lower concentration at comparable numbers of absorbed photons. Whereas an impressive TON_{Re} of 6000 was obtained, much higher values could have been expected when

comparing to the TON_{Re} of 2000 at 0.5 mM **12**, providing the cobalt WRC limits catalysis and gives fix TON_{Co}. Obviously this was not the case. Either this means the explanation for performance limitation by the cobalt WRC was (partially) wrong, or that TON_{Co} depends on the rate of H_2 production or that some other, unknown factors, changed. Interesting to note is that the initial rate displayed a different dependence on [HBF_4] as at the high concentration of **12**. Whereas before maximal TON's were obtained for 50 – 100 mM [HBF_4], best results at low [**12**] were obtained for [HBF_4] ≤ 20 mM. Very likely these two observations are related, and TON_{Co} indeed depends on the H_2 production rate. Further analysis is still required to clarify this. Nevertheless it was possible, in an extreme case, with [**12**] at 30 µM, [WRC] at 1 mM and 20 mM [HBF_4] to obtain the highest TON_{Re} measured in this system (7750). But again, if TON_{Co} was constant (as would be expected if decomposition of WRC was linear to the total H_2 produced) a TON_{Re} of 12'000 or more should have resulted.

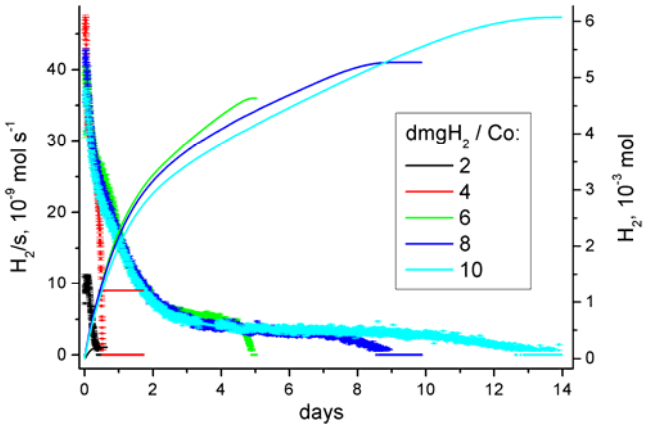

Figure 66. H_2 production as a function of [$dmgH_2$] (0.5 mM **12**, 0.5 mM $Co(BF_4)_2.6H_2O$, vary $dmgH_2$ per cobalt as indicated, 1 M TEOA, 0.1 M HBF_4, DMF, Ar, 10 ml, 480 nm).

If H_2 production profiles as a function of [$dmgH_2$] are analysed it is immediately clear that the abrupt stop of catalysis must be related to [$dmgH_2$] – the higher its concentration the longer it takes for it to be consumed and for PS decomposition to occur. One might expect though, if no other explanation is given, that H_2/s remained constant before this abrupt stop. But as noted before, H_2/s slowly decreases (in an exponential manner), no matter how much excess $dmgH_2$ was added, before the stop. This behaviour suggests

that an alternative mechanism to catalyst deactivation / modification plays, which yet needs to be unravelled. Possibly this behaviour is related to the decomposition of TEOA, a process which might change the media during catalysis (for details see Appendix II, section electron transfer). Diethanolamine, one decomposition product, might, although not a reductive quencher itself, increase the pH of the solution. In the upper case it could account for up to 0.5 M. Other decomposition products (also up to 0.5 M) were not tested, but might contribute to catalysis in their own specific manner too.

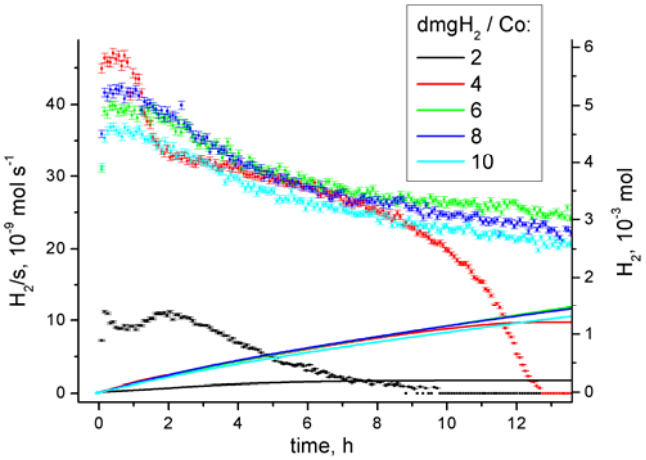

Figure 67. Magnification of Figure 66 showing [dmgH_2] dependence of H_2/s (0.5 mM **12**, 0.5 mM $Co(BF_4)_2.6H_2O$, vary dmgH_2 per cobalt as indicated, 1 M TEOA, 0.1 M HBF_4, DMF, Ar, 10 ml, 480 nm).

Another interesting observation in Figure 66 (magnified in Figure 67) concerns the experiment at dmgH_2 / cobalt = 2 (and 4): the initial rate of H_2 production displays two maxima. The author has no explanation for this behaviour.

Also, one experiment was run with all parameters as in Figure 66, but [dmgH_2] at 6 mM and $Co(BF_4)_2.6H_2O$ at 50 µM. Assuming that [$Co(dmgH)_2$] forms to 95 % at dmgH_2 : Co of 6, under this conditions complete formation of [$Co(dmgH)_2$] should be given. Thus, according to Appendix II, Figure 4, very low H_2/s should be observed because of the WRC cycle that limits catalysis, eventually causing it to stop. But in contrast to that, an initial H_2 production rate of 27×10^{-9} mol s^{-1} was obtained. This experiment was not run to completion, and no further tests were done to clarify it. But in less than 7 h a TON_{Co} of more than 1100 was obtained, the best value up to now!

2.6 Photocatalysis in a three Component System from pure H_2O

The following publication was in the process of revision when this manuscript was written. It deals with the first example of a photocatalytic three component system in pure H_2O solvent using rhenium PS. Two early kinetic studies using ruthenium type PS evidenced H_2 from pure H_2O before, but none of them has given any turnover numbers.[38,39] In view of future application in a full water decomposition cycle catalysis in pure H_2O is certainly a key prerequisite. It needs to be noted that up to date all water oxidation catalysts (the missing part in the three component system to H_2) only work in pure H_2O.[18,24,26,33,36]

2.6.1 Summary of Probst, B. *et al.*, *J. Am. Chem. Soc.* 2010, *in revision*.

Eight different PS's (**11**, **13** – **15**, **31**, **33** – **35**, see Scheme 30) in conjunction with 9 different WRC's have been examined for their ability to catalyse H_2 production from pure H_2O solvent. Their photochemical properties are given in Appendix III, Table 1.

Scheme 30. PS as tested in Appendix III.

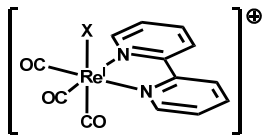

11: X = OH_2
13: X = pyridine
14: X = 4-(dimethylamino)pyridine
15: X = benzyl isocyanide

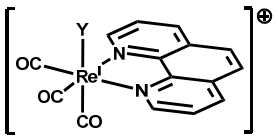

31: Y = OH_2
33: Y = pyridine
34: Y = 4-(dimethylamino)pyridine
35: Y = benzyl isocyanide

Four of them, namely the two pyridine and the two benzyl isocyanide complexes (**13**, **33**, **15**, **35**) do indeed catalyse H_2 production from pure H_2O (see Appendix III, Figure 1). Complexes **11**, **14**, **31**, **34** and $[Ru(bipy)_3]^{2+}$ did not catalyse proton reduction. The two aquo complexes were found to exhibit a chemistry of their own (see section 2.6.2), but were not reductively

quenched by TEOA and did therefore not catalyse proton reduction. As for the two dimethlyaminopyridine complexes **14** and **34**, H_2 production was too low to be integrated. Interestingly enough, all 4 complexes that did catalyse proton reduction gave identical TON_{Re} of ~110. Even more so, TON_{Co} remained constant if [PS] was varied. This was a strong indication that again the cobalt WRC limited catalysis.

Time resolved FT-IR measurements were performed to establish a catalytic cycle (see Appendix III, section Electron Transfer). We could show that catalysis for **13** and **33** proceeds, as in DMF, by reductive quenching of *PS ($k_q = 5 – 8 \times 10^7\ M^{-1}s^{-1}$; $\Phi_{cage} = 0.75$) and subsequent electron transfer to cobalt ($[Co^{III}(py)_2(dmgH)_2]^+$, $k_{CoIII} = 1.1 \times 10^9\ M^{-1}s^{-1}$). No transfer of a second electron from the decomposition of TEOA could be observed on a timescale up to 40 µs. Preliminary results indicated that, unlike in DMF solvent, no second order dependence of H_2/s on [Co] is followed (Appendix III, SI 1).

It was of special interest to study the low turn over numbers as compared to DMF. A screening of 9 different WRC's showed a strong correlation between WRC structure and long-term stability (see Appendix III, Figure 5). Unlike in DMF, the DOH complexes outperformed the $dmgH_2$ complex. The TIM complexes performed inferior to the other two, as in DMF. Interestingly enough is the case of $[CoBr(DOHpy)]PF_6$: whereas in DMF its performance was inferior to the analogue $[Co(Br)_2DOH]$, it was the WRC with the highest TON_{Co} in H_2O (~10). $[CoBr(DOHpy)]PF_6$, $[Co(Br)_2DOH]$ and $[Co(py)_2(dmgH)_2]^+$ were tested for catalysis in D_2O, and detection of D_2 instead of H_2 clearly showed that the solvent is indeed the source of protons. Apart from that, only in the case of $[CoBr(DOHpy)]PF_6$ could a significant (inverse) isotope effect be observed, underscoring that H_2 production with the latter likely differs from the other WRC's (see Appendix III, Table 3). A quantum yield of 0.3 was obtained for catalysis with the latter compound at the same concentrations as in Appendix III, Figure 5.

As expected, a strong pH dependency was found for H_2 production (tested for $[Co(py)_2(dmgH)_2]^+$, $[Co(Br)_2DOH]$ and $[CoBr(DOHpy)]^+$; see Appendix III, Figure 6, SI 4 and SI 5). It appeared as if though TON_{Co} constantly increases if pH was lowered. TON_{Co} up to 15 were achieved at pH ≤ 8 for the DOH

complexes. Interesting was also the observation that at high pH for $[Co(py)_2(dmgH)_2]^+$ accumulation of Co^I occurred (see Appendix III, SI 2, SI 3 and SI 6). Clearly this explained the low catalytic performance at high pH's, since accumulation of Co^I will cause accumulation of PS^-, which was shown to undergo loss of the axial ligand in H_2O on a timescale between 50 µs and several ms. Most likely the pK_a of Co^I is in the range of 10 – 12, thus making Co^{III}-H formation limiting at high pH. Another factor that might contribute to the observed pH dependency is the pK_a of 7.4 for $[Co^{III}(py)_2(dmgH)_2]^+$ / $[Co^{III}(py)_2(dmgH)(dmg)]$, even though this value might be different for the respective Co^{II} complexes. Possibly H_2 production is favoured over hydride shift if both oxime bridges are protonated. This could be due to intramolecular protonation of Co^{III}-H by one of the oxime bridges, as postulated before.[41] The presence of 1 M TEOA prohibited a further decrease of pH, and the fact that no catalysis was observed at pH ≤ 7.25 is most likely due to the ratio of $[HTEOA]^+$ to TEOA 4 to 1, meaning that only 0.2 M free TEOA is present for reductive quenching. Nevertheless reductive quenching could still be operative for the 3 longer lived complexes **15**, **33** and **35**, even though at lower rates, but this was not tested in this study.

2.6.2 Further Observations

As the data for the above publication was collected with a setup optimised for higher H_2/s, too large errors were obtained for small H_2/s and integration was not possible in all cases. In the mean time the setup was optimized for smaller H_2/s. It then allowed to show, as expected, that complexes **13** and **14** produce the same amount of H_2, even though at different rates (see Figure 68). This pinpoints the performance limiting steps once more to the cobalt WRC, since otherwise the performance of different PS should be expected to be different. Obviously H_2 release from Co^{III}-H for **72** has only a yield of ~0.9, and with a yield of ~0.1 decomposition of the WRC occurs.

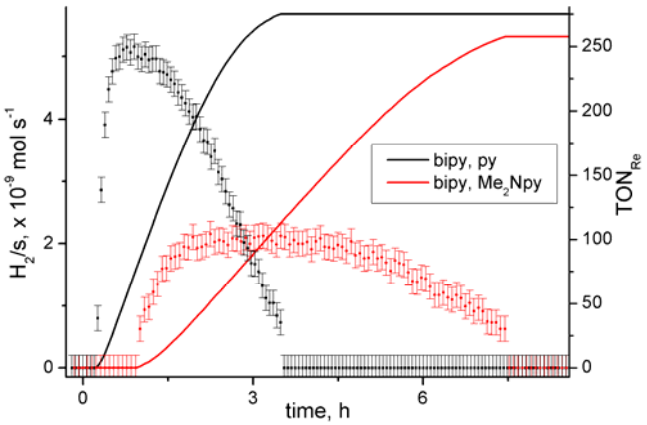

Figure 68. H_2 production profiles for **13** (bipy, py) and **14** (bipy, Me_2Npy) using a more sensitive setup (30 µM PS, 500 µM **72**, 1 M TEOA, 0.1 M HBF_4, H_2O, 380 nm, 10 ml).

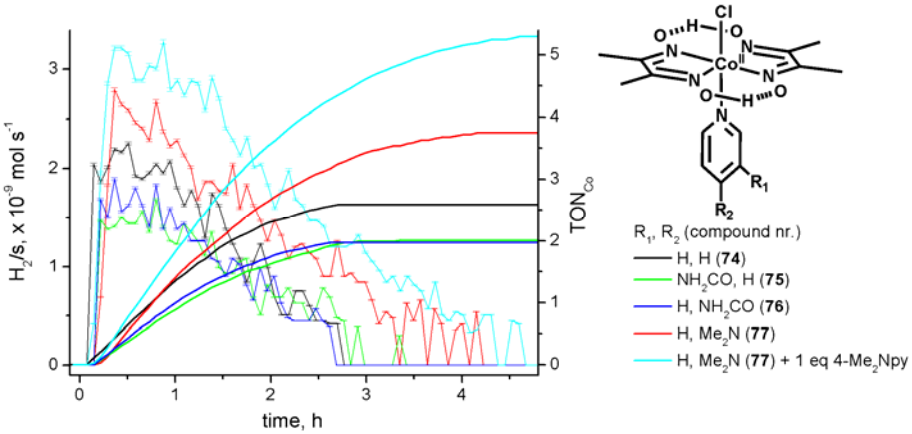

Figure 69. H_2 production profiles using **13** and different [CoCl(3-R_1-4-R_2-py)$(dmgH)_2$] derivatives (30 µM **13**, 500 µM Co, 1 M TEOA, 0.1 M HBF_4, H_2O, 380 nm, 10 ml).

As pointed out before, WRC limits catalytic performance. It has been postulated that protonation and H_2 release from [CoCl(4-R-py)$(dmgH)_2$] strongly depends on the nature of 4-R-py.[35] Faster H_2 release was observed for electron donating substituent's R than for electron accepting ones, correlating with their respective Hammett parameters. A screening with different axial ligands on **74** is shown in Figure 69. Clearly the above finding manifested here as well, and the complexes with the amide substituents were slower and the electron donating dimethylamino substituent was faster than H_2 production with unsubstituted pyridine, respectively. Furthermore, no effect was observed if the amide group was in the 3 or 4 position of pyridine, underlining that the effect is purely due to σ – interaction. It is interesting to note that a faster initial rate correlates with higher TON_{Co}. This means, in

other words, that the H_2 release step was modified but not so the decomposition. Furthermore, if 1 equivalent dimethlyaminopyridine (Me_2Npy) was added to the experiment with **77**, H_2/s increased even more. This could mean that Me_2Npy is labile towards substitution with solvent / TEOA, and an excess of Me_2Npy is required to assure complete formation of **77** under catalysis conditions. Clearly this study could help in optimising H_2 production from water. No pH dependence was recorded for those complexes jet, but even higher TON's are expected at lower pH.

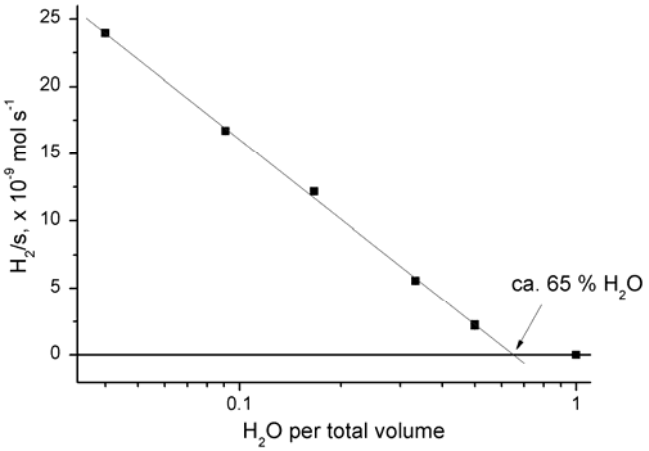

Figure 70. Illustration of initial H_2 production rates versus H_2O content for **11** (0.5 mM **11**, 1 mM **72**, 1 M TEOA, 0.1 M HBF_4, DMF with resp. (total) content of H_2O, 380 nm, Ar).

Interesting results were obtained when checking the two aquo complexes **11** and **31** by FT-IR, as shown in section 2.2.4 (Figure 47 and Figure 48), clearly explaining as to why no catalysis is to be expected. Before the successful system for H_2 production in H_2O, as described in Appendix III was established, trials were made with **11** and $[ReBr(CO)_3DH_3NCH_2bipy]Br_2$ (**53**) in H_2O. Figure 70 displays a study of the initial rates for H_2 production as a function of water content in DMF for **11**. The initial rates decrease exponentially, giving an estimate of 65 % water content as upper limit. It is clear now that in pure H_2O no catalysis takes place because ***11** can not be reductively quenched by TEOA. Obviously the pK_a of **11** is different in H_2O than in DMF. No H_2 production was observed for **53** under identical conditions from pure H_2O.

2.7 Effect of Solvents

A drastic solvent dependence for catalysis was observed, as also apparent from a comparison of the data in Appendixes I and II (DMF) with Appendix III (H_2O). An investigation of catalysis in DMF versus MeCN and of DMF versus H_2O is given below (Figure 71 resp. Figure 72).

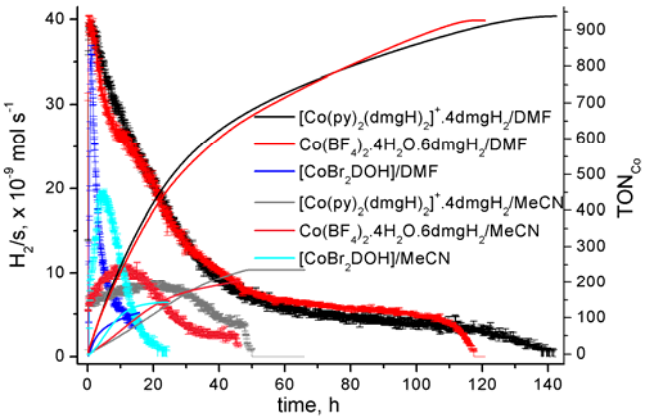

Figure 71. H_2 production profiles in DMF as compared to MeCN (0.5 mM **12**, 0.5 mM Cobalt as indicated, 1 M TEOA, 0.1 M HBF_4, Ar, solvent as indicated, 470 nm).

Catalysis in DMF, using [ReNCS(CO)$_3$bipy] (**12**, 0.5 mM) and irradiating at 470 nm (see Figure 71), gives about identical initial rates for **71** (black), in-situ prepared [Co(dmgH)$_2$] (red), both with an excess of $dmgH_2$, and [$CoBr_2$DOH] (blue). Whereas catalysis with the two $dmgH_2$ complexes gives identical TON_{Co} (~1000), TON_{Co} for the DOH complex is drastically reduced (~100). When switching to MeCN, under otherwise identical conditions, initial rates for the cobaloximes drop by about a factor of 4 and for the DOH complex by about a factor of 2. TON_{Co} remains about the same from DMF to MeCN for the DOH complex, but decrease by about a factor of 4 for the $dmgH_2$ complexes.

It is unclear as to why this happens. Surely the pH scale in MeCN is different from DMF. Further on reductive quenching could be affected as well. But if not that, it could reflect the higher likeliness of decomposition for the cobaloximes in MeCN versus DMF. Further investigations are needed to clarify this issue.

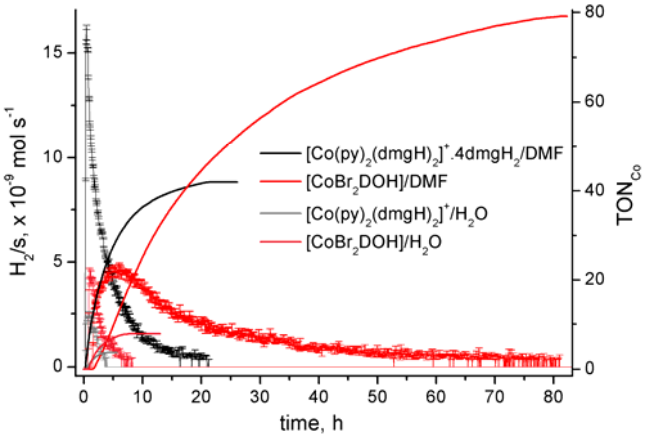

Figure 72. H_2 production profiles in DMF as compared to H_2O (30 µM **13**, 0.5 mM Cobalt as indicated, 1 M TEOA, 0.1 M HBF_4, Ar, solvent as indicated, 380 nm).

Catalysis in DMF for 30 µM $[Repy(CO)_3bipy]^+$ (**13**), irradiated at 380 nm (see Figure 72), gives about a 3 fold higher initial rate for **72** (black) than for $[CoBr_2DOH]$ (red). TON_{Co}, on the other hand, is about 2 fold higher for the latter complex, due to slow, but steady catalysis for about 80 h. This is in contrast to the experiments at 470 nm using 0.5 mM **12** as PS, where the cobaloximes usually outscored the DOH complexes. It is unclear as to why these differences occur. It seems unlikely that the PS or the wavelengths used are responsible – but possibly some of the experiments (eg. those with DOH in DMF and 0.5 mM **12**) were run in a domain that is limited by cobalt. This would mean that much higher turnovers would be possible for the DOH complexes under photon flux control. For the cobaloximes (in DMF and 0.5 mM **12**) it was shown that the reaction occurs under photon flux control (see Appendix I and II). So possibly the DOH complexes would be superior to the $dmgH_2$ complexes in DMF as well, if the right conditions were chosen.

As for catalysis in H_2O solvent, for both complexes (grey and pink) about a 10 fold decrease in TON occurred as compared to DMF. For the DOH complex comparable rates were obtained both in DMF and H_2O, whereas for the cobaloxime a 3 fold reduced initial rate was obtained. Again it would be crucial to reassure that all experiments were photon flux controlled. If so, then this behaviour could be interpreted as a general trend stating that decomposition of WRC is much more likely in H_2O than in DMF. On the other hand, one needs to remember that the pH scale in H_2O is quite different from the respective scale in DMF. Possibly catalysis in H_2O is far off its pH maxima.

3 Conclusion and Outlook

3.1 Photosensitiser

Our initial results have shown that $[ReX(CO)_3diimine]^+$ – type complexes are an attractive alternative in terms of stability to the commonly employed $[Ru(bipy)_3]^{2+}$ PS. Further on oxidised $[ReX(CO)_3diimine]^+$ is a more potent oxidizing agent than $[Ru(bipy)_3]^{3+}$, thus potentially facilitating future schemes for water oxidation. On the absorption side, we could show that $[ReX(CO)_3diimine]^+$ – type complexes can be tuned way into the visible domain, although $[Ru(bipy)_3]^{2+}$ – type complexes are clearly superior. Also concerning solubility, $[Ru(bipy)_3]^{2+}$ is superior to it's rhenium pendant. Future efforts in rhenium chemistry must though aim to overcome these two limits, without affecting properties such as lifetime and stability too much.

Concerning stability of the ground state PS, almost all $[ReX(CO)_3diimine]^+$ – type complexes are very attractive. Catalysis in a three component system by reductive quenching of *PS also requires that the reduced form of PS is stable. This criteria is best meet by the complexes with diimine = phen. Surely, when expanding the concept to eg. oxidative quenching of *PS by eg. WRC, stability of oxidised PS must be assessed.

Concerning absorption of $[ReX(CO)_3diimine]^+$, this work shows that using π – donor ligands for X and π – acceptor substituents on diimine results in a shift of λ_{max} up to 380 nm. Whereas this is still far off the λ_{max} of $[Ru(bipy)_3]^{2+}$ (454 nm), it clearly shows that an improvement is possible by a rational design of the rhenium PS. As predicted by the energy gap law, this increase in λ_{max} is accompanied by a decrease in lifetime, thus preventing at some point further improvements on $[ReX(CO)_3diimine]^+$. Further promising efforts in that direction aim though at substituting one carbonyl in $[ReX(CO)_3diimine]^+$. The compound $[ReBr(py)(CO)_2bipy]$, as an example, shows a significant shift of absorption into the visible domain ($\lambda_{max} \approx 500$ nm).

Since rhenium carbonyl PS's will always bear one positive charge only at the metal, alternative concepts to increase solubility must be sought. Surely the

approach of introducing charged substituents, as in compounds **53** – **55** or of introducing well soluble functional groups such as in compounds **60** – **65** is promising in that regard.

3.2 Water Reduction Catalyst

Although seemingly simple in synthesis, cobaloxime complexes are very potent WRC's. On the other hand, as has been shown in section 2.5 and 2.6, the cobaloxime WRC's are very likely the turnover limiting components in photocatalysis. As compared to the PS cycle, only limited and often indirect evidence for the WRC cycle is available to date.

Concerning the long-term stability much attention is presently devoted to the synthesis of new WRC's. Promising results where obtained with DOH type complexes, especially when bearing an intramolecular axial base. The effect of the axial base on cobalt must not be underestimated, as was shown by a comparison of catalysis with **74** – **77** in H_2O (see section 2.6.2). Clearly the pH of the reaction solution plays a major role, also in terms of long-term stability. Thus an interesting concept is that of using an intramolecular acid of appropriate pK_a close to the catalytic centre on cobalt, as nature uses in hydrogenases.

Concerning the elucidation of the WRC cycle, one focus is thus on the introduction of an IR probe on a cobaloxime, thus possibly allowing a direct observation of the rate limiting steps before H_2 release. This information would surely affect the design of novel WRC's.

3.3 Three Component System

The work in this project clearly showed that three component systems for the reductive halfreaction of water splitting are possible for $[ReX(CO)_3diimine]^+$ – type PS, and even more so, that they represent one of the most stable PS's up to date. Clearly photocatalysis in DMF, in terms of turnovers, is on the edge of becoming economically interesting. A detailed kinetic analysis of the

individual reaction steps is given, which was greatly facilitated by the characteristic IR bands of $[ReX(CO)_3diimine]^+$.

We could further show for the first time that photocatalysis in a three component system to H_2 is possible in pure H_2O solvent. Even though turnovers, especially in WRC, are still quite low, this step bears great potential in terms of future implementation as a functional part of a full photochemical water decomposition scheme. Clearly future efforts must aim at optimising catalysis in H_2O solvent.

Concerning the electron donor, it could be shown that besides the widely used TEOA several alternatives exist. When looking at other irreversible electron donors, this could be a proof of principle, showing that catalysis is not limited to the model donor TEOA, and on the other hand it could allow a wider range of test experiments, since up to now eg. the pH was limited to ≥ 7 in the TEOA system. Form all the reversible quenchers studied, cobaloximes are surely the most promising ones in term of future application. The most promising scheme, as hypothesized by the author, for a full water decomposition cycle, would consist of an aqueous buffered solution with a relatively long lived PS, to assure that oxidative quenching by WRC is possible, and an ideally molecular WOC, which would be oxidised by PS^+ in turn.

4 Experimental

4.1 Syntheses

All chemicals were of reagent grade and used without further purification. $Co(BF_4)_2.6H_2O$, methyl viologen dichloride hydrate, isonicotinamide, $[Et_3NH]Br$, phenothiazine, TflsOH, spectroscopic grade DMF, n-pentane, 7-diethylamino-4-methylcoumarin, 4,4'-dimethyl-2,2'-bipyridine, Cobalt(II) bromide hydrate, isonicotinylaldehyde and thionylchloride were purchased from Acros. Spectroscopy grade triethanolamine (TEOA), technical grade methyl-tert-butyl-ether (MTBE; distilled before use), $[Et_2OH]BF_4$, $[Co(AcO)_2(OH_2)_4]$, pyridine (py), benzylisocyanide (CNBz), 4-dimethylaminopyridine (4-Me_2Npy), dimethylglyoxime ($dmgH_2$), 2,2'-bipyridine (bipy), phenanthroline (phen), thiophenol, NaMeS, NaNCS, nicotinamide, CCl_3CCl_3, $[Et_3NH]Cl$, NaN_3, [TBA]I, Me_2NH (100 ml cylinder), MeOH, Hexane, $[TBA]PF_6$, $[NH_4]PF_6$, NaAcO, thiourea, Cobalt chloride hexahydrate, aluminium oxide, $NaBH_4$, NaCN, $NaNO_2$, AcOH, TFA, BuLi (2 M, hexane), CaH_2, HBr (aqueous, min. 62%), triethylamine (TEA) and trimethylsilylchloride were purchased from Fluka. 4,4'-dicarboxylic acid-2,2'-bipyridine and isonicotinoyl chloride hydrochloride were obtained from Lancaster. Silver trifluoromethansulfonate (AgTflsO) was obtained from Strem Chemicals. CsF was obtained from ABCR. Petroleumbenzin was obtained from Merck. 54 % aqueous HBF_4 and TEOA were obtained from RdH. Rhenium metal was generously donated by H. C. Starck, Berlin. Water was doubly distilled before use. Synthetic reactions were carried out under N_2 or Ar using standard Schlenk techniques. The synthesis of $[ReBr(CO)_5]$ (**1**),[126] $[ReBr_3(CO)_3](Et_4N)_2$ (**3**),[152] $[ReCl(CO)_3bipy]$ (**21**),[44] $[Re(CN)(CO)_3bipy]$ (**22**),[56] $[ReBr(CO)_3phen]$ (**30**),[44] $[Co(OH_2)_2(dmgH)_2]$ (**70**),[77] $[CoBr(py)(dmgH)_2]$ (**73**),[77] $[CoCl(py)(dmgH)_2]$ (**74**),[77] $[CoCl(3\text{-}H_2NCOpy)(dmgH)_2]$ (**75**),[77] $[CoCl(4\text{-}H_2NCOpy)(dmgH)_2]$ (**76**),[77] $[CoCl(4\text{-}Me_2Npy)(dmgH)_2]$ (**77**),[77] 2,2'-bipyridine-4,4'-dimethylester (**88**, $DMeCO_2bipy$)[135] have been described before.

4.1.1 Rhenium

[Re(OTfls)(CO)$_5$] (**2**). 644 mg (1.586 mmol) [ReBr(CO)$_5$] (**1**) were suspended in 20 ml CH_2Cl_2. 537 mg (2.09 mmol) AgOTfls was then added as a solid and the resulting suspension stirred in the dark for 3 h with occasional sonication. Excess AgOTfls and AgBr are then filtered off and the solution is concentrated in *vaccuo* to 5 ml, filtered, taken to dryness and dissolved again in a 1 – 2 ml dry CH_2Cl_2 and filtered again. Slow evaporation of CH_2Cl_2 resulted in crystalline, colourless needles which were suspended in hexane and filtered off to give 539.2 mg (1.13 mmol; 72 %) **2**. If complete removal of silver is necessary, the compound might be applied to column chromatography. Solid **2** was, although air-stable, quite hydroscopic and is best be stored in the dark and in a water free environment. Long-term storing is not recomanded. IR(KBr): 2152 (m), 2032 (s), 1975 (s), 1963 (s), 1252 (m), 1172 (m), 1034 (m). Anal. calcd. for $C_6F_3O_8ReS$ (%): C: 15.16, H: 0.00, N: 0.00. Found: C: 15.03, H: 0.21, N: 0.00.

[ReBr(CO)$_3$bipy] (**10**). 516 mg (3.3 mmol) 2,2'-bipyridine and 1.218 g (3 mmol) [ReBr(CO)$_5$] (**1**) were suspended in 80 ml petroleum benzine (boiling range 100-120 °C) and refluxed for 2 h. Filtration of the yellow residue and subsequent washings by MTBE and hexane gave 1.4865 g **10** as a yellow powder (2.936 mmol, 98 %). λ_{max}(DMF): 375 nm (ε = 3100 $M^{-1}cm^{-1}$). λ_{em}(DMF): 600 nm (Φ_{em} = 0.0018 ± 0.0001). IR(KBr): 2011 (s), 1902 (s), 1881 (s), 1602 (m), 1470 (m), 1444 (m), 770 (m). ^{1}H-NMR (300 MHz, d^6-dmso, ppm): 9.04 (*d*, 2 H), 8.78 (*d*, 2 H), 8.34 (*t*, 2 H), 7.76 (*t*, 2 H). ESI-MS(MeOH): *m/z* = 528.9 $[M+Na]^+$ (100 %), 427.1 $[M-Br]^+$ (20 %). HPLC (min): 15.05 (M-Br), 16.57 (M). Anal. calcd. for $C_{13}H_8BrN_2O_3Re$ (%): C: 30.84, H: 1.59, N: 5.53. Found: C: 30.62, H: 1.41, N: 5.59.

[Re(OH$_2$)(CO)$_3$bipy](TflsO) (**11**). [ReBr(CO)$_3$bipy] (**10**, 549 mg, 1.048 mmol) was suspended in 120 ml MeOH and AgTflsO (284.5 mg, 1.11 mmol), dissolved in 5 ml MeOH, was added. The suspension was, under exclusion of light, stirred for 7 h and sonicated several times to avoid formation of large colloidal particles. AgBr was removed quantitatively by filtration and the resulting, clear yellow solution evaporated to dryness. Column

chromatography (basic aluminium oxide, CH_2Cl_2) was performed to remove remaining impurities of silver. The yellow fraction was collected, dried over Na_2SO_4, filtered and evaporated to dryness to give [Re(OTfls)$(CO)_3$bipy]. IR(KBr): 2033 (s), 1931 (s), 1897 (s), 1339 (m), 1014 (m), 768 (m), 630 (m). ^{1}H-NMR (300 MHz, d^6-dmso, ppm): 9.13 (*d*, 2 H), 8.81 (*d*, 2 H), 8.44 (*t*, 2 H), 7.85 (*t*, 2 H). ESI-MS(MeOH): *m/z* = 445.0 [M-TflsO+H_2O]$^+$ (100 %), 427.1 [M-TflsO]$^+$ (80 %). HPLC: 15.12. Anal. calcd. for $C_{14}H_8F_3N_2O_6ReS$ (%): C: 29.22, H: 1.40, N: 4.87. Found: C: 28.50, H: 0.92, N: 4.70. (3 % impurities, probably AlOx). The residue was then refluxed for 2 h in 200 ml H_2O, filtered to remove any insoluble material, and the resulting, yellow solution lyophilized to give **11** as a off-yellow, shinny powder. λ_{max}(H_2O, 1 mM TflsOH): 347 nm (sh, ε = 3950 $M^{-1}cm^{-1}$). λ_{em}(H_2O, 1 mM TflsOH): 590 nm (Φ_{em} = 0.0015 ± 0.0001). IR(KBr): 2035 (s), 1919 (s), 1901 (s), 1603 (m), 1235 (m), 1200 (m), 1015 (m), 770 (m), 630 (m). ^{1}H-NMR (200 MHz, d^6-dmso, ppm): 9.1 (*2xd*, 2 H, Re-DMSO/OTfls (~60 %) and Re-OH_2 (~40 %)), 8.81 (*d*, 2 H), 8.43 (*t*, 2 H), 7.84 (*t*, 2 H), 7.59 (*s*, ~40 % Re-OH_2). ESI-MS(MeOH): *m/z* = 427.0 [M-TflsO-OH_2]$^+$ (100 %), 445.0 [M-TflsO]$^+$ (10 %). HPLC: 15.01. Anal. calcd. for $C_{14}H_{10}F_3N_2O_7ReS$ (%): C: 28.33, H: 1.70, N: 4.72. Found: C: 28.28, H: 1.69, N: 4.76.

[ReNCS(CO)$_3$bipy] (**12**). 253.0 mg **10** (0.5 mmol) was suspended in 50 ml MeOH and AgOTfls (128.0 mg, 0.499 mmol), dissolved in 2 ml MeOH added to under exclusion of light. The solution was agitated for 4 h in the dark and sonicated several times, after which AgBr was removed quantitatively by filtration to obtain a clear, yellow solution of **11**. Then 140 mg NaSCN (3.5 eq.), dissolved in little H_2O, was added and the solution heated to 70 °C for 6 h to ensure complete formation of the Re-NCS species (at low temperature an other species is first formed, most likely Re-SCN, which can be detected by HPLC and H-NMR). Evaporation of MeOH and suspension in H_2O allows isolation of **12** as a yellow solid by filtration and subsequent washings with H_2O and MTBE (218 mg, 90 %). As an alternative the reaction is carried out with **11** in H_2O (max. solubility of **11** in H_2O: ~5 mM). λ_{max}(DMF): 376 nm (ε = 2760 $M^{-1}cm^{-1}$). λ_{em}(DMF): 602 nm (Φ_{em} = 0.0011 ± 0.0001). IR(KBr): 2093 (s), 2020 (s), 1928 (s), 1914 (s), 1471 (m), 1444 (m), 765 (m). ^{1}H-NMR (200 MHz, d^6-dmso, ppm): 9.06 (*d*, 2 H), 8.82 (*d*, 2 H), 8.41 (*t*, 2 H), 7.82 (*t*, 2 H). ESI-

MS(MeOH): *m/z* = 552.0 $[M+Cl+MeOH]^-$ (90 %), 588 $[M+MeO+THF]^+$ (100 %). HPLC (min): 17.08. Anal. calcd. for $C_{14}H_8N_3O_3ReS$ (%): C: 34.71, H: 1.66, N: 8.67. Found: C: 34.65, H: 1.68, N: 8.65.

[Re(py)(CO)$_3$bipy](TflsO) (**13**). Complex **11** (296.5 mg, 0.5 mmol) was dissolved in 25 ml MeOH and pyridine (100 µl, 1.29 mmol) was added. The resulting solution was refluxed for 12 h, evaporated to dryness, suspended in 25 ml MTBE, filtered, washed with MTBE and dried in *vacuo*. Yield: 320.5 mg (98 %) of a shinny off-yellow powder. $\lambda_{max}(H_2O)$: 343 nm (ε = 3650 $M^{-1}cm^{-1}$). $\lambda_{em}(H_2O)$: 567 nm (Φ_{em} = 0.0098 ± 0.0003). IR(KBr): 2026 (s), 1923 (s), 1907 (s), 1280 (m), 1260 (m), 1030 (m), 637 (m). ^{1}H-NMR (200 MHz, d^6-dmso, ppm): 9.32 (*d*, 2 H), 8.70 (*d*, 2 H), 8.40 (*m*, 4 H), 7.92 (*m*, 3 H), 7.43 (*t*, 2 H). ESI-MS(MeOH): *m/z* = 506.0 $[M-TflsO]^+$ (100 %), 426.9 [M-TflsO-pyridine]$^+$ (2 %). HPLC: 15.08 min. Anal. calcd. for $C_{19}H_{13}F_3N_3O_6ReS$ (%): C: 34.86, H: 2.00, N: 6.42. Found: C: 34.66, H: 1.99, N: 6.62.

[Re(4-Me$_2$Npy)(CO)$_3$bipy](TflsO) (**14**). Complex **11** (30.5 mg, 51 µmol) was dissolved in 5 ml MeOH and 4-dimethylaminopyridine (20.5 mg, 0.17 mmol) was added. The resulting orange solution was refluxed for 4 h, evaporated to dryness, suspended in 5 ml MTBE, filtered, washed with MTBE and dried in *vacuo*. Yield: 31.4 mg (90 %) of a yellow powder. $\lambda_{max}(H_2O)$: 368 nm (ε = 2450 $M^{-1}cm^{-1}$). $\lambda_{em}(H_2O)$: 602 nm (Φ_{em} = 0.00029 ± 0.00001). IR(KBr): 2029 (s), 1935 (s), 1903 (s), 1627 (m), 1275 (m), 1230 (m), 1025 (m), 637 (m). ^{1}H-NMR (300 MHz, d^6-dmso, ppm): 9.29 (*d*, 2 H), 8.73 (*d*, 2 H), 8.41 (*t*, 2 H), 7.90 (*t*, 2 H), 7.65 (*d*, 2 H), 6.47 (*d*, 2 H), 2.90 (*s*, 6 H). ESI-MS(MeOH): *m/z* = 549.1 $[M-TflsO]^+$ (100 %). HPLC: 15.78. Anal. calcd. for $C_{21}H_{18}F_3N_4O_6ReS$ (%): C: 36.15, H: 2.60, N: 8.03. Found: C: 36.01, H: 2.67, N: 8.29.

[Re(CNBz)(CO)$_3$bipy](TflsO) (**15**). Complex **11** (29.7 mg, 50 µmol) was dissolved in 5 ml MeOH and benzylisocyanide (61 µl, 0.5 mmol) was added. The resulting solution was stirred for 36 h, evaporated to dryness, suspended in 5 ml MTBE, filtered, washed with MTBE and dried in *vacuo*. Yield: 33.5 mg (97 %) of a off-yellow powder. $\lambda_{max}(H_2O)$: 337 nm (sh; ε = 3800 $M^{-1}cm^{-1}$). $\lambda_{em}(H_2O)$: 527 nm (Φ_{em} = 0.087 ± 0.003). IR(KBr): 2223 (s), 2041 (s), 1956 (s), 1935 (s), 1281 (m), 1258 (m), 1030 (m), 773 (m). ^{1}H-NMR (200 MHz, d^6-dmso, ppm): 9.08 (*d*, 2 H), 8.81 (*d*, 2 H), 8.41 (*t*, 2 H), 7.82 (*t*, 2 H), 7.27 (*m*, 3

H), 6.89 (*m*, 2 H), 5.01 (*s*, 2 H). ESI-MS(MeOH): *m/z* = 544.1 $[M\text{-TflsO}]^+$ (100 %). HPLC: 15.79 min. Anal. calcd. for $C_{22}H_{15}F_3N_3O_6ReS$ (%): C: 38.15, H: 2.18, N: 6.07. Found: C: 38.14, H: 2.21, N: 6.04.

[Re(NCMe)(CO)$_3$bipy](TflsO) (**16**). 253.1 mg **10** was suspended in 25 ml MeCN and AgOTfls, dissolved in 2 ml MeCN, was added. After stirring for 1 day in the dark, the resulting suspension was filtered to remove AgBr (90.8 mg, 484 µmol, 97 %, off-white). Refluxing for 3 h and removal of the solvent resulted in 16 as a greenish powder (266.6 mg, 516 µmol, 103 %). $\lambda_{max}(H_2O)$: 340 nm (sh; ε = 3650 $M^{-1}cm^{-1}$). $\lambda_{em}(H_2O)$: 543 nm (Φ_{em} = 0.058 ± 0.013). IR(KBr): 2043 (s), 1932 (s), 1912 (s), 1265 (m), 1156 (m), 1033 (m), 770 (m), 639 (m). ^{1}H-NMR (200 MHz, d^6-dmso, ppm): 9.10 (*m*, 2 H), 8.82 (*m*, 2 H), 8.44 (*m*, 2 H), 7.84 (*m*, 2 H), 2.30 & 2.06 (*s*, 3 H). ESI-MS(MeOH): *m/z* = 468.0 $[M\text{-TflsO}]^+$ (100 %), 426.9 $[M\text{-MeCN}]^+$ (20 %). HPLC: 15.18 min. Anal. calcd. for $C_{16}H_{11}F_3N_3O_6ReS$ (%): C: 31.17, H: 1.80, N: 6.82. Found: C: 31.11, H: 1.90, N: 6.72.

[Re(SPh)(CO)$_3$bipy] (**17**). To 10 ml of an aqueous solution of **11** (29.4 mg, 50 µmol) was added 20 µl of thiophenol (196 µmol) and a spatula full of K_2CO_3. After stirring for 4 days the suspension was filtered and washed with water to afford 24.6 mg (46 µmol, 97 %) of **17** as a reddish powder. λ_{max}(DMF): 349 nm (sh; ε = 4800 $M^{-1}cm^{-1}$), 488 nm (ε = 550 $M^{-1}cm^{-1}$). No emission observed. IR(KBr): 2009 (s), 1896 (s), 1879 (s), 1602 (m), 1470 (m), 1443 (m), 768 (m). ^{1}H-NMR (200 MHz, d^6-dmso, ppm): 8.90 (*d*, 2 H), 8.51 (*d*, 2 H), 8.19 (*t*, 2 H), 7.65 (*t*, 2 H), 6.64 (*m*, 5 H). ESI-MS(MeOH): *m/z* = 537.0 $[M+H]^+$ (100 %), 559.1 $[M+Na]^+$ (70 %), 427.0 $[M\text{-SPh}]^+$ (50 %). HPLC: 17.54 min. Anal. calcd. for $C_{19}H_{13}N_2O_3ReS$ (%): C: 42.61, H: 2.45, N: 5.23. Found: C: 42.29, H: 2.46, N: 5.12.

[ReN$_3$(CO)$_3$bipy] (**18**). 29.3 mg **11** (50 µmol) was dissolved in 5 ml H_2O and 6.0 mg NaN_3 (92 µmol), dissolved in 1 ml H_2O, added to the stirred solution. The solution became turbid immediately, but was refluxed for 5 h. Filtration and washing with H_2O gave 21.5 mg **18** (46 µmol, 92 %) as a yellow powder. λ_{max}(DMF): 375 nm (ε = 2600 $M^{-1}cm^{-1}$). No emission observed. IR(KBr): 2074 (s), 2058 (s), 2018 (s), 2009 (s), 1896 (s), 1617 (m), 1474 (m), 1445 (m), 773 (m). ^{1}H-NMR (300 MHz, d^6-dmso, ppm): 9.03 (*d*, 2 H), 8.79 (*d*, 2 H), 8.38 (*t*, 2

H), 7.80 (*t*, 2 H). ESI-MS(CH_2Cl_2/THF): *m/z* = 445.1 $[M\text{-}N_3+H_2O]^+$ (100 %). HPLC: 15.05 ($M\text{-}N_3$), 16.57 min. Anal. calcd. for $C_{13}H_8N_5O_3Re$ (%): C: 33.33, H: 1.72, N: 14.95. Found: C: 32.40, H: 1.50, N: 13.50.

[Re(NO_2)(CO)$_3$bipy] (**19**). 29.1 mg **11** (50 µmol) was dissolved in 5 ml H_2O 17.5 mg $NaNO_2$ (253 µmol), dissolved in 1 ml H_2O, added. The solution was refluxed for 5 h, filtered and washed with H_2O to afford 19.0 mg (40 µmol; 80 %) of **19** as a yellow powder. It was shown by ^{1}H-NMR, HPLC, IR and X-ray diffraction that the compound consists of 2 isomers (Re-ONO and Re-NO_2), which were not further separated. λ_{max}(DMF): 354 nm (ε = 3775 $M^{-1}cm^{-1}$). λ_{em}(DMF): 587 nm (Φ_{em} = 0.00015 ± 0.00001). IR(KBr): 2024 (s), 1914 (s), 1620 (broad, m), 1470 (m), 1351 (m), 1322 (m), 1310 (m), 774 (m). ^{1}H-NMR (300 MHz, d^6-dmso, ppm): 9.09 & 8.99 (2x*d*, 2 H), 8.79 (2x*d*, 2 H), 8.38 (*t*, 2 H), 7.79 (*m*, 2 H). ESI-MS(MeOH): *m/z* = 427.0 $[M\text{-}NO_2]^+$ (100 %), 444.9 $[M\text{-}NO_2+OH_2]^+$ (90 %), 472.9 $[M\text{-}e^-]^+$ (5 %). HPLC (min): 15.05 ($M\text{-}NO_2$), 16.33. Anal. calcd. for $C_{13}H_8N_3O_5Re$ (%): C: 33.05, H: 1.71, N: 8.89. Found: C: 32.91, H: 1.61, N: 8.63.

[Re(OH_2)(CO)$_3$phen](TflsO) (**31**). **30** (529.9 mg, 1 mmol) was suspended in 80 ml MeOH and AgTflsO (256.5 mg, 1 mmol), dissolved in 10 ml MeOH, was added. The suspension was, under exclusion of light, stirred overnight and sonicated several times to avoid formation of large colloidal particles. AgBr was removed quantitatively by filtration and the resulting, clear orange solution evaporated to dryness. Column chromatography (basic aluminium oxide, CH_2Cl_2, 5 % MeOH) was performed to remove remaining impurities of silver. The residue was then reflux for 2 h in 200 ml H_2O, filtered to remove any insoluble material, and the resulting, yellow solution lyophilized. Yield: 673.0 mg (109 %) of a orange powder. λ_{max}(H_2O, 1 mM TflsOH): 360 nm (sh, ε = 3400 $M^{-1}cm^{-1}$). λ_{em}(H_2O, 1 mM TflsOH): 578 nm (Φ_{em} = 0.00099 ± 0.00002). IR(KBr): 2035 (s), 1919 (s), 1735 (m), 1618 (m), 1266 (m), 1231 (m), 1031 (m), 638 (m). ^{1}H-NMR (300 MHz, d^6-dmso, ppm): 9.52 (*dd*, 2 H), 9.06 (*d*, 2 H), 8.37 (*s*, 2 H), 8.19 (*dd*, 2 H), 7.50 (*s*, 2 H). ESI-MS(MeOH): *m/z* = 468.8 $[M\text{-TflsO}]^+$ (25 %), 450.9 $[M\text{-TflsO-}OH_2]^+$ (100 %). HPLC: 15.29. Anal. calcd. for $C_{16}H_{10}F_3N_2O_7ReS$ (%): C: 31.12, H: 1.63, N: 4.54. Found: C: 30.98, H: 1.79, N: 4.31.

[ReNCS(CO)$_3$phen] (**32**). Complex **31** (30.7 mg, 50 µmol) was dissolved in 5 ml MeOH. Upon addition of NaNCS (27 mg, 338 µmol) the solution was refluxed for 2 h, resulting in a shinny yellow precipitate, which was subsequently collected by filtration and washed with 2 ml H_2O and MTBE. Trying in *vacuo* yielded 20.7 mg (40.7 µmol, 81 %) **32** as a yellow powder. λ_{max}(DMF): 373 nm (ε = 3500 $M^{-1}cm^{-1}$). λ_{em}(DMF): 597 nm (Φ_{em} = 0.0045 ± 0.0001). IR(KBr): 2093 (s), 2022 (s), 1914 (s), 1427 (m), 849 (m), 723 (m). ^{1}H-NMR (300 MHz, d^6-dmso, ppm): 9.50 (*dd*, 2 H), 9.05 (*dd*, 2 H), 8.38 (*s*, 2 H), 8.17 (*dd*, 2 H). ESI-MS(THF): *m/z* = 451 $[M\text{-}NCS]^+$ (20 %). HPLC: 17.23 min. Anal. calcd. for $C_{16}H_8N_3O_3ReS$ (%): C: 37.79, H: 1.59, N: 8.26. Found: C: 37.67, H: 1.52, N: 8.31.

[Re(py)(CO)$_3$phen](TflsO) (**33**). Complex **31** (30.4 mg, 50 µmol) was dissolved in 5 ml pyridine and the resulting solution was stirred for 10 days, evaporated to dryness, suspended in 5 ml MTBE, filtered, washed with MTBE and dried in *vacuo*. Yield: 26.0 mg (77 %) of a off-yellow powder. λ_{max}(H_2O): 362 nm (ε = 3350 $M^{-1}cm^{-1}$). λ_{em}(H_2O): 550 nm (Φ_{em} = 0.039 ± 0.001). IR(KBr): 2030 (s), 1918 (s), 1263 (m), 1028 (m), 637 (m). ^{1}H-NMR (300 MHz, d^6-dmso, ppm): 9.77 (*d*, 2 H), 9.04 (*d*, 2 H), 8.46 (*d*, 2 H), 8.31 (*s*, 2 H), 8.26 (*dd*, 2 H), 7.86 (*t*, 1 H), 7.32 (*t*, 2 H). ESI-MS(MeOH): *m/z* = 530.0 $[M\text{-}TflsO]^+$ (100 %), 451.0 $[M\text{-}TflsO\text{-}pyridine]^+$ (10 %). HPLC: 15.30 min. Anal. calcd. for $C_{21}H_{13}F_3N_3O_6ReS$ (%): C: 37.17, H: 1.93, N: 6.19. Found: C: 37.23, H: 1.97, N: 6.39.

[Re(4-Me$_2$Npy)(CO)$_3$phen](TflsO) (**34**). Complex **31** (30.5 mg, 50 µmol) was dissolved in 20 ml MeOH and 4-dimethylaminopyridine (22 mg, 0.18 mmol) was added. The resulting orange solution was refluxed for 100 h, evaporated close to dryness, suspended in 5 ml MTBE, filtered, washed with MTBE and dried in *vacuo*. Yield: 23.6 mg (65 %) of a yellow powder. λ_{max}(H_2O): 368 nm (ε = 3000 $M^{-1}cm^{-1}$). λ_{em}(H_2O): 592 nm (Φ_{em} = 0.0011 ± 0.0001). IR(KBr): 2024 (s), 1936 (s), 1921 (s), 1628 (m), 1270 (m), 1032 (m), 637 (m). ^{1}H-NMR (300 MHz, d^6-dmso, ppm): 9.74 (*d*, 2 H), 9.04 (*d*, 2 H), 8.33 (*s*, 2 H), 8.24 (*dd*, 2 H), 7.71 (*d*, 2 H), 6.35 (*d*, 2 H), 2.82 (*s*, 6 H). ESI-MS(MeOH): *m/z* = 573.2 $[M\text{-}TflsO]^+$ (100 %). HPLC: 16.04. Anal. calcd. for $C_{23}H_{18}F_3N_4O_6ReS$ (%): C: 38.28, H: 2.51, N: 7.76. Found: C: 37.94, H: 2.38, N: 7.46.

[Re(CNBz)(CO)$_3$phen](TflsO) (**35**). Complex **31** (30.7 mg, 50 µmol) was dissolved in 5 ml MeOH and benzylisocyanide (20 µl, 0.17 mmol) was added. The resulting solution was stirred for 10 days, evaporated to dryness, suspended in 5 ml MTBE by sonication, filtered, washed with MTBE and dried in *vacuo*. Yield: 30.5 mg (85 %) of a off-yellow powder. λ_{max}(H_2O): 360 nm (sh; ε = 2600 $M^{-1}cm^{-1}$). λ_{em}(H_2O): 515 nm (Φ_{em} = 0.208 ± 0.004). IR(KBr): 2201 (m), 2044 (s), 1966 (s), 1938 (s), 1267 (m), 1031 (m), 637 (m). ^{1}H-NMR (300 MHz, d^6-dmso, ppm): 9.51 (*d*, 2 H), 9.03 (*d*, 2 H), 8.39 (*s*, 2 H), 8.16 (*dd*, 2 H), 7.22 (*t*, 1 H), 7.10 (*t*, 2 H), 8.62 (*d*, 2 H), 4.87 (*s*, 2 H). ESI-MS(THF): *m/z* = 568.0 $[M\text{-}TflsO]^+$ (100 %). HPLC: 15.79 min. Anal. calcd. for $C_{24}H_{15}F_3N_3O_6ReS$ (%): C: 40.22, H: 2.11, N: 5.86. Found: C: 40.32, H: 2.09, N: 5.95.

[ReBr(CO)$_3$phenNH$_2$] (**40**). 1 mmol (770.45 mg) **3** was dissolved in 20 ml MeOH and 195 mg 1,10-phenanthrolin-5-amine (1 mmol), dissolved in 10 ml MeOH, added to it. After stirring for 1 day, **40** was isolated by filtration and washing with H_2O as a orange solid (514.8 mg, 0.94 mmol, 94 %). λ_{max}(DMF): 440 nm (sh; ε = 2550 $M^{-1}cm^{-1}$). λ_{em}(DMF): 485 nm. IR(KBr): 2015 (s), 1925 (s), 1905 (s), 1640 (m), 1491 (w), 1461 (w), 1431 (w), 724 (w). ^{1}H-NMR (300 MHz, d^6-dmso, ppm): 9.39 (*d*, 1 H), 9.10 (*d*, 1 H), 8.95 (*d*, 1 H), 8.47 (*d*, 1 H), 8.04 (*dd*, 1 H), 7.78 (*dd*, 1 H), 7.06 (*s*, 1 H), 6.88 (*s*, 2 H). HPLC: 12.06 min. Anal. calcd. for $C_{15}H_9BrN_3O_3Re$ (%): C: 33.04, H: 1.66, N: 7.71. Found: C: 33.62, H: 173, N: 7.83.

[ReBr(CO)$_3$pAp] (**41**). 60 mg (0.2 mmol) N-(1,10-phenanthrolin-5-yl)-isonicotinamide (pAp, **93**) was dissolved in 25 ml warm MeOH and 154 mg (0.2 mmol) **3**, dissolved in 2 ml MeOH, was added. The solution turned immediately yellow and after 5 min some precipitate occurred. The mixture was brought to reflux for 1 h and stirred overnight at room temperature before the solvent was removed in *vaccuo*. The residue was washed with H_2O to remove $[Et_4N]Br$, dried and applied to column chromatography using basic aluminium oxide and CH_2Cl_2 with 2.5 % MeOH and 0.25 % aq. NH_3 as mobile phase. The first fraction was collected to yield 71 mg (109 µmol, 55 %) **41** as an orange solid, which still contained minor impurities of $[Et_4N]Br$. λ_{max}(DMF): 480 nm (sh; ε = 1100 $M^{-1}cm^{-1}$). λ_{em}(DMF): 575 nm. IR(KBr): 2024 (s), 1920

(s), 1888 (s), 1663 (w), 1629 (w), 1522 (w), 1424 (w), 727 (w). ^{1}H-NMR (200 MHz, d^6-dmso, ppm): 11.24 (*s*, 1 H), 9.49 (*d*, 1 H), 9.39 (*d*, 1 H), 9.08 (*d*, 1 H), 8.94 (*d*, 1 H), 8.86 (*d*, 2 H), 8.58 (*s*, 1 H), 8.1 (*m*, 4 H). HPLC: 14.65 (M-Br) and 16.16 min. Anal. calcd. for $C_{21}H_{12}BrN_4O_4Re$ (%): C: 38.78, H: 1.86, N: 8.61. Found: C: 42.20, H: 2.50, N: 8.46.

[ReBr(CO)$_3$pAmp] (**42**). 74.5 mg **3** (97 µmol) was dissolved in 2 ml MeOH and 25 mg (87 µmol) pAmp (**94**), dissolved in 3 ml MeOH, was added. A precipitate was observed 5 min after mixing, but stirring was continued for 4 h before the solvent was removed in *vaccuo*. The residue was then suspended in 5 ml H_2O and filtered. The crude product was applied to chromatography (basic aluminium oxide, CH_2Cl_2, 1.25 % MeOH, 0.125 % aq. NH_3) and collection of the first fraction gave, after removal of solvent and washing with Et_2O, 8.2 mg (13 µmol, 15 %) of **42** as a shinny yellow powder (purity: ~90 %). $\lambda_{max}(H_2O)$: 425 nm. IR(KBr): 2018 (s), 1900 (s), 1891 (s), 1624 (m), 1598 (m), 1423 (w), 724 (w). ^{1}H-NMR (300 MHz, d^6-dmso, ppm): 9.43 (*d*, 1 H), 9.25 (*d*, 1 H), 8.96 (*d*, 1 H), 8.51 (*d*, 2 H), 8.40 (*d*, 1 H), 8.11 (*dd*, 1 H), 8.04 (*t*, 1 H), 7.76 (*dd*, 1 H), 7.46 (*d*, 2 H), 6.82 (*s*, 1 H), 4.71 (*d*, 2 H). HPLC: 14.45 min.

[ReBr(CO)$_3$pImp] (**43**). Compound **43** was prepared by reaction of **40** and isonicotinylaldehyd in dry THF, and crystals of x-ray quality were obtained directly from the reaction (see 2.1.1). All attempts for further analysis were hampered by the high tendency of **43** to hydrolyse on the imine moiety, thus yielding **40** and isonicotinylaldehyd.

[ReBr(CO)$_3$DHOCH$_2$bipy] (**50**). 216 mg (1 mmol) 4,4'-Bis(hydroxymethyl)-2,2'-bipyridine (**85**) was dissolved in 10 ml MeOH and 25 ml H_2O, and $[ReBr_3(CO)_3](Et_4N)_2$ (770 mg, 1 mmol), dissolved in 25 ml H_2O, was added. The solution turned yellow, and after 10 min a yellow precipitate formed. The solution was stirred for 3 days, after which the precipitate was filtered off, washed with H_2O and little MeOH and dried in *vaccuo* to obtain 521 mg (0.92 mmol, 92 %) **50** as a yellow powder. λ_{em}(DMF): 594 nm. IR(KBr): 2027 (s), 1914 (s), 1868 (s), 1619 (m), 1415 (m), 1066 (m), 826 (m). ^{1}H-NMR (200 MHz, d^6-dmso, ppm): 8.95 (*d*, 2 H), 8.60 (*s*, 2 H), 7.68 (*d*, 2 H), 5.81 (*t*, 2 H), 4.77 (*d*, 4 H). ESI-MS(MeOH): *m/z* = 487.0 $[M\text{-}Br]^+$ (100 %). HPLC: 14.87 min (M-Br), 16.30 (M). Anal. calcd. for $C_{15}H_{12}BrN_2O_5Re$ (%): C: 31.81, H: 2.14, N: 4.95. Found: C: 32.12, H: 2.26, N: 4.81.

[Re(OH$_2$)(CO)$_3$DHOCH$_2$bipy](TflsO) (**51**). 283 mg (0.5 mmol) **50** was suspended in 15 ml H_2O, and AgOTfls (129 mg, 0.5 mmol), dissolved in 1.5 ml H_2O, was added along with 5 ml MeOH. The suspension was stirred for 5 hours and sonicated several times, after which AgBr was removed by filtration. MeOH was then removed, the product retiturated from H_2O and lyophilised to obtain 271 mg (415 µmol, 85 %) **51** as an off yellow powder. $\lambda_{max}(H_2O)$: 339 nm (sh; ε = 3900 $M^{-1}cm^{-1}$). $\lambda_{em}(H_2O)$: 594 nm. IR(KBr): 2031 (s), 1916 (s), 1898 (s), 1619 (m), 1422 (w), 1272 (m), 1250 (m), 1030 (m), 639 (m). ^{1}H-NMR (300 MHz, d^6-dmso, ppm): 9.03 (*d*, 2 H), 8.64 (*s*, 2 H), 7.76 (*d*, 2 H), 5.83 (*t*, 2 H), 4.78 (*d*, 4 H). ESI-MS(H_2O): *m/z* = 487.0 $[M\text{-}OH_2]^+$ (100 %), 504.9 $[M]^+$ (20 %). HPLC: 14.89 min (M-Br). Anal. calcd. for $C_{16}H_{14}F_3N_2O_9ReS$ (%): C: 29.40, H: 2.16, N: 4.29. Found: C: 29.32, H: 2.10, N: 4.33.

[ReNCS(CO)$_3$DHOCH$_2$bipy] (**52**). 191 mg **50** (337 µmol) was suspended in 14 ml MeOH, and 87 mg (337 µmol) AgOTfls, dissolved in 4 ml MeOH, was added. The mixture was stirred for 5 hours in the dark and sonicated occasionally, before AgBr was removed quantitatively by filtration. Then 116 mg (1.4 mmol) NaSCN, dissolved in 2 ml H_2O, was added to the clear yellow solution. Refluxing for 2 hours and removal of MeOH in a gentle stream of nitrogen caused precipitation of the product, which was then isolated by filtration and subsequent washings to afford 175.3 mg (322 µmol, 96 %) of **52** as a yellow powder. IR(KBr): 2098 (s), 2022 (s), 1902 (s), 1617 (m), 1420 (w), 1059 (w), 838 (w), 626 (w). ^{1}H-NMR (200 MHz, d^6-dmso, ppm): 8.97 (*d*, 2 H), 8.65 (*s*, 2 H), 7.75 (*d*, 2 H), 5.82 (*t*, 2 H), 4.79 (*d*, 4 H). ESI-MS(H_2O): *m/z* = 568.0 $[M+Na]^+$ (100 %), 583.9 $[M+K]^+$ (20 %). HPLC: 16.85 min. Anal. calcd. for $C_{16}H_{12}N_3O_5ReS$ (%): C: 35.29, H: 2.22, N: 7.72. Found: C: 35.23, H: 2.28, N: 7.69.

[ReBr(CO)$_3$DH$_3$NCH$_2$bipy]Br$_2$ (**53**). 21.4 mg (0.1 mmol) 4,4'-Bis(aminomethyl)-2,2'-bipyridine (**87**) was dissolved in 3 ml H_2O by the addition of 50 µl 48 % aqueous HBr (0.4 mmol). Then 77.0 mg (0.1 mmol) **3**, dissolved in 3 ml H_2O, was added to the solution and the resulting mixture stirred for 2 days, lyophilised to remove H_2O and washed several times with dry CH_2Cl_2 to remove excess $[Et_4N]Br$. This procedure yielded 63 mg of **53** as an orange, hydroscopic solid. Excess $[Et_4N]Br$ (~1/3) and a complex where one ammonium group was replaced by H, arising from ligand impurities, were

still present and might be removed by chromatography. IR(KBr): 2928 (m), 2022 (s), 1910 (s), 1893 (s), 1623 (m), 1422 (w), 1107 (w), 645 (w). ^{1}H-NMR (200 MHz, d^6-dmso, ppm): 9.16 (*d*, 2 H), 8.80 (*s*, 2 H), 8.49 (*s*, 6 H), 7.83 (*d*, 2 H), 4.35 (*s*, 4 H), 3.19 (*q*, [Et_4N]Br), 1.16 (*t*, [Et_4N]Br). ESI-MS(H_2O): *m/z* = 485.1 [M-Br-2HBr]$^+$ (100 %). HPLC (Et_3N gradient): 14.87 min (M-Br), 15.67 (M). Anal. calcd. for $C_{15}H_{16}Br_3N_4O_3Re.1/3C_8H_{20}NBr.2H_2O$ (%): C: 25.49, H: 3.23, N: 7.29. Found: C: 25.51, H: 3.08, N: 7.20.

[Re(OH$_2$)(CO)$_3$DH$_3$NCH$_2$bipy](TflsO)$_3$ (**54**). This compound was not isolated, but occurred in the synthesis of **55**. HPLC (Et_3N gradient): 14.93 min.

[ReNCS(CO)$_3$DH$_3$NCH$_2$bipy](TflsO)$_2$ (**55**). 21.3 mg (0.1 mmol) 4,4'-Bis(aminomethyl)-2,2'-bipyridine (**87**) was dissolved in 2 ml H_2O along with 2 equivalents of TflsOH (0.2 mmol, 17.5 µl). Then this solution was added to 47.8 mg (0.1 mmol) **2**, dissolved in 10 ml H_2O by refluxing for 30 min, and the resulting mixture was refluxed for 4 h under N_2 to give **54**. Then 9 mg (1.1 eq.) of NaNCS was added to the yellow solution and refluxing continued for another 2 h. After cooling the solution was filtered to remove a fine precipitate formed, which was discarded, and the filtrate then lyophilised to yield 82.4 mg **55** as an orange, hydroscopic solid. 1 eq. NaTflsO, 0.1 eq. NaNCS and a complex where one ammonium group was replaced by H, arising from ligand impurities, were still present and might be removed by chromatography. IR(KBr): 3070 (m), 2113 (m), 2029 (s), 1916 (s), 1626 (m), 1260 (s), 1173 (s), 1034 (s), 642 (m). ^{1}H-NMR (300 MHz, d^6-dmso, ppm): 9.22 (*d*, 2 H), 8.68 (*s*, 2 H), 8.45 (*s*, 6 H), 7.90 (*d*, 2 H), 4.36 (*s*, 4 H). ESI-MS(MeOH): *m/z* = 485.0 [M-2HOTfls-NCS]$^+$ (30 %), 544.0 [M-HOTfls-OTfls]$^+$ (80 %), 553.0 [M-2HOTfls-NCS-H$^+$CF$_3$]$^+$ (100 %). HPLC (Et_3N gradient): 16.31 min. Anal. calcd. for $C_{18}H_{16}F_6N_5O_9ReS_3.CF_3NaO_3S.6H_2O$ (%): C: 20.32, H: 2.51, N: 6.24. Found: C: 20.35, H: 2.02, N: 5.75.

[ReBr(CO)$_3$DMeCO$_2$bipy] (**60**). 83.5 mg (305 µmol) 2,2'-bipyridine-4,4'-dimethylester ($DMeCO_2$bipy) and 121.5 mg (300 µmol) [$ReBr(CO)_5$] were suspended in 10 ml petroleum benzin (100 - 120 °C) and refluxed for 14 h. The red coloured precipitate was then filtered off and washed with MTBE to afford 183.7 mg (295 µmol, 98 %) **60** as an orange-red powder. IR(KBr): 2033 (s), 1919 (s), 1899 (s), 1890 (s), 1870 (m), 1735 (m), 1400 (w), 1265 (m), 1230 (m), 767 (m). ^{1}H-NMR (300 MHz, d^6-dmso, ppm): 9.26 (*d*, 2 H), 9.24 (*d*,

2 H), 8.14 (*dd*, 2 H), 4.02 (*s*, 6 H). HPLC (min): 15.43 (M-Br), 17.37. Anal. calcd. for $C_{17}H_{12}BrN_2O_7Re$ (%): C: 32.81, H: 1.94, N: 4.50. Found: C: 32.72, H: 2.14, N: 4.82.

[Re(OH$_2$)(CO)$_3$DMeCO$_2$bipy](TflsO) (**61**). 175 mg (281 µmol) **60** was suspended in 10 ml MeOH and 72.2 mg (281 µmol) AgOTfls, dissolved in 5 ml MeOH, added and stirred for 7 h. The resulting precipitate (AgBr) was then removed quantitatively by filtration, the solution evaporated to dryness, suspended in 100 ml water, brought to reflux for 1 h, filtered and lyophilized to afford 185 mg (161 µmol, 93 %) **61** as an orange powder. Alternatively to aqueous workup the compound is applied to column chromatography to remove silver quantitatively. ^{1}H-NMR (300 MHz, d^6-dmso, ppm): 9.33 (*d*, 2 H), 9.28 (*m*, 2 H), 8.22 (*m*, 2 H), 7.69 (*s*, 20 % Re-OH$_2$), 4.03 (*s*, 6 H). HPLC (min): 15.40.

[Re(py)(CO)$_3$DMeCO$_2$bipy](TflsO) (**62**). 50 µmol (35.2 mg) **61** was dissolved in 10 ml MeOH and pyridine (50 µl, 621 µmol) added. The resulting solution was stirred for 3 days before the solvent was removed in vaccuo, the residue suspended in MTBE by sonication, filtered and washed with MTBE to afford 33.7 mg **62** (44 µmol, 87 %) as an orange powder. λ_{max}(H$_2$O): 381 nm (ε = 4650 M^{-1}cm^{-1}). λ_{em}(H$_2$O): 619 nm (Φ_{em} = 0.0010 ± 0.0001). IR(KBr): 2034 (s), 1943 (s), 1925 (s), 1745 (m), 1262 (s), 1031 (m), 638 (m). ^{1}H-NMR (200 MHz, d^6-dmso, ppm): 9.51 (*d*, 2 H), 9.17 (*s*, 2 H), 8.37 (*d*, 2 H), 8.23 (*d*, 2 H), 7.96 (*t*, 1 H), 7.41 (*t*, 2 H), 3.99 (*s*, 6 H). ESI-MS(MeOH): *m/z* = 622.1 [M-TflsO]$^+$ (100 %). HPLC (min): 15.62. Anal. calcd. for $C_{23}H_{17}F_3N_3O_{10}ReS$ (%): C: 35.85, H: 2.22, N: 5.45. Found: C: 34.90, H: 2.26, N: 5.15.

[ReBr(CO)$_3$DMe$_2$NCObipy] (**63**). 93.4 mg **60** (150 µmol) was dissolved in 10 ml MeOH and Me$_2$N was bubbled through the solution for 2 h. Then the solvent was removed in *vaccuo* and 40 ml H$_2$O and an excess LiBr added and refluxed for 3 h and the resulting precipitate filtered and washed with H$_2$O to afford 84.9 mg **63** (131 µmol, 87 %). Alternatively the compound might be obtained by reacting DMe$_2$NCObipy (from DMeCO$_2$bipy and Me$_2$N) directly with [ReBr(CO)$_5$]. IR(KBr): 2025 (s), 1907 (s), 1885 (s), 1636 (s), 1396 (m), 1229 (w), 1097 (w), 861 (w). ^{1}H-NMR (300 MHz, d^6-dmso, ppm): 9.10 (*d*, 2 H), 8.90 (*s*, 2 H), 7.75 (*d*, 2 H), 3.07 (*s*, 6 H), 2.94 (*s*, 6 H). ESI-

MS(MeOH/MeCN): *m/z* = 569.3 $[M\text{-}Br]^+$ (100 %), 671.1 $[M+Na]^+$ (100 %), 610.2 $[M\text{-}Br+MeCN]^+$ (80 %), 1217.2 [2 M –Br]$^+$ (70 %). HPLC (min): 14.37 (M-Br), 15.92. Anal. calcd. for $C_{19}H_{18}BrN_4O_5Re$ (%): C: 35.19, H: 2.80, N: 8.64. Found: C: 35.42, H: 2.98, N: 8.37.

[Re(OH$_2$)(CO)$_3$DMe$_2$NCObipy](TflsO) (**64**). 84 mg (130 µmol) **63** was dissolved in 10 ml MeOH and 33.9 mg (132 µmol) AgOTfls, dissolved in a minimum amount of MeOH, added. The resulting mixture was stirred for 3 d and sonicated several times in between, before AgBr was removed quantitatively by filtration. The resulting, clear orange solution was evaporated to dryness, taken up in a minimum amount of CH_2Cl_2 and applied to column chromatography (AlOx, CH_2Cl_2, 0 - 100 % MeOH). Half of the resulting yellow powder was directly used for the synthesis of **65**. HPLC (min): 14.34.

[Re(py)(CO)$_3$DMe$_2$NCObipy](TflsO) (**65**). Half of **64** was suspended in 10 ml MeOH, 50 µl pyridine (621 µmol) added and stirred for 4 days before the solvent was removed. The residue was then taken up in 5 ml CH_2Cl_2, filtered and 20 ml MTBE added to cause precipitation. Filtration and washing with MTBE afforded 16.1 mg **65** (20.2 µmol; 40 % based on **63**) as an orange, hydroscopic powder. $\lambda_{max}(H_2O)$: 371 nm (ε = 2600 $M^{-1}cm^{-1}$). $\lambda_{em}(H_2O)$: 604 nm (Φ_{em} = 0.0012 ± 0.0001). IR(KBr): 2035 (s), 1931 (s), 1637 (s), 1262 (s), 1033 (m), 640 (m). ^{1}H-NMR (300 MHz, d^6-dmso, ppm): 9.37 (*d*, 2 H), 8.83 (*s*, 2 H), 8.46 (*d*, 2 H), 7.99 (*t*, 1 H), 7.91 (*d*, 2 H), 7.47 (*t*, 2 H), 3.05 (*s*, 6 H), 2.91 (*s*, 6 H). ESI-MS(MeOH): *m/z* = 648.2 $[M\text{-}TflsO]^+$ (100 %). HPLC: 14.77 min. Anal. calcd. for $C_{19}H_{13}F_3N_3O_6ReS$ (%): C: 34.86, H: 2.00, N: 6.42. Found: C: 34.66, H: 1.99, N: 6.62.

4.1.2 Cobalt

$[Co(py)_2(dmgH)_2](PF_6)$ (**71**). 2.491 g (10 mmol) $Co(AcO)_2.4H_2O$ were dissolved in 70 ml MeCN under N_2 atmosphere and pyridine (8.05 ml, 100 mmol) was added. Then 2.322 g (20 mmol) dimethylglyoxime ($dmgH_2$), dissolved in 20 ml of MeCN under N_2, was added under exclusion of air, causing a brown precipitate. After stirring for 15 min air was passed through the solution for 15 min, turning the mixture into a clear, brown solution. This solution was filtered and 3.26 g (20 mmol) NH_4PF_6, dissolved in a minimum amount of H_2O, was added to the filtrate. The resulting coffee brown precipitate was then filtered and washed with H_2O to yield 5.802 g (9.8 mmol, 98 %) of **71**. IR(KBr): 1558 (m), 1453 (s), 1243 (m), 840 (s), 828 (s), 762 (m), 556 (m). ^{1}H NMR (300 MHz, d^6-DMSO, ppm): 18.14 (*s*, 2 H), 8.17 (*d*, 4 H), 8.01 (*t*, 2 H), 7.57 (*t*, 4 H), 2.30 (*s*, 12 H). Anal. calcd. for $C_{18}H_{24}CoF_6N_6O_4P$ (%): C: 36.50, H: 4.08, N: 14.19. Found: C: 36.93, H: 4.11, N: 14.40.

$[Co(py)_2(dmgH)(dmg)]$ (**72**). To $[Co(AcO)_2(OH_2)_4]$ (622.5 mg, 2.5 mmol) in 10 ml MeOH was added 2 ml pyridine (24.8 mmol) under stirring. The dark violet solution was degassed and flushed with argon several times before $dmgH_2$ (581 mg, 5 mmol) was added as a solid. Immediate formation of a brown precipitate occurs. After 5 minutes stirring under argon atmosphere air was gently bubbled through the suspension for 1 h and the solvent removed in *vacuo*. The residue was then taken up in 50 ml H_2O and filtered to remove any insoluble material. Slow addition of 1 M NaOH (5 ml, 2 equivalents) resulted in formation of brownish, cubic crystals. Filtration and washing with cold H_2O afforded 843.4 mg (1.89 mmol, 76 %) **72**. IR(KBr): 1291 (s), 772 (s), 698 (s), 515 (s). ^{1}H NMR (200 MHz, D_2O, ppm): 8.30 (*d*, 4 H), 7.76 (*t*, 2 H), 7.26 (*t*, 4 H), 2.13 (*s*, 6 H), 1.92 (*s*, 6 H). ESI-MS(MeOH): *m/z* = 447.1 $[MH]^+$ (35 %), 289.3 [MH- 2 pyridine]$^+$ (100 %). HPLC: 13.69 min. Anal. calcd. for $C_{18}H_{23}CoN_6O_4$ (%): C: 48.44, H: 5.19, N: 18.83. Found: C: 48.31, H: 5.18, N: 18.34.

4.1.3 Ligand syntheses

4,4'-Dimethyl-2,2'-bipyridine (DCH_3bipy, **81**). HPLC (min): 13.08.

4,4'-Bis[(trimethylsilyl)methyl]-2,2'-bipyridine (4,4'-$DTMSCH_2$bipy, **82**).[131,132] HPLC (min): 12.97.

4,4'-Bis(Chloromethyl)-2,2'-bipyridine (4,4'-$DClCH_2$bipy, **83**).[131,132] HPLC (min): 16.33.

4,4'-Bis(acetoxymethyl)-2,2'-bipyridine (4,4'-$DAcOCH_2$bipy, **84**).[131,132] HPLC (min): 14.10.

4,4'-Bis(hydroxymethyl)-2,2'-bipyridine (4,4'-$DHOCH_2$bipy, **85**).[131,132] HPLC (min): ~5.5 (broad).

4,4'-Bis(azidomethyl)-2,2'-bipyridine (4,4'-DN_3CH_2bipy, **86**). To a solution of **83** (253 mg, 1 mmol) in 20 ml DMF was added NaN_3 (174 mg, 2.74 mmol). The reaction was followed by HPLC and was usually complete after 1 h and DMF was removed in *vaccuo* followed by EtOAc extraction of the residue and washing with brine. Subsequent evaporation of the organic solvent afforded **86** as an of yellow powder (253 mg, 0.95 mmol, 95 %). ESI-MS(MeOH): *m/z* = 267.2 $[M+H]^+$ (100 %), 289.2 $[M+Na]^+$ (30 %).HPLC (min): 15.56.

4,4'-Bis(aminomethyl)-2,2'-bipyridine (4,4'-DH_2NCH_2bipy, **87**). To 253 mg **87** (0.95 mmol) was added a spatula tip of 10 % Pd/C (need not be fresh) and 25 ml MeOH. The mixture was degassed and stirred for 2 h at room temperature under a H_2 atmosphere. The reaction was followed by HPLC. After complete conversion Pd/C was filtered of over celite and the filtrate concentrated to dryness. If needed the residue was extracted with CH_2Cl_2 and washed with concentrated NaOH, the organic phase concentrated in *vaccuo* to afford **87** as a colourless white powder (110 mg, 0.51 mmol, 51 % based on **83**). The sample contained an impurity (~10 %) of monosubstituted product (eg. 4-aminomethyl-4'-methyl-2,2'-bipyridine) from the synthesis of **83**. ^{1}H-NMR (200 MHz, d^6-dmso, ppm): 8.56 (*d*, 2 H), 8.38 (*s*, 2 H), 7.39 (*d*, 2 H), 3.83 (*s*, 4 H), 1.99 (*s*, 4 H). ESI-MS(MeOH): *m/z* = 215.3 $[M+H]^+$ (100 %). HPLC (Et_3N gradient, min): 13.39. Anal. calcd. for $C_{12}H_{14}N_4$ (%): C: 67.27, H: 6.59, N: 26.15. Found: C: 67.15, H: 6.41, N: 24.81.

2,2'-bipyridine-4,4'-dimethylester ($DMeCO_2$bipy, **88**).[135] HPLC (min): 17.70.

2,2'-bipyridine-4,4'-diamide ($DH_2NHCObipy$, **89**). To 112 mg $DMeCO_2bipy$ (411 µmol) was added 20 ml of a saturated NH_3 solution in methanol. The mixture was stirred for 3 days at room temperature, filtered and washed with MeOH to obtain 99.5 mg (411 µmol, 100 %) **89** as a white solid. Solubility in all solvents except DMSO was very low. ^{1}H-NMR (200 MHz, d^6-dmso, ppm): 8.85 (*d*, 2 H), 8.79 (*s*, 2 H), 8.41 (*s*, 2 H), 7.85 (*d*, 2 H), 7.78 (*s*, 2 H). Anal. calcd. for $C_{12}H_{10}N_4O_2$ (%): C: 59.50, H: 4.16, N: 23.13. Found: C: 59.20, H: 4.47, N: 23.29.

1,10-phenanthroline (phen, **90**). HPLC (min): 12.30.

5-nitro-1,10-phenanthroline ($phenNO_2$, **91**).[136] HPLC (min): 13.75.

5-amino-1,10-phenanthroline ($phenNH_2$, **92**). 1.96 g (8.71 mmol) $phenNO_2$ (**91**) was dissolved in 130 ml of hot MeOH, and two spatula full of 10 % Pd/C (~100 mg) were added to the solution. The reaction mixture was degassed with H_2 and vigorously stirred at 50 °C for 5 h after which HPLC analysis indicated complete reaction. The mixture was then filtered over celite, evaporated to dryness and retiturated from H_2O and filtered to obtain 1.098 g (5.63 mmol, 65 %) of **92** as a brownish powder. Another portion of 316 mg (1.62 mmol, 19 %) **92** was obtained by evaporation of the motherliquid and extraction in EtOH. IR(KBr): 3417 (m), 3321 (m), 3225 (w), 1634 (s), 1594 (s), 1488 (s), 1428 (s), 1406 (s), 740 (s). ^{1}H-NMR (300 MHz, d^6-dmso, ppm): 9.05 (*d*, H), 8.6 (*m*, 2 H), 8.04 (*d*, H), 7.73 (*dd*, H), 7.50 (*dd*, H), 6.86 (*s*, H), 6.13 (*s*, 2 H). ESI-MS(MeOH): *m/z* = 196.0 $[M+H]^+$ (100 %), 218.0 $[M+Na]^+$ (30 %). HPLC: 12.20 min. Anal. calcd. for $C_{12}H_9N_3$ (%): C: 73.83, H: 4.65, N: 21.52. Found: C: 77.97, H: 4.97, N: 22.78 (EA H.Spring, 23.6.06 & 16.06.06, total 106 %, normalized to 100 %: C: 73.75, H: 4.70, N: 21.55).

N-(1,10-phenanthrolin-5-yl)-isonicotinamide (pAp, **93**). 185 mg (1.5 mmol) isonicotinic acid was refluxed for 150 min in 50 ml freshly distilled $SOCl_2$ along with 0.1 ml DMF, before $SOCl_2$ was removed under reduced pressure and the crude residue of isonicotinchloride dried for 1.5 days at an oil diffusion pump. 195 mg (1 mmol) **92** was dried for 2 days at an oil diffusion pump and then dissolved in 75 ml dry, refluxing THF along with 5 ml dry TEA. The former compound was then as well dissolved in 20 ml dry THF and added to the latter solution by cannula. There was an immediate, slightly orange coloured precipitate, but the mixture was refluxed for 7 h, before the precipitate was

filtered off and discarded (mainly [HTEA]Cl and [phenNH_3]Cl). The mother liquid was then taken to dryness and applied to column chromatography (basic aluminium oxide, CH_2Cl_2, 2.5 % MeOH, 0.25 % aq. NH_3, rf = 0.1). The first fractions were discarded, and parts of the product spontaneously crystallized in the latter fractions. Filtration yielded 53.4 mg of pure pAp, and evaporation of the solvent yielded another 55.5 mg of high purity pAp, both after washing. Combined yield of **93**: 108.9 mg (0.36 mmol, 36 %) of an off-yellow, crystalline product. IR(KBr): 1681 (s), 1568 (m), 1554 (s), 1285 (m), 738 (s), 697 (m). ^{1}H-NMR (200 MHz, d^6-dmso, ppm): 10.91 (*s*, H), 9.15 (*dd*, H), 9.10 (*dd*, H), 8.86 (*d*, 2 H), 8.57 (*dd*, H), 8.52 (*dd*, H), 8.17 (*s*, H), 8.03 (*d*, 2 H), 7.82 (*dd*, H), 7.78 (*dd*, H). ESI-MS(MeOH): *m/z* = 301 $[M+H]^+$ (100 %). HPLC (min): 10.5 (broad).

N-(pyridin-4-ylmethyl)-1,10-phenanthrolin-5-amine (pAmp, **94**). 195 mg (1 mmol) **92** was dissolved in 50 ml abs. EtOH and 3 Å molesieve added to the solution. Then 200 µl (2.1 mmol) isonicotinaldehyde were added and the mixture refluxed for 5 days, after which 100 mg $NaBH_4$ (2.6 mmol) were added and the solution stirred again for 2 h at room temperature. Filtration, removal of solvent, suspension in H_2O and filtration then yielded 189 mg (0.66 mmol, 66 %) of **94** in 95 % purity as an orange powder (the major impurity was identified as phenNH_2). Column chromatography can be applied to get pure **94** (basic aluminium oxide, CH_2Cl_2, 1.25 % MeOH, 0.125 % aq. NH_3, rf = 0.1, rf of phenNH_2 = 0.2). IR(KBr): 3366 (s), 3045 (m), 1616 (s), 1608 (s), 1595 (s), 1417 (s), 833 (m), 738 (s). ^{1}H-NMR (300 MHz, d^6-dmso, ppm): 9.08 (*d*, H), 8.83 (*d*, H), 8.68 (*d*, H), 8.49 (*d*, 2 H), 7.98 (*d*, H), 7.80 (*dd*, H), 7.47 (*dd*, H), 7.44 (*d*, 2 H), 7.38 (*t*, H), 6.56 (*s*, H), 4.64 (*d*, 2 H). HPLC: 11.38 min. Anal. calcd. for $C_{18}H_{14}N_4.0.5H_2O$ (%): C: 73.20, H: 5.12, N: 18.97. Found: C: 74.00, H: 4.99, N: 18.72.

4.2 Methods

Mass spectra were measured on a Bruker Esquire HCT (ESI) instrument and only characteristic fragments are given. The solvent flow rate for ESI measurements was 5 µl min^{-1}, a nebulizer pressure of 15 psi and a dry gas flow rate of 5 L min^{-1} at a dry gas temperature of 300°C were used.

Elemental analyses were performed on a LecoCHNS-932 elemental analyzer.

^{1}H NMR spectra were recorded on Varian Mercury and Varian Gemini-2000 spectrometers (^{1}H at 199.97 MHz and 300.08 MHz, respectively). The chemical shifts are reported relative to residual solvent protons as reference.

Luminescence measurements were performed on a Perkin-Elmer LS50B fluorescence spectrometer with argon-purged solution samples in 1 cm cells. Luminescence life time measurements were performed on an Edinburgh Instrument F900 equipped with a nF900 nanosecond flash lamp filled with hydrogen (operating at 0.4 bar and frequency 40 KHz). Luminescence quantum yields were determined relative to coumarin I in ethanol (0.64)[153] according to literature procedure.[154]

UV-Vis spectra were measured using a Cary 50 spectrometer with solution samples in 1 cm quartz cells. If necessary, cells with silicon septa lids were used to keep samples under an inert gas atmosphere during measurements.

IR spectra were recorded on a Bio PerkinElmer SpectrumBXFT-IR spectrometer with samples in compressed KBr-pellets.

Electrochemical measurements were carried out in DMF containing 0.1 M [TBA][PF_6] as conducting electrolyte. A Metrohm 757VA Computrace electrochemical analyzer was used with a standard three-electrode setup of glassy carbon working (ID = 3 mm) and Pt auxiliary electrodes and an Ag/AgCl reference electrode. All potentials are given vs. Ag/AgCl and are referenced with Fc/Fc^+ at +500 mV. Spectroelectrochemical analysis was performed in an optical transparent thin layer electrolysis (OTTLE) cell in the UV-Vis spectrometer described above. The working electrode was a platinum gaze immersed into the OTTLE cell, auxiliary electrode was a platinum wire in

a compartment separated by a diaphragm, and the reference electrode was an Ag/AgCl electrode.

HPLC measurements were performed on a VWR LaChrome Elite® using a Nucleodur C18 Gravity column operated in an oven (L-2350) at 40 °C and a PDA detector (L-2450). The gradient was as follows: A = 0.1 % TFA, 10 % MeOH, H_2O; D = MeOH; flow rate = 0.5 ml/min; 0 – 5 min 100 % A; 5 – 15 min 0 – 100 % D; 15 – 18 min 100 % D. Control runs before and after catalysis were systematically performed using 10 µl of the reaction solution in DMF. Under these conditions $dmgH_2$ gave a broad peak at 6.4 min and **1** a defined peak at 17.04 min.

Gas chromatograms with an automated setup were recorded using a Varian CP-3800 gas chromatograph with argon as carrier gas and a 3 m x 2 mm packed molecular sieve 13X 80-100 column. The gas flow was set to 20 ml/min. The oven was operated isothermal at 100 °C. Manual measurements were done by injecting 100 µl of headspace volume directly onto the column. Analysis then gave total amounts of H_2 produced by comparison with a calibration curve using pure H_2 in the same vessel containing the same buffer solution. Alternatively, an automated setup was used as follows: an argon flow of usually 10.8 ml/min (adjusted with a manual flow controller (Porter, 100) and referenced with a flow meter (MS Wil GmbH)) was passed through the reaction mixture and into the GC, where 100 µl gas samples were automatically injected in defined time intervals (usually 5 min) using a 6-Port-2-Position Valve from Vicci. The gases were detected using a thermal conductivity detector (Varian) operated at 150 °C. Hydrogen production rates were calibrated by introducing a known flow of pure hydrogen by a Single Syringe Pump (70-2208 from Harvard Apparatus, using a 2.5 ml Hamilton GASTIGHT® #1002 syringe and a Teflon® tube) to the 60 ml Schlenk containing 1 M TEOA in DMF. Plotting of the peak area for hydrogen versus the used flow rates of hydrogen gave linear fits. The slope of these fits depended linearly on the argon flow through the solution. Varying the argon flow thus allowed detecting smaller hydrogen production rates, although at a higher response time (20 min for 10.8 ml/min). This setup allowed us to detect $H_2/s \geq 0.3 \times 10^{-9}$ mol s^{-1} (standard deviation is $\leq 0.2 \times 10^{-9}$ mol s^{-1}).

Photochemical measurements were carried out in a 60 ml septum capped Schlenk tube containing a Teflon® stirrer at 500 rpm. 10 ml of a solution containing the respective mixture were prepared, wrapped in black foil and degassed using an argon-purged Schlenk-line. The mixture was equilibrated under 1.5 bar argon pressure for 15 min and then transferred to a dark room for illumination. The light source was either a 380 resp. 476 nm high flux LED from Rhopoint Components LTD (OTLH-0280-UV resp. OTLH-0010-BU; CPC reflector for Shark LED; irradiated directly from below; current control at usually 200 mA; hv/s = 1.75 x 10^{-7} mol/s resp. 2 x 10^{-7} mol/s). If necessary the radiant flux was varied by adjustment of the current through the LED. The radiant flux at different currents was calibrated using actinometry. A constant flow of usually 5.4 – 21.6 ml/min argon was passed through the solution and into a sixport valve at the GC, where 100 µl gas samples were injected into the GC-TCD gas analyzer in defined intervals. Integration of the production rate versus time gave the total amount of hydrogen produced. Alternative setup: the light source was a Leica Pradovit S AF slide projector equipped with a 250 W Osram Xenophot HLX lamp. The light was filtered by a 400 nm cut off filter (Schott GG 400, no transmission below 400 nm) before reaching the sample at 40 cm distance from the projector. If necessary the radiant flux was cut in $(1/2)^n$ by using n neutral density filters (OD = 0.3). 100 µl gas samples were drawn from the headspace above the solution and injected into the GC-TCD gas analyzer.

Actinometry for quantum yield determination was performed in a 1 cm quartz cell containing 2 ml of a 9 mM $K_3[Fe(ox)_3]$ in 0.1 N H_2SO_4 as chemical actinometer and was irradiated as described in Quantum Yields (1−T for $K_3[Fe(ox)_3]$ > 0.999). For calibration of the photon flux in the standard setup the identical setup as for hydrogen production (LED from below, varying current, 60 ml Schlenk, stirred, argon flow of 21.6 ml/min) was used with 10 ml of a 9 mM $K_3[Fe(ox)_3]$ in 0.1 N H_2SO_4 as chemical actinometer. Analysis of irradiated solutions: after a certain time at a certain LED current 100 µl of the irradiated solution were added to 100 µl of a 5 mM solution of phenanthroline in H_2O, agitated and left in the dark for 30 min. After this 50 µl of a 600 mM NaOAc / 360 mN H_2SO_4 buffer and 750 µl H_2O were added and the absorption at 511 nm was determined relative to a solution that was not

irradiated. Conversion to photon flux as a function of LED current was achieved by using ε[$Fe^{II}(phen)_3$], 511nm = 10750 ± 76 M^{-1} cm^{-1} and $\Phi(Fe^{III} \rightarrow Fe^{II})$ = 1.18 resp. 0.925 for 380 resp. 476 nm.[155]

Quantum Yields were determined in a 1 cm quartz cell using a 380 nm LED (OTLH-0280-UV, Rhopoint Components LTD) in series with an iris and a lens to ensure linear photon flux. The cells were filled with 2 ml solutions as follows: 0.5 mM **12** (1−T = 0.957 ± 0.0033) resp. **10** (1−T = 0.971 ± 0.0028), 0.5 mM {$[Co(OH_2)_6](BF_4)_2$, 6 $dmgH_2$} resp. 1 mM {$Co(ac)_2(H_2O)_4$], 6 $dmgH_2$}, 1 M TEOA, 0.1 M HBF_4 resp. AcOH, DMF, Ar. Total hydrogen was determined by manually sampling 20 µl of head space gas through a septum and subsequent injection in a GC/TCD system as described above. The photon flux as determined by actinometry was 4.81 ± 0.13 × 10^{-9} mol/s. It was corrected for the respective fractions of light absorbed. The hydrogen production rates measured were 2.18 ± 0.082 × 10^{-9} mol/s resp. 1.01 ± 0.069 × 10^{-9} mol/s for **12** resp. **10**.

UV-pump-IR-probe spectroscopy. The system for UV-pump-IR-probe spectroscopy consists of two synchronized[156] commercially available Ti:sapphire-oscillator/regenerative amplifier femtosecond laser systems operating at 800 nm (Spectra Physics, duration ~100 fs, repetition rate 1 kHz, energy ~600 µJ/pulse), allowing us to cover the time range from 2 ps to 10 µs. Laser system 1 was frequency-doubled with a BBO crystal. The obtained 400 nm pulses were subsequently focused into the sample cell (100 µm thick) with a spot size of ~200 µm diameter. Measurements were carried out using parallel and perpendicular polarized pump pulses generated by a computer-controlled half-wave plate, from which the magic angle signal was calculated. Laser system 2 pumped a white light seeded two-stage BBO optical parametric amplifier (OPA),[157] the signal and idler pulses of which were difference frequency mixed in an $AgGaS_2$ crystal. They were separated into two parts to achieve broadband probe and reference pulses. These IR-probe pulses were focused into the sample cell in spatial overlap with the 400 nm pump pulse. Reference and probe pulse were dispersed in a monochromator (SPEX Triax Series) and imaged onto a 2 x 64 pixel MCT (Mercury Cadmium Telluride) detector array (InfraRed Associates Inc.), revealing a spectral

resolution of 3.5 cm^{-1}. To ensure efficient exchange of the excited volume, the sample was pumped rapidly by a tubing pump (Ismatec BVP equipped with EasyLoad II pump-head, flow ~5.0 ml/min) to a small sealed reservoir (V ≈ 3 ml). The pressurized flow of the reservoir transferred the sample through the flow cell (path length 100 µm) and finally back to the tank, which was protected from light. Since TEOA is a very aggressive compound, the EasyLoad II pump-head was equipped with chemically resistant fluoroelastomer tubing from Gore™ (Chem-Sure®; 1.6 mm ID, 1.6 mm wall, 4.8 mm OD, 305 mm length). The solution was purged with argon continuously. During the course of the measurement, unwanted photo-products accumulated to less than 5%.

Crystallographic data were collected at 183(2) K with Mo K_α radiation (λ = 0.7107 Å) that was graphite-monochromated on either a Stoe IPDS diffractometer or an Oxford Diffraction CCD Xcalibur system with a Ruby detector. Suitable crystals were covered with oil (Infineum V8512, formerly known as Paratone N), mounted on top of a glass fibre or a CryoLoop™ (Hampton Research) and immediately transferred to the diffractometer. In the case of the IPDS, a maximum of eight thousand reflections distributed over the whole limiting sphere were selected by the program SELECT and used for unit cell parameter refinement with the program CELL.[158] Data were corrected for Lorentz and polarisation effects as well as for absorption (numerical). In case of the Oxford system, the program suite CrysAlis^{Pro} was used for data collection, semi-empirical absorption correction and data reduction.[159] Structures were solved with direct methods using SIR97[160] and were refined by full-matrix least-squares methods on F^2 with SHELXL-97.[161] The structures were checked for higher symmetry with help of the program Platon.[162]

4.3 Crystallographic Tables

	10	**11**	**12**
	bp070607	bp061109	bp160909
Empirical formula	$C_{13}H_8BrN_2O_3Re$	$C_{14}H_{10}F_3N_2O_7ReS$	$C_{14}H_8N_3O_3ReS$
Formula weight	506.32	593.5	484.49
Diffractometer	Oxford Xcalibur	Oxford Xcalibur	Oxford Xcalibur
Crystal system	Monoclinic	Monoclinic	Monoclinic
Space group	$P2_1/n$	$P2_1/n$	$P2_1/n$
a [Å]	6.8894(2)	10.79584(13)	7.29785(10)
b [Å]	15.1940(3)	9.76947(10)	15.32108(18)
c [Å]	13.4568(3)	17.51150(18)	13.12657(16)
α [°]	90	90	90
β [°]	97.110(3)	93.1248(10)	93.5750(12)
γ [°]	90	90	90
Volume [$Å^3$]	1397.79(6)	1844.19(3)	1464.84(3)
Z	4	4	4
calc. dens. [Mg/m^3]	2.406	2.138	2.197
Abs. coef. [mm^{-1}]	11.559	6.772	8.453
F(000)	936	1128	912
Crystal size [mm^3]	0.21 x 0.15 x 0.11	0.25 x 0.13 x 0.11	0.24 x 0.19 x 0.02
Crystal descr.	yellow plate	yellow block	yellow plate
Θ range [°]	2.68 to 29.13	2.81 to 30.51	2.66 to 34.34
Index ranges	-9<=h<=9, -20<=k<=20, -18<=l<=17	-15<=h<=15, -13<=k<=13, -25<=l<=23	-11<=h<=11, -24<=k<=24, -20<=l<=20
Refl. collected	24564	25840	45332
Indep. refl.	3721 [R_{int} = 0.0465]	5616 [R_{int} = 0.0243]	6134 [R_{int} = 0.0667]
Refl. obs.	2912	4454	4504
Compl. to Θ	98.9 % to 29.13°	99.9 % to 30.51°	99.9 % to 34.34°
Abs. cor.	Semi-empirical from equivalents	Semi-empirical from equivalents	Semi-empirical from equivalents
max. and min. transm.	0.3629 and 0.1511	0.571 and 0.369	0.8491 and 0.3909
Data/ restr./ param.	3721 / 66 / 212	5616 / 18 / 252	6134 / 0 / 199
GOF on F^2	1.301	1.045	0.880
Final R indices [I>2sigma(I)]	R1 = 0.0432, wR2 = 0.0979	R1 = 0.0310, wR2 = 0.0876	R1 = 0.0258, wR2 = 0.0473
R indices (all data)	R1 = 0.0646, wR2 = 0.1075	R1 = 0.0413, wR2 = 0.0900	R1 = 0.0453, wR2 = 0.0497
abs. struct. param.	-	-	-
Largest diff. peak and hole [$e.Å^{-3}$]	2.161 and -2.534	1.566 and -1.399	2.181 and -0.698

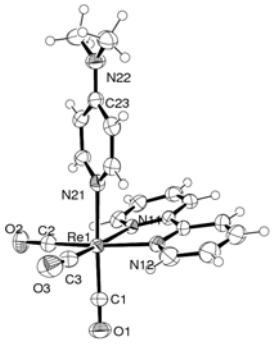

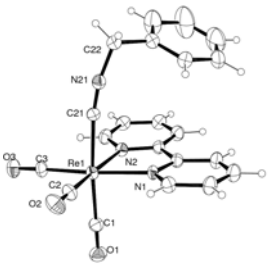

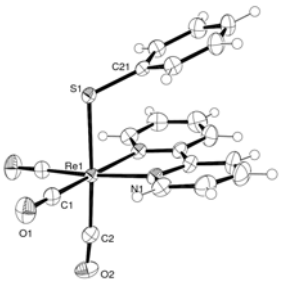

	14	**15**	**17**
	bp151209	bp280510	bp180509
Empirical formula	$C_{21}H_{19}F_3N_4O_{6.5}ReS$	$C_{22}H_{15}F_3N_3O_6ReS$	$C_{19}H_{13}N_2O_3ReS$
Formula weight	706.66	692.65	535.57
Diffractometer	Stoe IPDS	Stoe IPDS	Oxford Xcalibur
Crystal system	Monoclinic	Monoclinic	Orthorhombic
Space group	C2/c	$P2_1/n$	Pnma
a [Å]	25.7038(18)	14.5408(15)	11.37769(13)
b [Å]	12.7263(8)	12.8118(8)	12.11061(11)
c [Å]	14.9858(10)	12.9437(13)	13.19847(16)
α [°]	90	90	90
β [°]	95.430(8)	96.486(12)	90
γ [°]	90	90	90
Volume [$Å^3$]	4880.1(6)	2395.9(4)	1818.63(3)
Z	8	4	4
calc. dens. [Mg/m^3]	1.924	1.915	1.956
Abs. coef. [mm^{-1}]	5.136	5.226	6.817
F(000)	2744	1328	1024
Crystal size [mm^3]	0.21 x 0.12 x 0.08	0.23 x 0.12 x 0.09	0.30 x 0.25 x 0.10
Crystal descr.	yellow block	yellow block	orange block
Θ range [°]	2.87 to 30.40	2.55 to 26.37	2.28 to 33.14
Index ranges	-36<=h<=36, -18<=k<=18, -21<=l<=21	-18<=h<=18, -15<=k<=15, -16<=l<=16	-17<=h<=17, -18<=k<=18, -19<=l<=18
Refl. collected	40207	28220	31837
Indep. refl.	7323 [R_{int} = 0.0639]	4881 [R_{int} = 0.0414]	3544 [R_{int} = 0.0364]
Refl. obs.	4669	4107	2893
Compl. to Θ	99.1 % to 30.40°	99.7 % to 26.37°	98.1 % to 33.14°
Abs. cor.	Semi-empirical from equivalents	Numerical	Semi-empirical from equivalents
max. and min. transm.	0.4983 and 0.3198	0.6716 and 0.5068	0.5488 and 0.3337
Data/ restr./ param.	7323 / 1 / 335	4881 / 0 / 325	3544 / 0 / 127
GOF on F^2	0.876	0.986	1.137
Final R indices [I>2sigma(I)]	R1 = 0.0310, wR2 = 0.0728	R1 = 0.0287, wR2 = 0.0751	R1 = 0.0191, wR2 = 0.0549
R indices (all data)	R1 = 0.0557, wR2 = 0.0790	R1 = 0.0347, wR2 = 0.0779	R1 = 0.0281, wR2 = 0.0558
abs. struct. param.	-	-	-
Largest diff. peak and hole [$e.Å^{-3}$]	1.184 and -0.819	1.338 and -0.766	0.956 and -1.227

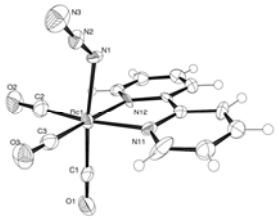
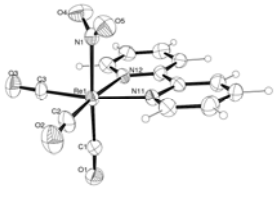
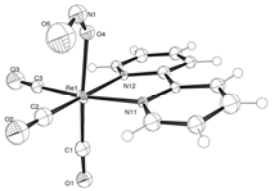

	18	**19-NO_2**	**19-ONO**
	bp070110	bp271109	bp08120t
Empirical formula	$C_{13}H_8N_5O_3Re$	$C_{13}H_8N_3O_5Re$	$C_{13}H_8N_3O_5Re$
Formula weight	468.44	472.42	472.42
Diffractometer	Oxford Xcalibur	Stoe IPDS	Oxford Xcalibur
Crystal system	Monoclinic	Triclinic	Monoclinic
Space group	$P2_1/c$	P-1	Cc
a [Å]	14.8659(9)	6.698(9)	15.2700(11)
b [Å]	10.9772(4)	10.716(15)	10.6479(4)
c [Å]	8.7306(5)	10.750(13)	9.2298(7)
α [°]	90	79.48(15)	90
β [°]	106.061(6)	73.07(15)	114.414(9)
γ [°]	90	72.10(16)	90
Volume [$Å^3$]	1369.11(13)	698.8(16)	1366.52(15)
Z	4	2	4
calc. dens. [Mg/m^3]	2.273	2.236	2.296
Abs. coef. [mm^{-1}]	8.896	8.719	8.921
F(000)	880	442	888
Crystal size [mm^3]	0.08 x 0.05 x 0.02	0.08 x 0.07 x 0.04	? x ? x ?
Crystal descr.	yellow plate	yellow block	yellow sheet
Θ range [°]	2.43 to 28.28	3.30 to 30.42	2.93 to 26.37
Index ranges	-19<=h<=18, -14<=k<=14, -11<=l<=11	-9<=h<=9, -15<=k<=15, -13<=l<=15	-19<=h<=18, -13<=k<=13, -9<=l<=11
Refl. collected	19792	7338	6412
Indep. refl.	3402 [R_{int} = 0.0865]	3823 [R_{int} = 0.0550]	2353 [R_{int} = 0.0835]
Refl. obs.	2213	2817	2028
Compl. to Θ	99.9 % to 28.28°	89.8 % to 30.42°	99.6 % to 26.37°
Abs. cor.	Semi-empirical from equivalents	Numerical	Semi-empirical from equivalents
max. and min. transm.	0.8421 and 0.7694	0.7388 and 0.5821	1.0000 and 0.65795
Data/ restr./ param.	3402 / 0 / 195	3823 / 0 / 199	2353 / 2 / 95
GOF on F^2	1.037	1.050	1.053
Final R indices [I>2sigma(I)]	R1 = 0.0523, wR2 = 0.1247	R1 = 0.0432, wR2 = 0.1019	R1 = 0.0577, wR2 = 0.1137
R indices (all data)	R1 = 0.0934, wR2 = 0.1333	R1 = 0.0658, wR2 = 0.1168	R1 = 0.0735, wR2 = 0.1186
abs. struct. param.	-	-	0.48(3)
Largest diff. peak and hole [$e.Å^{-3}$]	3.753 and -1.120	1.920 and -1.633	3.318 and -2.031

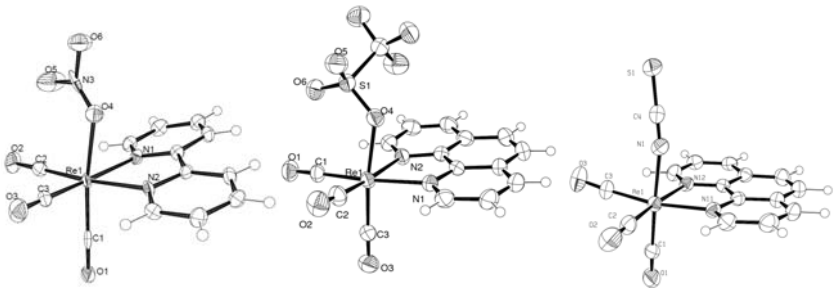

	20	**31**	**32**
	bp030609	bp221209	bp120110
Empirical formula	$C_{13}H_8N_3O_6Re$	$C_{16}H_8F_3N_2O_6ReS$	$C_{16}H_8N_3O_3ReS$
Formula weight	488.42	599.50	508.51
Diffractometer	Oxford Xcalibur	Stoe IPDS	Stoe IPDS
Crystal system	Monoclinic	Monoclinic	Monoclinic
Space group	Cc	$P2_1/c$	$P2_1/c$
a [Å]	15.6724(4)	8.3307(12)	7.9902(8)
b [Å]	10.72607(16)	14.1776(13)	9.7327(7)
c [Å]	9.0542(2)	15.222(3)	21.0550(16)
α [°]	90	90	90
β [°]	112.288(3)	101.54(2)	100.039(10)
γ [°]	90	90	90
Volume [$Å^3$]	1408.33(5)	1761.5(5)	1612.3(2)
Z	4	4	4
calc. dens. [Mg/m^3]	2.304	2.261	2.095
Abs. coef. [mm^{-1}]	8.665	7.087	7.685
F(000)	920	1136	960
Crystal size [mm^3]	0.23 x 0.10 x 0.04	0.16 x 0.08 x 0.06	0.18 x 0.14 x 0.05
Crystal descr.	yellow plate	yellow dart head	yellow pentagon
Θ range [°]	2.81 to 30.51	2.87 to 28.28	3.33 to 30.34
Index ranges	-22<=h<=22, -15<=k<=15, -12<=l<=12	-11<=h<=10, -18<=k<=18, -20<=l<=20	-11<=h<=11, -13<=k<=13, -28<=l<=28
Refl. collected	18660	17274	27214
Indep. refl.	4307 [R_{int} = 0.0503]	4359 [R_{int} = 0.0586]	4577 [R_{int} = 0.0446]
Refl. obs.	3883	3438	3596
Compl. to Θ	100.0 % to 30.51°	99.9 % to 28.28°	94.5 % to 30.34°
Abs. cor.	Semi-empirical from equivalents	Semi-empirical from equivalents	Numerical
max. and min. transm.	0.7232 and 0.4045	0.668 and 0.199	0.6066 and 0.3668
Data/ restr./ param.	4307 / 2 / 209	4359 / 0 / 262	4577 / 0 / 217
GOF on F^2	0.980	0.977	0.980
Final R indices [I>2sigma(I)]	R1 = 0.0268, wR2 = 0.0504	R1 = 0.0311, wR2 = 0.0731	R1 = 0.0282, wR2 = 0.0644
R indices (all data)	R1 = 0.0321, wR2 = 0.0512	R1 = 0.0428, wR2 = 0.0762	R1 = 0.0400, wR2 = 0.0670
abs. struct. param.	0.000(11)	-	-
Largest diff. peak and hole [$e.Å^{-3}$]	2.007 and -0.866	1.297 and -1.704	2.892 and -0.828

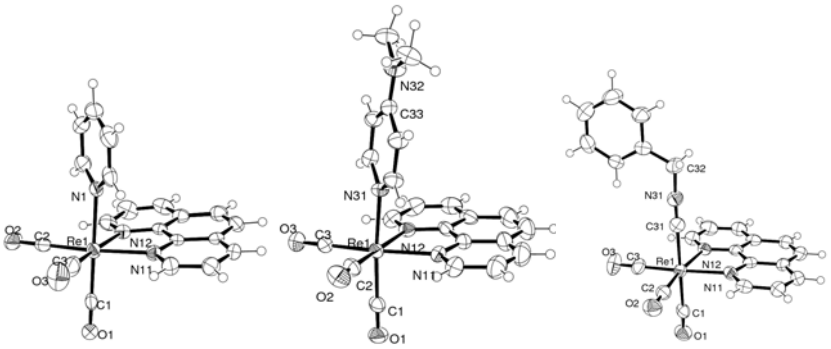

	33	**34**	**35**
	bp230909	bp210410	bp031209
Empirical formula	$C_{89}H_{57}F_{12}N_{13}O_{24}Re_4S_4$	$C_{23}H_{18}F_3N_4O_6ReS$	$C_{24}H_{15}F_3N_3O_6ReS$
Formula weight	2793.52	721.67	716.65
Diffractometer	Oxford Xcalibur	Stoe IPDS	Stoe IPDS
Crystal system	Triclinic	Monoclinic	Monoclinic
Space group	P-1	I2/a	$P2_1/c$
a [Å]	11.2444(2)	14.5365(13)	15.6272(13)
b [Å]	13.1398(2)	17.9350(13)	10.7013(13)
c [Å]	17.9128(4)	19.3964(17)	14.8192(13)
α [°]	91.7936(16)	90	90
β [°]	103.4450(18)	94.563(10)	96.506(10)
γ [°]	110.0450(17)	90	90
Volume [$Å^3$]	2400.23(8)	5040.8(7)	2462.3(4)
Z	1	8	4
calc. dens. [Mg/m^3]	1.933	1.902	1.933
Abs. coef. [mm^{-1}]	5.218	4.973	5.089
F(000)	1346	2800	1384
Crystal size [mm^3]	0.18 x 0.11 x 0.09	0.33 x 0.29 x 0.20	0.08 x 0.05 x 0.04
Crystal descr.	yellow block	orange block	yellow cube
Θ range [°]	2.55 to 30.51	2.83 to 30.56	2.31 to 25.95
Index ranges	-15<=h<=16, -18<=k<=18, -25<=l<=25	-20<=h<=20, -25<=k<=25, -27<=l<=27	-19<=h<=19, -13<=k<=13, -18<=l<=18
Refl. collected	38088	43291	23499
Indep. refl.	14627 [R_{int} = 0.0463]	7636 [R_{int} = 0.0964]	4500 [R_{int} = 0.0882]
Refl. obs.	8710	5340	2821
Compl. to Θ	99.9 % to 30.51°	98.8 % to 30.56°	93.3 % to 25.95°
Abs. cor.	Semi-empirical from equivalents	Semi-empirical from equivalents	Numerical
max. and min. transm.	0.6510 and 0.5709	0.675 and 0.208	0.8544 and 0.7347
Data/ restr./ param.	14627 / 53 / 702	7636 / 0 / 345	4500 / 0 / 405
GOF on F^2	0.800	0.993	0.870
Final R indices [I>2sigma(I)]	R1 = 0.0350, wR2 = 0.0507	R1 = 0.0334, wR2 = 0.0759	R1 = 0.0334, wR2 = 0.0610
R indices (all data)	R1 = 0.0807, wR2 = 0.0554	R1 = 0.0510, wR2 = 0.0790	R1 = 0.0699, wR2 = 0.0671
abs. struct. param.	-	-	-
Largest diff. peak and hole [$e.Å^{-3}$]	1.571 and -0.761	1.532 and -1.080	1.218 and -0.415

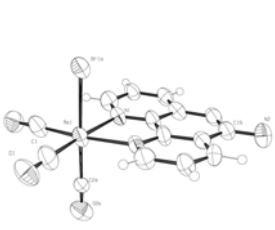
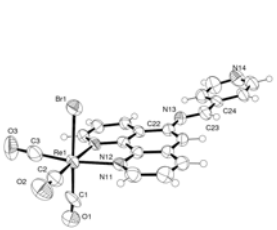
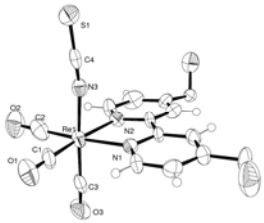

	40	**43**	**52**
	bp100706	bp050906	bp171108
Empirical formula	$C_{15}H_9BrN_3O_3Re$	$C_{21}H_{12}BrN_4O_3Re$	$C_{32.5}H_{27}Cl_{1.5}N_6O_{11.25}Re_2S_2$
Formula weight	545.36	634.46	1171.30
Diffractometer	Stoe IPDS	Stoe IPDS	Oxford Xcalibur
Crystal system	Monoclinic	Monoclinic	Monoclinic
Space group	I2/m	$P2_1/c$	C2/c
a [Å]	7.7571(11)	7.0078(13)	20.2023(4)
b [Å]	12.3526(11)	27.6866(13)	11.7090(2)
c [Å]	15.879(2)	20.4677(5)	33.5767(6)
α [°]	90	90	90
β [°]	101.791(16)	95.642(8)	91.3051(17)
γ [°]	90	90	90
Volume [$Å^3$]	1489.5(3)	3951.9(8)	7940.5(3)
Z	4	8	8
calc. dens. [Mg/m^3]	2.432	2.133	1.960
Abs. coef. [mm^{-1}]	10.859	8.204	6.363
F(000)	1016	2400	4492
Crystal size [mm^3]	0.07 x 0.06 x 0.05	0.20 x 0.16 x 0.11	0.16 x 0.04 x 0.04
Crystal descr.	orange block	orange block	yellow stick
Θ range [°]	2.11 to 25.95	2.92 to 26.37	2.34 to 26.37
Index ranges	-9<=h<=9, -15<=k<=14, -19<=l<=18	-8<=h<=8, -34<=k<=34, -25<=l<=25	-24<=h<=25, -14<=k<=14, -41<=l<=41
Refl. collected	4907	47432	49761
Indep. refl.	1521 [R_{int} = 0.1168]	8043 [R_{int} = 0.1018]	8133 [R_{int} = 0.0754]
Refl. obs.	1116	6381	4610
Compl. to Θ	99.3 % to 25.95°	99.4 % to 26.37°	99.9 % to 26.37°
Abs. cor.	Numerical	Numerical	Semi-empirical from equivalents
max. and min. transm.	0.6486 and 0.5498	0.4670 and 0.2924	0.7850 and 0.5035
Data/ restr./ param.	1521 / 1 / 118	8043 / 0 / 541	8133 / 0 / 524
GOF on F^2	0.945	0.924	0.854
Final R indices [I>2sigma(I)]	R1 = 0.0566, wR2 = 0.1308	R1 = 0.0517, wR2 = 0.1240	R1 = 0.0370, wR2 = 0.0705
R indices (all data)	R1 = 0.0774, wR2 = 0.1387	R1 = 0.0631, wR2 = 0.1314	R1 = 0.0854, wR2 = 0.0773
abs. struct. param.	-	-	-
Largest diff. peak and hole [$e.Å^{-3}$]	2.899 and -1.384	1.920 and -1.117	1.087 and -0.900

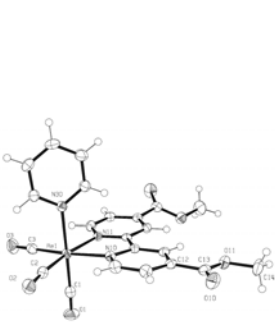

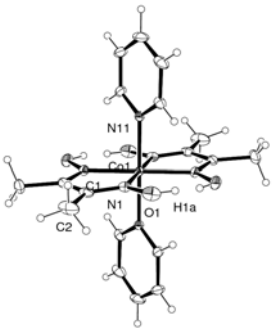

	62	**72**
	bp090610	bp300310
Empirical formula	$C_{23}H_{17}F_3N_3O_{10}ReS$	$C_{18}H_{23}CoN_6O_4$
Formula weight	770.66	446.35
Diffractometer	Oxford Xcalibur	Oxford Xcalibur
Crystal system	Monoclinic	Monoclinic
Space group	$P2_1/n$	I2/m
a [Å]	10.54319(15)	8.087(6)
b [Å]	20.8262(3)	12.686(4)
c [Å]	12.01112(14)	9.362(9)
α [°]	90	90
β [°]	91.8513(12)	90.141(13)
γ [°]	90	90
Volume [$Å^3$]	2635.96(6)	960.46(12)
Z	4	2
calc. dens. [Mg/m^3]	1.942	1.543
Abs. coef. [mm^{-1}]	4.772	0.933
F(000)	1496	464
Crystal size [mm^3]	0.17 x 0.11 x 0.05	0.10 x 0.07 x 0.05
Crystal descr.	orange block	brown block
Θ range [°]	2.53 to 33.14	2.70 to 30.51
Index ranges	-16<=h<=16, -32<=k<=32, -18<=l<=18	-11<=h<=11, -18<=k<=18, -13<=l<=13
Refl. collected	39445	5508
Indep. refl.	10044 [R_{int} = 0.0519]	1536 [R_{int} = 0.0319]
Refl. obs.	7006	1362
Compl. to Θ	100.0 % to 33.14°	99.9 % to 30.51°
Abs. cor.	Semi-empirical from equivalents	Semi-empirical from equivalents
max. and min. transm.	0.7963 and 0.6812	0.9548 and 0.9455
Data/ restr./ param.	10044 / 0 / 372	1536 / 0 / 73
GOF on F^2	0.860	1.061
Final R indices [I>2sigma(I)]	R1 = 0.0278, wR2 = 0.0430	R1 = 0.0345, wR2 = 0.0842
R indices (all data)	R1 = 0.0534, wR2 = 0.0468	R1 = 0.0402, wR2 = 0.0857
abs. struct. param.	-	-
Largest diff. peak and hole [$e.Å^{-3}$]	1.048 and -1.033	0.397 and -0.304

5 Literature

[1] Boltzmann, L.; McGuinness, B. *Theoretical physics and philosophical problems selected writings*; Reidel: Dordrecht, **1974**.

[2] Ciamician, G., *Science*, **1912**, *36*, 385-394.

[3] IEA, "*Key World Energy Statistics*", **2006**.

[4] Lewis, N. S.; Nocera, D. G., *PNAS*, **2006**, *103*, 15729-15735.

[5] Nocera, D. G., *Daedalus*, **2006**, *135*, 112-115.

[6] Nocera, D. G., "*The Solar Resource*" at *Summer School CUSO* in Villars-sur-Ollon, **2009**.

[7] http://en.wikipedia.org/wiki/Energy_density, accessed on 18.8.2010.

[8] Olah, G. A., *Angew. Chem. - Int. Ed.*, **2005**, *44*, 2636-2639.

[9] Chmielniak, T.; Sciazko, M., *Applied Energy*, **2003**, *74*, 393-403.

[10] Saito, M.; Takeuchi, M.; Watanabe, T.; Toyir, J.; Luo, S. C.; Wu, J. G., *Energy Convers. Mgmt.*, **1997**, *38*, S403-S408.

[11] IEA, *http://www.iea.org/textbase/nppdf/free/1990/autofuel99.pdf*, **1999**.

[12] data from http://en.wikipedia.org/wiki/Earth and http://www.nationmaster.com/graph/tra_roa_tot_net_km-transportation-roads-total-network-km#source; assumed 5 m road width, accessed on 18.8.2010.

[13] Armaroli, N.; Balzani, V., *Angew. Chem. - Int. Ed.*, **2007**, *46*, 52-66.

[14] Bolton, J. R., "*Solar photoproduction of hydrogen*", IEA, **1995**.

[15] Wegner, K.; Ly, H. C.; Weiss, R. J.; Pratsinis, S. E.; Steinfeld, A., *Int. J. Hyd. Ener.*, **2006**, *31*, 55-61.

[16] Steinfeld, A., *Int. J. Hyd. Ener.*, **2002**, *27*, 611-619.

[17] Caputo, G.; Felici, C.; Tarquini, P.; Giaconia, A.; Sau, S., *Int. J. Hyd. Ener.*, **2007**, *32*, 4736-4743.

[18] Yin, Q. S.; Tan, J. M.; Besson, C.; Geletii, Y. V.; Musaev, D. G.; Kuznetsov, A. E.; Luo, Z.; Hardcastle, K. I.; Hill, C. L., *Science*, **2010**, *328*, 342-345.

[19] Streich, D.; Astuti, Y.; Orlandi, M.; Schwartz, L.; Lomoth, R.; Hammarstrom, L.; Ott, S., *Chem. Europ. Jour.*, **2010**, *16*, 60-63.

[20] Probst, B.; Rodenberg, A.; Guttentag, M.; Hamm, P.; Alberto, R., *Inorg. Chem.*, **2010**, *49*, 6453-6460.

[21] Probst, B.; Kolano, C.; Hamm, P.; Alberto, R., *Inorg. Chem.*, **2009**, *48*, 1836-1843.

[22] Li, C.; Wang, M.; Pan, J.; Zhang, P.; Zhang, R.; Sun, L., *J. Organom. Chem.*, **2009**, *694*, 2814-2819.

[23] Lazarides, T.; McCormick, T.; Du, P. W.; Luo, G. G.; Lindley, B.; Eisenberg, R., *J. Am. Chem. Soc.*, **2009**, *131*, 9192-9194.

[24] Geletii, Y. V.; Huang, Z.; Hou, Y.; Musaev, D. G.; Lian, T.; Hill, C. L., *J. Am. Chem. Soc.*, **2009**, *131*, 7522-7523.

[25] Gartner, F.; Sundararaju, B.; Surkus, A. E.; Boddien, A.; Loges, B.; Junge, H.; Dixneuf, P. H.; Beller, M., *Angew. Chem. - Int. Ed.*, **2009**, *48*, 9962-9965.

[26] Duan, L.; Xu, Y.; Zhang, P.; Wang, M.; Sun, L., *Inorg. Chem.*, **2009**, *49*, 209-215.

[27] Du, P.; Schneider, J.; Luo, G.; Brennessel, W. W.; Eisenberg, R., *Inorg. Chem.*, **2009**, *48*, 4952-4962.

[28] Dempsey, J. L.; Brunschwig, B. S.; Winkler, J. R.; Gray, H. B., *Acc. Chem. Res.*, **2009**, *42*, 1995-2004.

[29] Fihri, A.; Artero, V.; Razavet, M.; Baffert, C.; Leibl, W.; Fontecave, M., *Angew. Chem. - Int. Ed.*, **2008**, *47*, 564-567.

[30] Fihri, A.; Artero, V.; Pereira, A.; Fontecave, M., *Dalton Transactions*, **2008**, 5567-5569.

[31] Du, P. W.; Knowles, K.; Eisenberg, R., *J. Am. Chem. Soc.*, **2008**, *130*, 12576-12577.

[32] Du, P.; Schneider, J.; Fan, L.; Zhao, W.; Patel, U.; Castellano, F. N.; Eisenberg, R., *J. Am. Chem. Soc.*, **2008**, *130*, 5056-5058.

[33] Cline, E. D.; Adamson, S. E.; Bernhard, S., *Inorg. Chem.*, **2008**, *47*, 10378-10388.

[34] Hu, X.; Brunschwig, B. S.; Peters, J. C., *J. Am. Chem. Soc.*, **2007**, *129*, 8988-8998.

[35] Razavet, M.; Artero, V.; Fontecave, M., *Inorg. Chem.*, **2005**, *44*, 4786-4795.

[36] Comte, P.; Nazeeruddin, M. K.; Rotzinger, F. P.; Frank, A. J.; Gratzel, M., *J. Mol. Cat.*, **1989**, *52*, 63-84.

[37] Hawecker, J.; Lehn, J. M.; Ziessel, R., *Nouv. J. Chim.*, **1983**, *7*, 271-277.

[38] Krishnan, C. V.; Creutz, C.; Mahajan, D.; Schwarz, H. A.; Sutin, N., *Isr. Jour. Chem.*, **1982**, *22*, 98-106.

[39] Krishnan, C. V.; Sutin, N., *J. Am. Chem. Soc.*, **1981**, *103*, 2141-2142.

[40] Chan, S. F.; Chou, M.; Creutz, C.; Matsubara, T.; Sutin, N., *J. Am. Chem. Soc.*, **1981**, *103*, 369-379.

[41] Chao, T. H.; Espenson, J. H., *J. Am. Chem. Soc.*, **1978**, *100*, 129-133.

[42] Barbir, F., *Solar Energy*, **2005**, *78*, 661-669.

[43] Hieber, W.; Fuchs, H., *Z. Anorg. Allg. Chem.*, **1941**, *248*, 269-275.

[44] Abel, E. W.; Wilkinson, G., *J. Chem. Soc.*, **1959**, 1501-1505.

[45] Wrighton, M.; Morse, D. L., *J. Am. Chem. Soc.*, **1974**, *96*, 998-1003.

[46] Giordano, P. J.; Fredericks, S. M.; Wrighton, M. S.; Morse, D. L., *J. Am. Chem. Soc.*, **1978**, *100*, 2257-2259.

[47] Luong, J. C.; Nadjo, L.; Wrighton, M. S., *J. Am. Chem. Soc.*, **1978**, *100*, 5790-5795.

[48] Kalyanasundaram, K., *J. Chem. Soc. - Faraday Transact.*, **1986**, *82*, 2401-2415.

[49] Hawecker, J.; Lehn, J. M.; Ziessel, R., *J. Chem. Soc. - Chem. Com.*, **1983**, 536-538.

[50] Kutal, C.; Weber, M. A.; Ferraudi, G.; Geiger, D., *Organometallics*, **1985**, *4*, 2161-2166.

[51] Hawecker, J.; Lehn, J. M.; Ziessel, R., *Helv. Chim. Acta*, **1986**, *69*, 1990-2012.

[52] Kutal, C.; Corbin, A. J.; Ferraudi, G., *Organometallics*, **1987**, *6*, 553-557.

[53] Tsubaki, H.; Sugawara, A.; Takeda, H.; Gholamkhass, B.; Koike, K.; Ishitani, O., *Res. Chem. Inter.*, **2007**, *33*, 37-48.

[54] Sato, S.; Sekine, A.; Ohashi, Y.; Ishitani, O.; Blanco-Rodriguez, A. M.; Vicek, A.; Unno, T.; Koike, K., *Inorganic Chemistry*, **2007**, *46*, 3531-3540.

[55] Sato, S.; Koike, K.; Inoue, H.; Ishitani, O., *Photochem. & Photobio. Sci.*, **2007**, *6*, 454-461.

[56] Kurz, P.; Probst, B.; Spingler, B.; Alberto, R., *Eur. J. Inorg. Chem.*, **2006**, 2966-2974.

[57] Hayashi, Y.; Kita, S.; Brunschwig, B. S.; Fujita, E., *J. Am. Chem. Soc.*, **2003**, *125*, 11976-11987.

[58] Sutin, N.; Creutz, C.; Fujita, E., *Com. Inorg. Chem.*, **1997**, *19*, 67-92.

[59] Johnson, F. P. A.; George, M. W.; Hartl, F.; Turner, J. J., *Organometallics*, **1996**, *15*, 3374-3387.

[60] Ishitani, O.; George, M. W.; Ibusuki, T.; Johnson, F. P. A.; Koike, K.; Nozaki, K.; Pac, C. J.; Turner, J. J.; Westwell, J. R., *Inorg. Chem.*, **1994**, *33*, 4712-4717.

[61] Takeda, H.; Koike, K.; Inoue, H.; Ishitani, O., *J. Am. Chem. Soc.*, **2008**, *130*, 2023-2031.

[62] Rodriguez, A. M. B.; Gabrielsson, A.; Motevalli, M.; Matousek, P.; Towrie, M.; Sebera, J.; Zalis, S.; Vlcek, A., *J. Phys. Chem. A*, **2005**, *109*, 5016-5025.

[63] George, M. W.; Johnson, F. P. A.; Westwell, J. R.; Hodges, P. M.; Turner, J. J., *J. Chem. Soc. - Dalton Trans.*, **1993**, 2977-2979.

[64] Dattelbaum, D. M.; Omberg, K. M.; Hay, P. J.; Gebhart, N. L.; Martin, R. L.; Schoonover, J. R.; Meyer, T. J., *J. Phys. Chem. A*, **2004**, *108*, 3527-3536.

[65] Stufkens, D. J.; Vlcek, A., *Coord. Chem. Rev.*, **1998**, *177*, 127-179.

[66] Worl, L. A.; Duesing, R.; Chen, P. Y.; Dellaciana, L.; Meyer, T. J., *J. Chem. Soc. - Dalton Trans.*, **1991**, 849-858.

[67] Macqueen, D. B.; Schanze, K. S., *J. Am. Chem. Soc.*, **1991**, *113*, 7470-7479.

[68] Schanze, K. S.; Macqueen, D. B.; Perkins, T. A.; Cabana, L. A., *Coord. Chem. Rev.*, **1993**, *122*, 63-89.

[69] Hanss, D.; Wenger, O. S., *Inorg. Chem.*, **2008**, *47*, 9081-9084.

[70] Bates, W. D.; Chen, P. Y.; Dattelbaum, D. M.; Jones, W. E.; Meyer, T. J., *J. Phys. Chem. A*, **1999**, *103*, 5227-5231.

[71] Kaim, W.; Scheiring, T.; Weber, M.; Fiedler, J., *Zeit. Anorg. Allg. Chem.*, **2004**, *630*, 1883-1893.

[72] Farrell, I. R.; Matousek, P.; Kleverlaan, C. J.; Vlcek, A., *Chem. Europ. J.*, **2000**, *6*, 1386-1394.

[73] Tschugaeff, L., *Zeit. Anorg. Chem.*, **1905**, *46*, 144-169.

[74] Tschugaeff, L., *Ber. Deut. Chem. Ges.*, **1906**, *39*, 2692-2702.

[75] Tschugaeff, L., *Ber. Deut. Chem. Ges.*, **1907**, *40*, 3498-3504.

[76] Schrauzer, G. N.; Kohnle, J., *Chem. Ber.*, **1964**, *97*, 3056-3064.

[77] Schrauzer, G. N.; Parshall, G. W.; Wonchoba, E. R. In *Inorganic Syntheses*; William, L. J., Ed.; McGraw-Hill Book Company, Inc.: **1968**; Vol. XI, p 61-70.

[78] Schrauzer, G. N., *Acc. Chem. Res.*, **1968**, *1*, 97-103.

[79] Schrauzer, G. N.; Holland, R. J., *J. Am. Chem. Soc.*, **1971**, *93*, 1505-1506.

[80] Mita, K., *Bull. Chem. Soc. Japan*, **1986**, *59*, 823-826.

[81] Tyrlik, S.; Kwiecinski, M.; Rockenbauer, A.; Gyor, M., *J. Coord. Chem.*, **1982**, *11*, 205-212.

[82] Rockenbauer, A.; Gyor, M.; Kwiecinski, M.; Tyrlik, S., *Inorg. Chim. Acta*, **1982**, *58*, 237-242.

[83] Tyrlik, S.; Kucharska, M. M.; Wolochowicz, I., *J. Mol. Cat.*, **1979**, *6*, 393-404.

[84] Simandi, L. I.; Szeverenyi, Z.; Budo-Zahonyi, E., *Inorg. Nucl. Chem. Letters*, **1975**, *11*, 773-777.

[85] Takeuchi, S.; Ohgo, Y.; Yoshimur.J, *Bull. Chem. Soc. Japan*, **1974**, *47*, 463-466.

[86] Ma, F.; Jagner, D.; Renman, L., *Anal. Chem.*, **1997**, *69*, 1782-1784.

[87] Kalyanasundaram, K.; Borgarello, E.; Duonghong, D.; Gratzel, M., *Angew. Chem. - Int. Ed.*, **1981**, *20*, 987-988.

[88] Lehn, J. M.; Sauvage, J. P.; Ziessel, R., *Nouv. J. Chim.*, **1980**, *4*, 623-627.

[89] Kalyanasundaram, K.; Gratzel, M., *Angew. Chem. - Int. Ed.*, **1979**, *18*, 701-702.

[90] Sauvage, J. P., **2009**, personal communication.

[91] Tseng, H. W.; Zong, R.; Muckerman, J. T.; Thummel, R., *Inorg. Chem.*, **2008**, *47*, 11763-11773.

[92] Hurst, J. K.; Cape, J. L.; Clark, A. E.; Das, S.; Qin, C. Y., *Inorg. Chem.*, **2008**, *47*, 1753-1764.

[93] Cape, J. L.; Hurst, J. K., *J. Am. Chem. Soc.*, **2008**, *130*, 827-829.

[94] Rotzinger, F. P.; Munavalli, S.; Comte, P.; Hurst, J. K.; Gratzel, M.; Pern, F. J.; Frank, A. J., *J. Am. Chem. Soc.*, **1987**, *109*, 6619-6626.

[95] Concepcion, J. J.; Jurss, J. W.; Templeton, J. L.; Meyer, T. J., *J. Am. Chem. Soc.*, **2008**, *130*, 16462-16463.

[96] Gersten, S. W.; Samuels, G. J.; Meyer, T. J., *J. Am. Chem. Soc.*, **1982**, *104*, 4029-4030.

[97] McDaniel, N. D.; Coughlin, F. J.; Tinker, L. L.; Bernhard, S., *J. Am. Chem. Soc.*, **2008**, *130*, 210-217.

[98] Suss-Fink, G., *Angew. Chem. - Int. Ed.*, **2008**, *47*, 5888-5890.

[99] Sartorel, A.; Carraro, M.; Scorrano, G.; De Zorzi, R.; Geremia, S.; McDaniel, N. D.; Bernhard, S.; Bonchio, M., *J. Am. Chem. Soc.*, **2008**, *130*, 5006-5007.

[100] Geletii, Y. V.; Botar, B.; Koegerler, P.; Hillesheim, D. A.; Musaev, D. G.; Hill, C. L., *Angew. Chem. - Int. Ed.*, **2008**, *47*, 3896-3899.

[101] Brimblecombe, R.; Swiegers, G. F.; Dismukes, G. C.; Spiccia, L., *Angew. Chem. - Int. Ed.*, **2008**, *47*, 7335-7338.

[102] Beckmann, K.; Uchtenhagen, H.; Berggren, G.; Anderlund, M. F.; Thapper, A.; Messinger, J.; Styring, S.; Kurz, P., *Energy & Environ. Sci.*, **2008**, *1*, 668-676.

[103] Lehn, J. M.; Sauvage, J. P.; Ziessel, R.; Hilaire, L., *Isr. Jour. Chem.*, **1982**, *22*, 168-172.

[104] Lehn, J. M.; Sauvage, J. P.; Ziessel, R., *Nouv. J. Chim.*, **1979**, *3*, 423-427.

[105] Lehn, J. M.; Sauvage, J. P.; Ziessel, R., *Nouv. J. Chim.*, **1980**, *4*, 355-358.

[106] Kanan, M. W.; Nocera, D. G., *Science*, **2008**, *321*, 1072-1075.

[107] Najafpour, M. M.; Ehrenberg, T.; Wiechen, M.; Kurz, P., *Angew. Chem.-Int. Ed.*, **2010**, *49*, 2233-2237.

[108] Kay, A.; Cesar, I.; Gratzel, M., *J. Am. Chem. Soc.*, **2006**, *128*, 15714-15721.

[109] Brown, G. M.; Brunschwig, B. S.; Creutz, C.; Endicott, J. F.; Sutin, N., *J. Am. Chem. Soc.*, **1979**, *101*, 1298-1300.

[110] Krishnan, C. V.; Brunschwig, B. S.; Creutz, C.; Sutin, N., *J. Am. Chem. Soc.*, **1985**, *107*, 2005-2015.

[111] Kölle, U.; Grätzel, M., *Angew. Chem. - Int. Ed.*, **1987**, *26*, 567-570.

[112] Lehn, J. M.; Sauvage, J. P.; Ziessel, R., *Nouv. J. Chim.*, **1981**, *5*, 291-295.

[113] Lehn, J. M.; Kirch, M.; Sauvage, J. P.; Ziessel, R., *Recherche*, **1980**, *11*, 203-205.

[114] Moradpour, A.; Amouyal, E.; Keller, P.; Kagan, H., *Nouv. J. Chim.*, **1978**, *2*, 547-549.

[115] Kalyanasundaram, K.; Kiwi, J.; Gratzel, M., *Helv. Chim. Acta*, **1978**, *61*, 2720-2730.

[116] Lehn, J. M.; Sauvage, J. P., *Nouv. J. Chim.*, **1977**, *1*, 449-451.

[117] Sakai, K.; Kizaki, Y.; Tsubomura, T.; Matsumoto, K., *J. Mol. Catal.*, **1993**, *79*, 141-152.

[118] Kirch, M.; Lehn, J. M.; Sauvage, J. P., *Helv. Chim. Acta*, **1979**, *62*, 1345-1384.

[119] Goldsmith, J. I.; Hudson, W. R.; Lowry, M. S.; Anderson, T. H.; Bernhard, S., *J. Am. Chem. Soc.*, **2005**, *127*, 7502-7510.

[120] Elvington, M.; Brown, J.; Arachchige, S. M.; Brewer, K. J., *J. Am. Chem. Soc.*, **2007**, *129*, 10644-10645.

[121] Rau, S.; Schafer, B.; Gleich, D.; Anders, E.; Rudolph, M.; Friedrich, M.; Gorls, H.; Henry, W.; Vos, J. G., *Angew. Chem. - Int. Ed.*, **2006**, *45*, 6215-6218.

[122] Ozawa, H.; Haga, M. A.; Sakai, K., *J. Am. Chem. Soc.*, **2006**, *128*, 4926-4927.

[123] Lei, P.; Hedlund, M.; Lomoth, R.; Rensmo, H.; Johansson, O.; Hammarstrom, L., *J. Am. Chem. Soc.*, **2008**, *130*, 26-27.

[124] Na, Y.; Wang, M.; Pan, J. X.; Zhang, P.; Akermark, B.; Sun, L. C., *Inorg. Chem.*, **2008**, *47*, 2805-2810.

[125] Probst, B.; Guttentag, M.; Rodenberg, A.; Hamm, P.; Alberto, R., *J. Am. Chem. Soc.*, **2010**, *in revision*.

[126] Schmidt, S. P.; Trogler, W. C.; Basolo, F., *Inorg. Synth.*, **1990**, *28*, 160-165.

[127] Lazarova, N.; James, S.; Babich, J.; Zubieta, J., *Inorg. Chem. Comm.*, **2004**, *7*, 1023-1026.

[128] Lukehart, C. M.; Torrence, G. P.; Zeile, J. V., *Inorg. Synth.*, **1990**, *28*, 199-202.

[129] Schmidt, S. P.; Nitschke, J.; Trogler, W. C.; Huckett, S. I.; Angelici, R. J., *Inorg. Synth.*, **1989**, *26*, 113-117.

[130] Marzilli, L. G., **2009**, personal communication.

[131] Smith, A. P.; Lamba, J. J. S.; Fraser, C. L., *Org. Synth.*, **2004**, *Col. Vol. 10*, 107.

[132] Smith, A. P.; Corbin, P. S.; Fraser, C. L., *Tetrahedron Lett.*, **2000**, *41*, 2787-2789.

[133] Izutsu, K. *Acid-base dissociation constants in dipolar aprotic solvents*; Blackwell Scientific Publications: Oxford, **1990**.

[134] Jessop, P., **2009**, personal communication.

[135] Zhang, K. Y.; Lo, K. K. W., *Inorg. Chem.*, **2009**, *48*, 6011-6025.

[136] Smith, G. F.; Cagle, F. W., *J. Org. Chem.*, **1947**, *12*, 781-784.

[137] Paw, W.; Eisenberg, R., *Inorg. Chem.*, **1997**, *36*, 2287-2293.

[138] Bodige, S.; MacDonnell, F. M., *Tetrahedron Lett.*, **1997**, *38*, 8159-8160.

[139] Holleman, A. F.; Holleman, W.; Wiberg, E.; Wiberg, N. *Lehrbuch der anorganischen Chemie*; 101., verb. und stark erw. Aufl. ed.; de Gruyter: Berlin, **1995**.

[140] Juris, A.; Balzani, V.; Barigelletti, F.; Campagna, S.; Belser, P.; Vonzelewsky, A., *Coord. Chem. Rev.*, **1988**, *84*, 85-277.

[141] Stor, G. J.; Hartl, F.; Vanoutersterp, J. W. M.; Stufkens, D. J., *Organometallics*, **1995**, *14*, 1115-1131.

[142] Kaim, W.; Kramer, H. E. A.; Vogler, C.; Rieker, J., *J. Organomet. Chem.*, **1989**, *367*, 107-115.

[143] Otoole, T. R.; Sullivan, B. P.; Bruce, M. R. M.; Margerum, L. D.; Murray, R. W.; Meyer, T. J., *J. Electroanal. Chem.*, **1989**, *259*, 217-239.

[144] Breikss, A. I.; Abruna, H. D., *J. Electroanal. Chem.*, **1986**, *201*, 347-358.

[145] Christensen, P.; Hamnett, A.; Muir, A. V. G.; Timney, J. A., *J. Chem. Soc. - Dalton Trans.*, **1992**, 1455-1463.

[146] Bullock, J. P.; Carter, E.; Johnson, R.; Kennedy, A. T.; Key, S. E.; Kraft, B. J.; Saxon, D.; Underwood, P., *Inorg. Chem.*, **2008**, *47*, 7880-7887.

[147] Kamenov, L. L.; Simov, D.; Golubev, V. B., *Theo. Exp. Chem.*, **1973**, *7*, 115-118.

[148] Gao, Y. H.; Chen, J. F.; Zhuang, X. J.; Wang, J. T.; Pan, Y.; Zhang, L. M.; Yu, S. Q., *Chem. Phys.*, **2007**, *334*, 224-231.

[149] Chen, P. Y.; Westmoreland, T. D.; Danielson, E.; Schanze, K. S.; Anthon, D.; Neveux, P. E.; Meyer, T. J., *Inorg. Chem.*, **1987**, *26*, 1116-1126.

[150] Porter, G.; Wright, M. R., *Discuss. Faraday Soc.*, **1959**, 18-27.

[151] Andrieux, C. P.; Blocman, C.; Dumasbouchiat, J. M.; Mhalla, F.; Saveant, J. M., *J. Electroanal. Chem.*, **1980**, *113*, 19-40.

[152] Alberto, R.; Egli, A.; Abram, U.; Hegetschweiler, K.; Gramlich, V.; Schubiger, P. A., *J. Chem. Soc. - Dalton Trans.*, **1994**, 2815-2820.

[153] Olmsted, J., *J. Phys. Chem.*, **1979**, *83*, 2581-2584.

[154] Williams, A. T. R.; Winfield, S. A.; Miller, J. N., *Analyst*, **1983**, *108*, 1067-1071.

[155] Hatchard, C. G.; Parker, C. A., *Proc. R. Soc. A*, **1956**, *235*, 518-536.

[156] Bredenbeck, J.; Helbing, J.; Hamm, P., *Rev. Sci. Instr.*, **2004**, *75*, 4462-4466.

[157] Hamm, P.; Kaindl, R. A.; Stenger, J., *Optics Letters*, **2000**, *25*, 1798-1800.

[158] STOE & Cie, GmbH, Darmstadt, Germany, **1999**.

[159] Oxford Diffraction Ltd., *Xcalibur CCD system 171.32*, Oxford, UK, **2007**.

[160] Altomare, A.; Burla, M. C.; Camalli, M.; Cascarano, G. L.; Giacovazzo, C.; Guagliardi, A.; Moliterni, A. G. G.; Polidori, G.; Spagna, R., *J. Appl. Cryst.*, **1999**, *32*, 115-119.

[161] Sheldrick, G. M., *Acta Cryst. Sect. A*, **2008**, *64*, 112-122.

[162] Spek, A. L., *J. Appl. Cryst.*, **2003**, *36*, 7-13.

Acknowledgments

At the beginning the ’photo-hydrogen’ project was somewhat ambitious and the outcome not clear at all. Even though it was a completely new avenue in his group, and experience was limited, Prof. Dr. Roger Alberto supported this work from the beginning and assisted it very closely and with a lot of passion. He was a never diminishing source of new ideas without which it would have been impossible to go so far!

Prof. Dr. Peter Hamm compensated for the lack of knowledge in photochemistry in our group. As a physicist he often times brought a different, but always constructive point of view into the project. Besides that, he was a great help in unravelling the kinetics of the catalytic cycle.

I want to thank Dr. Philipp Kurz for starting up the photochemistry group with Prof. Dr. Roger Alberto, and to introduce me to it during my Master time; Dr. Karljin Codee and Christine Männel-Croisé for their joint efforts in the syntheses and chromatography, but also the good time in the lab; Dr. Christoph Kolano for his help with the first experiments on the fast laser setup; Miguel Guttentag for being a motivated successor on the project and for countless interesting discussions on the balcony, ranging from chemistry to philosophy; and finally Nora Zuber and Stefan Sandriesser for the fresh wind they brought into the project!

The institute of inorganic chemistry was an excellent place to be both in terms of infrastructure and people – the latter helped a lot to make work enjoyable! Special thanks go to Dr. Bernhard Spingler and Dr. Henrik Braband for being good friends and for their help in crystallography, to Heinz Spring, Hanspeter Stalder and Manfred Jöhri for their excellent technical support, to Lukas Kromer, Patricia Santos, Philipp Antoni, Yuji Tooyama, Pillar Sanchez and Jae Kyoung Pak for being wonderful co-workers and good friends, and to all the alberto group for an excellent working atmosphere!

All of this would not have been possible without the support of my family and friends! Special thanks go to Matthias Gunsch, Marco Looser, Thomas Niederberger and Diego Sanchez, but also to the ZO gang, the lagerlager gang, the Parkring crew and the gARTengarten team!

In all this time I received a lot of support from both my parents and my parents-in-law – not only physically but also in terms of good advices and the time we spent together. It's great to know that there is always a place to go!

Last I want to thank Sandra, for being here for me every day, and Jarun, for giving all of this a meaning!

Personal data

Name:	Probst-Rüd Benjamin
Address:	Sihlfeldstrasse 122, 8005 Zürich
Civil status:	married to Sandra Probst-Rüd (18.1.1982)
Children:	Jarun Probst (15.11.2007)
Place of origin:	Bäretswil ZH and Finsterhennen BE
Place of birth:	Grenchen SO
Date of birth:	22.08.1980
Nationality:	CH
Languages:	German (mother language), English, French

Education

1987:	1. Class primary school, Trubschachen BE
1988 - 1992:	2.-6. Classes' primary school, Wetzikon ZH
1993 - 2000:	Matura (mathematical- and natural sciences), Wetzikon ZH
7.2000 - 3.2001:	Language stay in New Zeeland
10.2001 - 4.2006:	Master in Chemistry with emphasis on inorganic-, organic and physical chemistry and environmental sciences
10.2004 - 7.2005:	Diploma thesis entitled: "Photocatalytic Investigation on novel Rhenium(I)-tricarbonyl based homo- and heterobimetallic Systems" with Prof. R. Alberto, Inorganic Chemistry, University of Zürich
4.2006 – today:	PhD in inorganic chemistry, Prof. R. Alberto, University of Zürich, Topic: Photocatalytic water splitting in homogenous solution

Rewards

Reward of the Alfred Werner Legat for extraordinary Exams, 2002 & 2003.
Poster price for the best presentation on "*Chemistry for a Sustainable World"* in Villars-sur-ôllon, CH, 2009.

List of Publications

1. Kurz, P.; Probst, B.; Spingler, B.; Alberto, R. *Eur. J. Inorg. Chem.* **2006**, 2966-2974.
2. Mannel-Croise, C.; Probst, B.; Zelder, F. *Anal. Chem.* **2009**, *81*, 9493-9498.
3. Probst, B.; Kolano, C.; Hamm, P.; Alberto, R. *Inorg. Chem.* **2009**, *48*, 1836-1843.
4. Zhou, Y.; Vuille, K.; Heel, A.; Probst, B.; Kontic, R.; Patzke, G. R. *App. Cat. A: Gen.* **2010**, *375*, 140-148.
5. Probst, B.; Rodenberg, A.; Guttentag, M.; Hamm, P.; Alberto, R., *Inorg. Chem.*, **2010**, *49*, 6453-6460.
6. Probst, B.; Guttentag, M.; Rodenberg, A.; Hamm, P.; Alberto, R., *J. Am. Chem. Soc.*, **2010**, *in revision*.

Conference Contributions

Talks outside the University:

1. *"An efficient homogenous photocatalytic system for the reduction of protons to hydrogen using a rhenium based photosensitiser"*, Probst, B.; Alberto, R., *XXIInd IUPAC Symposium on Photochemistry*, Göteborg, SE, **2008**.

Posters:

1. *"Photocatalytic Investigation on novel rhenium(I)-tricarbonyl based mono- and bimetallic systems"*, Probst, B.; Kurz, P.; Alberto, R., *IPS 16*, Uppsala, SE, **2006**.
2. *"Photocatalytic energy storage: a case study on the reductive half-reaction"*, Probst, B.; van der Schilden, K.; Männel-Croisé, C.; Alberto, R., *SCS Fall meeting*, Zürich, CH, **2006**.
3. *"Photocatalytic energy storage: an artifical biomimetic model of PS I"*, Probst, B.; Alberto, R., *SCS Fall meeting*, Lausanne, CH, **2007**.
4. *"Homogenous photocatalytic hydrogen evolution"*, Guttentag, M.; Probst, B.; Alberto, R., *SCS Fallmeeting*, Zürich, CH, **2008**.
5. *"Photocatalytic dihydrogen production with a rhenium/cobalt system: tuning long term performance"*, Probst, B.; Alberto, R., *Chemistry for a Sustainable World*, Villars-sur ollon, CH, **2009**.
6. *"Photocatalytic Hydrogen Production with a Rhenium/Cobalt System: Understanding the longterm Performance"*, Probst, B.; Alberto, R., *SCS Fall meeting*, Lausanne, CH, **2009**.

Inorg. Chem. **2009**, *48*, 1836−1843

An Efficient Homogeneous Intermolecular Rhenium-Based Photocatalytic System for the Production of H_2

Benjamin Probst,[†] Christoph Kolano,[‡] Peter Hamm,*[,‡] and Roger Alberto*[,†]

Institute of Inorganic Chemistry, University of Zürich, Winterthurerstrasse 190, CH-8057 Zürich Switzerland, and Institute of Physical Chemistry, University of Zürich, Winterthurerstrasse 190, CH-8057 Zürich Switzerland

Received July 16, 2008

We present an artificial photocatalytic model for photosystem I (PSI) using [ReBr(CO)$_3$bipy)] (**1**) as a photosensitizer, [Co(dmgH)$_2$] (**2**) as a *hydrogen evolution reaction* catalyst, and triethanolamine as an irreversible reductive quencher. Complex **1** is more robust in the long run, and turnover numbers were more than doubled in the present study as compared to the commonly used photosensitizer $[Ru(bipy)_3]^{2+}$. The quantum yield for hydrogen production with **1** was found to be 26 ± 2% (H produced per absorbed photon). Forward electron transfer between $\mathbf{1}^-$ and **2** was found to occur at a rate close to diffusion control ($k_1 = 2.5 \pm 0.1 \times 10^8$ M^{-1} s^{-1}). The rate of hydrogen production exhibited a linear dependence on the photon flux and a quadratic dependence on the total concentration of Co ($k_{obs} = 3.7 \pm 0.1$ M^{-1} s^{-1}). Therefore, a second-order process in Co^{III}−H is proposed. The process showed a complex dependence on [AcOH]. An excess of dimethylglyoxime was systematically added to the system to ensure the complete formation of **2** and reduce the portion of free $[Co]_{solv}^{2+}$, an efficient quencher of the excited state of **1**.

Introduction

The energy supply of our modern society largely depends on fossil fuels. As is nowadays accepted, reserves of fossil fuels decrease while consumption steadily increases. Concerns about the influence of greenhouse gases on earth's climate are furthermore not in favor of using large amounts of fossil fuels in the future. Alternative and sustainable energy sources are not sufficiently developed to compensate for fossil fuels. This holds especially for use in transportation (land, air, and sea) and for energy storage. The main discussions focus nowadays on dihydrogen (H_2) or methanol (MeOH) as viable alternatives. Great efforts are being undertaken for the development of fuel cells running with H_2 or MeOH as well as for the development of efficient storage for H_2.[1,2] This technology is more extensively developed, but the production of H_2 from fossil fuels remains a drawback (from today's 65 million tons a year, 48% is derived from natural gas, 30% from refinery/chemical off-gases, 18% from coal, and 4% is produced electrochemically).[3]

The chemical storage of sunlight in H_2 by electrolysis using light-generated electrical energy is at an advanced state but remains inefficient. Alternatively, a direct conversion of sunlight into O_2 and H_2 would be a viable route in areas of high radiant flux, producing a fuel of high energy content which can be transported to metropolitan areas and converted to work and H_2O.

Since the late 1970s, remarkable results on artificial photosynthesis have been published, still setting today's benchmark. Brown et al. investigated photocatalytic water reduction with $[Ru(bipy)_3]^{2+}$ as a photosensitizer and macrocyclic cobalt complexes as catalysts for the *hydrogen evolving reaction* (*her*).[4] Efforts led by Lehn contributed substantial research both in H_2O oxidation[5] and reduction[6]

* To whom correspondence should be addressed. E-mail: ariel@aci.uzh.ch.
† Institute of Inorganic Chemistry.
‡ Institute of Physical Chemistry.

(1) Armaroli, N.; Balzani, V. *Angew. Chem.* **2007**, *119*, 52–67.
(2) Olah, G. A. *Angew. Chem., Int. Ed.* **2005**, *44*, 2636–2639.
(3) Simbolotti, G. *Hydrogen Production & Distribution*; IEA: Paris, 2007.
(4) Brown, G. M.; Brunschwig, B. S.; Creutz, C.; Endicott, J. F.; Sutin, N. *J. Am. Chem. Soc.* **1979**, *101*, 1298–1300.
(5) Lehn, J. M.; Sauvage, J. P.; Ziessel, R. *New J. Chem.* **1979**, *3*, 423–427.
(6) Hawecker, J.; Lehn, J. M.; Ziessel, R. *New J. Chem.* **1983**, *7*, 271–277.
(7) Hawecker, J.; Lehn, J. M.; Ziessel, R. *Helv. Chim. Acta* **1986**, *69*, 1990–2012.

10.1021/ic8013255 CCC: $40.75
Published on Web 01/27/2009

Intermolecular Rhenium-Based Photocatalytic System

Scheme 1. General Scheme for Photoreduction of H^+ by Light and an Irreversible Electron Donor, as Proposed by Lehn et al. (PS is $[Ru(bipy)_3]^{2+}$, D is triethanolamine, HA is the acid)[6]

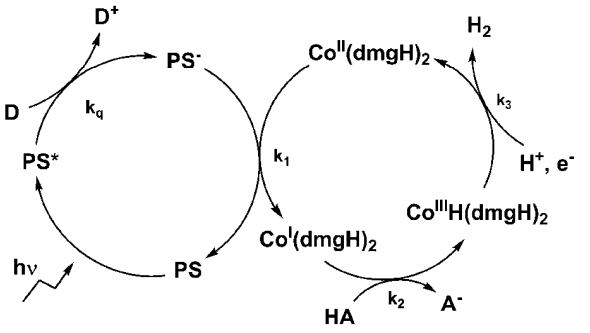

and in $CO_2 \rightarrow CO$ conversion.[7] Recent years have seen a revival of artificial photosynthesis, mainly employing the $[Ru(bipy)_3]^{2+}$ photosensitizer and noble metal catalysts to achieve proton reduction, the sacrificial electron donor mostly being a tertiary amine.[8−11] Lei et al. questioned the homogeneous character of these reactions, as they found H_2 production to correlate with colloid formation.[11] Rosenthal et al. studied systems involving rhodium-based dinuclear complexes,[12] and Fihri et al. studied systems involving heterodinuclear ruthenium−cobalt complexes.[13] Eisenberg used a platinum terpyridyl sensitizer in combination with cobalt dimethylglyoxime analogues,[14] and Bernhard used a series of iridium phenylpyridine sensitizers with rhodium *her* catalysts for photocatalytic homogeneous H_2 production.[15]

The vast majority of studies for photocatalytic H_2 production employed $[Ru(bipy)_3]^{2+}$ or derivatives as photosensitizers. The pioneering work by Lehn and co-workers showed that $[Ru(bipy)_3]^{2+}$, $[Co(dmgH)_2(OH_2)_2]$ (Co(II)-bisdimethylglyoxime-bisaquo) as a *her* catalyst, and triethanolamine as an irreversible electron donor in DMF produced H_2 under irradiation with light.[6] The principle of this dyad system, as proposed by the authors, is given in Scheme 1.

A drawback of this system was long-term stability, since after 10 h of irradiation, the rate of H_2 evolution decreased considerably. This was shown to be due to the decomposition of the sensitizer $[Ru(bipy)_3]^{2+}$. A substantial excess of dimethylglyoxime ($dmgH_2$) was required to increase the catalytic turnover. In the long run, tertiary amines as irreversible electron donors have to be replaced as well. A detailed mechanism of a similar system using $[Co(dmgH)_2]$ as a *her* catalyst and Et_3NH^+ as a proton source was provided by Razavet et al.[16] They showed by cyclic voltametry that H_2 production occurred by protonation of a $Co^{III}-H$ species (first-order in $Co^{III}-H$) with $k_{1.order} = 3 \times 10^2\ M^{-1}\ s^{-1}$ in DMF. In an electrochemical study, a second-order process in $Co^{III}-H$ with $k_{2.order} \approx 1 \times 10^6\ M^{-1}\ s^{-1}$ was observed in similar systems with $[Co(dmgBF_2)_2(CH_3CN)_2]$ as a catalyst in CH_3CN.[17] In a spectroscopic study in protic solvents, where $[HCo(dmgH)_2P(n\text{-}C_4H_9)_3]$ was employed as a *her* catalyst, a mixed mechanism with $k_{1.order} = 3.4 \times 10^4\ M^{-1}\ s^{-1}$ and $k_{2.order} = 4.2 \times 10^{-1}\ M^{-1}\ s^{-1}$ was reported.[18]

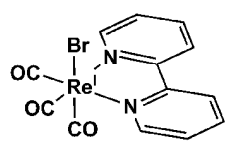

1

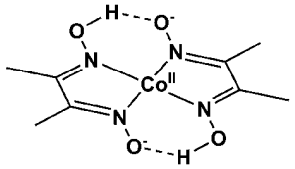

2

Thus far, most of the photocatalytic studies have employed $[Ru(bipy)_3]^{2+}$ as a photosensitizer.[4−6,8−10,13] Photocatalytic $CO_2 \rightarrow CO$ conversion catalyzed by $[ReBr(CO)_3bipy]$ (**1**) was published.[7,19−22] Heterodinuclear Ru−Re/ Zn−Re complexes, increasing the overlap with the solar spectrum, were reported for CO_2 reduction.[23−25] Reports about photocatalytic H_2 evolution with **1** are however rare. We, and later others, reported the influence of the axial ligand X in $[ReX(CO)_3bipy]$ for $CO_2 \rightarrow CO$ conversion.[19,26]

As shown in $[Ru(bipy)_3]^{2+}$ sensitized homogeneous systems, $[Co(dmgH)_2]$ (**2**) is a good choice for the reductive catalyst in *her*. Compound **2** is cheap, displays a low overpotential for proton reduction (30 mV) under neutral conditions, and achieves high turnover numbers.[16] The combination of **1** and **2** for photocatalytic H_2 production has, to the best of our knowledge, not yet been reported but is an important extension on the way to an improved system. We wish to present a detailed mechanistic and kinetic study for the photocatalytic production of H_2 in a homogeneous solution of **1** and **2** with triethanolamine (TEOA) as an irreversible electron donor. It turned out that the combination of rhenium complexes as photosensitizers and cobalt as a *her* catalyst is superior over the ruthenium−cobalt combination with respect to long-term performance.

(8) Ozawa, H.; Haga, M. A.; Sakai, K. *J. Am. Chem. Soc.* **2006**, *128*, 4926–4927.
(9) Rau, S.; Schafer, B.; Gleich, D.; Anders, E.; Rudolph, M.; Friedrich, M.; Gorls, H.; Henry, W.; Vos, J. G. *Angew. Chem., Int. Ed.* **2006**, *45*, 6215–6218.
(10) Elvington, M.; Brown, J.; Arachchige, S. M.; Brewer, K. J. *J. Am. Chem. Soc.* **2007**, *129*, 10644–10645.
(11) Lei, P.; Hedlund, M.; Lomoth, R.; Rensmo, H.; Johansson, O.; Hammarstrom, L. *J. Am. Chem. Soc.* **2008**, *130*, 26–27.
(12) Rosenthal, J.; Bachman, J.; Dempsey, J. L.; Esswein, A. J.; Gray, T. G.; Hodgkiss, J. M.; Manke, D. R.; Luckett, T. D.; Pistorio, B. J.; Veige, A. S.; Nocera, D. G. *Coord. Chem. Rev.* **2005**, *249*, 1316–1326.
(13) Fihri, A.; Artero, V.; Razavet, M.; Baffert, C.; Leibl, W.; Fontecave, M. *Angew. Chem., Int. Ed.* **2008**, *47*, 564–567.
(14) Du, P. W.; Knowles, K.; Eisenberg, R. *J. Am. Chem. Soc.* **2008**, *130*, 12576–12577.
(15) Cline, E. D.; Adamson, S. E.; Bernhard, S. *Inorg. Chem.* **2008**, *47*, 10378–10388.
(16) Razavet, M.; Artero, V.; Fontecave, M. *Inorg. Chem.* **2005**, *44*, 4786–4795.
(17) Hu, X.; Brunschwig, B. S.; Peters, J. C. *J. Am. Chem. Soc.* **2007**, *129*, 8988–8998.
(18) Chao, T. H.; Espenson, J. H. *J. Am. Chem. Soc.* **1978**, *100*, 129–133.
(19) Takeda, H.; Koike, K.; Inoue, H.; Ishitani, O. *J. Am. Chem. Soc.* **2008**, *130*, 2023–2031.
(20) Kutal, C.; Weber, M. A.; Ferraudi, G.; Geiger, D. *Organometallics* **1985**, *4*, 2161–2166.
(21) Hayashi, Y.; Kita, S.; Brunschwig, B. S.; Fujita, E. *J. Am. Chem. Soc.* **2003**, *125*, 11976–11987.
(22) Johnson, F. P. A.; George, M. W.; Hartl, F.; Turner, J. J. *Organometallics* **1996**, *15*, 3374–3387.
(23) Kiyosawa, K.; Masui, D.; Shimada, T.; Takagi, S.; Ishitani, O.; Inoue, H. *XXII IUPAC Symposium on Photochemistry*, Göteborg, Sweden, 2008.
(24) Sato, S.; Koike, K.; Inoue, H.; Ishitani, O. *Photochem. Photobiol. Sci.* **2007**, *6*, 454–461.
(25) Gholamkhass, B.; Mametsuka, H.; Koike, K.; Tanabe, T.; Furue, M.; Ishitani, O. *Inorg. Chem.* **2005**, *44*, 2326–2336.
(26) Kurz, P.; Probst, B.; Spingler, B.; Alberto, R. *Eur. J. Inorg. Chem.* **2006**, *296*, 6–2974.

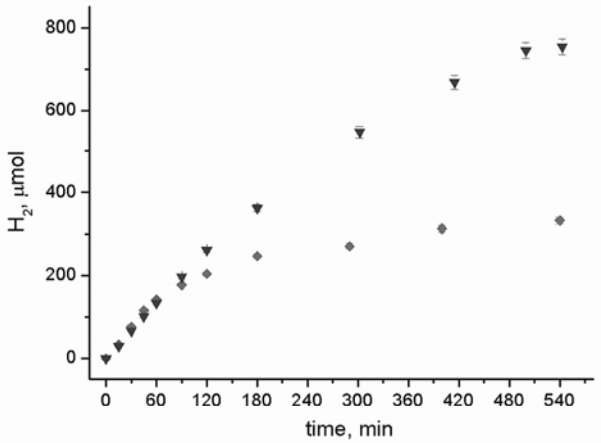

Figure 1. Comparison between $[ReBr(CO)_3bipy]$ (▼) and $[Ru(bipy)_3]^{2+}$ (♦) chromophores (0.5 mM in **1** and $[Ru(bipy)_3]^{2+}$ respectively, 1 mM $Co(OAc)_2 \cdot 4H_2O$, 6 mM $dmgH_2$, 1 M TEOA, 0.1 M AcOH, DMF, Argon).

Results and Discussion

To obtain detailed insight into the mechanism of H_2 production, the rate constants of the different elementary reaction steps, as shown in Scheme 1, were the focus of our study. Besides qualitative long-term stability as compared to the $[Ru(bipy)_3]^{2+}-[Co(dmgH)_2]$ system,[6] we investigated the influence of excess $dmgH_2$, [AcOH], photon flux and quantum yields, rate, and mechanism on the final H_2 evolution step.

The main methods employed are hydrogen measurements under continuous wave irradiation to determine dependencies of the composition of the system on dH_2/dt. On the other hand, time-resolved IR spectroscopy provided a tool for the study of the initial phase of the *her*, namely, the rhenium cycle.

1. Rhenium Cycle. Catalytic Performance. $[Ru(bipy)_3]^{2+}$ has been described as being moderately stable with respect to long-term performance.[6] In a first step, we qualitatively compared the rate of H_2 production under identical conditions for $[Ru(bipy)_3]^{2+}$ and **1**. A time-dependent comparison is given in Figure 1. When subjected to photolysis ($h\nu \geq 400$ nm), the two chromophores **1** and $[Ru(bipy)_3]^{2+}$ performed equally well in an initial phase of the experiment for about 60 min. The rate of H_2 evolution was 3.7 ± 0.05 $\mu M\ s^{-1}$ for **1** and 4.1 ± 0.09 $\mu M\ s^{-1}$ for $[Ru(bipy)_3]^{2+}$. When subjected to photolysis for a longer time, **1** continued producing H_2, whereas the $[Ru(bipy)_3]^{2+}$ system substantially slowed down. After about 9 h of irradiation, more than twice the amount of H_2 was observed for **1** as compared to $[Ru(bipy)_3]^{2+}$. The turnover number (defined as H_2 per photosensitizer) for **1** and $[Ru(bipy)_3]^{2+}$ was 150 and 65, respectively. In fact, whereas the AcOH and TEOA concentrations could be considered as constant for the first 60 min, H^+ from acetic acid was consumed after 5 h and about 15% of the reductive quencher TEOA after 9 h. The addition of more equivalents of TEOA and AcOH after 5 h did not increase long-term performance. Qualitatively, both systems seemed to undergo some deactivation pathway, but **1** shows an improved long-term stability.

Scheme 2. General Representation of a Second-Order Pathway in $Co^{III}-H$ to Hydrogen[a]

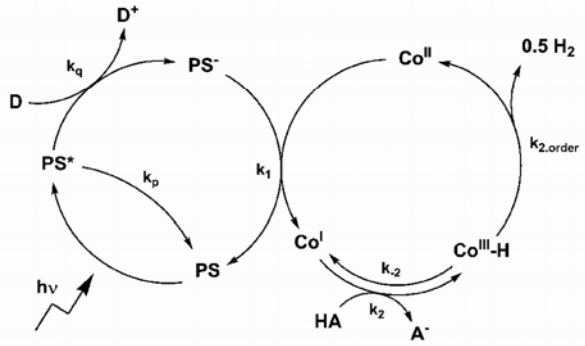

[a] PS represents the photosensitizer $[ReBr(CO)_3bipy]$. Co^{II} is $[Co^{II}(dmgH)_2]$. D is the donor TEOA, and HA is acetic acid.

Time-Resolved IR Spectroscopy. The first three reactions along the proposed catalytic cycle (k_{abs}, k_p, k_q, and k_1, Scheme 2) all involve the $[ReBr(CO)_3bipy]$ sensitizer in different electronic configurations (ground, excited, and reduced states). Time-resolved IR spectroscopy is therefore the method of choice for a kinetic analysis of this part of the system. The ground-state IR spectrum of **1** in DMF is shown in Figure 2a and exhibits strong and characteristic bands in the $1800-2100$ cm^{-1} region. The bands at 1897, 1918, and 2022 cm^{-1} have been assigned to a′(2) [asymmetric stretching of CO_{ax} and CO_{eq}], a″ [asymmetric stretching of CO_{eq}], and a′(1) [symmetric stretching of all CO's] modes, respectively. The photochemistry of **1** upon 400 nm excitation is well understood and has been described in detail.[21,27−33] Using an UV-pump−IR-probe setup[34] allowed us to follow the reaction from picoseconds to microseconds and to unravel the rate-limiting step. Our DFT calculations (B3LYP) at the LANL2DZ level of theory and previous experiments[28] showed that upon excitation or reductive quenching the symmetric and asymmetric set of CO stretching frequencies will undergo characteristic spectral shifts.

In a first series of experiments, we investigated the photochemistry of a 1 mM solution of **1** in degassed DMF upon 400 nm excitation. Within the response time of our setup, we observed the instantaneous formation of a new set of symmetric and asymmetric CO stretching bands, which were shifted to higher wavenumbers. A singular value decomposition (SVD) analysis and a fit of kinetic traces at selected spectral positions yielded a lifetime of $\tau_{1/2} = 51$ ns

(27) Glyn, P.; George, M. W.; Hodges, P. M.; Turner, J. J. *J. Chem. Soc., Chem. Commun.* **1989**, 1655–1657.
(28) George, M. W.; Johnson, F. P. A.; Westwell, J. R.; Hodges, P. M.; Turner, J. J. *J. Chem. Soc., Dalton Trans.* **1993**, 2977–2979.
(29) Turner, J. J.; George, M. W.; Johnson, F. P. A.; Westwell, J. R. *Coord. Chem. Rev.* **1993**, *125*, 101–114.
(30) Stufkens, D.; Vlcek, A. *Coord. Chem. Rev.* **1998**, *177*, 127–179.
(31) Bredenbeck, J.; Helbing, J.; Hamm, P. *J. Am. Chem. Soc.* **2004**, *126*, 990–991.
(32) Vlcek, A.; Busby, M. *Coord. Chem. Rev.* **2006**, *250*, 1755–1762.
(33) Busby, M.; Matousek, P.; Towrie, M.; Vlcek, A. *Inorg. Chim. Acta* **2007**, *360*, 885–896.
(34) Bredenbeck, J.; Helbing, J.; Hamm, P. *Rev. Sci. Instrum.* **2004**, *75*, 4462–4466.

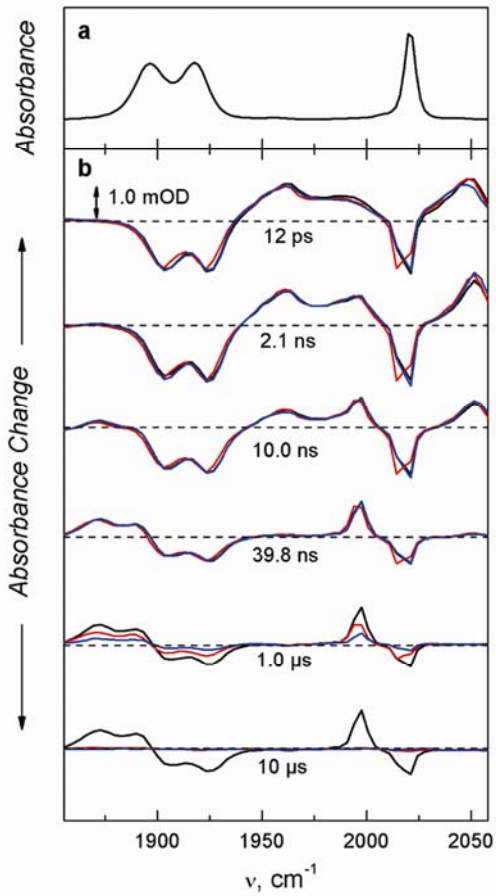

Figure 2. (a) FTIR spectrum of a 1 mM solution of **1** containing 1 M TEOA in degassed DMF (spectral resolution 2 cm^{-1}). (b) Magic angle pump−probe spectra (1 mM **1**, 1 M TEOA, 0.1 M AcOH, degassed DMF, spectral resolution 3.5 cm^{-1}) at different time delays after excitation at λ_{ex} = 400 nm. Bands appearing upon irradiation are pointing upward; bands disappearing are pointing downward. Black spectra, 0 mM of **2**; red spectra, 2 mM of **2**; blue spectra, 5 mM of **2**.

for this transient species. We assigned this transient species to the excited state of **1** (designated as ^{3}MLCT), in agreement with previous experiments,[20,28,30] reporting that the shift to higher wavenumbers is caused by a formal Re^{II} center coordinated to the bpy radical anion.

When the experiment was performed in the presence of an electron donor (1 M TEOA), a new, second transient evolved from the ^{3}MLCT state on a time scale of ~15 ns and remained constant for 10 μs, the maximum delay time of our setup (Figure 2b, 0 mM [$Co(dmgH)_2$], black spectrum). This lifetime is in good agreement with Stern−Volmer plots of luminescence intensities for **1** as a function of the TEOA concentration ($k_q = 6 \times 10^7$ M^{-1} s^{-1}).[20,26,35] The observed second transient gave rise to a new set of symmetric and asymmetric CO stretching bands, which were now red-shifted. We assign this transient to the reduced form $\mathbf{1}^-$. Accordingly, this assignment was consistent with a red shift of the corresponding set of $\nu_{C=O}$ vibrations. This was to be expected for a formally reduced 2,2′-bipyridine ligand coordinated to a Re^I center.[28] Together, $\tau_{1/2}$ and k_q would predict a quenching yield of 0.78 ± 0.04 according to eq 1.

(35) Luong, J. C.; Nadjo, L.; Wrighton, M. S. *J. Am. Chem. Soc.* **1978**, *100*, 5790–5795.

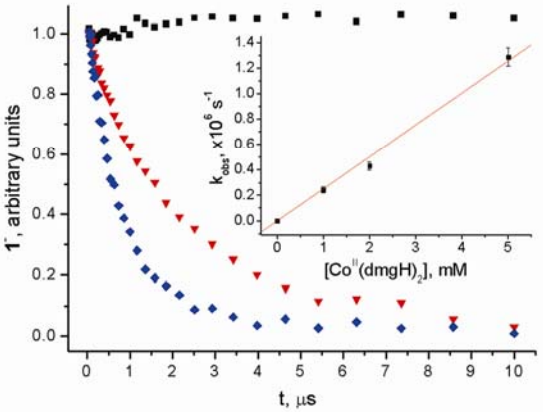

Figure 3. Transient kinetic traces for $\mathbf{1}^-$, monitored at ($\tilde{\nu}$) = 1997.5 cm^{-1}, in the presence of different cobalt concentrations (■, 0 mM of **2**; ▼, 2 mM of **2**; ♦, 5 mM of **2**). Inset: Decay rate of $\mathbf{1}^-$ as a function of $[Co]_{tot}$. The plot of k_{obs} vs concentration of **2** yields the rate for the forward electron transfer reaction ($\mathbf{1}^- + \mathbf{2} \rightarrow \mathbf{1} + [Co^I(dmgH)_2]^-$).

On the other hand, if we compare the intensities of the bleaching (negative) bands of the Re complex during the lifetime of the ^{3}MLCT state (10 ps to 10 ns) with that after the reductive quenching (Figure 2b), we estimate a yield of $\Phi_{red} \approx 0.3$. This analysis assumes that the vibrational bands of the unpumped Re complex are spectrally well separated from that of transient photoproducts (which is the case). In this case, the early bleach intensity is a direct measure of the number of molecules initially excited into the ^{3}MLCT state, whereas at later delay times it is a measure of the number of molecules that have not reacted back to the ground state. Obviously, the ^{3}MLCT of **1** was quenched in a nonproductive (~60%) and in a reductive (~40%) fashion on the same time scale, indicative of a cage escape yield of $\Phi_{cage} \approx 0.4$.

$$\Phi_q = \frac{k_q[\mathrm{TEOA}]}{k_q[\mathrm{TEOA}] + \tau_{1/2}^{-1}}, \quad \Phi_{red} = \Phi_q \Phi_{cage} \qquad (1)$$

In a next set of experiments, all of the components of the *her* system were combined and the spectra recorded in the presence of 1, 2, and 5 mM $Co(OAc)_2 \cdot 4H_2O$ and a 6-fold excess of $dmgH_2$ (Figure 2b, red and blue spectra). As can be seen in Figures 2b and 3, the signal for $\mathbf{1}^-$ was quenched depending on $[Co]_{tot}$. A fit of the kinetic traces at selected spectral positions (Figure 3) and a SVD analysis yielded lifetimes of 4.1 μs and 2.3 and 0.8 μs. The experimental C=O stretching vibrations of the observed species and the obtained global time constants are summarized in Table 1.

We estimated an upper limit for the concentration of $\mathbf{1}^-$ of 80 μM as calculated from the spectral overlap of **1** with a 400 nm laser pulse of 2.5 μJ. On the basis of this upper limit concentration, the kinetics were expected to be pseudo-first-order. Thus, for the forward electron transfer reaction between $\mathbf{1}^-$ and [$Co^{II}(dmgH)_2$], as shown in the inset of Figure 3, a rate constant of $k_1 = 2.5 \pm 0.1 \times 10^8$ M^{-1} s^{-1} was obtained. This is about 5% of the diffusion-controlled rate in DMF containing 1 M TEOA according to the Stokes−Einstein−Smoluchowski equation ($k_{dc} \sim 5 \times 10^9$ M^{-1} s^{-1}). This value is well in agreement

Table 1. Global Time Constants and Experimental C≡O Stretching Vibrations of the Species Observed Here and as Compared to the Literature

	$\nu_{C=Osym}$ [cm^{-1}]	$\nu_{C=Oasym}$ [cm^{-1}]	$\nu_{C=Osym}$ [cm^{-1}], lit.	$\nu_{C=Oasym}$ [cm^{-1}], lit.	global time constant (decay)	global time constant (decay), lit.
1	2021.9	1896.5, 1917.7	2023[a]	1902, 1914[a]		
			2019[b]	1893, 1914[b]		
^{3}MLCT of **1**	2051.4	1960.5, 1997.5	2068[a]	1957, 1989[a]	51.1 ± 1.3 ns	30 ns,[a] 50 ns,[b] 55 ns[d]
			2064[c]	1957, 1987[c]		
$\mathbf{1}^-$	1997.5	1872.9, 1889.8	1998[a]	1866, 1880[a]	15.4 ± 0.2 ns (formation)	>10 ms[a] (decay)
			1994[b]	1862, 1880[b]	>10 μs (decay)	>200 ms[b] (decay)
$\mathbf{1}^-$ (1 mM of **2**)					4.1 ± 0.4 μs	
$\mathbf{1}^-$ (2 mM of **2**)					2.3 ± 0.2 μs	
$\mathbf{1}^-$ (5 mM of **2**)					0.78 ± 0.04 μs	

[a] Data measured for $ReCl(CO)_3bipy$ in MeCN.[21] [b] Data measured for $ReCl(CO)_3bipy$ in DMF.[28] [c] Data measured for $ReCl(CO)_3bipy$ in CH_2Cl_2.[28] [d] Data measured for $ReBr(CO)_3bipy$ in DMF.[20]

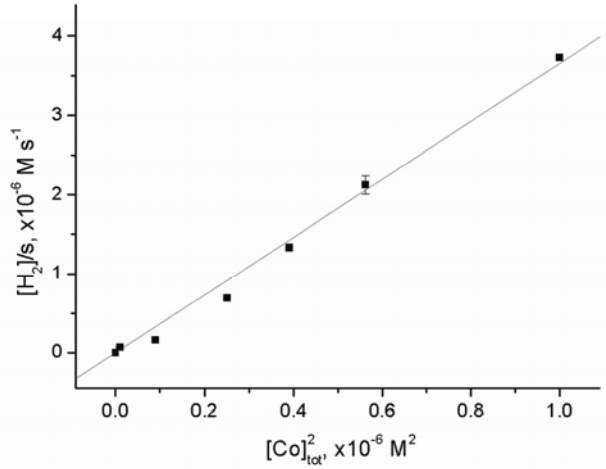

Figure 4. H_2 production rates as a function of $[Co]^2_{tot}$. An excess of 6 equiv of $dmgH_2$ was used per cobalt, 0.5 mM **1**, 1 M TEOA, 0.1 M AcOH, DMF, and argon.

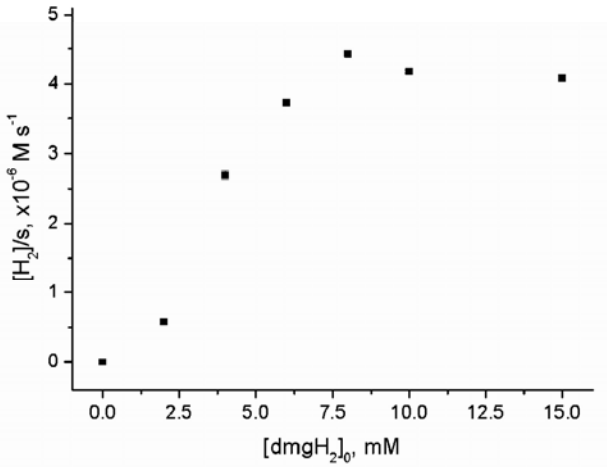

Figure 5. Initial turnover frequency as a function of $dmgH_2$ (0.5 mM **1**, 1 mM $Co(OAc)_2 \cdot 4H_2O$, 1 M TEOA, 0.1 M AcOH, DMF, and argon).

with results of a laser flash photolysis study for the forward electron transfer between $[Ru(bipy)_3]^+$ and $[Co^{II}(Me_6[14]dieneN_4)]^{2+}$ ($k = 1.8 \times 10^8$ M^{-1} s^{-1}) in a $Eu^{2+}/[Ru(bipy)_3]^{2+}/[Co^{II}(Me_6[14]dieneN_4)]^{2+}/H_2O/HCl$ system.[4]

2. Cobalt Cycle. Cobalt Dependence. The initial rate of H_2 formation as a function of the total Co concentration, $[Co]_{tot}$, should elucidate whether the major pathway was first- or second-order in cobalt. Accordingly, $[Co]_{tot}$ was varied while all of the other parameters were kept constant. For a first-order process, we expected a linear dependence since AcOH was constant over a time period of 120 min. We observed a marked dependence of the H_2 production rate on the total cobalt concentration (Figure 4). An excess of 6 equiv of $dmgH_2$ per cobalt was applied in order to keep the concentration of **2** constant (vide infra). The rate of H_2 production was found to have a square dependence on $[Co]_{tot}$, as is obvious from a corresponding linearization of the original curve. The observed second-order rate constant was $k_{obs} = 3.7 \pm 0.10$ M^{-1} s^{-1}. This square dependence implies hydrogen formation via a path second-order in $Co^{III}-H$ as is argued in the discussion and depicted in eq 5. Further increase of the cobalt concentration above 1 mM gave a constant rate of H_2 formation at about 3.75 μM s^{-1} (Supporting Information 1). We assume that at this concentration the photon flux became rate-limiting (see the Limiting Processes section).

Cobalt/$dmgH_2$ Ratio. One of the critical factors in the **1**−**2** system is the role of $dmgH_2$. As noted by Hawecker et al., an excess of $dmgH_2$ was required to achieve reasonable performance.[6] The overall stability constant (log β) for the formation of **2** from $[Co]_{solv}^{2+}$ and $dmgH_2$ has been reported to be in the range of 20 for a 1:1 dioxane−water mixture as determined by potentiometric titration.[36,37] The dependence of the H_2 formation rate as a function of $dmgH_2$ concentration confirmed that the initial turnover frequency of the system increased considerably with increasing $[dmgH_2]$ while keeping all other parameters constant. A plateau of about 4 μM s^{-1} H_2 was reached at 7.5 equiv of $dmgH_2$ per cobalt (Figure 5).

Complex **2** seemed to be less stable than expected. We found, in an electrochemical study, a conditional stability constant of $\beta_{cond.} \approx 10^6$ M^{-2} (eq 2, Supporting Information 2). The discrepancy to the literature value of $\log(\beta) = 20$ can be explained by the different solvent system used and the different definition of β. Accordingly, **2** was formed almost quantitatively upon the addition of 6 equiv of free ligand per cobalt as used in our photolysis experiments (95%). $[Co]_{solv}^{2+}$ should not interfere with excitation, quenching, and electron transfer. It is, however, known from other

(36) Freiser, H. *Analyst* **1952**, *77*, 830–845.
(37) Banks, C. V.; Anderson, S. *Inorg. Chem.* **1963**, *2*, 112–115.

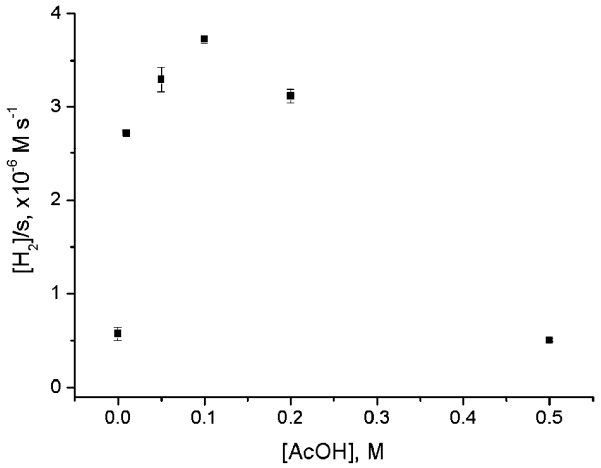

Figure 6. Dependence of hydrogen production rate on acid concentration (0.5 mM 1, 1 mM $Co(OAc)_2$, 6 mM $dmgH_2$, 1 M TEOA, DMF, and argon).

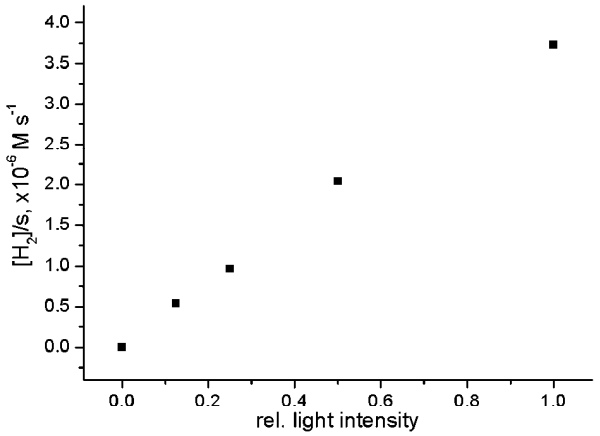

Figure 7. Variation of photon flux versus $[H_2]$/s (0.5 mM **1**, 1 mM **2**, 1 M TEOA, 0.1 M AcOH, DMF, and argon).

systems that paramagnetic cations rapidly quench triplet excited states (triplet−triplet quenching).[38] We investigated by Stern−Volmer fluorescence quenching whether $[Co]_{solv}^{2+}$ would act in the same way. We found that $[Co]_{solv}^{2+}$, added to the system in the form of $[Co(OAc)_2]$, efficiently quenched the excited state of **1** with $k_q = 2.57 \pm 0.07 \times 10^9\ M^{-1}\ s^{-1}$ (Supporting Information 3) in the absence of $dmgH_2$. Thus, an excess of $dmgH_2$ was required to optimize the amount of active *her* catalyst but also, more importantly, to avoid the presence of $[Co]_{solv}^{2+}$ since it abolished the H_2 formation process efficiently and at a rate which is close to diffusion control.

$$\beta_{cond} = \frac{[Co^{II}(dmgH)_2]}{[Co^{II}_{solv}][dmgH_2]^2} \qquad (2)$$

Dependence on Acidity. A further parameter in the system was the pH value. Although pH is difficult to define in a nonaqueous solution, the amount of added protons in the form of acetic acid might be representative for the amount of immediately available protons. We varied the concentration of acetic acid in the system while keeping the other parameters constant. In particular, the concentration of TEOA was not altered and remained constant at 1 M. The rate dependence on acetic acid concentration is shown in Figure 6.

Not surprisingly, a strong acetic acid concentration dependence on the formation rate of H_2 was found reaching a maximum at about 0.1 M acetic acid in 1 M TEOA ($3.72 \pm 0.04\ \mu M\ s^{-1}$). Interestingly, catalysis also took place without any acetic acid, although at a very slow rate ($0.57 \pm 0.07\ \mu M\ s^{-1}$). It is likely that residual protons coming from water in the system and the decomposition of TEOA[39] were responsible for this process. In the presence of 0.05 M water instead of acetic acid, the hydrogen production rate was $0.70 \pm 0.02\ \mu M\ s^{-1}$. Below and above 0.1 M, respectively, two processes decrease the H_2 production rate. The decrease observed at a high acetic acid concentration is likely to be caused by the instability of **2** at a high acid concentration, resulting in the generation of the quencher $[Co]_{solv}^{2+}$ as described before.[16] This is supported by the observation that at a low acetic acid concentration the system performed at a more constant rate over a long period of time. At a low acid concentration, the protonation of Co^I might have become limiting as acetic acid enters the overall equation.

3. Performance of the System. Quantum Yield. The photon flux was varied systematically in a series of experiments to study its influence on the hydrogen production rate. It was found to correlate linearly with hydrogen production at 1 mM **2** (Figure 7), indicating that the photon flux is rate-limiting under these conditions. The overall quantum yield of hydrogen production (0.5 H_2 per absorbed photon) was $26 \pm 2\%$ at 415 nm (see the Experimental Section) in this regime. This value was confirmed independently (within error) by ferrioxalat actinometry. Quantum yields in this range are well in accordance with literature reports on similar systems.[40] It has to be kept in mind though that the actual quantum yield might be smaller due to the generation of a second reducing equivalent by the decomposition process of TEOA.[39,41] The time-resolved experiments suggest (Figure 2) that the dominant contribution in limiting the overall quantum yield is the first electron transfer step, that is, the reductive quenching of the initially excited ^{3}MLCT state of the Re complex.

Limiting Processes. According to these observations, two rate-limiting factors for the Re−Co system were obvious. A second-order process in cobalt was the rate-limiting step when $[Co]_{tot}$ was in the range of 0−1 mM. By exceeding this concentration of *her* catalyst **2**, the photon flux became rate-limiting (Supporting Information 1). To confirm this conclusion, the rate of H_2 formation should no longer linearly depend on the photon flux at a concentration of **2** < 1 mM. Thus, we performed the same experiments as above and fixed the $[Co]_{tot}$ at 0.5 mM. The rate-limiting step changed from

(38) Porter, G.; Wright, M. R. *Discuss. Faraday Soc.* **1959**, 18–20.
(39) Kalyanasundaram, K. *J. Chem. Soc., Faraday Trans.* **1986**, *82*, 2401–2415.
(40) Sutin, N.; Creutz, C.; Fujita, E. *Comments Inorg. Chem.* **1997**, *19*, 67–92.
(41) Kutal, C.; Corbin, A. J.; Ferraudi, G. *Organometallics* **1987**, *6*, 553–557.

photon flux (at low photon flux) to a second-order process in cobalt (at high photon flux; Supporting Information 5).

Homogeneity. It has been noted for similar systems, using late transition metals as *her* catalysts, that hydrogen production correlated with colloid formation during irradiation.[11,42] On the basis of the kinetic results presented here, namely, the second-order dependence on cobalt, but also the dependence on $dmgH_2$ concentration and the fact that Co^I was produced, which is known to undergo the proposed reaction series, colloid formation as a main source of hydrogen seemed unlikely. Nevertheless, we probed a standard experiment (0.5 mM **1**, 1 mM **2**, 1 M TEOA, 0.1 M AcOH, DMF, Ar) at varying irradiation times for colloid formation by light scattering (see Supporting Information 6). The results clearly showed that, during 6 h of irradiation, no significant amounts of colloids (particle sizes from 0.5 to 1000 nm) were produced.

4. Discussion. The elucidation of essential parameters in the Re−Co system for photocatalytic H_2 formation showed that **1** is a viable alternative for $[Ru(bipy)_3]^{2+}$ used in similar experiments.[4,6,13,40] The long-term performance of **1** in particular is superior over that of $[Ru(bipy)_3]^{2+}$. Our time-resolved data unambiguously show that reductive quenching is the first step for the present system. The overall quantum yield is about 25%; however, the time-resolved measurements suggest that the dominating loss occurs during the reductive quenching of the ^{3}MLCT state of the Re complex. Further investigations elucidated the rate-controlling step. The forward electron transfer rate between $\mathbf{1}^-$ and **2** was $k_1 = 2.5 \pm 0.1 \times 10^8\ M^{-1}\ s^{-1}$ and was therefore not rate-controlling. Under mild conditions (e.g., solar irradiation), photon flux will limit the overall process. On the other hand, we could show that a second-order process in cobalt with a conditional rate constant of $k_{obs} = 3.7 \pm 0.1\ M^{-1}\ s^{-1}$ limited the rate, provided that the photon flux was high enough (Figure 4). In principle, two pathways to hydrogen can be followed after the protonation of Co^I (eq 3): either a first-order (eq 4) or a second-order process in Co^{III}−H (eq 5).

$$Co^I + HA \rightarrow Co^{III}{-}H + A^- \ (K_2, k_2) \quad (3)$$

$$Co^{III}{-}H + HA \rightarrow Co^{III} + H_2 + A^- \ (k_{1.order}) \quad (4)$$

$$2Co^{III}{-}H \rightarrow 2Co^{II} + H_2 \ (k_{2.order}) \quad (5)$$

Hu et al. demonstrate in their investigation that, for a second-order process, if the protonation of Co^I is fast (k_2), a square dependence of dH_2/dt on Co^I is found (eq 6).[17]

$$\frac{d[H_2]}{dt} = K_2^{\,2} k_{2.order} \left[\frac{[Co^I][HA]}{[A^-]}\right]^2 \quad (6)$$

This indicates that in the present system H_2 was formed by the reaction of two Co^{III}−H's and not by the protonation of the latter, as observed elsewhere.[16]

Scheme 2 summarizes the complete picture of the system under study. Thermodynamics should favor the second-order route to H_2, but kinetic reasons might favor the first-order process.[43] We believe that parallel mechanisms occur, depending on the concentration of Co^{III}−H, the concentration of the added acid, and its pK_a. In contrast to this Re−Co system, Razavet et al. found in an electrochemical system with **2** in DMF and $[Et_3NH]Cl$ as a H^+ donor a first-order process to H_2 with $k_2 = 10^4\ M^{-1}\ s^{-1}$ and $k_{1.order} = 300\ M^{-1}\ s^{-1}$.[16] This mechanism might result from the different acids ($[Et_3NH]Cl$ vs AcOH) and solvent mixtures in their experiments. Obviously both Et_3NH^+ and AcOH are acids strong enough to protonate Co^I, but only Et_3NH^+ also protonates Co^{III}−H (pK_a $Et_3NH^+ = 9.2$, AcOH = 13−14, in DMF).[44] Hu et al. found in an electrochemical study with $[Co^{II}(dmgBF_2)(MeCN)_2]$ as a *her* catalyst a predominant second-order route to H_2 with $k_{2.order} \approx 10^6\ M^{-1}\ s^{-1}$, using CF_3COOH ($pK_a = 12.7$), $Et_2O{\cdot}HCl$ ($pK_a = 8.9$), and other acids.[17,45] Chao et al. reported in a spectroscopic study with $[HCo^{III}(dmgH)_2P(n\text{-}C_4H_9)_3]$ in protic solvents a mixed first-/second-order process with $k_{2.order} = 3.4 \times 10^4\ M^{-1}\ s^{-1}$.[18] A detailed mechanistic analysis or a simulation might unravel the single components that contribute to k_{obs} in this study.

Conclusion

We presented in this study a new photocatalytic system for the efficient production of H_2 with a quantum yield essentially limited by the quenching process of TEOA and the ^{3}MLCT of **1**. The system showed a much better overall performance than that of the widely studied Ru−Co system, which requires additional optimization. The detailed kinetic studies performed for the different elementary steps in our catalytic cycle revealed a second-order process in cobalt as the final H_2 releasing step. This fundamental result has strong implications for the rational design of future *her* catalysts. Further studies are on the way to fully elucidating the parameters that govern the cobalt cycle. Currently, we are working on improving stability and efficiency of the *her* catalyst by tuning its electronic and steric properties.

Experimental Section

All chemicals were of reagent grade and used without further purification. Spectroscopic-grade DMF was purchased from Acros. Electrochemical-grade $TBA[PF_6]$, $Co(OAc)_2{\cdot}4H_2O$, and $dmgH_2$ were purchased from Fluka. Water was doubly distilled before use. Synthetic reactions were carried out under N_2 or Ar using standard Schlenk techniques. The synthesis of **1** and $[Ru(bipy)_3]^{2+}$ has been described in the literature.[46,47]

Fluorescence measurements were performed on a Perkin-Elmer LS50B fluorescence spectrometer with argon-purged solution samples in 1 cm cells.

Electrochemical measurements were carried out in DMF containing 0.1 M $TBA[PF_6]$ as a conducting electrolyte. A Metrohm 757VA Computrace electrochemical analyzer was used with a

(42) Du, P.; Schneider, J.; Fan, L.; Zhao, W.; Patel, U.; Castellano, F. N.; Eisenberg, R. *J. Am. Chem. Soc.* **2008**, *130*, 5056–5058.

(43) Kellett, R. M.; Spiro, T. G. *Inorg. Chem.* **1985**, *24*, 2373–2377.

(44) Izutsu, K. *Acid-Base Dissociation Constants in Dipolar Aprotic Solvents*; Blackwell Scientific Publications: Oxford, 1990.

(45) Hu, X. L.; Cossairt, B. M.; Brunschwig, B. S.; Lewis, N. S.; Peters, J. C. *Chem. Comm.* **2005**, 4723–4725.

(46) Abel, E. W.; Wilkinson, G. *J. Chem. Soc.* **1959**, 1501–1505.

(47) Burstall, F. H. *J. Chem. Soc.* **1936**, 173–175.

standard three-electrode setup of glassy carbon working and Pt auxiliary electrodes and a Ag/AgCl reference electrode. All potentials are given versus Ag/AgCl (Fc/Fc^+ at +500 mV).

Light scattering was measured on a DynaPro Titan TC (Wyatt Technology). The sample was ultracentrifuged and probed by an 828 nm laser in either a 50 μL (not stirred) or 2 mL (stirred) cuvette after various irradiation times (25 °C, 90° to the probe beam, 100% laser power). Each measurement consisted of 20 acquisitions (10 s each).

Gas chromatograms were recorded using a Varian CP-3800 gas chromatograph with argon as the carrier gas and a 3 m × 2 mm molecular sieve 13X 80−100. The gas flow was set to 20 mL/min. The oven was operated isothermally at 100 °C. The 100 μL gas samples were injected using a Hamilton (1825 RN) gastight microliter syringe. The gases were detected using a thermal conductivity detector (Varian) operated at 150 °C. Calibrations were performed by the injection of known quantities of pure hydrogen diluted in the same Schlenk tube containing the same volume of DMF as used for the measurements.

Photochemical Measurements. Typical reactions were carried out in a 54 mL septum-capped Schlenk tube. Exact volumes were determined gravimetrically. A total of 10 mL of a solution containing the respective mixture in DMF was prepared, wrapped in black foil and degassed using an argon-purged Schlenk line. The mixture was equilibrated under 1.5 bar of argon pressure for 15 min and then transferred to a dark room for illumination. The light source was a Leica Pradovit S AF slide projector equipped with a 250 W Osram Xenophot HLX lamp. The light was filtered with a 400 nm cutoff filter (Schott GG 400, no transmission below 400 nm, spectra see Supporting Information 7, black) before reaching the sample at a 40 cm distance from the projector. If necessary, the radiant flux was cut in $(1/2)^n$ by using n neutral density filters (OD = 0.3). The 100 μL gas samples were drawn from the headspace above the solution and injected into the GC-TCD gas analyzer.

Quantum Yield Measurments. Light at 415 nm was produced by frequency-doubling a Spectra-Physics Tsunami femtosecond laser system. It was then focused (beam diameter ~ 5 mm) on a SUPRASIL quartz cell (Helma, 20 mm). The radiant flux through the sample was determined by an Ophir Laser Power Meter (Model AN/2) before and after the addition of the chromophore to calculate the number of absorbed photons. Headspace sampling for hydrogen detection at respective times was done as described above.

To obtain an independent verification of the quantum yield, we also performed actinometry using $K_3[Fe(ox)_3]$ as the chemical actinometer and a 300 W Xe arc lamp (LOT Oriel) in line with a water filter and a 400 nm bandpass filter (Andover Corporation, 400FS10-50, 402 nm).

UV-Pump−IR-Probe Spectroscopy. The system for UV-pump−IR-probe spectroscopy consists of two synchronized[34] commercially available Ti:sapphire-oscillator/regenerative amplifier femtosecond laser systems operating at 800 nm (Spectra Physics; duration, ~100 fs; repetition rate, 1 kHz; energy, ~600 μJ/pulse), allowing us to cover the time range from 2 ps to 10 μs. Laser system 1 was frequency-doubled with a BBO crystal. The obtained 400 nm pulses were subsequently focused into the sample cell (100 μm thick) with a spot size of ~200 μm diameter. Measurements were carried out using parallel and perpendicular polarized pump pulses generated by a computer-controlled half-wave plate, from which the magic angle signal was calculated. Laser system 2 pumped a white-light-seeded two-stage BBO optical parametric amplifier (OPA),[48] the signal and idler pulses of which were difference-frequency mixed in a $AgGaS_2$ crystal. They were separated into two parts to achieve broadband probe and reference pulses. These IR-probe pulses were focused into the sample cell in spatial overlap with the 400 nm pump pulse. The reference and probe pulses were dispersed in a monochromator (SPEX Triax Series) and imaged onto a 2 × 64 pixel MCT (Mercury Cadmium Telluride) detector array (InfraRed Associates Inc.), revealing a spectral resolution of 3.5 cm^{-1}. To ensure efficient exchange of the excited volume, the sample was pumped rapidly by a tubing pump (Ismatec BVP equipped with EasyLoad II pump-head, flow ~5.0 mL/min) to a small sealed reservoir (V ≈ 3 mL). The pressurized flow of the reservoir transferred the sample through the flow cell (path length 100 μm) and finally back to the tank, which was protected from light. Since TEOA is a very aggressive compound, the EasyLoad II pump-head was equipped with chemically resistant fluoroelastomer tubing from Gore (Chem-Sure; 1.6 mm ID, 1.6 mm wall, 4.8 mm o.d., 305 mm length). The concentration of the Re sample (**1**) in DMF (Acros, spectroscopic-grade) was adjusted to 1 mM, and the solution was purged with argon continuously. During the course of the measurement, unwanted photoproducts accumulated to less than 5%.

Acknowledgment. We thank Alexander Rodenberg for technical assistance in the quantum yield measurements. We are grateful to the Swiss National Science Foundation (SNF) for financially supporting this work (Grant No. 200021-119798).

Supporting Information Available: H_2 formation as a function of $[Co(dmgH)_2]$ and photon flux, stability constant determination for $[Co(dmgH)_2]$, luminescence quenching of **1** by Co^{2+}, light scattering experiments, and the spectra of the light sources used. This material is available free of charge via the Internet at http://pubs.acs.org.

IC8013255

(48) Hamm, P.; Kaindl, R. A.; Stenger, J. *Opt. Lett.* **2000**, *25*, 1798–1800.

An efficient homogeneous intermolecular rhenium based photocatalytic system for the production of H_2.

Benjamin Probst, Christoph Kolano, Peter Hamm, Roger Alberto*.*

Institute of Inorganic Chemistry, University of Zürich, Winterthurerstrasse 190, CH-8057 Zürich Switzerland

Institute of Physical Chemistry, University of Zürich, Winterthurerstrasse 190, CH-8057 Zürich Switzerland.

SUPPORTING INFORMATION

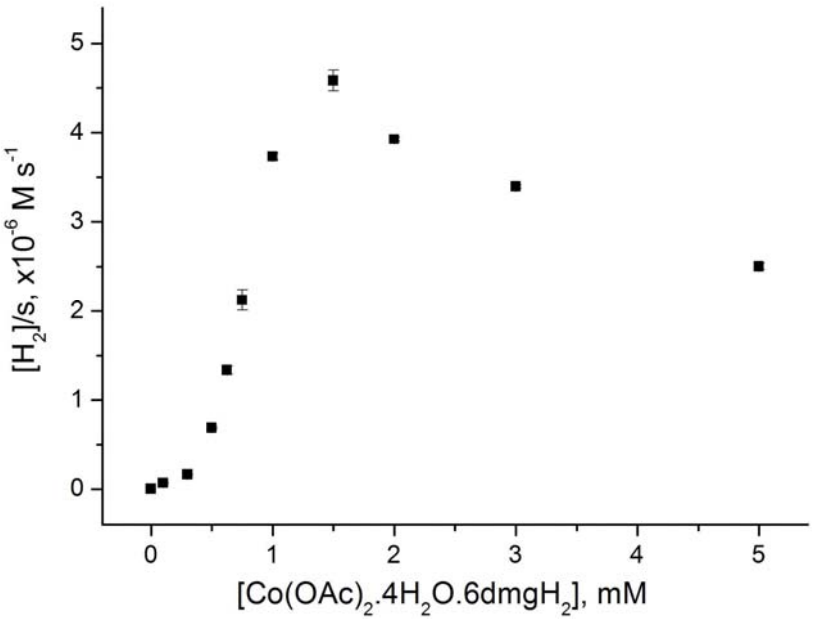

SI 1. Hydrogen production rate as a function of **2**, an excess of 6 equivalents of $dmgH_2$ was used per cobalt, 0.5 mM **1**, 1 M TEOA, 0.1 M AcOH, DMF, Argon.

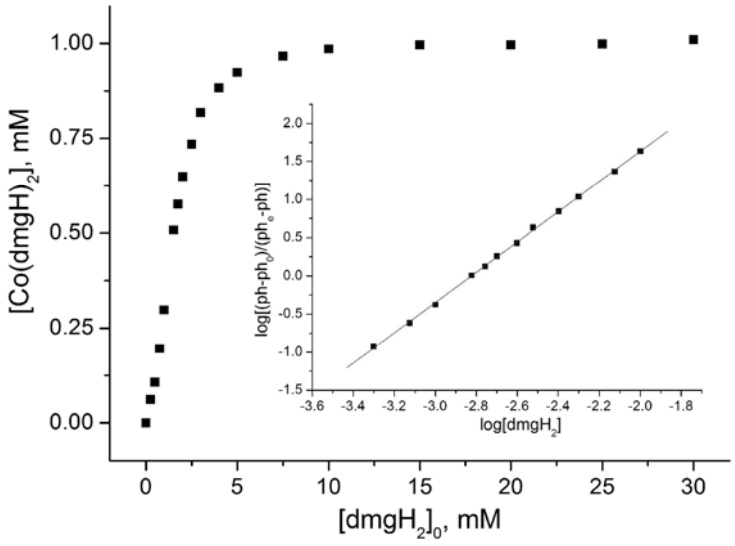

SI 2. Titration of $[Co]^{2+}_{solv}$ with $dmgH_2$, as monitored potentiometrically (1 mM $Co(OAc)_2 \cdot 4H_2O$, 0.1 M $TBAPF_6$, 1 M TEA, DMF, N_2). Linearization according to $\log\left(\frac{K}{F}\right) = -q \log[dmgH_2] + \log\left(\frac{[2]-[2]_0}{[2]_e-[2]}\right)$ gives $q \approx 2$ and $\log(\beta_{cond}) \approx 6$.

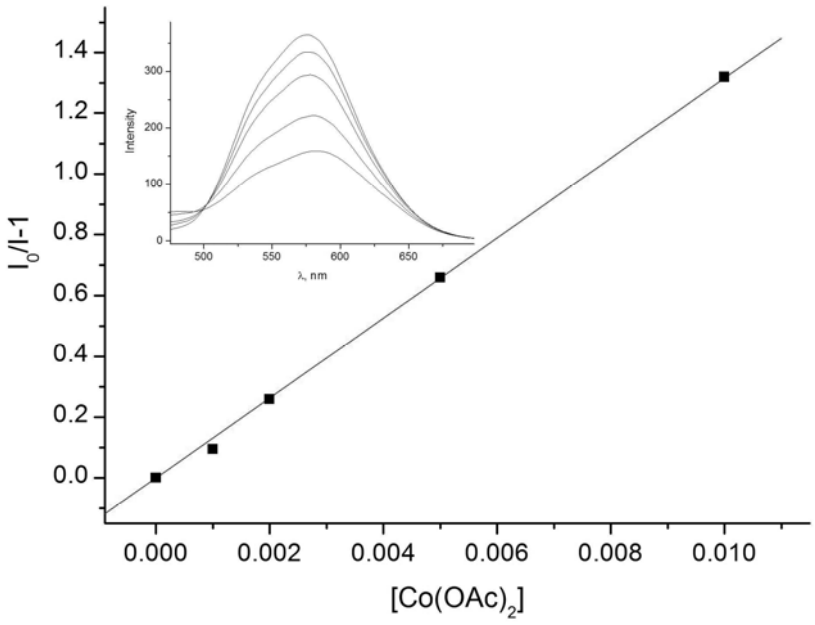

SI 3. Fluorescence quenching of a 1 mM solution of **1** by $Co(OAc)_2 \cdot 4H_2O$. Fitting according to Stern – Volmer (inset: emission spectra at respective concentrations of $Co(OAc)_2 \cdot 4H_2O$) gives a K_{SV} of 132 ± 1.7 M^{-1}, which corresponds to a k_q of 2.57 ± 0.07 x 10^9 M^{-1} s^{-1}.

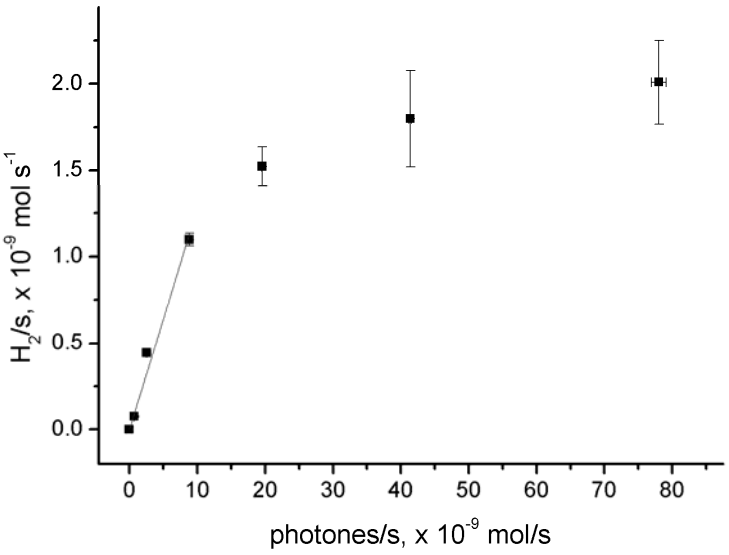

SI 4. Hydrogen production rate is plotted vs the number of absorbed photons. Linear fitting at low photon flux gives 0.128 ± 0.0078 H_2 per absorbed photon (R^2 = 0.98528; 1 M TEOA, 0.1 M AcOH, 0.5 mM **1**, 1 mM **2**, DMF, Ar, in a 5600 µl suprasil cell (Helma, 20 mm), irradiated with 415 nm laser light of varying power).

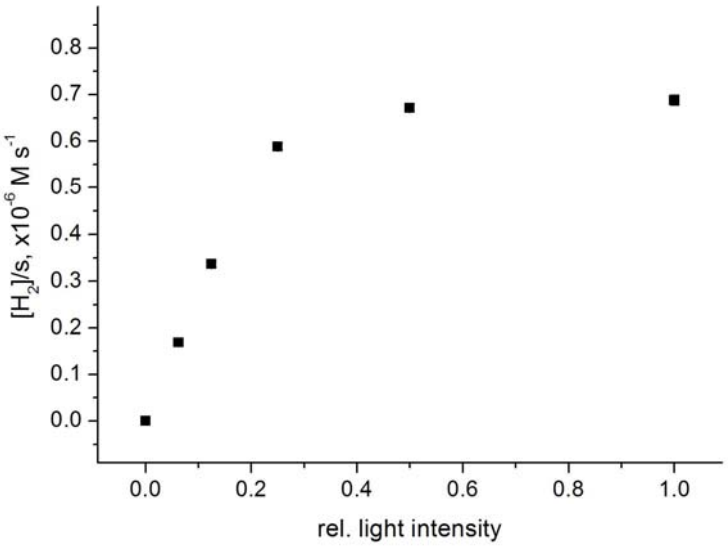

SI 5. $[H_2]$/s versus relative light intensity (0.5 mM **1**, 0.5 mM **2**, 1 M TEOA, 0.1 M AcOH, DMF, Argon).

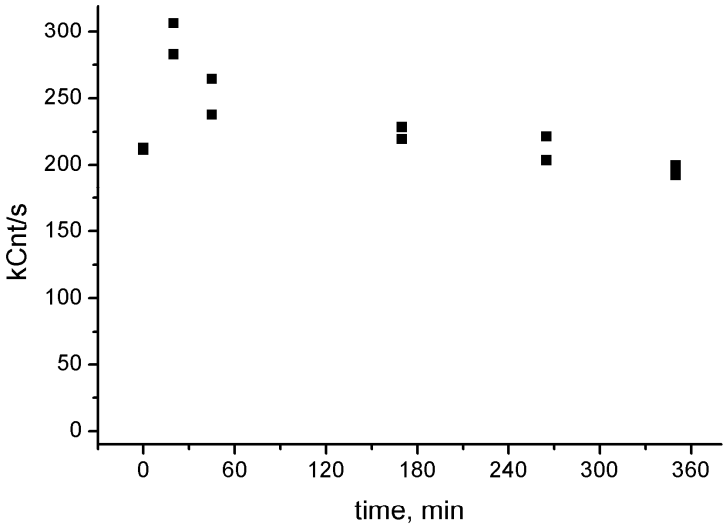

SI 6. Light scattering (90° degree angle, probe beam at 828 nm, kilo counts per second) during a six hour photolysis experiment (0.5 mM **1**, 1 mM **2**, 1 M TEOA, 0.1 M AcOH, DMF, Ar).

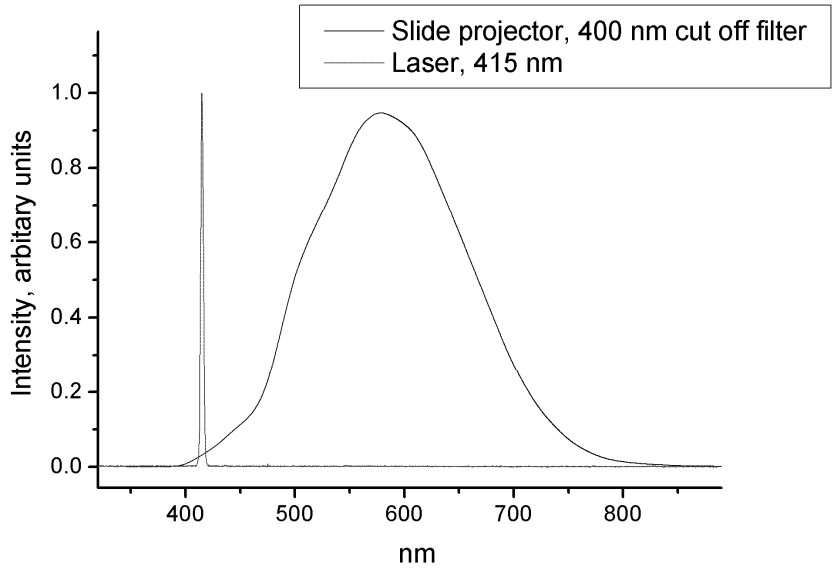

SI 7: Spectral distribution of the two light sources used for cw experiments.

Inorganic Chemistry
Article

Inorg. Chem. **2010**, *49*, 6453–6460 **6453**
DOI: 10.1021/ic100036v

A Highly Stable Rhenium−Cobalt System for Photocatalytic H_2 Production: Unraveling the Performance-Limiting Steps

Benjamin Probst,[†] Alexander Rodenberg,[‡] Miguel Guttentag,[†] Peter Hamm,*[,‡] and Roger Alberto*[,†]

[†]*Institute of Inorganic Chemistry,* [‡]*Institute of Physical Chemistry, University of Zürich, Winterthurerstrasse 190, CH-8057 Zürich Switzerland*

Received January 7, 2010

Increased long-term performance was found for photocatalytic H_2 production in a homogeneous combination of [Re(NCS)(CO)$_3$bipy] (**1**; bipy = 2,2′-bipyridine), [Co(dmgH)$_2$] (dmgH$_2$ = dimethylglyoxime), triethanolamine (TEOA), and [HTEOA][BF_4] in *N*,*N*-dimethylformamide, achieving TON_{Re} up to 6000 (H/Re). The system proceeded by reductive quenching of ***1** by TEOA, followed by fast ($k_1 = 1.3 \times 10^8$ M^{-1} s^{-1}) electron transfer to [Co^{II}(dmgH)$_2$] and subsequent protonation (K_2) and elimination (k_3, second-order process in cobalt) of H_2. Observed quantum yields were up to ∼90% (H produced per absorbed photon). The type of acid had a substantial effect on the long-term stability. A decomposition pathway involving cobalt is limiting the long-term performance. Time-resolved infrared (IR) spectroscopy confirmed that photooxidized TEOA generates a second reducing equivalent, which can be transferred to **1** (70%, $k_{2e^-} = 3.3 \times 10^8$ M^{-1} s^{-1}) if no [Co^{II}(dmgH)$_2$] is present.

Introduction

The long-term objective of this study is to find a photocatalytic cycle in a homogeneous solution for water splitting to H_2 and O_2 and is motivated by ongoing depletion of fossil energy sources in the years to come. Commercially available photovoltaic (PV) cells coupled to state-of-the-art water electrolyzers split water in high yields, but at prices that do not yet compete with H_2 produced by steam reforming of natural gas or coal gasification.[1] This intrinsic problem will, however, be overcome as soon as prices for fossil fuels rise significantly. Besides PV cells, the search for direct light-driven processes represents an incentive in current research. A particularly appealing one is the mimicking of natural photosynthesis: photons are absorbed by a photosensitizer to generate free electrons and holes. Ideally, the latter ones can be used for water oxidation, while the electrons reduce water (Scheme 1).

First literature reports about photocatalytic water splitting in homogeneous solutions appeared around 1980 with the pioneering work of Sutin and Lehn.[2,3] They presented systems that reduced protons to H_2 with [Ru(bipy)$_3$]$^{2+}$ as a photosensitizer (PS) and a cobalt-based water reduction catalyst (WRC). Cobalt macrocyclic complexes acted as WRCs in some more recent reports about photocatalytic proton reduction. Artero et al. applied [Co(dmgX)$_2$YZ]-type complexes (dmgH$_2$ = dimethylglyoxime, X = H$^+$ or BF_2^+, Y = halogen, Z = pyridine derivatives) and [ReBr(CO)$_3$phen]-, [Ru(diimine)$_3$]$^{2+}$-, and [Ir(ppy)(diimine)]$^+$-type PSs, with the latter two complexes also with a covalent link to the axial pyridine coordinated to cobalt, achieving up to 550 turnover numbers (TONs; for H/Re and 275 for H_2/Co) with the rhenium system.[4,5] Eisenberg et al. focused on [Co(dmgX)$_2$-YZ]-type complexes but with a platinum terpyridyl acetylide or, more recently, xanthene-type PSs, achieving up to 2400 TONs (for H/Pt and 2200 for H_2/Co) in the platinum system.[6,7] In our own work, [ReBr(CO)$_3$bipy] served as the PS and [Co(dmgH)$_2$] as the WRC.[8] Bernhard et al. used [M(bipy)$_3$]$^{3+}$ (M = Co^{III} or Rh^{III}) as WRC in combination with [Ir(ppy)$_2$(diimine)]$^+$ as the PS in MeCN or tetrahydrofuran/water mixtures with TONs up to a respectable 5000 (for H/Ir and 2500 for H_2/Rh).[9,10] Other more recent systems were all based on [Ru(bipy)$_3$]$^{2+}$-type PSs and platinum, palladium, or rhodium complexes as WRCs.[11−14] Besides displaying low TONs (5−50), the homogeneous character of

*To whom correspondence should be addressed. E-mail: ariel@aci.uzh.ch.

(1) Drennen, T. E.; Rosthal, J. E. *Pathways to a hydrogen future*; Elsevier: Amsterdam, The Netherlands, 2007.
(2) Brown, G. M.; Brunschwig, B. S.; Creutz, C.; Endicott, J. F.; Sutin, N. *J. Am. Chem. Soc.* **1979**, *101*, 1298–1300.
(3) Hawecker, J.; Lehn, J. M.; Ziessel, R. *New J. Chem.* **1983**, *7*, 271–277.
(4) Fihri, A.; Artero, V.; Razavet, M.; Baffert, C.; Leibl, W.; Fontecave, M. *Angew. Chem., Int. Ed.* **2008**, *47*, 564–567.
(5) Fihri, A.; Artero, V.; Pereira, A.; Fontecave, M. *Dalton Trans.* **2008**, 5567–5569.
(6) Du, P.; Schneider, J.; Luo, G.; Brennessel, W. W.; Eisenberg, R. *Inorg. Chem.* **2009**, *48*, 4952–4962.
(7) Lazarides, T.; McCormick, T.; Du, P. W.; Luo, G. G.; Lindley, B.; Eisenberg, R. *J. Am. Chem. Soc.* **2009**, *131*, 9192–.
(8) Probst, B.; Kolano, C.; Hamm, P.; Alberto, R. *Inorg. Chem.* **2009**, *48*, 1836–1843.
(9) Cline, E. D.; Adamson, S. E.; Bernhard, S. *Inorg. Chem.* **2008**, *47*, 10378–10388.
(10) Goldsmith, J. I.; Hudson, W. R.; Lowry, M. S.; Anderson, T. H.; Bernhard, S. *J. Am. Chem. Soc.* **2005**, *127*, 7502–7510.

Published on Web 06/16/2010

Scheme 1. General Representation of a Photocatalytic Relay for Water Decomposition into H_2 and O_2 Proceeding via Reductive Quenching of the Excited *PS by a WOC and Subsequent Reduction of a WRC by PS^-

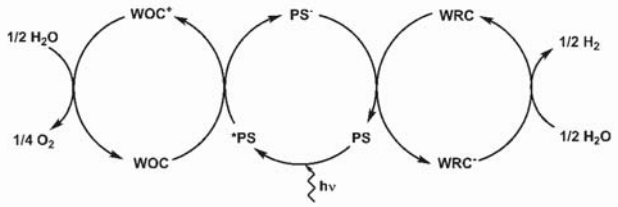

these latter systems was put into question.[12] Great efforts have been put into the development of water oxidation catalysts (WOCs),[15−20] and the first examples of photocatalytic water oxidation reactions (to our knowledge) were only recently reported by Hill et al.[21] and Sun et al.[22]

Our initial studies focused on the kinetics and short-term performance of a homogeneous system using triethanolamine (TEOA) as the sacrificial electron donor, [ReBr(CO)$_3$bipy] as the PS, and [Co(dmgH)$_2$] as the WRC. We found that reductive quenching of *PS by TEOA was followed by fast ($k_{1,Br}$ = 2.5 × 10^8 M^{-1} s^{-1}) electron transfer to [Co^{II}(dmgH)$_2$]. The resulting Co^I species produced H_2 in a second-order process in cobalt. The long-term performance of the process was limited by [ReBr(CO)$_3$bipy]. The labile Br^- ligand was lost under photocatalytic conditions after a short time of irradiation, thereby interrupting the cycle. We also found that acetic acid had a negative influence on the long-term performance of the system.

Addressing these two drawbacks, we present in this report a substantially improved system. Replacing Br^- in [ReBr(CO)$_3$bipy] by $[NCS]^-$ and acetic acid by [HTEOA][BF$_4$] increased the long-term stability significantly (TON_{Re} up to 6000). Electron transfer between the reduced PS and Co^{II} was very fast (k_1 = 1.3 × 10^8 M^{-1} s^{-1}). The transfer of a second reducing equivalent to the PS, tentatively assigned to originate from decomposition of TEOA, could be observed. Potential rhenium decomposition pathways were identified in a domain where the cobalt concentration was rate-limiting. We confirmed a second-order process in cobalt for the final formation of H_2 and a strong correlation between [HTEOA$^+$]

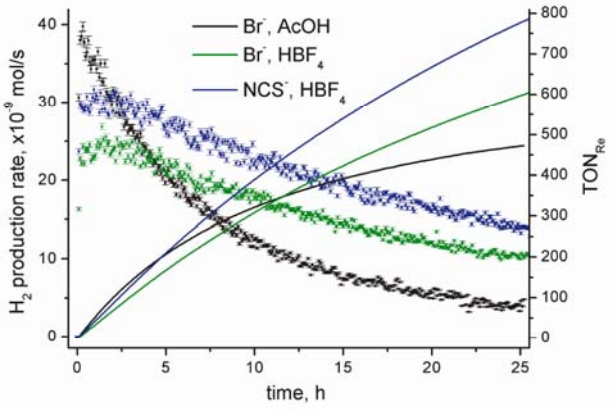

Figure 1. H_2 production rate (left scale, ■) and TON_{Re} (right scale, solid lines) as a function of time with AcOH or HBF_4, respectively, and with X = Br^- or NCS^- (0.5 mM [ReX(CO)$_3$bipy], 1 mM [Co(OH$_2$)$_6$](BF$_4$)$_2$, 6 mM dmgH$_2$, 1 M TEOA, 0.1 M acid, DMF, Ar, 476 nm).

and the initial turnover frequency (TOF) and the end TON, respectively.

Results and Discussion

Influence of Acid and X in [ReX(CO)$_3$bipy] on H_2 Production. Analysis of the reaction mixtures in the TEOA/AcOH/[ReBr(CO)$_3$bipy]/[Co(dmgH)$_2$]/DMF system after irradiation revealed the quantitative loss of Br^- in [ReBr(CO)$_3$bipy]. The addition of a 10-fold excess of tetra-*n*-butylammonium bromide ([TBA]Br) did not increase the catalytic performance (see SI 1 in the Supporting Information). Replacing acetic acid (pK_a = 13−14)[23] by [HTEOA][BF$_4$] (pK_a = 7.5)[23] considerably increased the long-term performance, although at lower rates (see Figure 1). The axial bromide ligand now remained coordinated to rhenium, as evidenced by high-performance liquid chromatography (HPLC). Obviously, acetic acid accelerates the loss of Br^- from [ReBr(CO)$_3$bipy], possibly via formation of an acetate or a solvato complex. Accordingly, comparative experiments were performed with [Re(OH$_2$)(CO)$_3$bipy][O$_3$SCF$_3$], where axial-bound OH_2 served as a leaving group. Indeed, we found catalysis to proceed at a much lower, albeit a constant rate, as found for [ReBr(CO)$_3$bipy] after the initial burst in H_2 production (see SI 1 in the Supporting Information). This confirmed our hypothesis that loss of axial Br^- in [ReBr(CO)$_3$bipy] limited H_2 production in the previous system. We hypothesized that the lower TOF for [Re(OH$_2$)(CO)$_3$bipy]$^+$ is due to a reduced overlap with the 476 nm LED (Table 1 and SI 7 in the Supporting Information). This assumption was supported by experiments with a 380 nm LED (see SI 5 in the Supporting Information), where extinction of [Re(OH$_2$)(CO)$_3$bipy]$^+$ and [ReBr(CO)$_3$bipy] and H_2 production were almost equal.

To further evidence the influence of the axial ligand X^-, we replaced [ReBr(CO)$_3$bipy] by [Re(NCS)(CO)$_3$bipy] (**1**). We found previously that **1** exerts a very high stability[24] while maintaining physicochemical properties

(11) Elvington, M.; Brown, J.; Arachchige, S. M.; Brewer, K. J. *J. Am. Chem. Soc.* **2007**, *129*, 10644–.
(12) Lei, P.; Hedlund, M.; Lomoth, R.; Rensmo, H.; Johansson, O.; Hammarstrom, L. *J. Am. Chem. Soc.* **2008**, *130*, 26–27.
(13) Ozawa, H.; Haga, M. A.; Sakai, K. *J. Am. Chem. Soc.* **2006**, *128*, 4926–4927.
(14) Rau, S.; Schafer, B.; Gleich, D.; Anders, E.; Rudolph, M.; Friedrich, M.; Gorls, H.; Henry, W.; Vos, J. G. *Angew. Chem., Int. Ed.* **2006**, *45*, 6215–6218.
(15) Chen, H. Y.; Tagore, R.; Das, S.; Incarvito, C.; Faller, J. W.; Crabtree, R. H.; Brudvig, G. W. *Inorg. Chem.* **2005**, *44*, 7661–7670.
(16) Geletii, Y. V.; Botar, B.; Koegerler, P.; Hillesheim, D. A.; Musaev, D. G.; Hill, C. L. *Angew. Chem., Int. Ed.* **2008**, *47*, 3896–3899.
(17) Gersten, S. W.; Samuels, G. J.; Meyer, T. J. *J. Am. Chem. Soc.* **1982**, *104*, 4029–4030.
(18) McDaniel, N. D.; Coughlin, F. J.; Tinker, L. L.; Bernhard, S. *J. Am. Chem. Soc.* **2008**, *130*, 210–217.
(19) Sartorel, A.; Carraro, M.; Scorrano, G.; De Zorzi, R.; Geremia, S.; McDaniel, N. D.; Bernhard, S.; Bonchio, M. *J. Am. Chem. Soc.* **2008**, *130*, 5006–5007.
(20) Tseng, H. W.; Zong, R.; Muckerman, J. T.; Thummel, R. *Inorg. Chem.* **2008**, *47*, 11763–11773.
(21) Geletii, Y. V.; Huang, Z.; Hou, Y.; Musaev, D. G.; Lian, T.; Hill, C. L. *J. Am. Chem. Soc.* **2009**, *131*, 7522–7523.
(22) Duan, L.; Xu, Y.; Zhang, P.; Wang, M.; Sun, L. *Inorg. Chem.* **2009**, *49*, 209–215.
(23) Izutsu, K. *Acid−base dissociation constants in dipolar aprotic solvents*; Blackwell Scientific Publications: Oxford, U.K., 1990.
(24) Kurz, P.; Probst, B.; Spingler, B.; Alberto, R. *Eur. J. Inorg. Chem.* **2006**, 2966–2974.

Table 1. Physicochemical Properties of $[ReX(CO)_3bipy]$ in DMF

X	λ_{MLCT}, nm (ε, M^{-1} s^{-1})	λ_{phos}, nm ($\Phi \times 10^3$)	τ, ns	$k_{q,TEOA}$, $\times 10^6$ M^{-1} s^{-1}	E_{red},[a] V	$\nu_{CO,\ sym}$,[b] cm^{-1}
Br	375 (3110 ± 50)	600 (1.8 ± 0.11)	42.2 ± 0.19	64.8 ± 0.4	−1.235	2011
OH_2	347 (sh; 3950 ± 20)	590 (1.5 ± 0.07)	33.3 ± 0.16	236 ± 3.2	−1.080	2035
NCS	376 (2910 ± 99)	602 (1.1 ± 0.05)	25.5 ± 0.22	92 ± 1.2	−1.185	2020

[a] Reversible one-electron reduction potentials in V vs Ag/AgCl. [b] In KBr pellet.

Scheme 2. Sequence of Reactions (As Assumed) for TEOA upon Interaction with *PS

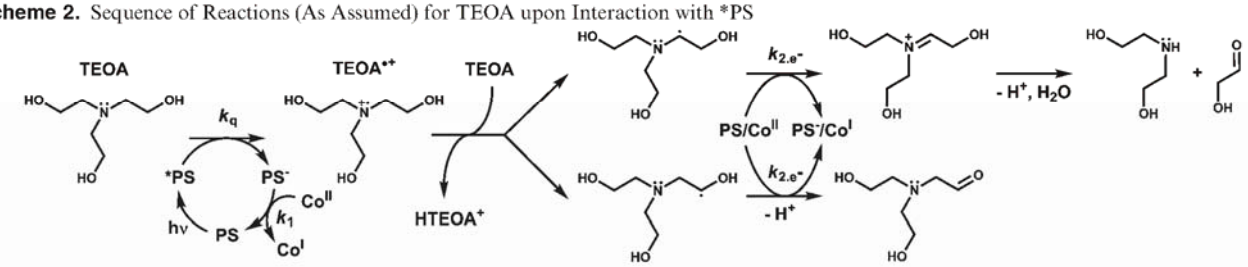

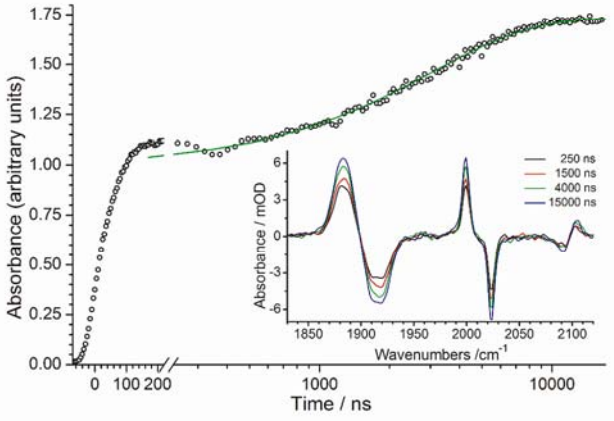

Figure 2. Transient kinetic trace of $\mathbf{1}^-$ (integrated absorbance of CO and NCS bands) in DMF with 1 M TEOA after excitation with λ = 355 nm (black circles). Oscillation of the signal between ~150 and ~450 ns is caused by amplifier ringing. Green line: Exponential fit of a second rise from 200 ns to 18 μs. Inset: Transient spectra measured at different delay times. Bands pointing downward belong to CO and NCS vibrations of the ground state of **1**, positive bands to those of the reduced complex $\mathbf{1}^-$.

similar to those of $[ReBr(CO)_3bipy]$ (Table 1). As is evident from HPLC analysis, **1** proved to be very inert toward $[NCS]^-$ substitution in DMF. Comparative H_2 formations are given in Figure 1. Further experiments were done to clarify the kinetics in the modified system, namely, the sequence of the catalytic cycle, the influence of the concentration of both $[HTEOA][BF_4]$ and $[Co(dmgH)_2]$, and the long-term performance.

Electron-Transfer Steps. To allow observation of the eventual secondary electron-transfer processes following the first, very fast reduction (k_q; Scheme 2), step-scan IR spectroscopy was applied to cover the time domain from 100 ns to 500 μs. The kinetics of $\mathbf{1}^-$, originating from reductive quenching of ***1** by TEOA (Scheme 2, left side), could thus be analyzed in more detail.[8] The first step after excitation, i.e., quenching of the triplet metal-to-ligand charge-transfer (^{3}MLCT) state of **1**, is not resolved with this method because its time scale is beyond the resolution of the step-scan technique (~11 ns in DMF with [TEOA] = 1 M; Table 1).

A 1 mM solution of **1** with 1 M TEOA in DMF was prepared and purged with Ar for 60 min before irradiation and measurement. Figure 2 shows the kinetic trace of $\mathbf{1}^-$ and difference spectra at various delay times after excitation with 355 nm light. The IR bands at 1918, 2024, and 2092 cm^{-1} correspond to the asymmetric and symmetric CO stretching vibrations and the NCS stretching vibration, respectively. These bands are bleached upon excitation and subsequent reductive quenching of ***1** by TEOA.[8,25] The corresponding ν_{CO} transients of $\mathbf{1}^-$ are found at slightly lower wavenumbers (1884 and 1999 cm^{-1}), indicative of an increased back-bonding in $\mathbf{1}^-$,[8,26,27] while ν_{NCS} of $\mathbf{1}^-$ appears at 2103 cm^{-1}. The kinetic trace of $\mathbf{1}^-$ consists of two processes occurring at different time scales. While the reductive quenching of the ^{3}MLCT state takes place within a few nanoseconds, the signal first rises within the response time of the detector and amplifier, reaching a first plateau after ~200 ns. Subsequently, a second step of the signal with a first-order time constant of 3.1 μs was observed. The amplitude of the second step is ~70% relative to the first one. Reductive quenching of ***1** with TEOA (amplitude: 100%) generates the nitrogen-centered radical-cation $TEOA^{\bullet+}$ $\{N^{\bullet}(CH_2CH_2OH)_3^{+}\}$ (Scheme 2). H$^{\bullet}$ abstraction at TEOA by $TEOA^{\bullet+}$/deprotonation of $TEOA^{\bullet+}$ by TEOA yields the carbon-centered radicals $(HOCH_2C^{\bullet}H)N(CH_2CH_2OH)_2$ and/or $(HOC^{\bullet}HCH_2)N(CH_2CH_2OH)_2$, as shown before (Scheme 2, right side).[28−34] Unlike the aminyl radical $TEOA^{\bullet+}$, these carbon-centered radicals are strong reducing agents[28,32]

(25) Rodriguez, A. M. B.; Gabrielsson, A.; Motevalli, M.; Matousek, P.; Towrie, M.; Sebera, J.; Zalis, S.; Vlcek, A. *J. Phys. Chem. A* **2005**, *109*, 5016–5025.
(26) George, M. W.; Johnson, F. P. A.; Westwell, J. R.; Hodges, P. M.; Turner, J. J. *J. Chem. Soc., Dalton Trans.* **1993**, 2977–2979.
(27) Hayashi, Y.; Kita, S.; Brunschwig, B. S.; Fujita, E. *J. Am. Chem. Soc.* **2003**, *125*, 11976–11987.
(28) Chan, S. F.; Chou, M.; Creutz, C.; Matsubara, T.; Sutin, N. *J. Am. Chem. Soc.* **1981**, *103*, 369–379.
(29) Delaive, P. J.; Foreman, T. K.; Giannotti, C.; Whitten, D. G. *J. Am. Chem. Soc.* **1980**, *102*, 5627–5631.
(30) Kalyanasundaram, K. *J. Chem. Soc., Faraday Trans.* **1986**, *82*, 2401–2415.
(31) Neshvad, G.; Hoffman, M. Z. *J. Phys. Chem.* **1989**, *93*, 2445–2452.
(32) Kishore, K.; Dey, G. R.; Mukherjee, T. *Res. Chem. Intermed.* **2004**, *30*, 837–845.
(33) Kirch, M.; Lehn, J. M.; Sauvage, J. P. *Helv. Chim. Acta* **1979**, *62*, 1345–1384.
(34) Kalyanasundaram, K.; Kiwi, J.; Gratzel, M. *Helv. Chim. Acta* **1978**, *61*, 2720–2730.

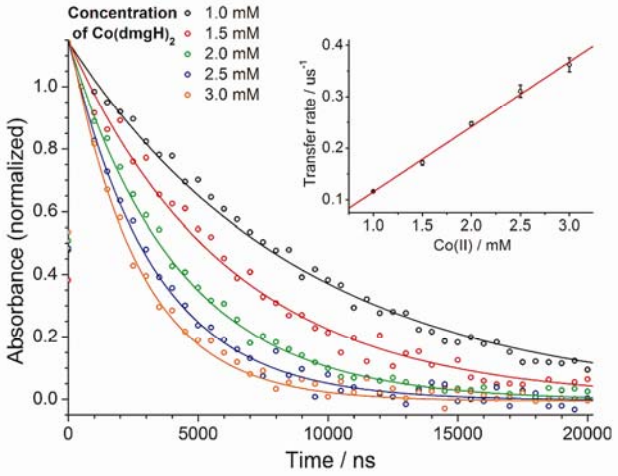

Figure 3. Transient kinetic traces for $\mathbf{1}^-$ (integrated absorbance of CO and NCS bands) in the presence of different concentrations of [Co(dmgH)$_2$] after excitation with λ = 355 nm. Inset: Time constants of the decay of $\mathbf{1}^-$ as a function of the concentration of [Co(dmgH)$_2$]. Linear fitting gives the rate for the forward electron-transfer reaction ($\mathbf{1}^-$ + [Co^{II}(dmgH)$_2$] → **1** + [Co^{I}(dmgH)$_2$]$^-$).[38]

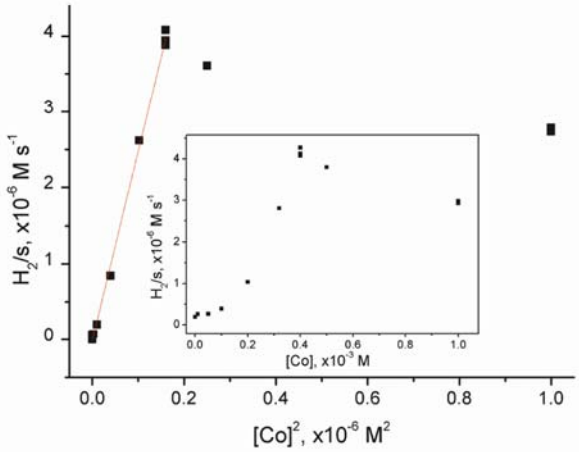

Figure 4. Initial H_2 production rates as a function of [Co]^2. Inset: Initial H_2 production rates as a function of [Co]; 0.5 mM **1**, varying {[Co(OH$_2$)$_6$](BF$_4$)$_2$, 6 dmgH$_2$}, 1 M TEOA, 0.1 M HBF$_4$, DMF, Ar, 476 nm.

that prevent back electron transfer from $\mathbf{1}^-$. In addition, they donate a second electron[28−31,33,35,36] to **1** with a yield of ~70%, rationalizing the kinetic trace depicted in Figure 2. An upper limit of ~40 μM for $\mathbf{1}^-$ and, therefore, for (HOCH$_2$C$^{\bullet}$H)N(CH$_2$CH$_2$OH)$_2$ and/or (HOC$^{\bullet}$HCH$_2$)-N(CH$_2$CH$_2$OH)$_2$ after reductive quenching was calculated from the spectral overlap of **1** and the laser pulse (355 nm and 2 mJ). Thus, after transfer of the second electron, the concentration of $\mathbf{1}^-$ is ~70 μM. Because of the large excess of **1**, its concentration can be considered to be constant. The resulting pseudo-first-order kinetics for transfer of the second electron gives a rate constant of $k_{2e^-} = 3.3 \times 10^8$ M^{-1} s^{-1}. The yield of less than 100% might result from other deactivation pathways such as recombination or disproportionation, which radicals typically undergo.

In order to quantify the electron-transfer rates in this new system, we kept all components constant (1 mM **1**, 1 M TEOA, and 0.1 M HBF$_4$) but varied Co^{II} from 1.0 to 3.0 mM in 0.5 mM steps. [Co(OH$_2$)$_6$](BF$_4$)$_2$ was dissolved with a 6-fold excess of dmgH$_2$ to ensure the complete formation of [Co^{II}(dmgH)$_2$]. Transient kinetic traces of $\mathbf{1}^-$ are shown in Figure 3. $\mathbf{1}^-$ transfers its electron to [Co^{II}(dmgH)$_2$], thereby generating a Co^{I} species. Because of a large excess, the Co^{II} concentration remains almost constant, which results in pseudo-first-order kinetics for the decay of $\mathbf{1}^-$. An exponential fit gave the following lifetimes with increasing concentrations of Co^{II}: 8.9, 6.1, 4.2, 3.3, and 2.7 μs. The corresponding rates depend linearly on the Co^{II} concentration, thus giving $k_1 = 1.3 \times 10^8$ M^{-1} s^{-1} for the electron-transfer step (Figure 3). This rate is in good agreement with a similar report in the literature[2] and compares well with electron transfer between [ReBr(CO)$_3$bipy]$^-$ and [Co^{II}(dmgH$_2$)] ($k_{1,Br} = 2.5 \times 10^8$ M^{-1} s^{-1}).[8] From Table 1 and E(Co$^{II/I}$) = −1.040 V, the corresponding backward electron-transfer rate is estimated as $k_{-1} \approx 4.1 \times 10^5$ M^{-1} s^{-1} ($\Delta_R G$ = −14.3 kJ mol^{-1}) and $k_{-1,Br} \approx 1.1 \times 10^5$ M^{-1} s^{-1} ($\Delta_R G$ = −19.1 kJ mol^{-1}) for **1** and [ReBr(CO)$_3$bipy], respectively, as was expected for an electron transfer in the normal region according to the Marcus theory. As found for similar systems (PS = ruthenium, platinum, or iridium complex; WRC = cobalt or rhodium complex),[6,9,37] quenching of ***1** by cobalt occurs at a rate close to diffusion control (see SI 8 in the Supporting Information; $k_d = 5 \times 10^9$ M^{-1} s^{-1} in 1 M TEOA, DMF).[8,36] Because $k_{q,TEOA} = 9.2 \times 10^7$ M^{-1} s^{-1} and [TEOA] = 1 M in all of our experiments, negligible contribution from quenching by cobalt is expected.

Cobalt Dependence. By systematically varying the cobalt concentrations, we showed that H_2 evolution in the original [ReBr(bipy)(CO)$_3$]/acetic acid system occurred along a second-order process in cobalt with k_{obs} = 4 M^{-1} s^{-1}.[8] In the new and improved system, a linear fitting of dH_2/dt vs [Co]$_{tot}$ gave k_{obs} = 25 M^{-1} s^{-1} (Figure 4).

The second-order process was rationalized by a bimolecular reaction of two cobalt hydrides as the rate-limiting elementary step (eqs 1−3), as postulated elsewhere.[39,40] Assuming a fast preequilibrium for eq 2 and with substitution of [Co^{I}] for c[Co]$_{tot}$, where c is the fraction of Co^{I} with respect to [Co]$_{tot}$, eq 4 describes the relationship

(35) Kutal, C.; Corbin, A. J.; Ferraudi, G. *Organometallics* **1987**, *6*, 553–557.

(36) Kutal, C.; Weber, M. A.; Ferraudi, G.; Geiger, D. *Organometallics* **1985**, *4*, 2161–2166.

(37) Krishnan, C. V.; Brunschwig, B. S.; Creutz, C.; Sutin, N. *J. Am. Chem. Soc.* **1985**, *107*, 2005–2015.

(38) It should be noted that the treatment of the transients as simple exponential decays ignores a possible influence of the second electron being transferred from the oxidized form of TEOA. In fact, this contribution is detectable for small concentrations of Co^{II} (i.e., < 1 mM), while it is negligible for larger ones, as is obvious from Figure 3. It is therefore reasonable to consider also a direct electron transfer from (HOCH$_2$C$^{\bullet}$H)-N(CH$_2$CH$_2$OH)$_2$ and/or (HOC$^{\bullet}$HCH$_2$)N(CH$_2$CH$_2$OH)$_2$ to [Co^{II}(dmgH)$_2$] in addition to the transfer to **1**. The former route becomes dominant for higher concentrations of [Co^{II}(dmgH)$_2$]. The direct transfer does not alter the kinetic trace of $\mathbf{1}^-$, provided that [Co^{II}] remains approximately constant.

(39) Dempsey, J. L.; Winkler, J. R.; Gray, H. B. *J. Am. Chem. Soc.* **2010**, *132*, 1060–1065.

(40) Hu, X.; Brunschwig, B. S.; Peters, J. C. *J. Am. Chem. Soc.* **2007**, *129*, 8988–8998.

Scheme 3. Schematic Representation of the Proposed Reaction Cycles to H_2

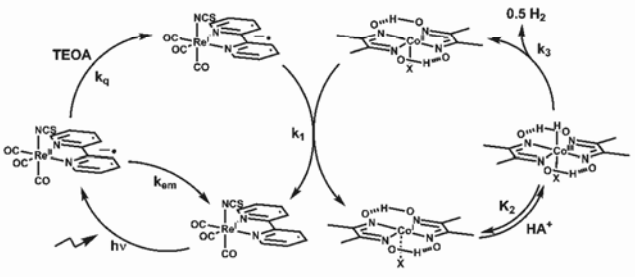

between the rate of H_2 formation and the total cobalt concentration.

$$Co^{II} + \mathbf{1}^- \rightarrow Co^{I} \quad (k_1) \tag{1}$$

$$Co^{I} + HA^+ \rightarrow Co^{III}\text{-}H + A \quad (K_2) \tag{2}$$

$$2Co^{III}\text{-}H \rightarrow 2Co^{II} + H_2 \quad (k_3) \tag{3}$$

$$\frac{dH_2}{dt} = k_3 K_2{}^2 \left(\frac{[HA^+]}{[A]}\right)^2 c^2 [Co]_{tot}{}^2 = k_{obs}[Co]_{tot}{}^2 \tag{4}$$

A systematic variation of $[HA^+]/[A]$ would allow one to identify $k_3K_2{}^2c^2$. This experiment is hardly possible with acetic acid because it is not clear if AcOH or internally generated $[HTEOA]^+$ did serve as the proton source. In the present study, $[HA^+]/[A]$ was fixed at 0.11 and $k_3K_2{}^2c^2$ thus equals 2025 M^{-1} s^{-1}.

We observed a very poor long-term performance when cobalt became rate-limiting ([Co] < 0.4 mM). When the reaction was run to completion under these conditions (H_2 evolution ceased), a black precipitate formed, the solution became colorless, and **1** could no longer be detected by HPLC. When cobalt becomes rate-limiting, complex $\mathbf{1}^-$, a strong reductant (−1.185 V vs Ag/AgCl) with a lifetime well above 10 ms as determined by transient IR spectroscopy in DMF/TEOA solutions, accumulates in the solution (Scheme 3). While being sufficiently long-lived to react with Co^{II} (≈16 μs for $[Co^{II}]$ = 0.5 mM with $k_1 = 1.3 \times 10^8$ M^{-1} s^{-1}), this radical has a chemistry of its own. In the complete absence of cobalt but with $[HTEOA]^+$, 3−5 equiv of H_2 and a black precipitate were observed (end $TON_{Re} = 4 \pm 1$), revealing a competitive, destructive pathway ending the catalytic cycle.

Acid Dependence. Replacement of acetic acid by $[HTEOA][BF_4]$ substantially improved the long-term performance. There are several reasons why acetic acid affects H_2 production, namely, its interaction with the PS (see before), but also its high pK_a in DMF ($pK_{a,AcOH}$ = 13−14; $pK_{a,TEOA}$ = 7.5; both in DMF),[23] making it a less likely proton source in eq 2. To quantify the role of $[HTEOA][BF_4]$, its concentration was varied systematically from 0 to 0.2 M, while all other parameters were kept constant (Figure 5). A distinct dependence was found for the initial TOFs, reaching a plateau at $[HBF_4] \geq 0.1$ M,

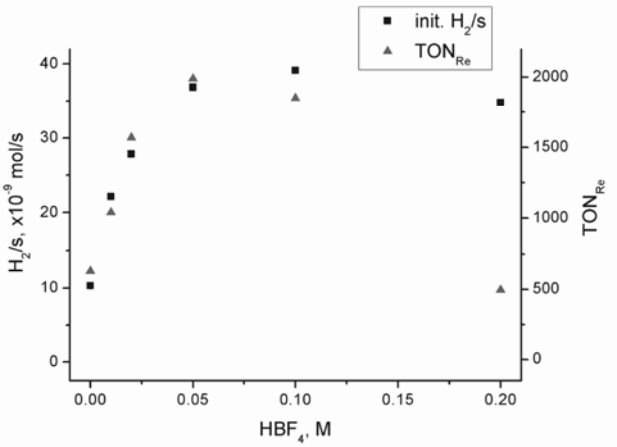

Figure 5. Left scale: initial H_2 production rates. Right scale: total TON_{Re} as a function of $[HBF_4]$ (0.5 mM **1**, 0.5 mM $[Co(OH_2)_6](BF_4)_2$, 3 mM $dmgH_2$, 1 M TEOA, DMF, Ar, 476 nm).

Table 2. HPLC Analysis of Free $dmgH_2$ and **1** during Catalysis (See Also SI 2 in the Supporting Information)[a]

irradiation time, h	$dmgH_2$, %	**1**, %	TOF_{Re}, H/Re/h	TON_{Re}, H/Re
0	100	100	56	0
16	80	100	32	670
55	0	80	10	1380
120	0	0	0	1850

[a] 1 M TEOA, 0.1 M HBF_4, 0.5 mM **1**, 0.5 mM {$[Co(OH_2)_6](BF_4)_2$, 6 $dmgH_2$}, DMF, Ar, 476 nm.

indicating rate-limiting protonation of $[Co^I]$ (eq 2) for $[HBF_4] \leq 0.1$ M. Slow H_2 formation was observed even in the absence of acid. Obviously, HBF_4 is not the sole proton source because the photocatalytic oxidation of TEOA generates two protons, compensating for the formal H^+ loss by H_2 formation (see Scheme 2).[30,41] In fact, for most experiments, more H_2 was produced than protons added in the form of HBF_4, thus underscoring the importance of proton release upon decomposition of $TEOA^{\bullet+}$ (Scheme 2, right side).

Besides the acid-dependent TOFs, the acid concentration had a marked influence on the final TON_{Re}. At $[HBF_4]$ = 0.2 M, the initial TOF (TOF_{ini}) compares well with the fastest one at 0.1 M, but the final TON_{Re} was only ≈25% of the maximum TON at 50 mM HBF_4 (2000 H/Re). At low $[HBF_4]$, the final TON_{Re} correlated well with TOF_{ini}. Analyzing the solutions after H_2 formation ceased, we found that $dmgH_2$ and **1** disappeared. A continuous analysis of the reaction with 0.1 M HBF_4 first revealed the disappearance of $dmgH_2$, followed by subsequent decomposition of **1** (Table 2).

The time-dependent concentrations, as shown in Table 2, imply a slow decomposition of the cobalt catalyst as the primary reason for the decay of the TOF over time. This deactivation pathway occurs slowly and is indirectly evidenced by the consumption of free $dmgH_2$. The fact that H_2 production ceased quite abruptly after 120 h is also in support of this interpretation (see SI 2 in the Supporting Information). To corroborate this hypothesis, we quantified the TON as a function of the $dmgH_2$ concentration (see SI 3 in the Supporting Information).

(41) Sun, H.; Hoffman, M. Z. *J. Phys. Chem.* **1994**, *98*, 11719–11726.

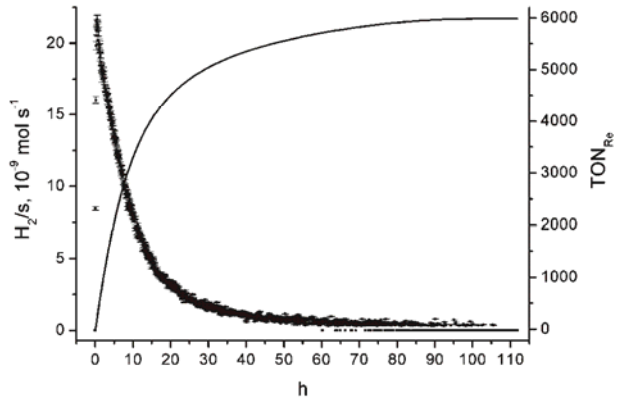

Figure 6. H_2 production rate (left scale, ■) and TON_{Re} (right scale, black line) as a function of time (30 μM **1**, 0.5 mM $[Co(OH_2)_6](BF_4)_2$, 3 mM $dmgH_2$, 1 M TEOA, 20 mM HBF_4, DMF, Ar, 380 nm).

The addition of more than 4−6 equiv of $dmgH_2$ did not significantly change the rate of H_2 formation. However, TON_{Re} increased steadily with increasing [$dmgH_2$], supporting $dmgH_2$ consumption to be the TON-limiting process. It was postulated before that [Co^{III}-H], in a slow reaction, undergoes intramolecular hydride shift to the coordinated oxime moiety of dmgH to give a hydroxylamine derivative.[42]

Long-Term Performance. Long-term stability with the new system is among the best reported so far (TON_{Re} up to 2000), but catalysis still slowed down over time. In these long-term experiments, a substantial part of TEOA was sacrificed (up to 50% for 2 electrons per TEOA). According to our analyses, decomposition of [$Co(dmgH)_2$] dominates the rate decrease and long-term stability. Depletion of TEOA, as a substrate in the process, contributes to the activity loss but not to the long-term performance because the addition of TEOA up to the original concentration at a late time point did not increase TOF or final TONs. Consequently, when the concentration of **1** was decreased to 30 μM and upon irradiation with a 380 nm high-flux LED, TON_{Re}'s up to 6000 were observed (Figure 6 and SI 4 in the Supporting Information) while less than 10% TEOA (for 2 electrons) was consumed. These high TON_{Re}'s can only be achieved if decomposition of **1** is not limiting. The fact that TON_{Co} (H_2 per cobalt) never exceeded ~1000 (~200 per $dmgH_2$) was a further strong indication for decomposition of [$Co(dmgH)_2$] to be the responsible factor for performance limitation.

Dependence on Photon Flux, Quantum Yield, and Colloids. The rates of H_2 formation depended linearly on the photon flux as determined by actinometry (see SI 5 in the Supporting Information). Quantification of the quantum yields should be addressed with care because of two systematic uncertainties, namely, the second electron released upon oxidation of TEOA and absorption of the reduced cobalt catalyst. The former uncertainty potentially gives an upper limit of $\Phi_{H/h\nu} = 200\%$, whereas the latter alters the observed $\Phi_{H/h\nu}$ as a function of the wavelength and can only be eliminated if the concentration and extinction of the reduced cobalt catalyst are known. The observed quantum yield for a standard experiment (0.5 mM **1**, 0.5 mM $[Co(OH_2)_6](BF_4)_2$, 3 mM $dmgH_2$, 1 M TEOA, 0.1 M HBF_4, DMF, Ar, 380 nm) was found to be $\Phi_{H/h\nu,380nm} \approx 90\%$ (observed H/absorbed photon), as compared to $\Phi_{H/h\nu,380nm} \approx 40\%$ (observed H/absorbed photon) for the original [$ReBr(CO)_3bipy$]/acetic acid system (0.5 mM [$ReBr(CO)_3bipy$], 1 mM $[Co(ac)_2(H_2O)_4]$, 6 mM $dmgH_2$, 1 M TEOA, 0.1 M AcOH, DMF, Ar, 380 nm). We previously reported an observed quantum yield of 26%, which was obtained in a different setup at 415 nm, thus at different optical densities in cobalt.[8] If the yield of the second electron released by $(HOCH_2C^{\bullet}H)N(CH_2CH_2OH)_2$ and/or $(HOC^{\bullet}HCH_2)N(CH_2CH_2OH)_2$ (see the section Electron-Transfer Steps) is taken into account, the quantum yield reduces to 90%/1.7 ≈ 50%.

To exclude colloids as catalytically active species, as established for similar systems with noble metal WRC catalysts,[11−14,43] it was of special interest to assess a homogeneous reaction in the present system. Evidence for homogeneous H_2 formation with [$Co(dmgH)_2$] was already received from light scattering,[8] from mercury poisoning experiments,[6] and, indirectly, from electrochemical studies.[40,44] The squared dependence of H_2 formation in $[Co]_{tot}$ as reported herein is not expected for a heterogeneous system. Because Hg^0 is known to poison colloidal catalysts, qualitative poisoning studies as reported in the literature for other systems were performed.[9,45,46] If a colloidal species would be the source of H_2 formation, the addition of elemental mercury would affect the long-term performance. In a test experiment, two solutions (0.5 mM **1**, 0.5 mM $[Co(OH_2)_6](BF_4)_2$, 3 mM $dmgH_2$, 1 M TEOA, 0.1 M HBF_4, DMF, Ar, 476 nm) were irradiated for 13.5 h with or without Hg^0 (200 μL and 2500 equiv relative to rhenium and cobalt, respsectively). Mercury was then removed and the experiment continued (see SI 6 in the Supporting Information). The shapes of the curves $[H_2]$/s vs time were identical, with or without mercury, being in agreement with a homogeneous process.[47]

Conclusion

Photocatalytic systems for H_2 formation based on [$ReX(bipy)(CO)_3$] as the PS and [$Co(dmgH)_2$] as the H_2 evolution reaction catalyst are alternatives to the widely studied ruthenium systems. Identifying the deactivation pathways in such a system is key for the development of long-term stable systems. The loss of the axial Br^- ligand in the PS is one of these pathways. Exchanging Br^- with $[NCS]^-$

(42) Simandi, L. I.; Szeverenyi, Z.; Budozahonyi, E. *Inorg. Nucl. Chem. Lett.* **1975**, *11*, 773–777.

(43) Du, P.; Schneider, J.; Fan, L.; Zhao, W.; Patel, U.; Castellano, F. N.; Eisenberg, R. *J. Am. Chem. Soc.* **2008**, *130*, 5056–.

(44) Razavet, M.; Artero, V.; Fontecave, M. *Inorg. Chem.* **2005**, *44*, 4786–4795.

(45) Paklepa, P.; Woroniecki, J.; Wrona, P. K. *J. Electroanal. Chem.* **2001**, *498*, 181–191.

(46) Anton, D. R.; Crabtree, R. H. *Organometallics* **1983**, *2*, 855–859.

(47) Because our reaction flasks were irradiated with an LED from below, effective photon flux in the mercury experiment was lower than that without mercury (reflected in the lower TOF but identical shape of the curve in SI 6 in the Supporting Information). If mercury would poison our catalysts, one would par contra expect that catalysis would not take place at all or come to a stop shortly after the start. To further confirm the hypothesis about the reduced photon flux, mercury was removed after 13.5 h and the experiment continued. H_2 production now indeed proceeds at rates identical with those in an experiment in which no mercury was added in the first place.

and replacing AcOH by $[HTEOA]^+$ with noncoordinating $[BF_4]^-$ as the counterion increased the efficiency considerably in terms of both the quantum yield and final TON, thus underlining the crucial importance of X^-. With the new and very stable PS [Re(NCS)(bipy)$(CO)_3$], the stability of [Co$(dmgH)_2$] became performance-limiting, most likely because of an intramolecular hydride shift of [Co^{III}-H] to a coordinated oxime moiety. To further improve this system requires thus stabilization of the cobalt complex toward hydride shift or an increase in the rate of H_2 formation with respect to the hydride shift, while keeping further physicochemical parameters intact. Detailed studies about the decomposition pathways of the cobalt complex are underway.

Experimental Section

All chemicals were of reagent grade and were used without further purification. Spectroscopic-grade DMF, $Co(BF_4)_2 \cdot 6H_2O$, and coumarin I were purchased from Acros. Electrochemical-grade [TBA](PF_6), [TBA]Br, TEOA, $[Et_2OH](BF_4)$, $[Co(ac)_2(H_2O)_4]$, $dmgH_2$, phenanthroline, and ethanol were purchased from Fluka. Water was doubly distilled before use. Synthetic reactions were carried out under N_2 or Ar using standard Schlenk techniques. HBF_4 in the text refers to $[HTEOA](BF_4)$, synthesized from TEOA and $[Et_2OH](BF_4)$.[48] The syntheses of **1**, [ReBr$(CO)_3$bipy], [Re$(OH_2)(CO)_3$bipy](TflsO), [Co$(dmgH)_2$], and $K_3[Fe(ox)_3]$ have been described in the literature.[8,24]

Luminescence measurements were performed on a Perkin-Elmer LS50B fluorescence spectrometer with Ar-purged solution samples in 1 cm cells. Luminescence lifetime measurements were performed on an Edinburgh Instrument F900 equipped with an F900 ns flash lamp filled with H_2 (operating at 0.4 bar and a frequency of 40 kHz). Luminescence quantum yields were determined relative to coumarin I in ethanol (0.64)[49] according to a literature procedure.[50]

UV−vis spectra were measured using a Cary 50 spectrometer with solution samples in 1 cm quartz cells. If necessary, cells with silicon septa lids were used to keep samples under an inert-gas atmosphere during measurements.

IR spectra were recorded on a Bio-Rad FTS-45 spectrometer with samples in compressed KBr pellets.

Electrochemical measurements were carried out in DMF containing 0.1 M [TBA][PF_6] as the conducting electrolyte. A Metrohm 757VA Computrace electrochemical analyzer was used with a standard three-electrode setup of glassy carbon working (i.d. = 3 mm) and platinum auxiliary electrodes and an Ag/AgCl reference electrode. All potentials are given vs Ag/AgCl and are referenced with Fc/Fc^+ at +500 mV.

HPLC measurements were performed on a VWR LaChrome Elite using a Nucleodur C18 gravity column operated in an oven (L-2350) at 40 °C and a PDA detector (L-2450). The gradient was as follows: A = 0.1% TFA, 10% MeOH, and H_2O; D = MeOH; flow rate = 0.5 mL min^{-1}; 0−5 min, 100% A; 5−15 min, 0−100% D; 15−18 min, 100% D. Control runs before and after catalysis were systematically performed using 10 μL of the reaction solution in DMF. Under these conditions, $dmgH_2$ gave a broad peak at 6.4 min and **1** a defined peak at 17.04 min.

Gas chromatograms were recorded using a Varian CP-3800 gas chromatograph with Ar as the carrier gas and a 3 m × 2 mm packed molecular sieve 13X 80-100 column. The gas flow was set to 20 mL min^{-1}. The oven was operated isothermally at 100 °C. An Ar flow of usually 21.6 mL min^{-1} [adjusted with a manual flow controller (Porter, 100) and referenced with a flowmeter (MS Wil GmbH)] was passed through the reaction mixture and into the gas chromatograph, where 100 μL gas samples were automatically injected in defined time intervals (usually 5 min) using a 6-port−2-position valve from Vicci. The gases were detected using a thermal conductivity detector (Varian) operated at 150 °C. H_2 production rates were calibrated by introducing a known flow of pure H_2 by a single syringe pump (70-2208 from Harvard Apparatus, using a 2.5 mL Hamilton GASTIGHT #1002 syringe and a Teflon tube) to the 60 mL Schlenk containing 1 M TEOA in DMF. Plotting of the peak area for H_2 versus the used flow rates of H_2 gave linear fits. The slopes of these fits depended linearly on the Ar flow through the solution. Varying the Ar flow thus allowed the detection of smaller H_2 production rates, although at a higher response time (10 min for 21.6 mL min^{-1}).

Photochemical measurements were carried out in a 60 mL septum-capped Schlenk tube containing a Teflon stirrer at 500 rpm. A total of 10 mL of a solution containing the respective mixture in DMF was prepared, wrapped in black foil, and degassed using an Ar-purged Schlenk line. The mixture was equilibrated under 1.5 bar of Ar pressure for 15 min and then transferred to a dark room for illumination. The light source was either a 380 or 476 nm high-flux LED from Rhopoint Components Ltd. (OTLH-0280-UV or OTLH-0010-BU, respectively; CPC reflector for Shark LED; irradiated directly from below; current control at usually 200 mA; $hv/s = 1.75 \times 10^{-7}$ and 2×10^{-7} mol s^{-1}, respectively). If necessary, the radiant flux was varied by adjustment of the current through the LED. The radiant flux at different currents was calibrated using actinometry. A constant flow of usually 21.6 mL min^{-1} of Ar was passed through the solution and into a six-port valve at the gas chromatograph, where 100 μL gas samples were injected into the gas chromatography/thermal conductivity detector (GC/TCD) gas analyzer in defined intervals. Integration of the production rate versus time gave the total amount of H_2 produced.

Quantum yields were determined in a 1 cm quartz cell using a 380 nm LED (OTLH-0280-UV, Rhopoint Components Ltd.) in series with an iris and a lens to ensure linear photon flux. The cells were filled with 2 mL solutions as follows: 0.5 mM **1** ($1 - T = 0.957 \pm 0.0033$) and [ReBr$(CO)_3$bipy] ($1 - T = 0.971 \pm 0.0028$), 0.5 mM {$[Co(OH_2)_6](BF_4)_2$, 6 $dmgH_2$} and 1 mM {$Co(ac)_2(H_2O)_4$], 6 $dmgH_2$}, 1 M TEOA, and 0.1 M HBF_4 for AcOH, DMF, and Ar, respectively. The total H_2 was determined by manual sampling of 20 μL of head-space gas through a septum and subsequent injection into a GC/TCD system as described above. The photon flux as determined by actinometry was $4.81 \pm 0.13 \times 10^{-9}$ mol s^{-1}. It was corrected for the respective fractions of light absorbed. The H_2 production rates measured were $(2.18 \pm 0.082) \times 10^{-9}$ and $(1.01 \pm 0.069) \times 10^{-9}$ mol s^{-1} for **1** and [ReBr$(CO)_3$bipy], respectively.

Actinometry for the quantum yield determination was performed in a 1 cm quartz cell containing 2 mL of 9 mM $K_3[Fe(ox)_3]$ in 0.1 N H_2SO_4 as the chemical actinometer and was irradiated as described in quantum yields ($1 - T$ for $K_3[Fe(ox)_3] > 0.999$). For calibration of the photon flux in the standard setup, a setup identical with that for H_2 production (LED from below, varying current, 60 mL Schlenk, stirred, Ar flow of 21.6 mL min^{-1}) was used with 10 mL of a 9 mM $K_3[Fe(ox)_3]$ in 0.1 N H_2SO_4 as the chemical actinometer. Analysis of irradiated solutions: after a certain time at a certain LED current, 100 μL of the irradiated solution was added to 100 μL of a 5 mM solution of phenanthroline in H_2O, agitated, and left in the dark for 30 min. After this, 50 μL of a 600 mM NaOAc/360 mN H_2SO_4 buffer and 750 μL

(48) Ono, H.; Seki, R.; Ikeda, R.; Ishida, H. *J. Mol. Struct.* **1995**, *345*, 235–243.
(49) Olmsted, J. *J. Phys. Chem.* **1979**, *83*, 2581–2584.
(50) Williams, A. T. R.; Winfield, S. A.; Miller, J. N. *Analyst* **1983**, *108*, 1067–1071.

of H_2O were added and absorption at 511 nm was determined relative to a solution that was not irradiated. Conversion to photon flux as a function of the LED current was achieved by using $\varepsilon_{[Fe^{II}(phen)_3],511nm} = 10750 \pm 76\ M^{-1}\ cm^{-1}$ and $\eta_{Fe^{III} \rightarrow Fe^{II}} = 1.18$ and 0.925 for 380 and 476 nm, respectively.[51]

Time Resolved Step-Scan FTIR Spectroscopy. The kinetics of the electron transfer from reductively quenched $\mathbf{1}^-$ to cobalt were measured through time-resolved step-scan IR spectroscopy. The system consists of a FT-IR spectrometer (Bruker Vertex 80 V) equipped with a PV mercury−cadmium−telluride detector and a frequency-tripled Nd:YAG laser generating pulses of ~2 mJ per < 10 ns at 355 nm with a repetition rate of 10 Hz used for sample excitation. The nominal time resolution that is reached with this setup is about 100 ns. The sample was continuously pumped through a 200 μm cell with 19.5 mL min^{-1}, giving an exchange rate for the probe volume of 14.5 s^{-1} in our case. A small sealed reservoir ($V \approx 3$ mL) was included between the peristaltic pump and the sample cell to minimize pulsation inside the latter. To avoid any interference of the pumping system with the aggressive sample mixture, a calcium fluoride sample cell with Teflon tubing was used. For sealings and the peristaltic pump tubing, chemically resistant perfluoroelastomers (ChemSure) were chosen. The samples were prepared by mixing all components except for $[Co(OH_2)_6](BF_4)_2$ in the form of standardized solutions in DMF, followed by filtration through a Teflon syringe filter (0.2 μm pore size). The solution was then purged for 30 min, after which $Co(BF_4)_2$ was added as a degassed solution in DMF. The measurements were started after an additional 30 min of purging, while the sample was already pumped through the flow cell. After the measurements, all samples were checked via static IR spectroscopy, entirely showing negligibly small degradation caused by irradiation at 355 nm.

(51) Hatchard, C. G.; Parker, C. A. *Proc. R. Soc. London A* **1956**, *235*, 518–536.

Acknowledgment. We are grateful to the Swiss National Science Foundation for financially supporting this work (Grant 200021-119798).

Supporting Information Available: H_2 formation as a function of the bromide concentration, in a typical experiment, as a function of the [Co]/[$dmgH_2$] ratio, at low [**1**], and as a function of photon flux, with added mercury and quenching rates of ***1** by different cobalt complexes. This material is available free of charge via the Internet at http://pubs.acs.org.

Supporting Information for

A highly stable rhenium - cobalt system for photocatalytic H_2 production: Unraveling the performance limiting steps.

Benjamin Probst[#], Alexander Rodenberg[§], Miguel Guttentag[#], Peter Hamm*[§] and Roger Alberto*[#]

[#] *Institute of Inorganic Chemistry, University of Zürich, Winterthurerstrasse 190, CH-8057 Zürich Switzerland*

[§] *Institute of Physical Chemistry, University of Zürich, Winterthurerstrasse 190, CH-8057 Zürich Switzerland.*

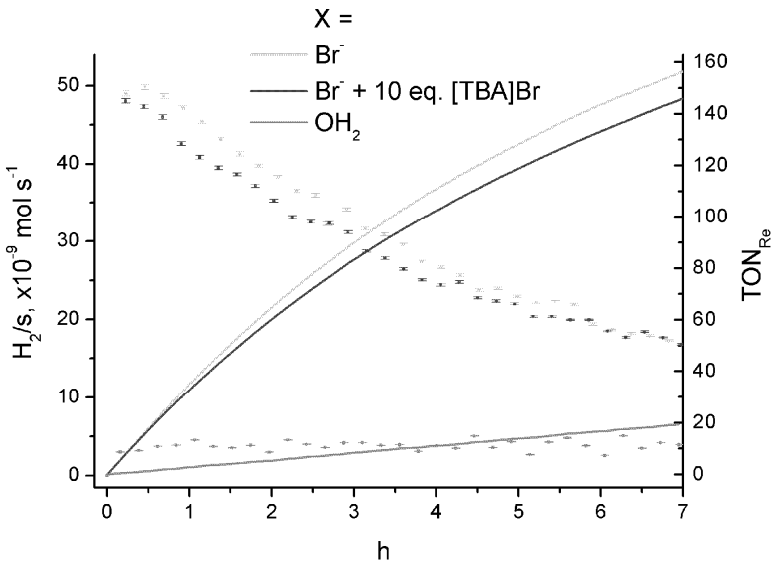

SI 1. Hydrogen production rate (left scale, ■) and TON_{Re} (right scale, line) as a function of time (0.5 mM $[ReX(CO)_3bipy]$, 1 mM $[Co(OH_2)_6](BF_4)_2$, 6 mM $dmgH_2$, 1 M TEOA, 0.1 M AcOH, DMF, Ar, 400 nm cut off, slide projector).

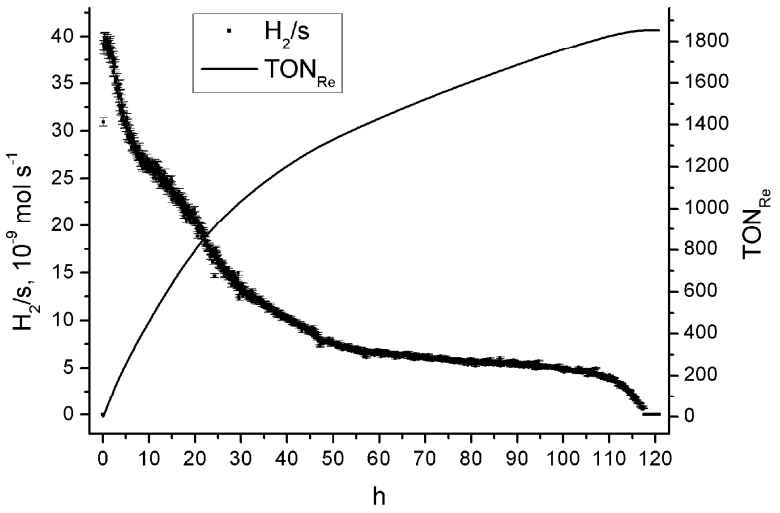

SI 2. Hydrogen production rate (left scale, ■) and TON_{Re} (right scale, black line) as a function of time (0.5 mM [Re(NCS)$(CO)_3$bipy], 0.5 mM [$Co(OH_2)_6$]$(BF_4)_2$, 3 mM $dmgH_2$, 1 M TEOA, 0.1 M HBF_4, DMF, Ar, 476 nm).

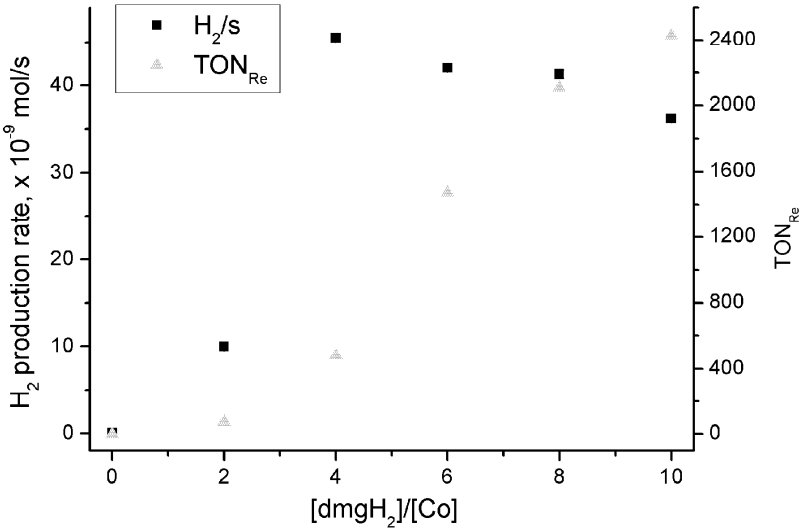

SI 3: Left scale: initial H_2 production rates – right scale: total TON_{Re} as a function of [$dmgH_2$] (0.5 mM [$Re(NCS)(CO)_3bipy$], 0.5 mM [$Co(OH_2)_6](BF_4)_2$, varying $dmgH_2$, 1 M TEOA, 0.1 M [HBF_4], DMF, Ar, 471 nm).

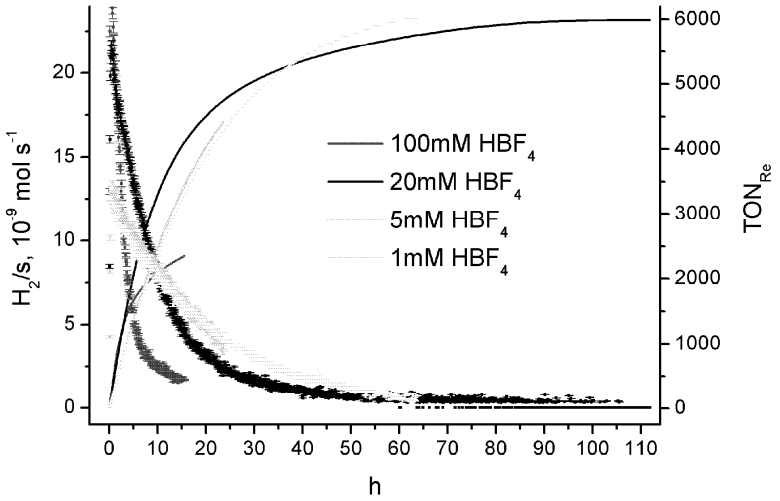

SI 4. Hydrogen production rate (left scale, ■) and TON_{Re} (right scale, black line) as a function of time (30 μM $[Re(NCS)(CO)_3bipy]$, 0.5 mM $[Co(OH_2)_6](BF_4)_2$, 3 mM $dmgH_2$, 1 M TEOA, varying HBF_4, DMF, Ar, 380 nm).

Equation	y = a * x			
		Value	Standard Error	Adj. R-Square
[ReBr(CO)3bipy]	Slope	2.37295E-10	7.33356E-13	0.99964
[Re(NCS)(CO)3bipy	Slope	3.59517E-10	1.27897E-12	0.99911
[Re(OH2)(CO)3bipy]	Slope	2.78217E-10	4.38722E-13	0.99999

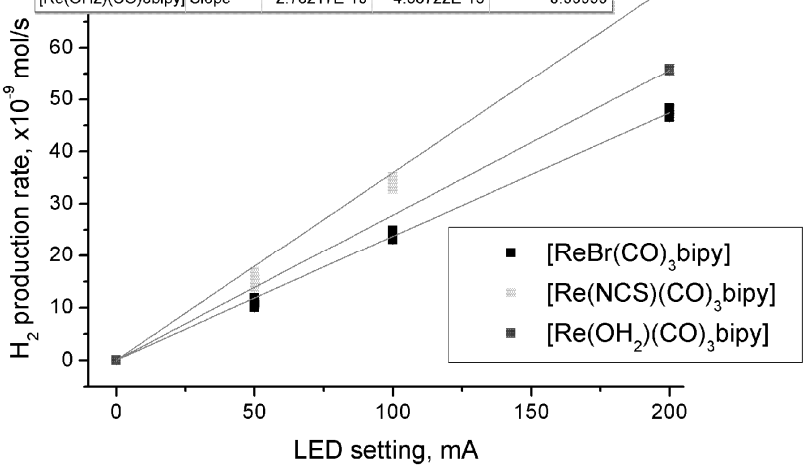

SI 5. Dependence of H_2/s on LED current (in mA), linearization serves as an indicator for the relative performance (0.5 mM [ReX(CO)$_3$bipy], 1 mM [Co(OH$_2$)$_6$](BF$_4$)$_2$, 6 mM dmgH$_2$, 1 M TEOA, 0.1 M HBF$_4$, DMF, Ar, 380 nm).

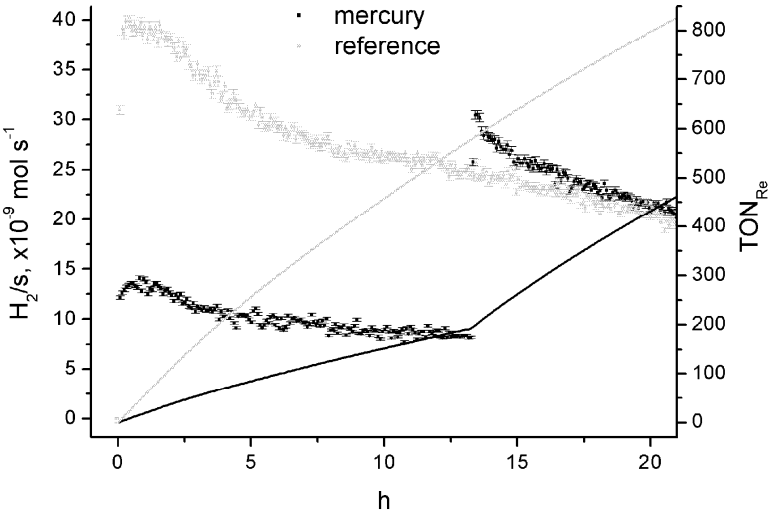

SI 6. Hydrogen production with 200 µl (black) and without (green) added mercury. Mercury was removed after 13.5 h. Left scale (■): hydrogen production rate, right scale (line): TON_{Re} (0.5 mM $[Re(NCS)(CO)_3bipy]$, 0.5 mM $[Co(OH_2)_6](BF_4)_2$, 3 mM $dmgH_2$, 1 M TEOA, 0.1 M HBF_4, DMF, Ar, 476 nm).

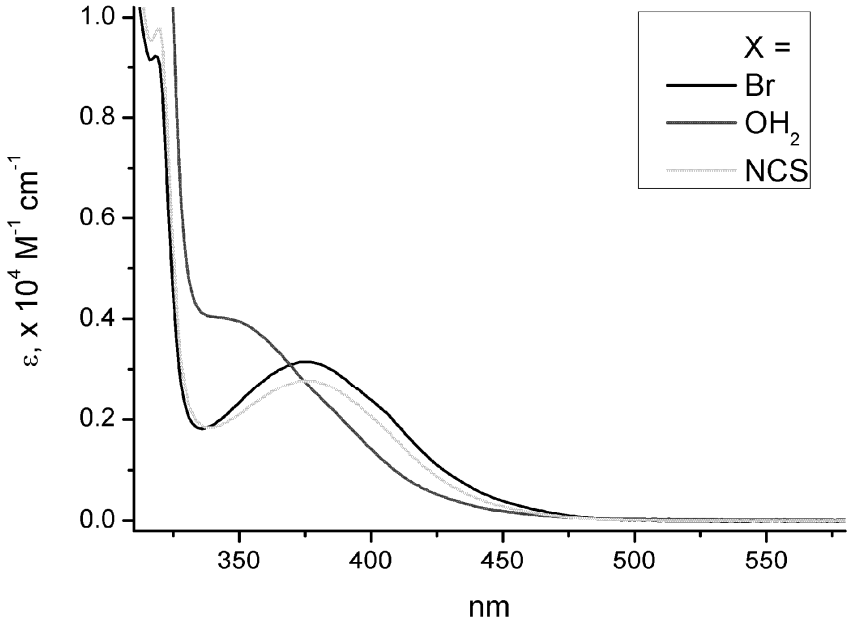

SI 7. Absorption spectra for [ReX(CO)$_3$bipy] in DMF.

SI 8. Quench rates obtained from Stern-Vollmer analysis of lifetimes of *__1__ in DMF vs [Co].

Quencher =	$k_{q,\ *\mathbf{1}}$ ($\times 10^9$ M^{-1} s^{-1})[a]	E (V vs Ag/AgCl)[b]
$[Co^{III}(py)_2(dmgH_2)](PF_6)$	2.86 ± 0.16	-0.24 (E_{pc}, $Co^{III/II}$)
$[Co^{III}Cl(py)(dmgH)_2]$	2.05 ± 0.04	-0.61 (E_{pc}, $Co^{III/II}$)
$[Co^{II}(dmgH)_2]$	1.23 ± 0.02	-1.04 ($Co^{II/I}$)

[a]: DMF, 1 mM **1**, 60 mM $dmgH_2$; [b]: 0.1 M [TBA](PF_6), DMF.

Photocatalytic H_2 Production from Water with Rhenium and Cobalt Complexes.

Benjamin Probst[#], Miguel Guttentag[#], Alexander Rodenberg[§], Peter Hamm[§], Roger Alberto*[#].*

Institutes of [#]Inorganic and [§]Physical Chemistry, University of Zürich, Winterthurerstrasse 190, CH-8057 Zürich Switzerland.

ariel@aci.uzh.ch

RECEIVED DATE (to be automatically inserted after your manuscript is accepted if required according to the journal that you are submitting your paper to)

ABSTRACT. Photocatalytic hydrogen production in pure water for three component systems using a series of rhenium based photosensitizers (PS) and cobalt based water reduction catalysts (WRC), with triethanolamine (TEOA) as irreversible electron donor, is described. Besides the feasibility of this reaction in water, key findings are reductive quenching of the excited state of the PS by TEOA (k_q = 5 – 8 × 10^7 $M^{-1}s^{-1}$; Φ_{cage} = 0.75) and subsequent transfer of an electron to the WRC ($k_{Co^{III}}$ = 1.1 × 10^9 $M^{-1}s^{-1}$). Turnover numbers in rhenium (TON_{Re}, H/Re) above 500 were obtained, whereas TON_{Co} (H_2/Co) did not exceed 17. It is shown that the cobalt based WRC limits long term performance. Long term performance critically depends on pH and the type of WRC used, but is unaffected by the type of PS or the concentration of WRC. A quantum yield of 30 % was obtained (H/photon). An inverse isotope effect is observed for one WRC.

KEYWORDS. Rhenium, Cobalt, Hydrogen, Photocatalysis, Isotope effect, Electron Transfer, Kinetics, Time resolved vibrational spectroscopy.

Introduction

The limited fossil and nuclear fuel reserves will make alternative energy resources crucial for the 21st century. Solar energy plays a key role and all modalities to harvest and convert light must be explored in great detail.[1] Classical PV cells convert sunlight into electrical energy which can be used for e.g. water splitting. An appealing alternative is direct, photocatalytic water splitting into H_2 and O_2, mimicking

photosynthesis. Conceptually, a photosensitizer (PS) harvests sunlight and water oxidation and reduction catalysts (WOC and WRC) complete the overall reaction. The system can be split into its reductive and oxidative parts and then be studied independently. Ideally, these processes run directly in water as a solvent.

Closed cycles for photochemical water splitting in homogeneous solution with visible light are not yet available. Since the 80's, detailed studies for the reductive half reaction have been presented with $[Ru(bipy)_3]^{2+}$, $[ReBr(CO)_3bipy]$, $[Ir(ppy)_2(bipy)]^+$, $[Pt(tpy)acetylide]^+$ or xanthine as PSs.[2-13] The WRC is often $[M(bipy)_3]^{3+}$ (M = Rh or Co), MV^{2+} in combination with colloidal Pt/Pd or cobalt macrocycles and e.g. TEOA or Eu^{2+} as sacrificial electron donors. These systems produced H_2 in organic or mixtures of organic solvents and H_2O. Some early kinetic and mechanistic studies by Sutin and coworkers with Ru/Co catalysts evidenced H_2 formation in homogeneous aqueous solution.[14,15] More recent work showed that increasing amounts of water in organic solvents rapidly decreased TON and TOF (turn over number and frequency) of H_2 formation.[3,6,16] No homogeneous system with rhenium in water has been reported so far. A limited number of photocatalytic oxidative half reactions in homogeneous, pure aqueous solution were described.[17-20]

The maximal TON (H_2 resp. O_2 per catalyst) reported in H_2 was 2500[2] and in O_2 350.[19] Whereas oxidative half reactions do run in H_2O, well defined water reducing systems have not been described so far. It stands to reason that a complete, homogeneous water splitting cycle must combine WOC and WRC and ultimately be performed in this solvent. We report herein on a homogeneous Re/Co-based system for photocatalytic water reduction in pure H_2O.

Results and Discussion

Eight photosensitizers, based on the *fac*-{$Re(CO)_3$} core (**1** – **8**, Scheme 1), for photophysical properties see Table 1) and nine cobalt based WRCs (**10** – **18**, Scheme 2) were investigated for photocatalytic hydrogen production in water. Irradiating 10 ml of an aqueous solution containing 30 μM **1**, **2**, **5** or **6**, 500 μM **10**, 1 M TEOA and 0.1 M HBF_4 produced ≈ 16 μmol H_2 (TON_{Re} ≈ 110, H/Re; TON_{Co} ≈ 3, H_2/Co), as depicted in Figure 1. No H_2 formation within our detection limits was observed in water for **4**, **7**, **8** or $[Ru(bipy)_3]^{2+}$ as PS or if no PS, WRC or TEOA was added. It is known that $[Ru(bipy)_3]^{2+}$ ($\tau \approx 900$ ns) does not interact with TEOA,[6,10] even though it does produce H_2 in a similar scheme using DMF as a solvent.[5,8] It is anticipated that oxidative quenching of excited $[Ru(bipy)_3]^{2+}$ by cobalt plays a major role in DMF but it remains to be elucidated why this does not happen in H_2O. Since H_2 production with **3** proceeded at very low rates, a direct comparison is not given here, but total amounts of H_2 formed were equal to the amounts as observed for **1**, **2**, **5** and **6**.[21] In the case of **7**, solubility issues in the buffer system used for catalysis prevented H_2 production experiments. Catalysis

for the two aquo complexes **4** and **8** is inhibited by deprotonation of coordinated H_2O in the ground (pK_a(**4**, H_2O) = 8.5) and in the excited state (see section Electron Transfer).

Scheme 1. Schematic drawings of photosensitizers **1** – **8**.

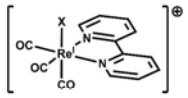

1: X = pyridine
2: X = benzyl isocyanide
3: X = 4-(dimethylamino)pyridine
4: X = OH_2

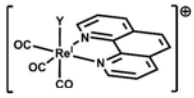

5: Y = pyridine
6: Y = benzyl isocyanide
7: Y = 4-(dimethylamino)pyridine
8: Y = OH_2

Time resolved vibrational spectroscopy was applied for complexes **1**, **4**, **5** and **8** in order to quantitatively study the initial reaction steps in the ps to μs domain (see section Electron Transfer).[22] Since these may be different from organic solvents, we focused on the initial set of reactions in rhenium. It is of fundamental interest to elucidate whether oxidative or reductive quenching of the excited state takes place and how fast it is (k_q).[23] It was of further interest to quantify the efficiency of the potential reductive quenching process and to observe electron transfer to Co^{III}.

Table 1. Photophysical properties of **1**–**8** in H_2O.

compd.	λ_{MLCT}, nm (ε, M^{-1} s^{-1})	λ_{phos}, nm ($\Phi \times 10^3$)	τ, ns
1	343 (3650)	567 (10)	200
2	337 (*sh*, 3800)	527 (90)	1'200
3	368 (2450)	602 (0.30)	13
4	339 (*sh*, 4000)[a]	585 (0.25)[a]	8.5[a]
5	362 (3350)	550 (40)	1'200
6	360 (*sh*, 2600)	515 (210)	12'800
7	368 (3000)	592 (1.0)	58
8	360 (*sh*, 3400)[a]	578 (1.0)[a]	28[a]

[a]: 1 mM TflsOH, H_2O.

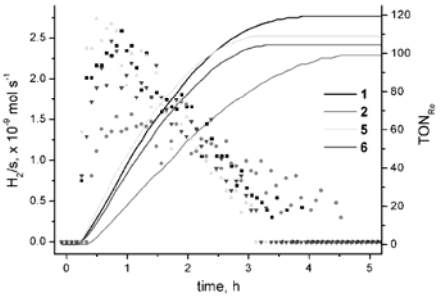

Figure 1. H_2 production of **1**, **2**, **5**, **6** (mol/s, left scale, dots; TON_{Re}, right scale, solid lines). Conditions: 30 μM PS, 500 μM **10**, 1 M TEOA, 0.1 M HBF_4, H_2O, 10 ml, 380 nm, $q_{n,p}$ = 1.75 x 10^{-7} einstein/s.

Electron Transfer. In DMF, photocatalytic H_2 production is initiated by reductive quenching of the excited PS.[8,24] To assess the mechanistic sequence in H_2O, we performed time resolved vibrational spectroscopy in the ps to μs time range in D_2O.[25] Upon excitation with a 400 nm laser pulse we see within the response time of our setup instantaneous formation of the ^{3}MLCT state ***1**, characterized by a blue shift in absorption (depopulation of **1** results in a bleach of $\nu_{CO,sym}$ at 2034 cm^{-1} and overlapping $2 \times \nu_{CO,asym}$ at 1932 cm^{-1} resp., whereas population of ***1** gives positive readings at 2070, 2016 and 1971 cm^{-1} for $\nu_{CO,sym}$ and $2 \times \nu_{CO,asym}$), its lifetime being 200 ns (Figure 2, yellow trace). In the presence of 1 M TEOA and 0.1 M HBF_4, we again see immediate formation of ***1**, followed by reductive quenching yielding $\mathbf{1}^-$ (characterized by a red shift of absorption, $\nu_{CO,sym}$ at 2012 and overlapping $2 \times \nu_{CO,asym}$ at 1895 cm^{-1}) (Figure 2, blue trace). An exponential fit yielded a time constant of 20 ns, thus, resulting in a bimolecular quench rate of about 5×10^7 M^{-1} s^{-1} (Table 2). The yield of reductive quenching, Φ_{red}, can be estimated by a comparison of the bleach of the ground state at the respective times directly after excitation and when quenching is completed (Table 2). An equivalent experiment was carried out for PS **5**. Since **1** and **5** are relatively long-lived, only minor contributions of radiative and non-radiative deactivation did occur on the timescale of reductive quenching, giving rough estimates for the cage escape yield (Φ_{cage}) of 0.75 for both complexes (Table 2).

Table 2. Kinetic parameters obtained from global fitting analysis of UV-pump-IR-probe experiments with **1** and **5** as PS in D_2O.

compd.	k_q, $\times 10^6$ $M^{-1}s^{-1}$	Φ_{red}	Φ_{cage}	$k_{Co^{III}}$, $\times 10^9$ $M^{-1}s^{-1}$
1[a]	51	0.70	0.75	1.1
5[a]	78	0.75	0.75	1.1

[a]: 0.25 mM PS, varying **[10]**, 1 M TEOA, 0.1 M HBF_4, D_2O, solution degassed with Ar, excitation by 400 nm laser pulse.

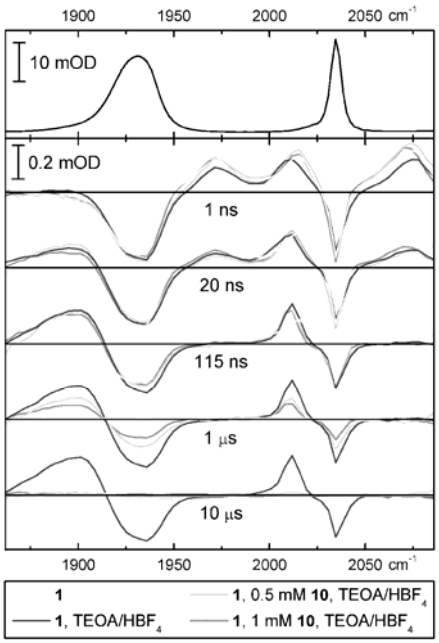

Figure 2. Top: FT-IR spectrum of the ground state of **1**, showing the characteristic $\nu_{CO,sym}$ at 2034 and overlapping $2 \times \nu_{CO,asym}$ at 1932 cm^{-1}, respectively. Below: Difference spectra after 400 nm excitation pulse at given delays, negative bands are due to depopulation of the ground state of **1**, positive bands are due to the population of new transient species: ***1** ($\nu_{CO,sym}$ at 2070 and $2 \times \nu_{CO,asym}$ at 2016 and 1971 cm^{-1}, resp.) and $\mathbf{1}^-$ ($\nu_{CO,sym}$ at 2012 and overlapping $2 \times \nu_{CO,asym}$ at 1895 cm^{-1}). Conditions: 0.25 mM **1**, varying **10**, except for yellow trace 1 M TEOA and 0.1 M HBF_4, solvent: D_2O. An animated image of a related experiment is available in the HTML version of this manuscript as Web Enhanced Object.

Although $\mathbf{1}^-$ decomposed in solution (see section long term performance), it was found to be stable on the timescale up to 40 µs (see Figure 2 and Figure 3, blue traces). In contrast to similar experiments in DMF no transfer of a second electron from $(HOCH_2C^{\bullet}H)N(CH_2CH_2OH)_2$ and/or $(HOC^{\bullet}HCH_2)N(CH_2CH_2OH)_2$ could be observed on this timescale.[24] In a solution containing **1**, 1 M TEOA, 0.1 M HBF_4 and **10** we again observed rapid formation of $\mathbf{1}^-$ and subsequent decay of $\mathbf{1}^-$ to **1** via electron transfer to **10** ($k_{1,10} = 1.1 \times 10^9$ $M^{-1}s^{-1}$, Figure 3). Hence, the catalytic cycle in water follows the same sequence as in DMF: reductive quenching of ***1** to $\mathbf{1}^-$ with subsequent electron transfer to cobalt.[8]

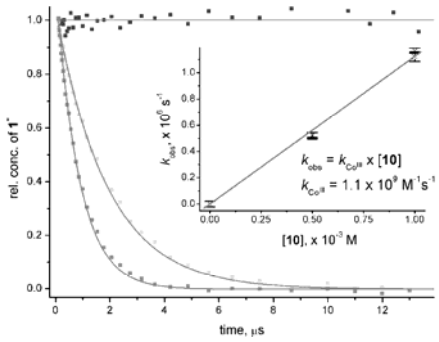

Figure 3. Relative concentration of $\mathbf{1}^-$ upon 400 nm excitation at ■ 0, ■ 0.5, ■ 1 mM **10** (0.25 mM **1**, 1 M TEOA, 0.1 M HBF_4, D_2O). Inset: Plot of k_{obs} vs. [**10**] according to a pseudo first order rate law.

In addition to elucidating the reaction mechanisms for the PSs **1** and **5** above, the question was tackled why catalytic systems employing the aquo complexes **4** and **8** do not produce any hydrogen. To resolve this issue UV-pump-IR-probe spectra were measured for **4** and **8** under identical reaction conditions as before for **1** and **5** (Figure 4). At pH 8.7 **4** is found as a mixture of its aquo ($\nu_{CO,sym}$ at 2034 and overlapping $2 \times \nu_{CO,asym}$ at 1927 cm^{-1}) and its deprotonated form, hydroxo-**4** ($\nu_{CO,sym}$ at 2016 and $2 \times \nu_{CO,asym}$ at 1909 and 1892 cm^{-1}, resp.). After excitation at 400 nm the excited state of hydroxo-**4** decays with a time constant of ~0.5 ns, therefore being too short lived for reductive quenching. In contrast, ***4** itself is longer lived and reacts as a photoacid, i.e. loses a proton (~5 ns) yielding positive absorptions at 1892, 1909 and 2016 cm^{-1}, which correspond to the ground state absorption of hydroxo-**4** as shown in (**Figure 4**). Afterwards equilibrium is restored with a time constant of ~70 ns, which is beyond the diffusion controlled ($k_{d,H2O} \sim 10^{10}$ $M^{-1}s^{-1}$), maximal possible electron transfer rate to **10**. This finding supports the assumption that ***4** and *8 react as photoacids while not being reductively quenched with TEOA and therefore not initiating the catalytic cycle for hydrogen generation.

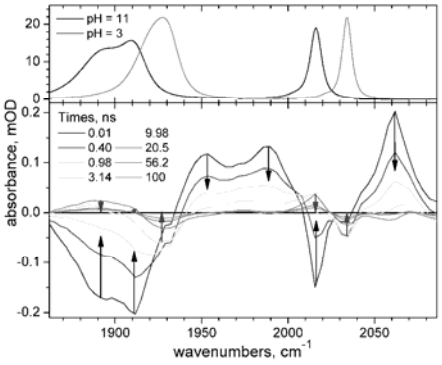

Figure 4. Top: FT-IR spectra of **4** at pH = 3 (aquo form, red line) and pH = 11 (hydroxo form, black line). Bands at 2034 and 1927 cm^{-1} belong to $\nu_{CO,sym}$ and $2 \times \nu_{CO,asym}$ of **4**, respectively, while the bands at 2016, 1909 and 1892 cm^{-1} are caused by the deprotonated form i.e. hydroxo-**4**. Bottom: Difference absorption spectra at indicated delays after 400 nm excitation of an aqueous solution containing 0.5 mM **4**, 0.5 mM **10**, 1 M TEOA, 0.1 M HBF_4, D_2O under Ar. Black arrows indicate the decay (~0.5 ns) of the excited state and bleach recovery of hydroxo-**4**, while the blue arrows point out protonation of hydroxo-**4** going along with simultaneous recovery of **4** (~70 ns).

Longterm Performance. Although good turnovers in Re were obtained ($TON_{Re} \geq 200$; H/Re), similar systems in DMF produced TON_{Re}'s up to 6'000.[24] Furthermore, TON_{Co}'s from **10** in water are very low (up to 7.5; H_2/Co) compared to the 1000 turnovers as obtained in DMF.[24] The first evidence concerning long term performance came from H_2 production with different PSs: TON_{Re}'s were constant for the four PS **1**, **2**, **5** and **6** (see Figure 1) indicating that decomposition of **10** rather than the PS is decisive. Varying the concentration of **10** but keeping all other parameters constant, TON_{Co}'s did not change (see SI 1), evidencing once more the cobalt WRC being the performance limiting factor. Addition of an excess of $dmgH_2$ relative to **10** increased TON_{Co} but did not change the rate of H_2 formation. Obviously, consumption of $dmgH_2$ limits the overall performance (increased TON_{Co}) while dissociation of $dmgH_2$ from **10** is not limiting in water (constant rate). Solutions of **10** in water are stable both in the dark and under irradiation with visible light. Only in 1 M TEOA / 0.1 M HBF_4 and after several days, partial replacement of one pyridine of **10** was observed. The decomposition pathway of the WRC, rationalizing the low TON_{Co}, is unknown so far. Decomposition has been observed before[7,24] and the reduction of coordinated dmgH to 2-aminobutan-3-one oxime was proposed,[26] rationalizing the observed [$dmgH_2$] dependence.

Scheme 1. Schematic drawings of water reduction catalysts **10** – **18**.

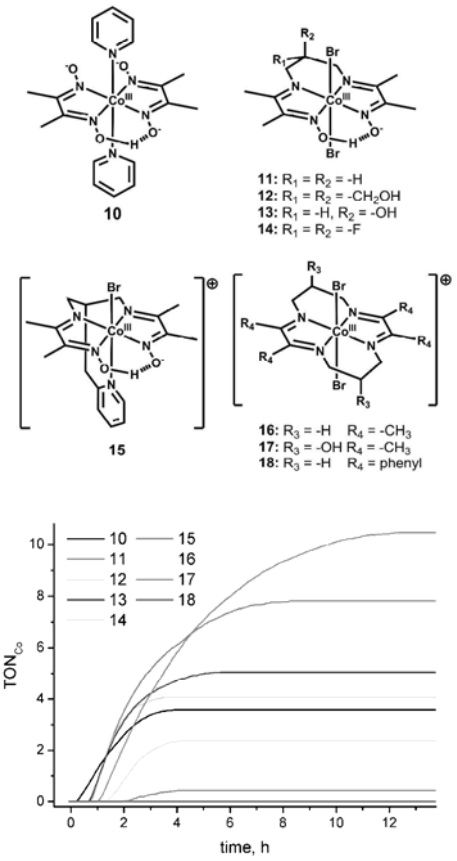

Figure 5. H_2 production for **1** with different WRCs. Conditions: 30 μM **1**, 500 μM Co, 1 M TEOA, 0.1 M HBF_4, H_2O, 10 ml, 380 nm, $q_{n,p} = 1.75 \times 10^{-7}$ einstein/s.

To improve the TON_{Co}, a series of WRCs (**11** – **18**), containing the tetradentate ligand frameworks 2,3,9,10-tetramethyl-1,4,8,11-tetraazaundecane-1,3,8,10-tetraene-1,11-diol (DOH_2) or the 2,3,9,10-tetramethyl-1,4,8,11-tetraazacyclotetradeca-1,3,8,10-tetraene (TIM), were evaluated under identical conditions as **10** Scheme 2 and Figure 5). In DMF, WRC **10** is clearly the best catalyst but in water, some of the other WRCs performed better than **10**. For instance, $TON_{Co} > 10$ were achieved for **15** (QY = 30 %; H/einstein). Unlike in DMF, **11** and **15** exhibited a better performance than **10** and **12** – **14**

are about equal. For both solvents, complexes containing the TIM macrocycle (**16** – **18**) are inferior to the other WRCs. The nature of the WRC thus determines long term stability which increases along the series TIM < dmgH < DOH. The comparison of **11** and **15** reveals a distinct effect on catalysis imposed by the pendant pyridine moiety in **15**. Identical experiments with **11** in the presence of free pyridine did not change the performance, indicating that the higher TONs as observed for **15** compared to **11** are related to the intramolecular base.

To complement stability studies of WRCs, we studied the behavior of the PS with respect to long term stability. Compound **1** rapidly disappeared upon irradiation in deaerated solution in the presence of TEOA but in the absence of WRC. HPLC analysis evidenced loss of the axial pyridine ligand and formation of the solvato-complex **4**. Since reductive quenching of *__1__ did take place, the product $\mathbf{1}^-$ underwent further reactions ultimately resulting in the loss of the axial pyridine. In the same experiment but without TEOA or in the presence of O_2, **1** remained completely stable. In CV experiments in H_2O, the reduction of **1** is irreversible (0.01 – 5 V/s). This indicated that reduced $\mathbf{1}^-$ is unstable in water and undergoes ligand loss on the upper μs to ms timescale. Since electron transfer to cobalt occurs within 1 μs however, this decomposition does not limit catalytic performance of the studied systems in water.

pH dependence. The pH dependencies of initial H_2 production and final TON_{Co} are shown inFigure 6, SI 3 and SI 4 for **10**, **11** and **15**. The initial H_2 formation rates for all three WRCs decreased rapidly when going to more acidic solutions. Since the pK_a of $[HTEOA]^+$ is 7.8,[27] the concentration of free TEOA to reductively quench *__1__ becomes small and the reaction slow at lower pH. On the other hand, all systems were more stable at lower pH and the TON_{Co} reached a maximum at around pH 8. The pK_a of **10** in H_2O is 7.3 (but will be different for the corresponding Co^{II}, Co^{I} and Co^{III}-H species), suggesting that most WRCs in these experiments are actually deprotonated on one oxime moiety. At higher pH values, both TOF and TON decrease. We observed a red shift in absorption at pH 10.5 in an irradiation experiment with **10**, indicative of a Co^{I} species accumulating in solution (see ***SI 3***). Possibly, at high pH protonation of Co^{I} becomes limiting which explains the decrease in TOF. Accumulation of Co^{I} goes along with PS^- accumulation, leading to decomposition of PS (see section Longterm Performance) and explaining the decrease in TON.

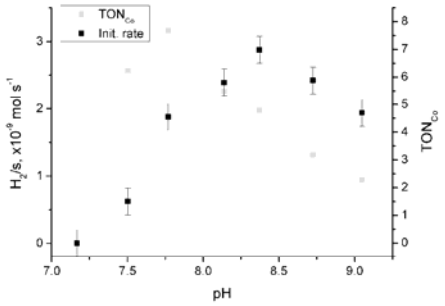

Figure 6. Initial H_2 production rates (left scale, ■, mol/s) and end TON_{Co} (right scale, ■) as a function of pH. Conditions: 30 μM **1**, 500 μM **10**, 1 M TEOA, varying HBF_4, H_2O, 10 ml, 380 nm, $q_{n,p}$ = 1.75 x 10^{-7} einstein/s.

Mechanism of hydrogen release: While in organic solvents, the nature of the hydrogen release step from Co^{III}-H for cobaloximes is believed to be homolytic,[8,24,28,29] heterolytic and homolytic routes might be at work in parallel in protic media, depending on [Co] and pH.[30] Unlike in DMF,[8,24] no square dependence of H_2/s on [Co] was found in H_2O for **10** (SI 1). The color change observed during irradiation (SI 2) strongly suggested initial build up of Co^{II} (λ_{max} = 463 nm, SI 6)[31,32] which then remained the predominant component during catalysis. Over time, its absorption bleached, indicating decomposition. All other species such as Co^{III}, Co^{I} or Co^{III}-H seem to be too short lived to be detected. When the pH was increased to 10.5 (SI 3), new absorption bands at 625 and 550 nm appeared, characteristic for Co^{I},[28,29,31] as shown by comparison with an electrochemical reduction of a derivative of **10** in aprotic media (SI 6). Presumably, Co^{I} accumulates due to its pK_a in the range of 11.[33-35] Therefore TONs are substantially reduced at high pH because Co^{I} and, subsequently, also PS^{-} accumulate in solution.

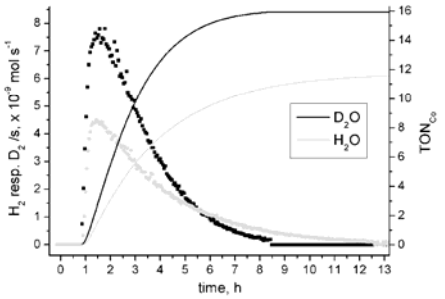

Figure 7. Comparison of catalytic performance in D_2O vs H_2O for **15**. Conditions: 30 μM **1**, 0.5 mM **15**, 1 M TEOA, 0.1 M HBF_4, H_2O resp. D_2O, Ar, 10 ml, 380 nm, $q_{n,p}$ = 1.75 x 10^{-7} einstein/s.

Table 3. Isotope effects as determined for **10**, **11**, **11** + 1 eq. pyridine and **15**.[a]

compound	$\frac{TON_{Co,D_2O}}{TON_{Co,H_2O}}$	$\frac{TOF_{max,D_2O}}{TOF_{max,H_2O}}$
10	0.7 ± 0.1	1.1 ± 0.2
11	1.0 ± 0.1	0.9 ± 0.3
11 + 1 eq pyridine[b]	1.2 ± 0.2	1.1 ± 0.3
15	1.5 ± 0.1	2.0 ± 0.3

[a]: 30 μM **1**, 0.5 mM WRC, 1 M TEOA, 0.1 M HBF_4, H_2O resp. D_2O, Ar, 10 ml, 380 nm, $q_{n,p}$ = 1.75 x 10^{-7} einstein/s. [b]: quantitative formation of [CoBr(py)DOH]Br.

Finally, it was of interest if a kinetic isotope effect could be observed. Experiments in D_2O, using 30 μM **1**, 500 μM WRC (**10**, **11** or **15**), 1 M TEOA, 0.1 M HBF_4, D_2O (~95 %) produced, as expected, D_2 instead of H_2 as observed in H_2O, thereby showing that the source of protons is the solvent indeed. Whereas in case of **10** or **11** no significant isotope effect could be observed, both in terms of TON_{Co}'s and TOF_{max}'s, we found a distinct, inverse isotope effect for **15** (see Table 3 andFigure 7). Catalyst **11**, in the presence of 1 eq. of pyridine, did not show a significant isotope effect (see Table 3) indicating once more that the mechanism of H_2 production depends on the ligand framework of the WRC. The presence of the pendent pyridine in **15** alters the mechanism with respect to **10** and **11** with free pyridine.

Conclusion

In conclusion, we present the first Re/Co based, light driven reductive half reaction to H_2 in H_2O. The catalytic cycle was investigated by time resolved Infrared Spectroscopy. Upon excitation of the PS,

reductive quenching by TEOA takes place ($k_q = 5 - 8 \times 10^7$ M^{-1} s^{-1}; $\Phi_{cage} = 0.75$) followed by electron transfer from PS^- to Co^{III} ($k_{CoIII} = 1.1 \times 10^9$ M^{-1} s^{-1}). Thus, under our conditions, the mechanism is not different from the one found in DMF. The reduced PS is stable on the timescale of the UV-pump IR-probe experiments which is up to 40 μs. Within this timeframe, the electron must be transferred to the WRC.

The highest TON_{Re} was 550 while TON_{Co} did not exceed 17. Although TON_{Co}'s are low, our study is a proof of principle for the feasibility of H_2 formation in pure water with a Re/Co system. It serves as a base for further development of PSs and WRCs in particular. Our kinetic studies clearly showed that the WRC needs to be improved for achieving systems competitive with those in organic solvents. The WRC, most likely as Co^{III}-H, undergoes side reactions, thus limiting turnovers achieved. A pronounced pH dependence indicates that WRC deactivation is favored under basic conditions whereas hydrogen elimination is favored under acidic conditions respectively. The deactivation process decreases the hydrogen yield per WRC in water by about two orders of magnitude as compared to DMF as a solvent. We emphasize that kinetic, mechanistic and thermodynamic studies are better defined in water than in organic solvents and will facilitate spectroscopic investigations and WRC design.

Experimental

Luminescence measurements were performed on a Perkin-Elmer LS50B fluorescence spectrometer with argon-purged solution samples in 1 cm cells. Luminescence life time measurements were performed on an Edinburgh Instrument F900 equipped with a nF900 nanosecond flash lamp filled with hydrogen (operating at 0.4 bar and frequency 40 KHz). Luminescence quantum yields were determined relative to coumarin I in ethanol (0.64)[36] according to literature procedure.[37]

Gas chromatograms were recorded using a Varian CP-3800 gas chromatograph with argon as carrier gas and a 3 m x 2 mm packed molecular sieve 13X 80-100 column. The gas flow was set to 20 ml/min. The oven was operated isothermal at 100 °C. An argon flow of usually 10.8 ml/min (adjusted with a manual flow controller (Porter, 100) and referenced with a flow meter (MS Wil GmbH)) was passed through the reaction mixture and into the GC, where 100 μl gas samples were automatically injected in defined time intervals (usually 5 min) using a 6-Port-2-Position Valve from Vicci. The gases were detected using a thermal conductivity detector (Varian) operated at 150 °C. Hydrogen production rates were calibrated by introducing a known flow of pure hydrogen by a Single Syringe Pump (70-2208 from Harvard Apparatus, using a 2.5 ml Hamilton GASTIGHT® #1002 syringe and a Teflon® tube) to the 60 ml Schlenk containing 1 M TEOA in DMF. Plotting of the peak area for hydrogen versus the used flow rates of hydrogen gave linear fits. The slope of these fits depended linearly on the argon flow through the solution. Varying the argon flow thus allowed detecting smaller hydrogen production rates,

although at a higher response time (20 min for 10.8 ml/min). This setup allowed us to detect $H_2/s \geq 0.3 \times 10^{-9}$ mol s^{-1} (standard deviation is $\leq 0.2 \times 10^{-9}$ mol s^{-1}).

Photochemical measurements were carried out in a 60 ml septum capped Schlenk tube containing a Teflon® stirrer at 500 rpm. 10 ml of a solution containing the respective mixture in DMF were prepared, wrapped in black foil and degassed using an argon-purged Schlenk-line. The mixture was equilibrated under 1.5 bar argon pressure for 15 min and then transferred to a dark room for illumination. The light source was a 380 nm high flux LED from Rhopoint Components LTD (OTLH-0280-UV; CPC reflector for Shark LED; irradiated directly from below; current control at usually 200 mA; $q_{n,p} = 1.75 \times 10^{-7}$ einstein/s). If necessary the radiant flux was varied by adjustment of the current through the LED. The radiant flux at different currents was calibrated using actinometry. A constant flow of usually 10.8 ml/min argon was passed through the solution and into a sixport valve at the GC, where 100 µl gas samples were injected into the GC-TCD gas analyzer in defined intervals. Integration of the production rate versus time gave the total amount of hydrogen produced. Quantum yields were measured in a 1 x 1 cm, 3.5 ml quartz cell from Helma, equipped with a septa cap for gas sampling during photolysis. The degassed solution was stirred and irradiated with a 380 nm high flux LED from Rhopoint Components LTD (OTLH-0280-UV), projected on to the cell ($q_{n,p} = 4.8 \times 10^{-9}$ einstein/s). 92 % of these photons are absorbed by a 0.5 mM solution of **1** ($\varepsilon_{380nm} = 2150$ cm^{-1} M^{-1}). Quantum yields are given as H per absorbed einstein.

UV-pump-IR-probe spectroscopy. The system for UV-pump-IR-probe spectroscopy consists of two synchronized[25] Ti:sapphire-oscillator/regenerative amplifier femtosecond laser systems operating at 800 nm (Spectra Physics, pulse duration ~100 fs, repetition rate 1 kHz, energy ~600 µJ/pulse), allowing us to cover the time range from 2 ps to 40 µs. Laser system 1 was frequency-doubled with a BBO crystal. The obtained 400 nm pulses were subsequently focused into the sample cell (100 µm thick) with a spot size of ~200 µm diameter. Laser system 2 pumped a white light seeded two-stage BBO optical parametric amplifier (OPA),[38] the signal and idler pulses of which were difference frequency mixed in an $AgGaS_2$ crystal. They were separated into two parts to achieve broadband probe and reference pulses. These IR-probe pulses were focused into the sample cell; the probe pulse in spatial overlap with the 400 nm pump pulse, while polarization of pump and probe pulses were set to an relative angle of 54.7° to allow for direct measurement of the anisotropy free magic angle signal. Reference and probe pulse were dispersed in a monochromator (SPEX Triax Series) and imaged onto a 2 x 64 pixel MCT (Mercury Cadmium Telluride) detector array (InfraRed Associates Inc.), resulting in a spectral resolution of 3.5 cm^{-1}. To ensure efficient exchange of the excited volume, the sample was pumped rapidly by a peristaltic pump (Ismatec BVP equipped with EasyLoad II pump-head) to a small sealed reservoir (V ≈ 3 ml). The pressurized flow of the reservoir transferred the sample through the flow cell and finally

back to the sample tank, which was protected from light. Since TEOA is an aggressive compound, the pump-head was equipped with chemically resistant fluoroelastomer tubing from Gore™ (Chem-Sure®). To exclude any oxygen the sample solution was purged with argon for at least 60 min before and during measurements. During the course of a measurement sample degradation remained negligibly small (< 5 %), which was checked via HPLC analysis before and afterwards.

Acknowledgment. We acknowledge the Swiss National Science Foundation (SNF grant No. 200021-119798) and the Kanton Zürich for financial support.

Supporting Information Available: H_2 production as a function of [Co] and pH, absorption changes during catalysis, spectroelectrochemistry and CV of $[Co(py)_2(dmgH)_2]PF_6$ and synthetic procedures for photosensitizers **1** – **8** and WRC catalysts **10** – **17** are available free of charge via the Internet at http://pubs.acs.org.

References

(1) Nicola Armaroli, V. B. *Angew. Chem.* **2007**, *119*, 52-67.
(2) Cline, E. D.; Adamson, S. E.; Bernhard, S. *Inorg. Chem.* **2008**, *47*, 10378-10388.
(3) Du, P.; Schneider, J.; Luo, G.; Brennessel, W. W.; Eisenberg, R. *Inorg. Chem.* **2009**, *48*, 4952-4962.
(4) Fihri, A.; Artero, V.; Razavet, M.; Baffert, C.; Leibl, W.; Fontecave, M. *Angew. Chem. Int. Ed.* **2008**, *47*, 564-567.
(5) Hawecker, J.; Lehn, J. M.; Ziessel, R. *New J. Chem.* **1983**, *7*, 271-277.
(6) Krishnan, C. V.; Brunschwig, B. S.; Creutz, C.; Sutin, N. *J. Am. Chem. Soc.* **1985**, *107*, 2005-2015.
(7) Lazarides, T.; McCormick, T.; Du, P. W.; Luo, G. G.; Lindley, B.; Eisenberg, R. *J. Am. Chem. Soc.* **2009**, *131*, 9192-9194.
(8) Probst, B.; Kolano, C.; Hamm, P.; Alberto, R. *Inorg. Chem.* **2009**, *48*, 1836-1843.
(9) Li, C.; Wang, M.; Pan, J.; Zhang, P.; Zhang, R.; Sun, L. *J. Organomet. Chem.* **2009**, *694*, 2814-2819.
(10) Kalyanasundaram, K.; Kiwi, J.; Grätzel, M. *Helv. Chim. Acta* **1978**, *61*, 2720-2730.
(11) Moradpour, A.; Amouyal, E.; Keller, P.; Kagan, H. *Nouv. J. De Chim.* **1978**, *2*, 547-549.
(12) Lehn, J. M.; Sauvage, J. P. *Nouv. J. de Chim.* **1977**, *1*, 449-451.
(13) Pac, C.; Ishii, K.; Yanagida, S. *Chem. Lett.* **1989**, 765-768.
(14) Krishnan, C. V.; Sutin, N. *J. Am. Chem. Soc.* **1981**, *103*, 2141-2142.
(15) Krishnan, C. V.; Creutz, C.; Mahajan, D.; Schwarz, H. A.; Sutin, N. *Isr. J. Chem.* **1982**, *22*, 98-106.
(16) Hawecker, J.; Lehn, J. M.; Ziessel, R. *New J. Chem.* **1983**, *7*, 271-277.
(17) Duan, L.; Xu, Y.; Zhang, P.; Wang, M.; Sun, L. *Inorg. Chem.* **2009**, *49*, 209-215.
(18) Comte, P.; Nazeeruddin, M. K.; Rotzinger, F. P.; Frank, A. J.; Grätzel, M. *J. Mol. Cat.* **1989**, *52*, 63-84.
(19) Geletii, Y. V.; Huang, Z.; Hou, Y.; Musaev, D. G.; Lian, T.; Hill, C. L. *J. Am. Chem. Soc.* **2009**, *131*, 7522-7523.

(20) Yin, Q. S.; Tan, J. M.; Besson, C.; Geletii, Y. V.; Musaev, D. G.; Kuznetsov, A. E.; Luo, Z.; Hardcastle, K. I.; Hill, C. L. *Science* **2010**, *328*, 342-345.
(21) Modification of the loop size (to 500 µl), reduction of Ar flow rate (5 ml/min) and reduction of the head space (2 ml), as compared to the setup described in Experimental, provided sufficient sensitivity for H_2 measurements with **3**.
(22) Experiments with **2**, **3**, **6** and **7** were not possible due to solubility issues in the buffer system at concentrations needed for UV-pump-IR-probe measurements.
(23) Classical Stern Vollmer plots of luminescence intensities vs. [TEOA] are not possible in H_2O because intensity changes due to viscosity / polarity changes in the solvent upon addition of TEOA. Further, dearated solutions of **1** and TEOA in H_2O were not photostable.
(24) Probst, B.; Rodenberg, A.; Guttentag, M.; Hamm, P.; Alberto, R. *Inorg. Chem.* **2010**, *49*, 6453-6460.
(25) Bredenbeck, J.; Helbing, J.; Hamm, P. *Rev.Sci. Inst.* **2004**, *75*, 4462-4466.
(26) Simandi, L. I.; Szeverenyi, Z.; Budozahonyi, E. *Inorg. Nulc. Chem. Let.* **1975**, *11*, 773-777.
(27) Izutsu, K. *Acid-base dissociation constants in dipolar aprotic solvents*; Blackwell Scientific Publications: Oxford, 1990.
(28) Dempsey, J. L.; Winkler, J. R.; Gray, H. B. *J. Am. Chem. Soc.* **2010**, *132*, 1060-1065.
(29) Hu, X.; Brunschwig, B. S.; Peters, J. C. *J. Am. Chem. Soc.* **2007**, *129*, 8988-8998.
(30) Chao, T. H.; Espenson, J. H. *J. Am. Chem. Soc.* **1978**, *100*, 129-133.
(31) Du, P. W.; Knowles, K.; Eisenberg, R. *J. Am. Chem. Soc.* **2008**, *130*, 12576-12577.
(32) Heckman, R. A.; Espenson, J. H. *Inorg. Chem.* **1979**, *18*, 38-43.
(33) Schrauze.Gn; Holland, R. J. *J. Am. Chem. Soc.* **1971**, *93*, 1505-&.
(34) Kellett, R. M.; Spiro, T. G. *Inorg. Chem.* **1985**, *24*, 2373-2377.
(35) Baffert, C.; Artero, V.; Fontecave, M. *Inorg. Chem.* **2007**, *46*, 1817-1824.
(36) Olmsted, J. *J. Phys. Chem.* **1979**, *83*, 2581-2584.
(37) Williams, A. T. R.; Winfield, S. A.; Miller, J. N. *Analyst* **1983**, *108*, 1067-1071.
(38) Hamm, P.; Kaindl, R. A.; Stenger, J. *Optics Letters* **2000**, *25*, 1798-1800.

TOC

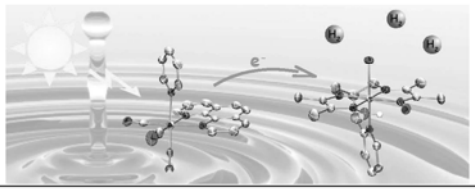

Photocatalytic hydrogen production from a homogeneous, aqueous solution with a series of rhenium based photosensitizers (PS) and cobalt based water reduction catalysts is reported for the first time. Catalysis was found to proceed by reductive quenching of the excited *PS and subsequent electron transfer to the cobalt based water reduction catalyst (WRC), as evidenced by UV-pump-IR-probe spectroscopy. Turnover numbers in rhenium above 500 along with a marked influence of pH were

found. Experiments in D_2O confirmed that the solvent is the proton source for hydrogen production. Catalysis was limited by decomposition of the WRC.

Supporting Information - Photocatalytic H_2 Production from Water with Rhenium and Cobalt Complexes.

Benjamin Probst[#], Miguel Guttentag[#], Alexander Rodenberg[§], Peter Hamm*[§], Roger Alberto*[#].

[#] *Institutes of Inorganic and* [§] *Physical Chemistry, University of Zürich, Winterthurerstrasse 190, CH-8057 Zürich Switzerland*

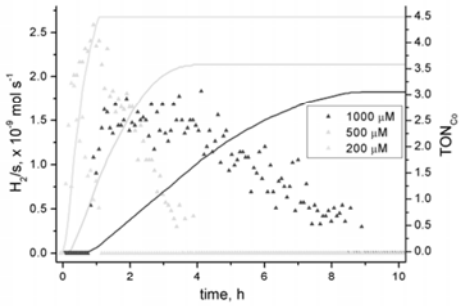

SI 1. H_2 production for different concentrations of **10** (mol/s, left scale, dots; TON_{Co} ,right scale, solid lines). Conditions: 30 µM **1**, 200, 500 or 1000 µM **10**, 1 M TEOA, 0.1 M HBF_4, H_2O, 10 ml, 380 nm, $q_{n,p}$ = 1.75 x 10^{-7} einstein/s.

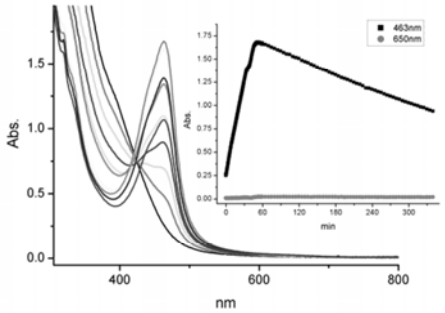

SI 2. Typical absorption change during photolysis (30 µM **1**, 500 µM **10**, 1 M TEOA, 0.1 M HBF_4, H_2O, 3 ml, 380 nm, $q_{n,p} \approx 10^{-9}$ einstein/s).

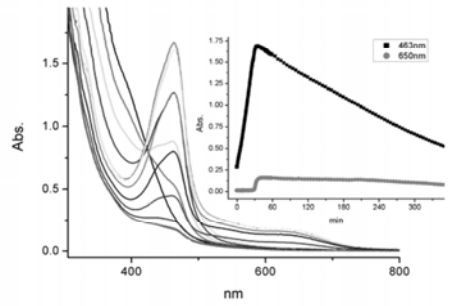

SI 3. Typical absorption change during photolysis (30 µM **1**, 500 µM **10**, 1 M TEOA, 1 mM HBF_4, H_2O, 3 ml, 380 nm, $q_{n,p} \approx 10^{-9}$ einstein/s).

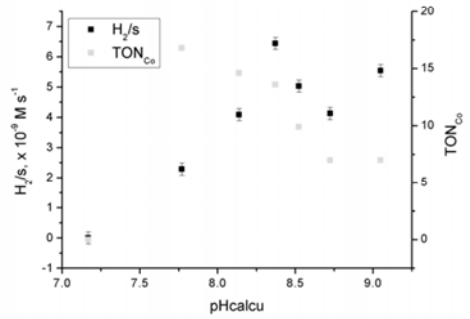

SI 4. Initial H_2 production rates (left scale, ■, mol/s) and end TON_{Co} (right scale, ▫) as a function of pH. Conditions: 30 µM **1**, 500 µM **11**, 1 M TEOA, varying HBF_4, H_2O, 10 ml, 380 nm, $q_{n,p} = 1.75 \times 10^{-7}$ einstein/s.

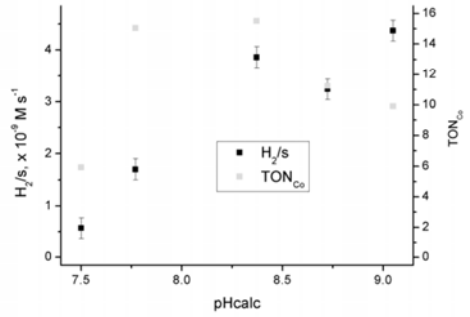

SI 5. Initial H_2 production rates (left scale, ■, mol/s) and end TON_{Co} (right scale, ▫) as a function of pH. Conditions: 30 µM **1**, 500 µM **15**, 1 M TEOA, varying HBF_4, H_2O, 10 ml, 380 nm, $q_{n,p} = 1.75 \times 10^{-7}$ einstein/s.

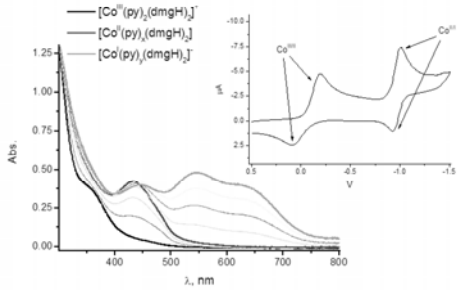

SI 6. Absorption change upon applying a potential of -1.2 V on a 2.5 mM solution of $[Co(py)_2(dmgH)_2]PF_6$ in DMF (selected traces, 0.1 M $[TBA]PF_6$, Ar). Inset: cyclic voltametry on a 1 mM solution of the latter complex (0.1 M $[TBA]PF_6$, DMF, Ar, 0.1 V/s), showing the irreversible $Co^{III/II}$ couple (upon reduction one axial pyridine is lost) and the reversible $Co^{II/I}$ couple (reversibility on the CV timescale does not necessarily mean reversibility in the bulk experiment, eg. it is possible that the d^8 species $[Co(dmgH)_2]^-$ is formed in the spectroelectrochemical experiment).

Experimental section

All chemicals were of reagent grade and used without further purification. 1,3-diaminopropane, 1,3-diamino-2-propanol, 2,2-bis(bromomethyl)-1,3-propanediol, picolyl chloride, diethyl malonate, benzil and 2,3-butandion were purchased from Aldrich, diethyl difluoromalonate and 2,3-butane monoxime from Alfa Aesar and $CoBr_2 \cdot x\ H_2O$, 54 % aqueous HBF_4 and silver trifluoromethansulfonate (AgTflsO) were purchased from Acros. Spectroscopy grade triethanolamine (TEOA), technical grade methyl-tert-butyl-ether (MTBE; distilled before use), $[Co(ac)_2(OH_2)_4]$, pyridine (py), benzylisocyanide (CNBz), 4-dimethylaminopyridine (4-Me_2Npy), dimethylglyoxime ($dmgH_2$), 2.2'-bipyridine (bipy) and phenanthroline (phen) were purchased from Fluka. Water was doubly distilled before use. Synthetic reactions were carried out under N_2 or Ar using standard Schlenk techniques. The synthesis of $[Re(OH_2)(CO)_3bipy](TflsO)$ (**4**),[1] $[ReBr(CO)_3phen]$,[1] $[Co(DOHpyr)Br](PF_6)$ (**15**),[2] $[Co(TIM^{Me})Br_2]$ (**16**),[3] $[Co(TIM^{Ph})Br_2]$ (**18**)[4] as well as the ligand fragment 2,2-bis(aminomethyl)propane-1,3-diol[5] have been described in the literature.

Syntheses

[Re(py)(CO)$_3$bipy](TflsO) (**1**). Complex **4** (296.5 mg, 0.5 mmol) was dissolved in 25 ml MeOH and pyridine (100 µl, 1.29 mmol) was added. The resulting solution was refluxed for 12 h, evaporated to dryness, suspended in 25 ml MTBE, filtered, washed with MTBE and dried in *vacuo*. Yield: 320.5 mg (98 %) of a off-yellow powder. $\lambda_{max}(H_2O)$: 343 nm (ε = 3650 $M^{-1}cm^{-1}$). $\lambda_{em}(H_2O)$: 567 nm (Φ_{em} = 0.0098 ± 0.0003). IR(KBr): 2026 (s), 1923 (s), 1907 (s), 1280 (m), 1260 (m), 1030 (m), 637 (m). ^{1}H-NMR (200 MHz, d^6-dmso, ppm): 9.32 (*d*, 2 H), 8.70 (*d*, 2 H), 8.40 (*m*, 4 H), 7.92 (*m*, 3 H), 7.43 (*t*, 2 H). ESI-MS(MeOH): *m/z* = 506.0 $[M\text{-}TflsO]^+$ (100 %), 426.9 $[M\text{-}TflsO\text{-}pyridine]^+$ (2 %). HPLC: 15.08 min. Anal. calcd. for $C_{19}H_{13}F_3N_3O_6ReS$ (%): C: 34.86, H: 2.00, N: 6.42. Found: C: 34.66, H: 1.99, N: 6.62.

[Re(CNBz)(CO)$_3$bipy](TflsO) (**2**). Complex **4** (29.7 mg, 50 µmol) was dissolved in 5 ml MeOH and benzylisocyanide (61 µl, 0.5 mmol) was added. The resulting solution was stirred for 36 h, evaporated to dryness, suspended in 5 ml MTBE, filtered, washed with MTBE and dried in *vacuo*. Yield: 33.5 mg (97 %) of a off-yellow powder. $\lambda_{max}(H_2O)$: 337 nm (sh; ε = 3800 $M^{-1}cm^{-1}$). $\lambda_{em}(H_2O)$: 527 nm (Φ_{em} = 0.087 ± 0.003). IR(KBr): 2223 (s), 2041 (s), 1956 (s), 1935 (s), 1281 (m), 1258 (m), 1030 (m), 773 (m). ^{1}H-NMR (200 MHz, d^6-dmso, ppm): 9.08 (*d*, 2 H), 8.81 (*d*, 2 H), 8.41 (*t*, 2 H), 7.82 (*t*, 2 H), 7.27 (*m*, 3 H), 6.89 (*m*, 2 H), 5.01 (*s*, 2 H). ESI-MS(MeOH): *m/z* = 544.1 $[M\text{-}TflsO]^+$ (100 %). HPLC: 15.79 min. Anal. calcd. for $C_{22}H_{15}F_3N_3O_6ReS$ (%): C: 38.15, H: 2.18, N: 6.07. Found: C: 38.14, H: 2.21, N: 6.04.

[Re(4-Me$_2$Npy)(CO)$_3$bipy](TflsO) (3). Complex **4** (30.5 mg, 51 µmol) was dissolved in 5 ml MeOH and 4-dimethylaminopyridine (20.5 mg, 0.17 mmol) was added. The resulting orange solution was refluxed for 4 h, evaporated to dryness, suspended in 5 ml MTBE, filtered, washed with MTBE and dried in *vacuo*. Yield: 31.4 mg (90 %) of a yellow powder. $\lambda_{max}(H_2O)$: 368 nm (ε = 2450 $M^{-1}cm^{-1}$). $\lambda_{em}(H_2O)$: 602 nm (Φ_{em} = 0.00029 ± 0.00001). IR(KBr): 2029 (s), 1935 (s), 1903 (s), 1627 (m), 1275 (m), 1230 (m), 1025 (m), 637 (m). ^{1}H-NMR (300 MHz, d^6-dmso, ppm): 9.29 (*d*, 2 H), 8.73 (*d*, 2 H), 8.41 (*t*, 2 H), 7.90 (*t*, 2 H), 7.65 (*d*, 2 H), 6.47 (*d*, 2 H), 2.90 (*s*, 6 H). ESI-MS(MeOH): *m/z* = 549.1 [M-TflsO]$^+$ (100 %). HPLC: 15.78. Anal. calcd. for $C_{21}H_{18}F_3N_4O_6ReS$ (%): C: 36.15, H: 2.60, N: 8.03. Found: C: 36.01, H: 2.67, N: 8.29.

[Re(OH$_2$)(CO)$_3$phen](TflsO) (8). [ReBr(CO)$_3$phen] (529.9 mg, 1 mmol) was suspended in 80 ml MeOH and AgTflsO (256.5 mg, 1 mmol), dissolved in 10 ml MeOH, was added. The suspension was, under exclusion of light, stirred overnight and sonicated several times to avoid formation of large colloidal particles. AgBr was removed quantitatively by filtration and the resulting, clear orange solution evaporated to dryness. The residue was then reflux for 2 h in 200 ml H_2O, filtered to remove any insoluble material, and the resulting, yellow solution lyophilized. Yield: 673.0 mg (109 %) of a orange powder. $\lambda_{max}(H_2O)$: 360 nm (sh, ε = 3400 $M^{-1}cm^{-1}$). $\lambda_{em}(H_2O)$: 578 nm (Φ_{em} = 0.00099 ± 0.00002). IR(KBr): 2035 (s), 1919 (s), 1735 (m), 1618 (m), 1266 (m), 1231 (m), 1031 (m), 638 (m). ^{1}H-NMR (300 MHz, d^6-dmso, ppm): 9.52 (*dd*, 2 H), 9.06 (*d*, 2 H), 8.37 (*s*, 2 H), 8.19 (*dd*, 2 H), 7.50 (*s*, 2 H). ESI-MS(MeOH): *m/z* = 468.8 [M-TflsO]$^+$ (25 %), 450.9 [M-TflsO-OH$_2$]$^+$ (100 %). HPLC: 15.29. Anal. calcd. for $C_{16}H_{10}F_3N_2O_7ReS$ (%): C: 31.12, H: 1.63, N: 4.54. Found: C: 30.98, H: 1.79, N: 4.31.

[Re(py)(CO)$_3$phen](TflsO) (5). Complex **8** (30.4 mg, 50 µmol) was dissolved in 5 ml pyridine and the resulting solution was stirred for 10 days, evaporated to dryness, suspended in 5 ml MTBE, filtered, washed with MTBE and dried in *vacuo*. Yield: 26.0 mg (77 %) of a off-yellow powder. $\lambda_{max}(H_2O)$: 362 nm (ε = 3350 $M^{-1}cm^{-1}$). $\lambda_{em}(H_2O)$: 550 nm (Φ_{em} = 0.039 ± 0.001). IR(KBr): 2030 (s), 1918 (s), 1263 (m), 1028 (m), 637 (m). ^{1}H-NMR (300 MHz, d^6-dmso, ppm): 9.77 (*d*, 2 H), 9.04 (*d*, 2 H), 8.46 (*d*, 2 H), 8.31 (*s*, 2 H), 8.26 (*dd*, 2 H), 7.86 (*t*, 1 H), 7.32 (*t*, 2 H). ESI-MS(MeOH): *m/z* = 530.0 [M-TflsO]$^+$ (100 %), 451.0 [M-TflsO-pyridine]$^+$ (10 %). HPLC: 15.30 min. Anal. calcd. for $C_{21}H_{13}F_3N_3O_6ReS$ (%): C: 37.17, H: 1.93, N: 6.19. Found: C: 37.23, H: 1.97, N: 6.39.

[Re(CNBz)(CO)$_3$phen](TflsO) (6). Complex **8** (30.7 mg, 50 µmol) was dissolved in 5 ml MeOH and benzylisocyanide (20 µl, 0.17 mmol) was added. The resulting solution was stirred for 10 days, evaporated to dryness, suspended in 5 ml MTBE by sonication, filtered, washed with MTBE and dried in *vacuo*. Yield: 30.5 mg (85 %) of a off-yellow powder. $\lambda_{max}(H_2O)$: 360 nm (sh; ε = 2600 $M^{-1}cm^{-1}$). $\lambda_{em}(H_2O)$: 515 nm (Φ_{em} = 0.208 ± 0.004). IR(KBr): 2201 (m), 2044 (s), 1966 (s), 1938 (s), 1267 (m), 1031 (m), 637 (m). ^{1}H-NMR (300 MHz, d^6-dmso, ppm): 9.51 (*d*, 2 H), 9.03 (*d*, 2 H), 8.39 (*s*, 2 H), 8.16

(*dd*, 2 H), 7.22 (*t*, 1 H), 7.10 (*t*, 2 H), 8.62 (*d*, 2 H), 4.87 (*s*, 2 H). ESI-MS(THF): *m/z* = 568.0 [M-TflsO]$^+$ (100 %). HPLC: 15.79 min. Anal. calcd. for $C_{24}H_{15}F_3N_3O_6ReS$ (%): C: 40.22, H: 2.11, N: 5.86. Found: C: 40.32, H: 2.09, N: 5.95.

[Re(4-Me$_2$Npy)(CO)$_3$phen](TflsO) (7). Complex **8** (30.5 mg, 50 μmol) was dissolved in 20 ml MeOH and 4-dimethylaminopyridine (22 mg, 0.18 mmol) was added. The resulting orange solution was refluxed for 100 h, evaporated close to dryness, suspended in 5 ml MTBE, filtered, washed with MTBE and dried in *vacuo*. Yield: 23.6 mg (65 %) of a yellow powder. $\lambda_{max}(H_2O)$: 368 nm (ε = 3000 $M^{-1}cm^{-1}$). $\lambda_{em}(H_2O)$: 592 nm (Φ_{em} = 0.0011 ± 0.0001). IR(KBr): 2024 (s), 1936 (s), 1921 (s), 1628 (m), 1270 (m), 1032 (m), 637 (m). ^{1}H-NMR (300 MHz, d^6-dmso, ppm): 9.74 (*d*, 2 H), 9.04 (*d*, 2 H), 8.33 (*s*, 2 H), 8.24 (*dd*, 2 H), 7.71 (*d*, 2 H), 6.35 (*d*, 2 H), 2.82 (*s*, 6 H). ESI-MS(MeOH): *m/z* = 573.2 [M-TflsO]$^+$ (100 %). HPLC: 16.04. Anal. calcd. for $C_{23}H_{18}F_3N_4O_6ReS$ (%): C: 38.28, H: 2.51, N: 7.76. Found: C: 37.94, H: 2.38, N: 7.46.

[Co(py)$_2$(dmgH)(dmg)] (10). To $[Co(ac)_2(OH_2)_4]$ (622.5 mg, 2.5 mmol) in 10 ml MeOH was added 2 ml pyridine (24.8 mmol) under stirring. The dark violet solution was degassed and flushed with argon several times before $dmgH_2$ (581 mg, 5 mmol) was added as a solid. Immediate formation of a brown precipitate occurs. After 5 minutes stirring under argon atmosphere air was gently bubbled through the suspension for 1 h and the solvent removed in *vacuo*. The residue was then taken up in 50 ml H_2O and filtered to remove any insoluble material. Slow addition of 1 M NaOH (5 ml, 2 equivalents) resulted in formation of brownish, cubic crystals. Filtration and washing with cold H_2O afforded 843.4 mg (1.89 mmol, 76 %) **10**. IR(KBr): 1291 (s), 772 (s), 698 (s), 515 (s). ^{1}H NMR (200 MHz, D_2O, ppm): 8.30 (*d*, 4 H), 7.76 (*t*, 2 H), 7.26 (*t*, 4 H), 2.13 (*s*, 6 H), 1.92 (*s*, 6 H). ESI-MS(MeOH): *m/z* = 447.1 [MH]$^+$ (35 %), 289.3 [MH- 2 pyridine]$^+$ (100 %). HPLC: 13.69 min. Anal. calcd. for $C_{18}H_{23}CoN_6O_4$ (%): C: 48.44, H: 5.19, N: 18.83. Found: C: 48.31, H: 5.18, N: 18.34.

2,2-difluoro-1,3-diaminopropane. Diethyl difluoromalonate (1.7 g, 8.71 mmol) was dissolved in a solution of ammonia in methanol (saturated at 0 °C). After 2 days the solvent was removed and the residue was dissolved in 8 ml dry THF. To the resulting suspension (kept at 0 °C) was added cautiously over 20 min 80 ml of a 1 M solution of $BH_3 \cdot$ THF. Once the addition was complete the mixture was refluxed for 4 hours. After cooling to 0 °C 7ml of H_2O were added very carefully to destroy excess diborane. The solution was evaporated to dryness and the residue was slowly treated with 35 ml 6 N HCl. After refluxing for another 4 hours the solution was left to stand overnight. The precipitate was filtered off and the solvent was removed. Addition of 17 ml H_2O and 12 ml 6 N NaOH and extraction with CH_2Cl_2 yielded 872 mg (7.9 mmol, 91%) 2,2-difluoro-1,3-diaminopropane as a colorless oil. ^{1}H NMR (200 MHz, DMSO, ppm): 2.88 (*t*, 4 H).

General Procedure for CoDOH-type complexes. After steering a solution of the corresponding diamine (0.4 M) and 2,3-butanedione monoxime (0.8 M) in EtOH for seven days, the solution was

degassed and combined with a degassed solution of $CoBr_2 \cdot x\,H_2O$ (2 eq, 0.8 M) in EtOH. After addition air was bubbled through the reaction for 10 minutes, and then left to stand several days for crystallization. Filtration and washing with cold water afforded a green, crystalline product with typical yields between 5 – 25 %.

[CoDOHBr$_2$] (11). IR(KBr): 1521 (m), 1136 (m). ^{1}H NMR (200 MHz, Acetone, ppm): 19.58 (*s*, NOH, 1 H), 4.14 (*m*, CH_2, 6 H), 2.68 (*s*, CH_3, 6 H), 2.52 (*s*, CH_3, 6 H). ESI-MS(MeOH): *m/z* = 480.8 $[M + Na]^+$ (100 %). Anal. calcd. for $C_{11}H_{19}Br_2CoN_4O_2$ (%): C: 28.84, H: 4.18, N: 12.23. Found: C: 29.05, H: 4.21, N: 12.30.

[Co(DOH(COH)$_2$)Br$_2$] (12). IR(KBr): 1509 (m), 1041 (m). ^{1}H NMR (200 MHz, DMSO, ppm): 19.07 (*s*, NOH, 1 H), 4.75 (*t*, OH, 2 H), 4.02 (*s*, NCH_2, 4 H), 3.70 (*d*, OCH_2, 4 H), 2.64 (*s*, CH_3, 6 H), 2.51 (*s*, CH_3, 6 H). ESI-MS(MeOH): *m/z* = 427 $[M\text{-}Br]^+$ (100 %). Anal. calcd. for $C_{13}H_{23}Br_2CoN_4O_4$ (%): C: 30.14, H: 4.47, N: 10.81. Found: C: 29.97, H: 4.57, N: 10.80.

[CoDOHOHBr$_2$] (13). IR(KBr): 1513 (m), 1146 (m). ^{1}H NMR (200 MHz, DMSO, ppm): 19.29 (*s*, NOH, 1 H), 5.69 (*d*, OH, 1 H), 4.54 (*m*, CH, 1 H), 4.32 (*d*, HCH, 2 H), 3.70 (*dd*, HCH, 2 H), 2.66 (*s*, CH_3, 6 H). ESI-MS(MeOH): *m/z* = 314 $[M\text{-}2Br]^+$ (100 %). Anal. calcd. for $C_{11}H_{19}Br_2CoN_4O_3$ (%): C: 27.87, H: 4.04, N: 11.82. Found: C: 27.76, H: 3.88, N: 12.04.

[CoDOHF$_2$Br$_2$] (14). IR(KBr): 1499 (m), 1302 (m), 1134 (m), 1093 (m). ^{1}H NMR (200 MHz, DMSO, ppm): 19.12 (*s*, NOH, 1 H), 4.59 (*t*, CH_2, 4 H), 2.71 (*s*, CH_3, 6 H). ESI-MS(MeOH): *m/z* = 343 $[M\text{-}2Br]^+$ (100 %). Anal. calcd. for $C_{11}H_{17}Br_2CoF_2N_4O_2$ (%): C: 26.74, H: 3.47, N: 11.34. Found: C: 26.72, H: 3.39, N: 11.38.

[Co(TIMOH)Br$_2$]Br (17) was synthesized according to a literature procedure for 16.[3] IR(KBr): 1420 (m), 1215 (m), 1098 (m). ^{1}H NMR (200 MHz, Acetone, ppm): 5.95 & 5.82 (2 *s*, CH, 2 H), 4.62 (*s*, OH, 2 H), 4.37 (*d*, HCH, 4 H), 3.76 (*t*, HCH, 4 H), 2.52 (*s*, CH_3, 12 H). ESI-MS(MeOH): *m/z* = 499 $[M]^+$ (100 %). Anal. calcd. for $C_{14}H_{24}Br_2CoF_2N_4O_2$ (%): C: 29.04, H: 4.17, N: 9.68. Found: C: 29.05, H: 4.16, N: 9.64.

Spectroscopy

Mass spectra were measured on a Bruker Esquire HCT (ESI) instrument and only characteristic fragments are given. The solvent flow rate for ESI measurements was 5 µl min^{-1}, a nebulizer pressure of 15 psi and a dry gas flow rate of 5 L min^{-1} at a dry gas temperature of 300°C were used.

Elemental analyses were performed on a LecoCHNS-932 elemental analyzer.

^{1}H NMR spectra were recorded on Varian Mercury and Varian Gemini-2000 spectrometers (^{1}H at 199.97 MHz and 300.08 MHz, respectively). The chemical shifts are reported relative to residual solvent protons as reference.

UV-Vis spectra were measured using a Cary 50 spectrometer with solution samples in 1 cm quartz cells. If necessary, cells with silicon septa lids were used to keep samples under an inert gas atmosphere during measurements.

IR spectra were recorded on a Bio PerkinElmer SpectrumBXFT-IR spectrometer with samples in compressed KBr-pellets.

Electrochemical measurements were carried out in DMF containing 0.1 M [TBA][PF_6] as conducting electrolyte. A Metrohm 757VA Computrace electrochemical analyzer was used with a standard three-electrode setup of glassy carbon working (ID = 3 mm) and Pt auxiliary electrodes and an Ag/AgCl reference electrode. All potentials are given vs. Ag/AgCl and are referenced with Fc/Fc^+ at +500 mV. Spectroelectrochemical analysis was performed in an optical transparent thin layer electrolysis (OTTLE) cell in the UV-Vis spectrometer described above. The working electrode was a platinum gaze immersed into the OTTLE cell, auxiliary electrode was a platinum wire in a compartment separated by a diaphragm, and the reference electrode was an Ag/AgCl electrode.

HPLC measurements were performed on a VWR LaChrome Elite® using a Nucleodur C18 Gravity column operated in an oven (L-2350) at 40 °C and a PDA detector (L-2450). The gradient was as follows: A = 0.1 % TFA, 10 % MeOH, H_2O; D = MeOH; flow rate = 0.5 ml/min; 0 – 5 min 100 % A; 5 – 15 min 0 – 100 % D; 15 – 18 min 100 % D. Control runs before and after catalysis were systematically performed using 10 µl of the reaction solution in DMF. Under these conditions $dmgH_2$ gave a broad peak at 6.4 min and **1** a defined peak at 17.04 min.

References

(1) Kurz, P.; Probst, B.; Spingler, B.; Alberto, R. *Eur. J. Inorg. Chem.* **2006**, 2966-2974.
(2) Gerli, A.; Sabat, M.; Marzilli, L. G. *J. Am. Chem. Soc.* **1992**, *114*, 6711-6718.
(3) Jackels, S. C.; Busch, D. H.; Barefiel.Ek; Rose, N. J.; Farmery, K. *Inorg. Chem.* **1972**, *11*, 2893-&.
(4) Welsh, W. A.; Reynolds, G. J.; Henry, P. M. *Inorg. Chem.* **1977**, *16*, 2558-2561.
(5) Virta, P.; Leppanen, M.; Lonnberg, H. *J. Org. Chem.* **2004**, *69*, 2008-2016.